JOHANNES GUTENBERG UNIVERSITÄT MAINZ

Max-Planck-Institut für Polymerforschung
Max Planck Institute for Polymer Research

Flow-based techniques for the analysis of nanocarriers in biological environments

Dissertation

zur Erlangung des Grades

„Doktor der Naturwissenschaften“

im Promotionsfach Chemie

am Fachbereich Chemie, Pharmazie und Geowissenschaften

der Johannes Gutenberg-Universität Mainz

D77

Claudia Weber

geb. in Frankfurt am Main, Deutschland

Mainz, 2018

The presented thesis was carried out from January 2016 until December 2018 in the department of Physical Chemistry of Polymers at the Max Planck Insitute for Polymer Research in Mainz (Germany).

Dekan:

1. Gutachter:

2. Gutachter:

Tag der mündlichen Prüfung:19. Dezember 2018

Eigenständigkeitserklärung

I hereby declare that I wrote the dissertation submitted without any unauthorized external assistance and used only sources acknowledged in the work. All textual passages, which are appropriated verbatim or paraphrased from published and unpublished texts, as well as all information obtained from oral sources are duly indicated and listed in accordance with bibliographical rules. In carrying out this research, I complied with the rules of standard scientific practice as formulated in the statutes of the Johannes Gutenberg University Mainz to ensure standard scientific practice.

Mainz, November 2018

Abstract

The use of nanomedicine has recently opened new perspectives in the field of drug delivery, while the comprehension on how nanocarriers interact with biological systems still remains to be a big challenge. Upon contact of the nanomaterial with a biological fluid like blood plasma, a 'protein corona' develops from the adsorption of proteins and other biomolecules on the nanocarrier surface. The adsorbed proteins determine the biological response and, therefore, understanding the processes involved in the protein corona formation is crucial to make nanomedicine reliable, successful and safe. Currently, the main focus in the protein corona analysis is the investigation of the 'hard corona', which describes the strongly adsorbed proteins usually separated via centrifugation. However, there are more aspects contributing to the protein corona, leading to a discrepancy between the *in vitro* and *in vivo* characterization.

In the presented thesis, asymmetric flow field-flow fractionation (AF4) has been introduced as a new separation technique for the isolation of differently sized components like nanocarrier-protein complexes or plasma protein fractions. Combining this technique with subsequent analysis steps, new insights into the protein corona formed from human blood plasma have been highlighted for the first time.

With the AF4, also loosely bound proteins contributing to the 'soft corona' on polystyrene nanoparticles could be preserved. The obtained corona could be compared with the hard corona after centrifugation in terms of size, composition and cellular uptake. The separation process was adopted to liposomes as potential drug carriers. The influence of hyperbranched polyglycerol as surface functionality on liposomes was investigated for its potential 'stealth effect', meaning a minimized unspecific protein adsorption and cell uptake. Furthermore, AF4 proved to be a valuable tool for the separation of plasma into smaller entities, enabling a more detailed data evaluation of the complex protein mixture. After removal of the silica nanoparticles including their protein corona, the protein residue of plasma was investigated. This way, a depletion of the most prominent protein of the protein corona could be identified, as well as a changed retention behavior of the supernatant. Additionally, considering the flow after intravenous injection of nanocarriers, a light scattering set-up was used to observe the influence of the blood flow on the protein corona formation.

From the presented results, a broader knowledge of the various parameters influencing the protein corona was obtained, and new techniques were introduced for the analysis of the nanocarrier-protein interactions that can be related to realistic *in vivo* conditions.

Zusammenfassung

Im Gebiet der Nanomedizin eröffnet die Anwendung von Wirkstoffträgern neue, vielversprechende Perspektiven. Allerdings sind die Interaktionen dieser Nanoträger mit biologischen Systemen noch weitestgehend unklar und bilden damit die größte Herausforderung in diesem Gebiet. In dem Moment, in dem ein Nanomaterial mit einer biologischen Flüssigkeit wie Blutplasma in Kontakt kommt, adsorbieren Proteine und andere Biomoleküle auf dessen Oberfläche und bilden die sogenannte ‚Proteinkorona'. Diese adsorbierten Proteine bestimmen von nun an die biologische Antwort des Körpers auf den Nanoträger. Daher ist es wichtig, die Prozesse, die an der Proteinkorona-Bildung beteiligt sind, zu verstehen und so Nanomedizin zuverlässig, effektiv und sicher zu machen. Derzeit liegt der Schwerpunkt der Proteinkorona-Analyse auf der Untersuchung der ‚harten Korona', die die stark adsorbierten Proteine beschreibt, und die üblicherweise durch Zentrifugation erhalten wird. Es gibt jedoch mehr Aspekte, die zur Proteinkorona beitragen, was zu einer Diskrepanz der *in vitro* und der *in vivo* Daten führt.

In der vorliegenden Arbeit wurde eine neue Trennmethode zur Isolierung von Nanoträgern unter Zuhilfenahme der asymmetrischen Fluss Feld-Fluss Fraktionierung (AF4) vorgestellt. Durch die Kombination dieser Technik mit nachfolgenden Analyseschritten wurden erstmals neue Einblicke in die aus menschlichem Blutplasma gebildete Proteinkorona gewonnen.

Mittels AF4 konnten zusätzlich zu der harten Korona auch lose gebundene Proteine als Teil der Proteinkorona erhalten werden, die zur ‚weichen Korona' auf Polystyrol-Nanopartikeln gezählt werden. Die nach AF4 isolierte Korona konnte mit der harten Korona nach Zentrifugation hinsichtlich Größe, Zusammensetzung und Zell-Aufnahme verglichen werden. Das Trennverfahren wurde anschließend auf Liposome als potentielle Wirkstoffträger übertragen. Dabei wurde hyperverzweigtes Polyglycerol auf der Oberfläche von Liposomen auf seinen potentiellen ‚Stealth-Effekt' hin untersucht, der sich in einer minimierten Proteinadsorption und einer minimierten unspezifischen Zellaufnahme zeigt. Darüber hinaus erwies sich AF4 als ein geeignetes Werkzeug für die Trennung von Plasma in kleinere Einheiten, was eine detailliertere Analyse der komplexen Proteinmischung ermöglicht. Nach Abtrennung von Silica-Nanokapseln mit Proteinkorona wurde der Proteinrückstand des Plasmas untersucht und auf diese Weise ein Mangel des prominentesten Proteins der Proteinkorona sowie ein verändertes Retentionsverhalten des Überstandes festgestellt. Zur zusätzlichen Analyse des Einflusses des Blutflusses auf die Proteinkorona-Bildung wurden Nanoträger im Fluss mittels eines speziell designten Lichtstreuaufbaus untersucht.

Durch die hier vorgestellten Ergebnisse wurde das Wissen um die verschiedenen Parameter, die die Proteinkorona beeinflussen, erweitert und neue Techniken für die weitere Analyse der Nanoträger-Protein-Wechselwirkungen eingeführt.

Contents

1 Motivation

Nowadays, many severe diseases require a harsh treatment, and even in cases where the disease cannot be cured, it is usually treated to provide a higher quality of life and a prolonged lifetime for the patient. Unfortunately, most of the used drugs are not only toxic to the diseased cells, but also to the rest of the body cells. The systemic exposure to toxic drugs often causes many unwanted side effects, which weaken the patients even more. Moreover, to guarantee an appropriate dosage in the target cells, high amounts of the drug must be administered because of metabolic degradation. For the listed reasons, even a successful therapy still has many disadvantages on the patient's general health.[1, 2]

One prominent example for a disease treated with toxic drugs is cancer, which is currently the second leading cause of death[3] and therefore a topic that concerns the majority of the population. Therefore, drug delivery is a promising new approach especially in cancer therapy.[4-6] In those cases, a drug is embedded in a nanocarrier with the main purpose to selectively deliver the active pharmaceutical ingredient (API) to the target location in the body. By incorporating the drug into the nanocarrier, several advantages could be achieved: (i) The API is protected from degradation by the metabolism, thus resulting in a decrease of the necessary applied dosage; (ii) the API is selectively released at the affected target tissue, ensuring that the full dosage reaches the site of action; and (iii) most importantly, the body is protected from the API, preventing the systemic exposure and therefore minimizing the side effects.

Today, many different nanomaterials are available as potential carrier systems, each with different characteristics and designed for different applications. These synthetic systems can be characterized in detail; however, the chemical attributes are not the only essential traits of an ideal drug carrier. The limiting factor in the field of nanomedicine is the lack of knowledge on the interactions of the nanocarrier with the biological surrounding and the resulting physiological responses. Indeed, the understanding and prediction of the behavior of the nanocarrier in the biological system (e.g. the patient) is still limited. As drug carriers are usually applied to the patient via intravenous injection, the nanomaterial is directly exposed to the flowing blood and confronted with a high excess and variety of biomolecules. Upon the first contact with the biological fluid, such as blood, the surrounding proteins and other biomolecules adsorb on the surface of the nanomaterial and form the so-called 'protein' or 'biomolecule corona'. The formed protein layer covers the chemical identity of the nanocarrier and gives it a new biological identity, thus determining the interactions with the surrounding.[7, 8] From now on, the adsorbed proteins affect the physiological response and are crucial for all following mechanisms like cellular uptake and else. Generally, the protein corona is divided into two parts. The 'hard' corona supposedly consists of high affinity proteins, which

adsorb strongly to the nanocarrier and interact directly with the nanomaterial. The surrounding 'soft' corona is defined as such to be more loosely bound with the proteins showing a lower affinity to the nanomaterial, adsorbing amongst others via protein-protein interactions to the complex. Considering that the newly formed bio-nano-interface affects the outcome of nanomedicine treatment, it is essential to investigate the different types of protein corona, as well as the consequences resulting from the protein adsorption.

For the detailed analysis of the protein corona, it is crucial to choose experimental conditions, which are as close to the physiological conditions as possible. However, in many cases, the nanocarrier-protein complex must be removed from the surrounding medium containing free proteins and other biomolecules. The analysis is not trivial since the separation procedure itself has an additional influence on the outcome of the protein corona composition. The most commonly used separation techniques like centrifugation remove also loosely bound proteins and only the hard corona can be further investigated.[9] Accordingly, many studies on the hard corona have already been conducted, showing also that the protein adsorption depends strongly on the underlying material. Up to now, the soft corona analysis has been challenging due to the lack of appropriate sample preparation methods. Therefore, the composition, as well as the impact of the soft corona remain unknown for the moment.

Besides the analysis of the bio-nano-interactions, it is also important to investigate the influence the nanocarrier has on the surrounding biological system. When analyzing the protein corona, usually only the proteins attached to the nanocarriers are further investigated. However, the nanocarriers most likely have some effects on free proteins as well, as these might come in contact with the nanocarriers without adsorbing to them. These effects might change the conformation of proteins, denature them, lead to aggregation and more, which might result in severe consequences in the blood of the patient. As a result, the focus on the surrounding medium should not be neglected in terms of realistic experimental conditions.

Regarding realistic experimental conditions, another important factor is that the nanocarriers injected intravenously are additionally exposed to a flowing system as opposed to static incubation in most experimental set-ups. The blood flow is constantly moving all blood components through the body, and transports nutrients, oxygen, etc. to cells. [10] As the nanocarrier is ideally circulating in the blood stream, it is also influenced by the flow and consequently the protein corona formation, stability and equilibrium state can be altered. However, current methods for the protein corona analysis cannot integrate these flow conditions and the consequences of the blood flow on the delivery system stay unrecognized.

In the presented thesis, the asymmetrical flow field-flow fractionation (AF4) is introduced as an innovative separation method for the sample preparation of the corona analysis. The great

advantage of the AF4 is the size separation depending only on a flowing carrier liquid, which makes it a very mild separation technique. By applying the AF4 separation on the protein corona analysis and comparing the results to the classically obtained corona by centrifugation, the influence of the sample preparation on the corona outcome was observed. This way, potentially also proteins with lower binding affinities can be characterized. Furthermore, the effect of different surface functionalities on liposomes as potential drug carriers was investigated in terms of protein corona composition as well as on the cellular uptake behavior. This, in principle, paves the way for analyzing systems which cannot be separated from the biological medium by other methods like centrifugation or magnetic separation. Additionally, the reverse case was analyzed, looking at the influence, which the nanocarrier had on the unbound blood plasma proteins by investigating the individual plasma fractions and evaluate protein size changes. In a last step, the influence of the flow on the protein corona was evaluated by the use of a light scattering set-up capable of measuring during an applied flow.

2 Background

2.1 Drug delivery

Nanocarriers are a promising approach in the field of nanomedicine, for example as therapeutic or diagnostic agents.[11-13] With their small size (minimum one dimension 1-100 nm),[14] large surface area and vast design options, they provide new possibilities to access biological functions on a subcellular level. In the presented thesis we focused on the application of nanomaterials as drug delivery systems, which is especially promising in the field of cancer treatment as the potentially toxic drugs are incorporated into the nanomaterial. In this way, the drug will be protected from degradation by the metabolism and unwanted systemic side effects are minimized, since the drug is ideally released only at the targeted cell population, e.g. the tumor tissue.[12] Thereby, the therapeutic benefit is increasing with a reduced dosage. Additionally, nowadays many new drugs are lipophilic and therefore not bioavailable without an appropriate carrier system. A targeting effect can in principle be achieved either actively by the attachment of specific ligands on the surface of the nanocarriers, e. g. antibodies to target special cell receptors,[15] or by passive targeting which relies on the enhanced permeability and retention (EPR) effect.[16] Many different materials are promising in this field - each with their own advantages and disadvantages, and therefore they must be chosen carefully for the corresponding applications. Examples are nanoparticles, micelles, liposomes, capsules, etc. However, even with the great advantages provided by drug delivery systems and the large variety of applicable nanocarriers, one major challenge to overcome are the interactions of the nanomaterial with biological fluids, influencing the behavior of the nanocarrier in a biological system.

2.2 Interactions of nanocarriers in biological environments

The nanocarriers used for drug delivery are usually injected intravenously into the body and consequently the nanocarriers are immediately surrounded by a great excess of plasma proteins. Due to the high surface energy of the nanomaterial the free proteins adsorb on the surface and form the so-called ‘protein corona’. Thereby, the chemical identity of the nanomaterial is covered, and the new biological identity given by the adsorbed proteins is responsible for the biological reaction.[7, 8, 17, 18]

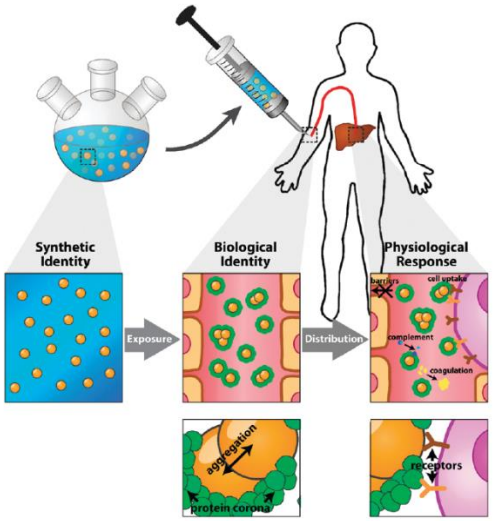

Figure 2.1: The chemical identity of the synthesized nanomaterial is covered by proteins upon injection, and the adsorbed proteins are accountable for the physiological response.[7] Reproduced by permission of The Royal Society of Chemistry.

Admittedly, the chemical identity of the carrier determined by size, shape, surface charge, polymer material, surface functionalization, stabilization agents, etc. affects the binding affinity of proteins to the used nanomaterial.[19] The adsorption of the proteins is of physical, non-covalent nature: The relevant forces are Van der Waals forces, hydrogen bonds, hydrophobic and electrostatic interactions. The mentioned forces might influence the proteins, leading to conformational changes or denaturation and consequently change their activity.[20]

Upon the injection of the nanocarriers, they are surrounded by highly abundant proteins, which do not necessarily show a high affinity to the nanomaterial. Nevertheless, they initially adsorb onto the nanocarrier surface quite fast. Over time, these low affinity proteins might be substituted by high affinity but low abundance proteins of the blood plasma, forming the protein corona in its equilibrium state. The responsible effect is called Vroman effect and describes why the abundance of certain proteins in the corona is not necessarily proportional to the abundance of proteins in the blood plasma.[21, 22] However, during the journey of the nanomaterial through the body, passing different organs and cell compartments, the biological medium around the nanocarrier will change and the protein corona will be altered as well. This indicates how sensitive the formation and stability of the protein corona is.[23]

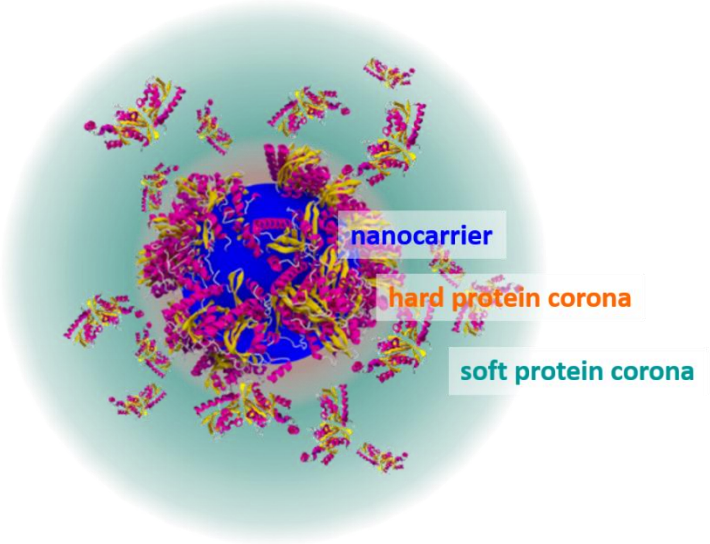

Figure 2.2: Schematic structure of the protein corona.

Generally, the structure of the protein corona can be divided into two different layers: the soft and the hard protein corona.[7, 24] The hard corona consists of proteins with a high binding affinity to the nanomaterial and adsorbs directly to its surface. The proteins are considered as irreversibly bound, meaning they are attached longer than the duration of the relevant biological response. The hard corona is stable during the separation process as well as during the journey through different cell compartments.[23] Therefore, a lot of analysis has already been executed investigating the hard corona.[25] The soft protein corona, which is adsorbed in addition to the hard corona, presumably is of highly dynamic nature and consists of proteins with lower binding affinities. It is considered to be attached on top of the hard corona via protein-protein interactions. Due to the dynamics of the soft corona it is difficult to analyze, and its relevance and composition are mostly unknown. Considering that the adsorbed proteins influence the interactions with the cells and the distribution in the body, the necessity to analyze and understand the protein corona and the following interactions becomes clear.

2.3 Blood flow

All research done in the field of nanomedicine serves the goal of applying the potential drug carriers successfully in the body. Therefore, great efforts are made to evaluate the interactions of the nanomaterial with biological systems *in vitro*, for example with plasma proteins, cells etc. However, all these methods neglect one major aspect of the actual biological dynamics, which is the blood flow. The heart is constantly pumping the blood through the blood vessels, and consequently through the body, to supply all cells with the necessary nutrients. Whenever a nanocarrier is injected

intravenously, it is directly confronted not only with the large excess of proteins and other biomolecules, but also with the blood flow. This permanent movement is most likely changing the characteristics of the environment tremendously and so far, the influence of the flow on the nanocarrier as well as on the protein corona is unknown.

The importance of the influence of the flow becomes clear, when considering that the blood moves through the aorta for example with a velocity of up to 40 cm s^{-1}.[26] Besides the velocity of the blood flow, one critical parameter induced by the streaming blood is the shear stress. Induced by the flow, this stress occurs along the endothelial walls of the blood vessels and it acts in the direction of the blood flow velocity vector very close to the wall. Assuming the vessels are cylindrical, the flow profile is considered to be parabolic, meaning that fluid layers the furthest away from the wall move the fastest. Therefore, the flow profile is stronger developed for either faster flow rates or smaller vessel diameters. The opposite force acting from the wall on the blood is called friction.[27] For the mathematical description of the blood flow and the shear stress, certain assumptions are made to simplify the system: (i) Blood vessels are considered to be cylindrical, rigid tubes, even though they are formed from a combination of elastic layers.[28] (ii) The blood is assumed to be a Newtonian fluid, which in reality is not correct because of the red blood cells, and (iii) the flow is considered to be constant, neglecting pulses due to the heartbeat. With these simplifications Haagen-Poisseuille's law can be applied to calculate the shear stress in the flowing blood.[27, 29]

$$\tau = 8 \cdot \mu \cdot \frac{u}{d} \tag{2.1}$$

(τ: shear stress; μ: viscosity; u: velocity of the flow; d: diameter of the vessel). The equation shows how the shear stress is directly proportional to the velocity and the reciprocal diameter of the corresponding vessel. As an example, the shear stress in the large aorta is only 6-10 dyn cm^{-1}, while in the smallest arterioles and capillaries it reaches up to 44-55 dyn cm^{-1}. Additionally to these theoretical approaches, the blood flow and consequently the wall shear stress can be measured by velocity-encoded magnet resonance imaging directly in the patient, which is relevant for atherogenic changes of the endothelial wall.[30]

2.4 Possibilities and limitations of different separation techniques for the analysis of the protein corona

As the understanding of the interactions of a nanocarrier with a biological system is essential, a detailed ananlysis of the protein corona must be performed. One option to approach the challenge of analyzing the protein corona are *in situ* measurements, which do not influence the corona composition, because no separation from the surrounding medium is required. However, since the

analysis takes place in the protein solution itself, the amount of information obtained by *in situ* measurements is limited. When the formed nanocarrier-protein complexes are separated from unbound biomolecules, the used characterization methods are classified as *ex situ* measurements.[31, 32] Generally, all separation techniques have a certain influence on the corona itself, considering that they alter the equilibrium of adsorbed and free proteins. During most separation processes the loosely bound proteins that form the soft corona (if present) will be removed, and little is known about their composition, binding behavior, or biological relevance. Currently, the hard corona is defined as the proteins that are still adsorbed to the nanocarrier after removal of the free proteins and subsequent washing of the complex. However, since many different methods for the separation of free proteins exist, it becomes clear, why there is no sharp border in the definition of the hard and soft corona and the differentiation between the two layers is an existing challenge.[31] Moreover, the analysis of the isolated hard protein corona includes a desorption of the proteins from the nanocarrier for further analysis. New data suggests that possibly some of the proteins cannot be detached with the usual methods, and thus will not be analyzed. These particularly tightly bound proteins are referred to as an "interfacial protein corona" in a recent study.[33] However, the question is, whether truly significant amounts of protein remains on the surface of every nanocarrier.

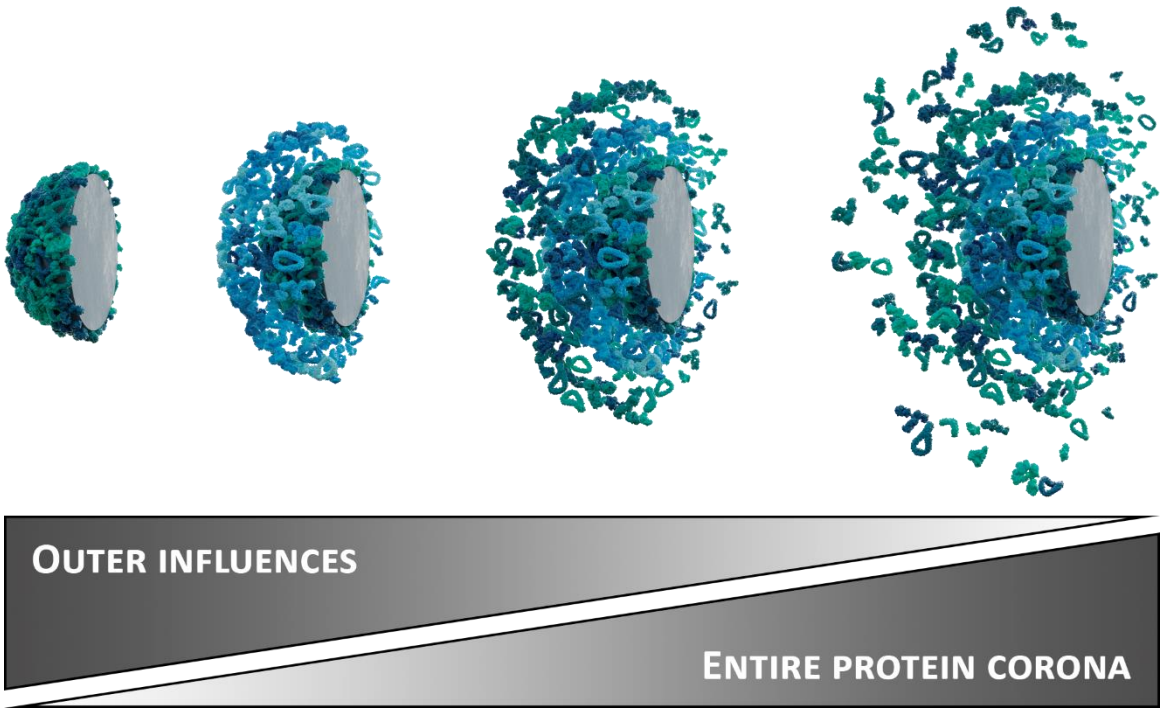

Figure 2.3: Outer influences like shear force or dilution alter the protein corona and remove parts of it.

Looking at all these aspects, a deeper understanding of the biological impact and importance of the hard as well as the soft protein corona is necessary to proceed in the field of nanomedicine. Therefore, in this section, we give an overview about how the sample preparation of commonly established separation methods – meaning the separation of nanocarrier-protein complexes form

the surrounding medium – influences the outcome of the protein corona analysis. Special focus was put on the requirements and limitations of the sample preparation process itself as the different characterization techniques used subsequently have already been reviewed extensively.[31, 32, 34, 35]

2.4.1 Separation of the nanocarrier-protein corona complex from free proteins

2.4.1.1 Protein corona isolations based on washing steps

The most common method for the separation of nanocarriers with their protein corona from the surrounding medium is centrifugation. Generally, by pelleting the nanocarrier-protein complex the unbound proteins are segregated. After the first centrifugation step, it is likely that loosely bound proteins are still attached to the surface. Subsequently, the sample is subjected to several washing steps in the according buffer. In each of these washing steps, the equilibrium of the protein corona readjusts and the loosely bound proteins are fully removed before further analysis can be executed.[9, 36] To date, centrifugation is probably the most established method to isolate only the strongly bound proteins.[9, 23, 37] If the sample possesses nanocarriers, which posess a structure stable during the centrifugation, it is a straightforward method that only requires a density difference of the sample compared to the surrounding medium. Throughout the separation process, which usually takes up to one hour, the nanocarriers are still surrounded by the incubation medium, although the actual contact area is reduced because of the pellet formation. To avoid this unintentional contact during the separation step, the centrifugation can also be performed in the presence of a sucrose cushion.[38-40] The nanocarriers with protein corona are applied on top of the cushion inside a tube and enter it within the first moments of the centrifugation. Free proteins stay on top of the cushion. Like this, any further undefined contact between sample and medium is eliminated. By combining this separation or regular centrifugation with protein identification techniques like liquid chromatography – mass spectrometry (LC-MS), detailed information of the composition of the hard corona on different nanomaterials could already be obtained.[38-42]

In any case, separation by centrifugation must be executed with great care, because protein aggregates can easily precipitate with the nanocarrier-protein complex and highly abundant proteins can be mistaken for parts of the protein corona if not washed off thoroughly. To minimize this effect and remove protein aggregates and other perturbing components, the pristine plasma should be centrifuged before use.

Another simple separation method for the isolation of the protein corona can be applied for the class of magnetic nanocarriers. In general, magnetic materials are interesting for certain applications in

nanomedicine, e. g. to direct magnetic nanocarriers to and focus them on a target region by an outer magnetic field[43-45] or to kill cancer cells by magnetically induced hyperthermia.[46, 47] Moreover, magnetism can be exploited as an advantage for the separation of the nanocarrier-protein complex from the excess biological medium, where different separation set-ups are possible. The basic separation is to bring a magnet into close vicinity to the sample and remove the supernatant as long as the nanoparticles are concentrated near the magnet, similar to pellet formation. After resuspension in buffer, the procedure is repeated to wash the sample. Over all, the applied steps to obtain the corona via magnetism are similar to the centrifugation process and further analysis can be applied subsequently. Protein corona analysis following the magnetic separation, e.g. identification of the adsorbed proteins by LC-MS, was already done, although without any information about the binding affinities of the proteins that were present.[48, 49] Looking at the influence of the separation technique onto the outcome of the identified protein corona pattern, there are certain similarities between the magnetic isolation and the centrifugation method. Both methods rely on repetitive washing steps to remove excess proteins and therefore the resulting protein corona is dependent on the adopted procedure. Thus, diluting the sample every time, new equilibriums are reached.

Looking deeper into the differentiation of the soft and the hard corona, Bonvin *et al.*[50] compared two different magnetic separation methods: (i) a magnetic bed reactor, and (ii) a magnetic multi-step centrifugation. The first consists of a static magnet around a column, thus magnetic nanocarriers are kept in place, while the washing solution passes by, which makes the sample preparation straightforward. According to Bonvin *et al.*, the soft corona proteins are entrapped within agglomerates that form upon increasing concentration of the used iron oxide nanocarriers (IONs) close to the magnet. To prevent the latter effect, a magnet is put in vicinity to the sample vial, while centrifugation is performed. Hence, a thorough washing is ensured. Since both methods result in different protein corona compositions, only those proteins which were found after both separations were considered to be part of the hard protein corona.[50] Also Sakulkuh *et al.*[51, 52] made a clear statement by specifying that in their tested system only the hard corona was isolated. They compared the hard corona of superparamagnetic iron oxide nanocarriers (SPIONs) in rat plasma *in vitro* and *in vivo* and found that the corona differs significantly, depending on the sample preparation.[51] They also analyzed different surface functionalizations on SPIONs [52] and for both works the above mentioned magnetic bed reactor was used. Since the SPIONs used by Sakulkuh *et al.* were smaller than the iron oxide particles used by Bonvin *et al.*, there was no agglomeration inside the reactor. By using magnetic separation, a generally versatile procedure is provided, however it is limited to certain materials and can certainly not be applied as a general procedure.

2.4.1.2 Protein corona isolation based on chromatographic methods

Besides these two methods based on density differences and magnetism, there is a large class of chromatographic and chromatography-like techniques that rely on separation according to hydrodynamic size. One of these chromatography-like techniques is the asymmetric flow field-flow fractionation (AF4). Hereby, the sample is separated by applying a perpendicular cross-flow in a trapezoidal separation channel and allowing subsequent diffusion of the sample species back into the middle of the channel.[53, 54] This diffusion depends on the diffusion coefficient and thus, the sample is separated according to size. With no stationary phase present, only the cross-flow is acting on the sample, making AF4 a very mild separation technique, which is especially suitable for sensitive samples like protein aggregates and nanocarrier-protein-complexes.[55, 56] Based on the separation mechanism, where smaller species elute faster than larger ones, the relative change of nanomaterial size due to protein adsorption and potentially aggregation can be evaluated by AF4 via a comparison of the retention times.[57-59] As highlighted by Maskos and coworkers even absolute particle sizes can be calculated from the retention times by calibrating the system with standard-size particles.[60] However, up to very recently, AF4 was not commonly adopted to separate free proteins from particle-protein complexes for further corona analysis. In summary, the above-mentioned works have exploited AF4 as an analytical method to evaluate the change of retention time due to size increase, but not as a separation tool for further protein corona analysis with *ex situ* measurements.

Focusing on the protein corona analysis, Ashby *et al*. tried to approach the challenge of separating both protein coronas, the hard and the soft one, with different methods to analyze the dynamic behavior of the corona. However, they assumed that AF4 would wash off the soft corona, while centrifugation, including one washing step, would lead to co-precipitation of all proteins of the entire corona,[61, 62] as opposed to the general assumption of loosely bound proteins being removed by centrifugation und subsequent washing steps. In contrast, we previously reported the application of AF4 to isolate nanocarrier-protein complexes from the medium containing free proteins. In that case, highly abundant but low affinity proteins like human serum albumin (HSA) were identified in the corona in high amounts after AF4 treatment while after centrifugation proteins with higher affinity were present. The presence of the high affinity proteins "underneath" a higher number of loosely bound proteins was confirmed by combining centrifugation and subsequent separation via AF4. Thus, we concluded that AF4 is more suitable to isolate nanocarriers with most of their soft protein corona while centrifugation yields the hard protein corona.[63]

Another chromatography-like technique, the hydrodynamic chromatography (HDC), works similar to AF4 and separates the sample according to hydrodynamic size. Inside of a capillary or a column packed with nonporous beads a hydrodynamic flow profile is developing. Since the center of mass

of larger particles cannot come as close to the wall as small particles, they will move in faster stream lines of the flow profile and elute first.[64, 65] Because the separation is only flow-driven, a minimum of outer forces is working on the sample, very similar to AF4. Roman *et al*. used this method to show that it is generally possible to isolate the nanocarrier-protein complex, but they did not perform further analysis on the protein corona so far.[66]

A commonly used separation technique in the field of polymer and protein analysis is size exclusion chromatography (SEC), which also separates the sample according to its hydrodynamic volume. The SEC columns are filled with beads that contain pores allowing only the smaller molecules to enter, thus making bigger molecules elute first while the smaller ones have a longer diffusion pathway until they reach the detector. During this process, no interactions between the sample and the stationary phase should occur.[67, 68] The drawback of this method in terms of protein corona analysis is the shear stress occurring between the samples and the packing material of the column, which increases with the flow rate.[69] Shear stress is likely to change the protein corona composition by removing certain (more loosely bound) proteins or protein layers. One method to apply SEC in protein corona analysis is to investigate dissociation rates of proteins. The idea is that the stronger a protein is bound to the nanomaterial, the faster it elutes, since it moves through the column together with the larger nanomaterial. Hence, proteins dissociating slowly from the nanomaterial surface – and thus compose the hard protein corona - could potentially be identified. Different results for the protein corona after SEC compared to the one after centrifugation showed the high impact of the applied separation technique. This makes it unclear, in which way the SEC separation influenced the protein corona composition, and thereby, which corona is actually analyzed.[37, 70] Focusing not on dissociating proteins, but on the nanocarrier-protein complex, Liu *et al*.[71] found that proteins adsorb reversibly on nanocarriers of the same size. Only aggregates of proteins on larger particles were eluted from the SEC, when analyzing the interactions of cerium oxide-nanocarriers with fetal bovine serum (FBS) spiked with immunoglobulin G (IgG) or bovine serum albumin (BSA). In their opinion, the attractive forces between proteins and nanocarriers of the same size were minimized due to the surface curvature and the proteins were replaced by the column material of the SEC, retaining the particles in the column. Since in general only stable aggregates, whose proteins are not exchanged for the column material, elute from the SEC, the protein binding is considered as irreversible and consequently a hard protein corona is formed.

All above mentioned chromatographic methods are based on hydrodynamic size, thus making a significant difference in size between free proteins, nanocarriers and nanocarrier-protein complexes a prerequisite in order to apply these techniques for successful separation.

A separation technique not based on the hydrodynamic volume, but on the size-to-charge ratio is the capillary electrophoresis (CE). Like in AF4 and HDC, no stationary phase is present, which

makes it a potentially mild separation technique. The driving force for separation is the movement through an electric field.[72, 73] The work of Matczuk *et al*. on gold nanocarriers (AuNCs) showed that CE is a very precise separation method. They were able to identify conjugates of different Au-nanocarriers with individual proteins by the specific migration time.[74, 75] Remarkably, even the differentiation between AuNC-transferrin conjugates with or without complexed iron ions was possible. By varying the incubation time of the AuNCs in human blood serum, they evaluated the dynamic development of the protein corona formation. Their findings showed an increasing amount of albumin on the nanocarrier surface with an increasing incubation time. Thus, CE proves to be a mild separation technique, allowing also reversibly bound proteins to be analyzed.[76] In another study, it was demonstrated that the dissociation constant of BSA-nanocarrier complexes could be calculated by CE measurements, indicating whether BSA might be part of the soft or hard corona.[35] With the mentioned insights into the protein corona, CE is a promising technique in the field of corona separation and the isolated complexes could be used for further analysis.

2.4.1.3 Assessment of the influences of the different separation methods

Reasons to choose a chromatographic separation method over others could be the minimization of the experimental time span compared to centrifugation and magnetic separation with their washing steps. This might be important, because the experimental duration plays a critical role in defining the biological relevance of the entire protein corona. Referring to a corona protein as irreversibly bound to the nanomaterial first of all means that their dissociation takes longer than the duration of a relevant biological response, e.g. cellular uptake, etc.[37] In this context, also the experimental set-up and as such the protein corona preparation steps should take place within the corresponding relevant time frame. Otherwise the interpretation of the data will be difficult, because it is unclear whether the identified corona proteins are involved into biological processes afterwards. Consequently, alongside with the mild separation process, the advantage of most of the here introduced chromatographic methods is the shortened sample preparation time. Accordingly, more loosely bound proteins can be preserved, which will help in understanding more about the biological relevance of the soft corona.

Another parameter of the equilibrium formation of the protein corona is the Vroman effect, as described above. However, any effect influencing the equilibrium only takes place on the accessible surface of the nanocarriers and only if free proteins are available to exchange with those adsorbed. If the free proteins are removed at the very beginning of the separation process as during the centrifugation through a sucrose cushion, the contact between the nanocarrier-protein complex and the free proteins is immediately eliminated and the corona cannot undergo any further changes. The same is valid for chromatographic methods, because the protein corona is isolated already in the

beginning of the separation process. In case the Vroman effect is not prevented, it will eventually change the protein corona composition during the separation process itself. Assuming that there is no protein excess in the solution of the formed protein corona, its formation can still be influenced by the applied separation method. With every dilution step, like the washing in centrifugation and magnetic separation or the constant flow of carrier liquid in chromatographic methods, the equilibrium is more or less disturbed and re-formed, constantly shaping the protein corona. Thereby, the dilution is a crucial factor, which makes it complicated to predict the protein corona outcome.

Consequently, *ex situ* measurements, which require the isolation of the protein corona, are the only way to gain detailed insights into the protein corona composition, however the biggest drawback of these methods is the unknown interference with the protein corona formation and stability. An overview on the separation techniques discussed in this section together with their limitations can be found in Table 2.1.

Table 2.1: Overview on the here introduced separation techniques with their requirements and limitations.

Method	*Requirements and Limitations*	*Literature*
Centrifugation	Density difference between medium with free proteins and nanomaterial	9, 23, 26-42, 92
Magnetism	Magnetic particles or nanocarriers with magnetic core	49-52
AF4	Difference in hydrodynamic radius between nanocarrier-protein complexes and free proteins	57-63
HDC		66
SEC		37, 70-71
CE	different size to charge ratios of the free proteins and the nanocarrier-protein complexes	35, 74-76

2.4.2 *In situ* measurements of the entire corona

To avoid any alteration of the protein corona, *in situ* methods are used, for which the nanocarrier-protein complex is characterized directly in the surrounding medium, i.e. the protein solution. On one hand, this reflects the most natural state of the protein corona that is possible to achieve *ex vivo*. On the other hand, the gain of information is limited, as well as the varieties of sample preparation.

For example, using dynamic light scattering the apparent diffusion coefficient of the sample can be determined and via the Stokes-Einstein equation translated into the hydrodynamic radius .[77] But the excess of free proteins after incubating nanocarriers in a biological fluid also limits the applicability of the method, as they interfere with the signal obtained from the nanocarrier-protein complex.

Thus, these signal interferences in complex mixtures like blood serum or plasma need to be avoided to measure the size increase of a nanocarrier due to protein corona or aggregate formation *in situ*. Consequently, Rausch *et al.* developed a method where the scattered light from free proteins and pure nanocarriers is considered as background, while the scattered light originating from newly formed larger species can be analyzed.[78, 79] Alternatively, AF4 could be used as an upstream separation step to remove the free proteins and thus allow DLS measurements of the particle-protein complexes without interfering background.[80] Performing centrifugation as a separation step in contrast does not give reliable results as usually the formed pellet cannot be perfectly resuspended.

Similar to DLS, fluorescence correlation spectrometry (FCS) also allows for calculation of the hydrodynamic radius and accordingly the size of the protein-nanocarrier complex can be observed.[81] The disadvantage of FCS is the necessity of a fluorescence label on either the nanocarrier or the protein. Certainly, by introducing such a label the system itself will be changed and the applicability of the results becomes difficult. The advantage on the other hand is that free proteins do not need to be separated. Since only the fluorescently labeled species are visible, other components in the solution do not interfere with the signal. Via FCS, different information regarding the dimensions of a formed protein corona were obtained. For example, Nienhaus and coworkers found that a monolayer of adsorbed proteins was formed on their nanocarriers investigated by FCS in many cases.[82, 83] These findings differ from other studies on protein corona formation. Monopoli *et al*. investigated the differences of the soft and hard protein corona by FCS, where they observed a fast formation of a monolayer of transferrin on carboxylated or sulfonated polystyrene nanocarriers, which was stable over a long time. When adding further proteins they concluded that multiple layers were formed via protein-protein interactions, which formed slower and were less stable.[17] Probably, the dimension of the formed hard and soft corona thus depends on many factors like the type and size of nanomaterial. However, this demonstrates that FCS is a very versatile tool to characterize the soft and hard corona without the need to remove free proteins from the medium.

In addition to the here discussed methods, other more rare techniques were applied to characterize the protein corona *in situ* and can be found in the literature. [84-91] Generally, it is advisable to combine *in situ* and *ex situ* characterization techniques to obtain a detailed picture of the protein corona as discussed in previous studies, keeping in mind that every preparation procedure potentially changes the investigated system.[25, 92]

2.4.3 Conclusion of the different separation methods

In summary, many different techniques have already been applied for the analysis of the protein corona. However, it is not possible to define a clear cut-off between the different corona layers or types and the question of what is part of the hard and soft corona cannot easily be answered. Currently, the differentiation is determined by the performed separation and analysis, not taking into account how the experiment already alters the protein corona itself. The different possibilities of separating the protein corona for analysis already demonstrate that the influence of factors like dilution, shear force, contact with the medium or experiment duration cannot be neglected. For future works it is important to mention that only if a variety of different methods is applied, a more and more complete picture of the entire protein corona and its implications can be obtained. However, even with a broad knowledge about the *in vitro* protein corona, the results are difficult to compare to *in vivo* conditions, as information about interactions with other biomolecules, cells and other biological dynamics are missing. Furthermore, not all separation methods are suitable for a given sample and more efforts should be made to streamline preparation procedures such that also studies conducted in different labs could easily be compared and the information be transferred to other nanomaterials.

3 Characterization methods

3.1 Asymmetric flow field-flow fractionation

Asymmetric flow field-flow fractionation (AF4) is used for the separation of nanoparticles according to their diffusion coefficient and the most commonly used technique among field-flow fractionations.[93, 94] Being proportional to the diffusion coefficient, the hydrodynamic radius of the separated particles can be calculated, making AF4 a size-dependent separation method. The separable particle size range is only limited by the channel geometry. The AF4 set-up (Figure 3.1) consists of a spacer with a trapezoidal cutout, which defines the shape and the height of the channel. A poly(methyl methacrylate) plate on the top and a frit at the bottom confine the separation channel. The frit is covered with a porous membrane, thus defining the lower size limit of the analyzed particles by the membrane's cut-off. Only the carrier liquid can pass the membrane, not the analyte, enabling a cross flow without sample loss.[53, 54, 95]

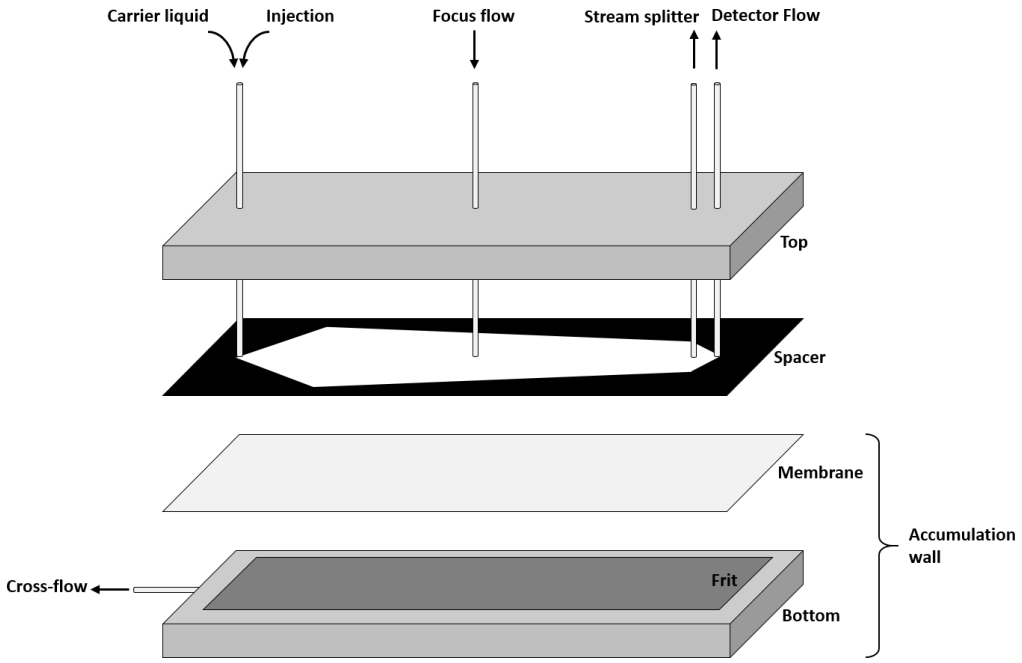

Figure 3.1: Set-up of the used AF4 separation channel.

To move the sample from the site of injection towards the detector, a laminar flow is pumped through the separation channel. Perpendicular to the flow transporting the sample, a cross-flow pushes the sample towards the accumulation wall placed at the bottom of the channel. Due to the higher concentration of the sample at the accumulation wall, a diffusion of the particles in the opposite direction is induced. The diffusion and the cross-flow act against each other until a

stationary condition is reached. The forces reach an equilibrium and the particles are present at specific distances from the accumulation wall at a given cross-flow, depending on their diffusion coefficient (Figure 3.2A). Because of the narrow shape of the separation channel, the laminar flow exposes a strongly parabolic flow profile, thus meaning that inner layers move faster than outer ones. Consequently, the particles placed in the middle move faster through the channel than the ones close to the accumulation wall. Since the diffusion coefficient is proportional to the particle size, the small particles show a higher diffusion and elute faster (Figure 3.2B).

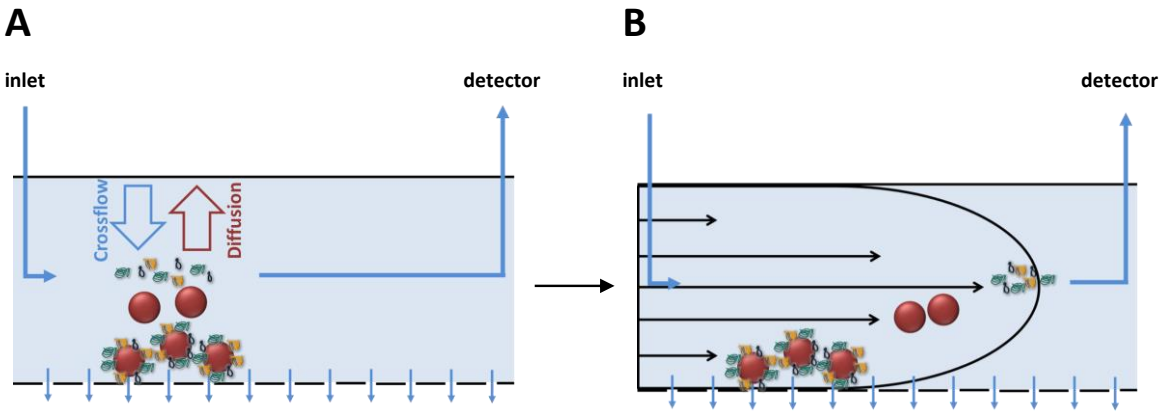

Figure 3.2: Separation mechanism of the AF4: (A) the cross flow and the diffusion compete against each other, which causes diffusion of smaller particles to the inner part of the channel; (B) the parabolic flow profile is pushing the particles towards the detector. Those close to the accumulation wall move slower than those with an increasing distance to it.

The separation is achieved only by the presence of the flows, thus making AF4 a very mild separation technique, perfectly suitable for sensitive protein- and particle aggregates.[55, 56] In summary, the parameters that influence the separation are the injection flow, the focus flow, the cross flow and the detector flow. Optimization of these parameters together with the right choice of the carrier liquid and the membrane are the crucial steps for a successful separation by AF4.

The main characteristic for AF4 separations[96] is the retention level (*RL*), which describes the ratio between the retention time (t_r) and the void time (t^0):

$$RL = \frac{t_r}{t^0} \tag{3.1}$$

The width of the signal on its basis ($\bar{w}_b$) depends on the retention level and it influences the resolution (R_s), calculated as followed:

$$R_s = \frac{\Delta t_r}{\bar{w}_b} \tag{3.2}$$

It is difficult to determine the void time used in equation 3.1 experimentally. Instead, it should be calculated according to the following equation:

$$t^0 = \frac{V^0}{F_{cross}} ln \left[1 + \frac{F_{cross}}{F_{out}} \left(1 - \frac{w\left(b_0 z' - \frac{b_0 - b_L}{2L} z'^2 - y \right)}{V_0} \right) \right] \tag{3.3}$$

Thereby, V^0 represents the void volume, F_{cross} the cross flow and F_{out} the detector flow. The other parameters describe the geometric characteristics of the separation channel (w: channel height, b_0: channel width at the inlet, z': channel width at the injection point, b_L: channel width at the outlet, L: channel length, y: area of the spare area at the channel inlet).

Another important parameter is the so-called retention parameter λ^*, which is defined as:

$$\lambda^* = \frac{l}{w} \tag{3.4}$$

w represents the channel thickness and l the distance of the center of concentration of the sample to the wall and can be calculated by:

$$l = \frac{D}{u_0} \tag{3.5}$$

D gives the diffusion coefficient and u_0 the speed of the cross flow on the membrane surface. The retention parameter and the retention level are connected as followed:

$$RL = \frac{1}{6\lambda^*} \tag{3.6}$$

With equation 3.4 and 3.5, the retention level can be converted to:

$$RL = \frac{w u_0}{6D} = \frac{w F_{cross}}{6AD} \tag{3.7}$$

with A as the area of the accumulation wall. Equation 3.7 demonstrates that as soon as the cross flow or the channel height are increased, the retention level is increasing as well. By rearranging equation 3.1 and inserting in equation 3.3 and 3.7, the retention time can be calculated:

$$t_r = \frac{w^2}{6V^0 D} F_{cross} t^0 \tag{3.8}$$

$$t_r = \frac{w^2}{6D} ln \left(1 + \frac{F_{cross}}{F_{out}} \left(1 - \frac{w\left(b_0 z' - \frac{b_0 - b_L}{2L} z'^2 - y \right)}{V^0} \right) \right) \tag{3.9}$$

Since the geometry of the channel is given, and the diffusion coefficient is defined by the sample, equation 3.9 displays that the retention of a particles is only dictated by the ratio of F_{cross} to F_{out}. Consequently, by experimentally determining the retention time, the diffusion coefficient is calculated and finally the hydrodynamic diameter of a particle can be calculated.[96] Therefore, AF4 is a highly sensitive technique to separate particles according to their size and can be applied for

even highly sensitive samples. The method is perfectly suitable for the separation of particle-protein complexes from free proteins.

3.2 Light scattering

All matter consists of positively and negatively charged molecules and incoming light will alter their spatial charge distribution. Consequently, when a molecule is hit by a light wave, it becomes an oscillating dipole. The generated dipole will also emit electromagnetic radiation of the same wavelength as the incoming light. This effect is exploited in light scattering measurements. The following chapter will cover theoretical parts relevant in the presented thesis, a detailed description of light scattering theory can be found in literature.[77, 97-100]

3.2.1 Static light scattering (SLS)

Static light scattering is usually used to calculate several characteristics of a scattering object, such as the radius of gyration or the molar mass. Therefore, the sample is irradiated with a light wave and the excited molecules, which form oscillating dipoles, will send out an electric field with an energy of:

$$E_s = \left(\frac{\partial^2 m}{\partial t^2}\right)\frac{1}{r_D c^2} = \frac{-4\pi^2 \nu^2 \alpha E_0}{r_D c^2}\exp\left(i\left(2\pi\nu t - \vec{k}\vec{r}_D\right)\right) \tag{3.10}$$

where r_D is the distance of the scattering sample to the detector, c is the sample concentration, ν is the frequency, α is the polarizability and E_0 the incoming energy. Of course, the electric wave vector amplitude cannot be measured, so rather the emitted intensity I_s is detected, which correlates to the electric wave as in the following equation:

$$I_s = E_s E_s^* = |E_s|^2 \tag{3.11}$$

Since the scattering volume is changed with the scattering angle, the measured intensity must be normalized with the sinus of the scattering angle θ. Additionally, the scattering intensity also depends on the experimental set-up. To overcome the two latter dependencies, an absolute scattering intensity, called Rayleigh ratio R can be calculated from constant parameters:

$$R = K \cdot \frac{cM}{N_L} = \frac{4\pi^2}{{\lambda_0}^4}\, {n_{D,0}}^2 \left(\frac{\partial n_D}{\partial c}\right)^2 \frac{cM}{N_L} = (I_{solution} - I_{solvent})\,\frac{{r_D}^2}{V} \tag{3.12}$$

with M: molar mass, N_L: nanoparticle number, n_D: refractive index of the solute, $n_{D,0}$: refractive index of the solvent, V: scattering volume and the experimentally determined intensities $I_{solvent}$ and $I_{solution}$. The parameter K represents the contrast factor, originated in the scattering power of the corresponding nanoparticles:

$$K = \frac{4\pi^2}{\lambda_0{}^4 N_L} {n_{D,0}}^2 \left(\frac{\partial n_D}{\partial c}\right)^2 \tag{3.13}$$

with $\frac{\partial n_D}{\partial c}$ representing the refractive index increment:

$$\frac{\partial n_D}{\partial c} \simeq \frac{n_D - n_{D,0}}{c} \tag{3.14}$$

The absolute scattering intensity R (Rayleigh ratio) of a sample can be determined experimentally with the measured parameters $I_{solvent}$ and $I_{solution}$ together with the intensity of the scattering standard I_{std}, which is usually measured for pristine toluene. The latter is renormalized by the absolute scattering intensity of the standard (Raleigh ratio of toluene) $I_{std,abs}$, resulting in the absolute scattering intesity:

$$R = (I_{solution} - I_{solvent}) \cdot \frac{I_{std,abs}}{I_{std}} \tag{3.15}$$

Because in larger nanoparticles several dipoles are generated within the same macromolecule, phase differences of the emitted light waves occur, thus causing interferences. This anisotropic development of radiation results in an angular dependency of the observed scattering intensity. The arising interference pattern is characteristic for each scattering species and is called the particle form factor $P(q)$:

$$P(q) = \frac{1}{N^2 Z^2 K} I(q) = \frac{1}{Z^2} \sum_{i=1}^{Z} \sum_{j=1}^{Z} \exp\left(i\vec{q}\overrightarrow{r_{ij}}\right) = \frac{1}{Z^2} \sum_{i=1}^{Z} \sum_{j=1}^{Z} \left(1 - \frac{1}{6} q^2 {r_{ij}}^2 + \cdots\right) \tag{3.16}$$

However, for larger nanoparticles also the scattering angle must be considered, which is converted to the scattering vector $\vec{q}$:

$$|\vec{q}| = q = \frac{4\pi n_D sin\left(\frac{\theta}{2}\right)}{\lambda} \tag{3.17}$$

Transferring the form factor from equation 3.16 into a coordinate system based on the center of mass and substituting r_{ij} with $\vec{s_i}$,= R_g equation 3.16 can be simplified to $P(q) = 1 - \frac{1}{3} q^2 {R_g}^2$.

Therefore, the Zimm equation results in:

$$\frac{Kc}{R} = \frac{1}{M} \left(1 + \frac{1}{3} {R_g}^2 q^2\right) + 2A_2 c \tag{3.18}$$

In the Zimm plot, $\frac{Kc}{R}$ is plotted against q^2 according to equation 3.18, so that the radius of gyration $< {R_g}^2 >^{\frac{1}{2}}$, the absolute molar mass M, and the second Virial coefficient A_2 can be determined from a linear fit. The latter is a quantitative measure of the sample polydispersity. In case, K cannot be determined for a sample, R_g can still be calculated from the slope of the linear regression, but a determination of M is not possible.

3.2.2 Dynamic light scattering (DLS)

A main particle characteristic in the area of polymer analysis is the hydrodynamic radius of the sample. It can be obtained by dynamic light scattering, using the same set-up as described for SLS measurements; however, DLS is based on another phenomenon:

For samples in solution, the solvent is subjected to constant thermic fluctuation in density, which causes a random movement of the nanoparticles in solution, the so-called Brownian motion. The nanoparticles alter their position relative to each other, thus changing their interference pattern and as a consequence the resulting scattering intensity. The measured fluctuation can be described in a self-correlation function according to van Hove:

$$G_s(\vec{r},\tau) = \langle n(\vec{0},t)n(\vec{r},t+\tau)\rangle_{V,T} \tag{3.19}$$

n describes the partible number density. For small nanoparticles, concerning the isotropic and diffusive particle motion, the equation can be simplified as followed:

$$G_s(r,\tau) = \left[\frac{2\pi}{3}\langle\Delta R(\tau)^2\rangle\right]^{\frac{3}{2}} exp\left[-\frac{3r(\tau)^2}{2\langle\Delta R(\tau)^2\rangle}\right] \tag{3.20}$$

with the mean square displacement of the scattering nanoparticles $\langle\Delta R(\tau)^2\rangle$ being described as:

$$\langle\Delta R(\tau)^2\rangle = 6D_s\tau \tag{3.21}$$

and D_s representing the self-diffusion coefficient.

Applying the Fourier transformation on the self-correlation function 3.19 to introduce the dependency on the scattering vector, the dynamic scattering factor F_s can be obtained:

$$F_s(\vec{q},\tau) = \int G_s(\vec{r},\tau)\exp(i\vec{q}\vec{r})d\vec{r} = exp\left[-q^2\langle R^2(\tau)\rangle_T\frac{\tau}{6}\right] = \exp(-D_sq^2\tau) \tag{3.22}$$

By using the Stokes-Einstein equation, the hydrodynamic radius of the scattering nanoparticles can be calculated from the diffusion coefficient:

$$D_s = \frac{kT}{f} = \frac{kT}{6\pi\eta R_h} \Leftrightarrow R_h = \frac{kT}{6\pi\eta D_s} \tag{3.23}$$

As the dynamic scattering factor F_s cannot be measured directly; instead, the hardware-correlator transfers the autocorrelation function based on intensity into a time dependent autocorrelation function. Therefore, the intensity is multiplied with itself after a time shift by τ. This is done for different τ and each product is averaged over the time of a measurement:

$$\langle I(q,t)I(q,t+\tau)\rangle \tag{3.24}$$

The Siegert relation gives the connection to the dynamic scattering factor:

$$F_s(q,\tau) = \exp(-D_sq^2\tau) = \langle E_s(q,t)E_s^*(q,t+\tau)\rangle = \sqrt{\frac{\langle I(q,t)I(q,t+\tau)\rangle}{\langle I(q,t)^2\rangle} - 1} \tag{3.25}$$

As expected, polydisperse samples show a size distribution $P(R_h)$. To overcome this issue, an average self-diffusion coefficient is calculated, which is given by a distribution function $P(D_s)$. This function is depending on the number particle density n_i, the mass M_i and form factor $P_i(q)$:

$$I \sim n_i \cdot M_i^2 \cdot P_i(q) \tag{3.26}$$

The form factor results in an overlay of several exponential functions, which are weighted according to the distribution function of the self-diffusion coefficients:

$$F_s(q,\tau) = \int_0^\infty P(D_s) \exp(-q^2 D_s \tau)\, dD_s \tag{3.27}$$

The quantitative data analysis of polydisperse samples is done by a cumulant analysis, even though this approach is only valid for minor polydispersity ranges:

$$\ln F_s(q,\tau) = -\kappa_1 \tau + \frac{1}{2!}\kappa_2 \tau^2 - \frac{1}{3!}\kappa_3 \tau^3 + \cdots \tag{3.28}$$

The first cumulant κ_1 represents the diffusion coefficient, while the second cumulant κ_2 displays the quantitative measurement of the polydispersity of the diffusion coefficient distribution function (σ_D):

$$\sigma_D = \frac{\sqrt{(\langle D_s^2 \rangle - \langle D_s \rangle^2)}}{\langle D_s \rangle} = \sqrt{\frac{\kappa_2}{\kappa_1}} \tag{3.29}$$

Assuming a Gaussian size distribution, the size polydispersity can be calculated by:

$$\sigma_R = \frac{\sqrt{(\langle R_h^2 \rangle - \langle R_h \rangle^2)}}{\langle R_h \rangle} \tag{3.30}$$

As mentioned earlier, the scattering angle cannot be neglected for polydisperse samples. Consequently, not the actual diffusion coefficient of one species in the sample is determined, but the apparent one:

$$D_{app}(q) = \frac{\sum n_i M_i^2 P_i(q) D_i}{\sum n_i M_i^2 P_i(q)} \tag{3.31}$$

Reformulated for nanoparticles between 10-100 nm this apparent diffusion coefficient can be simplified to:

$$D_{app}(q) = \langle D_s \rangle_z (1 + k \langle R_g^2 \rangle_z q^2) \tag{3.32}$$

For monodisperse samples $k = 0$ is valid. If the apparent diffusion coefficient it then plotted against q^2, a linear function is obtained, which gives the real diffusion coefficient when extrapolated to 0. For diluted solutions with no intermolecular interactions, the hydrodynamic radius can be calculated from the diffusion coefficient.

3.2.3 Evaluation of dynamic light scattering in a complex environment

Whenever dynamic light scattering is used as an *in situ* method for the analysis of the protein corona, the nanomaterial will be measured in the protein solution (for example blood plasma) itself. When measuring light scattering in such a complex environment, the excess of free proteins is interfering with the signal of the nanoparticles. Rausch *et al.* established a method to overcome this issue, by introducing a new data evaluation procedure.[79]

To measure the third unknown component that forms upon incubation of the nanonanoparticles in the protein solution, background measurements of the pristine nanoparticles and the protein solution are done and evaluated. The protein solution is (in the case of plasma) fitted with the sum of three exponential functions:

$$g_{protein}(t) = a_{1,protein}\exp\left(-\frac{t}{\tau_{1,protein}}\right) + a_{2,protein}\exp\left(-\frac{t}{\tau_{2,protein}}\right) + a_{3,protein}\exp\left(-\frac{t}{\tau_{3,protein}}\right) \tag{3.33}$$

and the nanoparticles with a biexponential fit, taking their polydispersity into account:

$$g_{NP}(t) = a_{1,NP}\exp\left(-\frac{t}{\tau_{1,NP}}\right) + a_{2,NP}\exp\left(-\frac{t}{\tau_{2,NP}}\right) \tag{3.34}$$

$a_{i,j}$ represents the amplitudes of the corresponding scattering contributions, t the time and τ_i the relaxation time:

$$\tau_i = \frac{1}{q^2 D_i} \tag{3.35}$$

When no interactions between the components inside of the complex mixture occur, the correlation function of the measured mixture can easily be described by the sum of the above-mentioned fit functions 3.33 and 3.34. Therefore, only the intensity contributions of the functions are variable:

$$g_{\,mixture}(t) = f_{protein}g_{protein}(t) + f_{NP}g_{NP}(t) \tag{3.36}$$

However, interactions between different species are likely and additional compounds like aggregates are formed. In this case, the measured correlation function can no longer be described by only the above given fit functions, but an additional equation term needs to be introduced. The formed, unknown aggregate is described by a single exponential function:

$$g_{aggregate}(t) = a_{1,aggregate}\exp\left(-\frac{t}{\tau_{1,aggregate}}\right) \tag{3.37}$$

This equation is added as a term to equation 3.36, now describing a mixture of proteins, nanoparticles and aggregates with the following autocorrelation function:

$$g_{mixture\ with\ aggregate}(t) = f_{protein}g_{protein}(t) + f_{NP}g_{NP}(t) + f_{aggregate}g_{aggregate}(t) \tag{3.38}$$

All parameters of the protein- and nanoparticle-correlation functions are given from the evaluation of the pristine solutions. Only the intensity contributions in the mixture and the parameters of the aggregate function are variables. The described data evaluation enables a determination of the size increase due to protein adsorption on nanoparticles or the formation of aggregates in a complex environment like blood plasma.

3.2.4 ρ-ratio

By combining the results of static and dynamic light scattering, the so-called ρ-ratio can be determined, which provides information on the topology of the scattering object:

$$\rho\text{-}ratio = \frac{R_g}{R_h} \tag{3.39}$$

However, eq. 3.39 is valid only for nanoparticles in the size range between 10-100 nm. It is used whenever the detailed analysis of the nanoparticles form factor is not possible. Relevant for this thesis are ρ-ratio = 1, which refers to a hollow sphere, and ρ-ratio = 0.775, which represents a homogenous sphere.

3.3 Protein analysis

3.3.1 Protein quantification

The protein quantification is usually the first step in the analysis of the protein corona. In this work, we followed the calorimetric protein quantification based on the complexation of the proteins with the Coomassie-Brilliant-Blue G250 dye as described by Bradford.[101] In acidic solutions the dye changes from red to blue color with a shift of the absorption maximum from 465 nm to 595 nm. The blue, active form of the dye is stabilized by non-covalent complexation with cationic and non-polar side chains of the amino acids forming the proteins. The resulting increase of the absorption at 595 nm coming from the binding to proteins can be measured photometrically. From a calibration with bovine serum albumin as a standard, the protein concentration can then be calculated. [102, 103]

3.3.2 Protein identification by sodium dodecyl sulfate-polyacrylamide gel electrophoresis (SDS-PAGE)

To evaluate the composition of the protein corona, the SDS-PAGE is the first applied technique to obtain a fast result. During the gel electrophoresis, the proteins move according to their net charge through the applied electric field. Acting as a sieve, the used polyacrylamide gel contains pores,

through which larger proteins travel slower than small ones. To achieve a separation based only on size, but not on charge, sodium dodecyl sulfate (SDS) is added to the sample. This surfactant is used in an excess to cover the net charge of the molecules so that it can be neglected, and a constant charge-to-mass ratio is achieved. Moreover, SDS destroys the tertiary structure of the proteins by preventing the non-covalent interactions necessary for the protein folding. Additionally, in a reducing SDS-PAGE disulfide bonds are broken by the addition of dithiothreitol. The gel is run at a certain voltage and the proteins travel towards the anode in the applied electrical field resulting in a size separation.[104-107] A marker containing proteins of known size is used as a reference. Subsequently, the proteins in the gel are visualized by a staining procedure. For this thesis, a silver staining procedure was used, in which silver ions bound to the proteins are reduced to metallic silver.[108, 109]

3.3.3 Protein identification by liquid chromatography - mass spectrometry (LC-MS)

For the qualitative and quantitative identification of proteins, analysis by LC-MS using the shotgun approach is performed.[38, 110, 111] Before the actual analysis of the sample, the proteins are digested with trypsin. The latter is an enzyme, which cuts proteins behind the C-terminus of lysin and arginine into smaller polypeptides of about 14 amino acids.[112] The created polypeptides are separated by high-performance liquid chromatography (HPLC) according to their polarity. The polypeptides are in solution with the mobile phase transporting the analyte along the stationary phase that consists of a hydrophobic (reversed-phase) column material. The eluting samples are separated according to their polarity upon interactions with the stationary phase. Since in mass spectrometry the mass-to-charge (m/z) ratio of a molecule is detected, the polypeptides must be ionized in the following step. Therefore, an electrospray ionization (ESI) is used in a positive ionization mode. The analyte solution is sprayed into an electric field, where the voltage between the capillary and the counter electrode leads to ionization and gas formation. As soon as the analyte leaves the small capillary and enters the strong electric field, a charge separation in the analyte droplet takes place, during which positive ions are moved to the outside of the droplet. The so-called Taylor cone is formed from the equilibrium of the electric field and the surface tension. With the increasing distance of the droplet to the capillary, a droplet with a positive charge is emitted. Subsequently, the droplet size is decreased by the evaporation of solvent molecules until only a charged residue is left. The following analyzer is then separating the formed ions according to their mass to charge ratio. In the used set-up, three analyzers are connected in series: A first quadrupole is separating the analytes, while a second quadrupole is used for the fragmentation of the ions. As third, a time of flight (TOF) analyzer separates the fragment ions according to their m/z-ratio and

the ratios are detected. Generally, the quadrupole analyzer consists of four cylindric electrodes, which are arranged parallel to each other. A hyperbolic alternating electrical field is applied to the electrodes, resulting in stable trajectories for the ions at a given voltage. Upon variation of the alternating field, ions with different m/z-ratios are released from the analyzer and can be detected. The TOF analyzer on the other hand accelerates the ions in an electric field. Depending on their m/z-ratios, the ions require different flight times until they reach the detector. The combination of quadrupole with fragmentation and TOF is also referred to as Q-TOF (Figure 3.3), in which the fragmentation is used to generate characteristic ion fragments of a molecule. The collected mass spectra are compared to a database containing all protein sequences, which leads to the identification of the proteins.

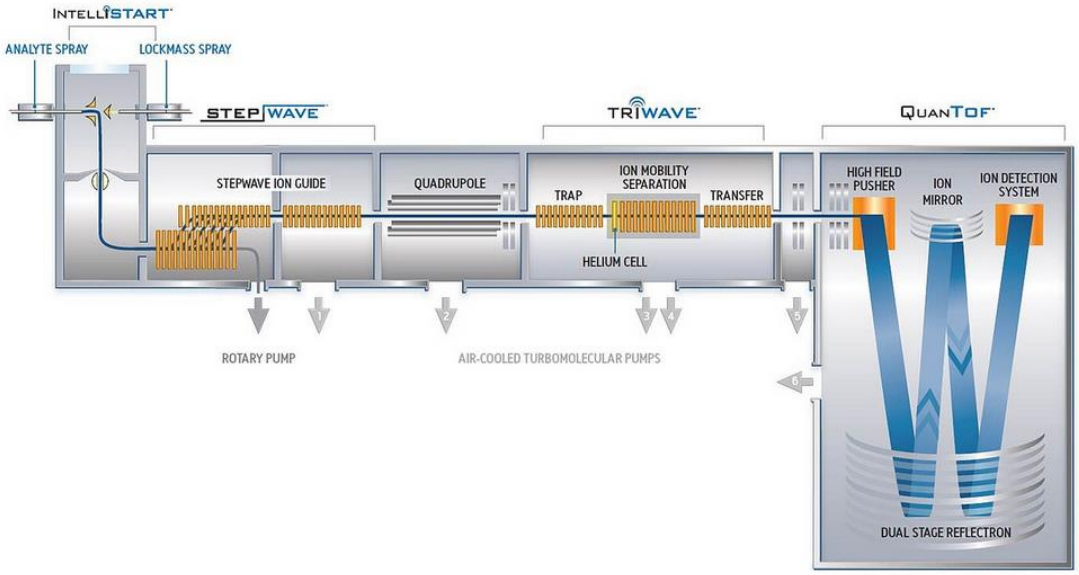

Figure 3.3: Schematic set-up of the used MS instrumentation (Waters Synapt G2-SI) by Waters.[113]

3.4 Other characterization methods

3.4.1 Zeta potential

To characterize the surface charge of dispersed particles, the zeta potential is used, since the actual surface charge cannot be measured directly. If a particle is in solution, opposite charges will adsorb on the surface and form the so-called Stern layer. Around this a more diffuse layer of ions is formed. As soon as an electric field is applied to the dispersion, the particle together with the Stern layer will move into the direction of the oppositely charged electrode. The particle movement does not influence the diffuse layer of ions and a slipping plane results due to the movement of the Stern

layer along the diffuse ions. This slipping plane is referred to as the zeta potential, which is measured via the electrophoretic mobility and calculated using the Smoluchowski equation.[114]

3.4.2 Behavior of nanocarriers including cellular uptake

For successful drug delivery, nanocarriers containing the cargo must be taken up by the target cells. Hence, the interactions between the nanomaterial and the cells are the most crucial step in the delivery process. However, the protein corona covers the nanocarrier surface, and consequently the adsorbed proteins play a major role in the cellular uptake mechanisms. Thereby, the characteristics of the nanocarrier, like the polymeric material or the surface functionalizations influence which proteins are adsorbed on the surface. In case opsonins (proteins like fibrinogen, immunoglobulin G, complement factor or else) adsorb, the nanocarriers are rapidly cleared out of the system by the immune cells. This process is called opsonization,[12] and it can be investigated by the cellular uptake in macrophages (e.g. RAW cells), which are the main phagocyting cells. If the nanocarriers are removed rapidly by the cells of the immune system, the probability that they reach their target decreases tremendously. Thus, the aim is to ideally avoid unspecific cell uptake of nanocarriers into macrophages. Besides analyzing the clearance from the body also the efficacy of the targeted drug delivery can be investigated. Therefore, HeLa cells are often used as a tumor model cell line for the uptake in cancer cells.[115] The evaluation of these cell uptake experiments is done by flow cytometry analysis, also called fluorescence activated cell sorting (FACS).[116] The sample flows through a cuvette small enough to only let an individual cell pass at a time. A laser beam is passing through the cuvette, resulting in a light scattering effect of the cell in the measurement volume. Depending on the size and the complexity of the cell, the laser light is scattered differently, providing information on the cell type, morphology, etc. Additionally, a variety of fluorescence labels can be attached to cells or proteins, and the different signals can be detected. Using the fluorescence labelling of proteins, also nanoparticle-protein complexes can be detected by flow cytometry, if they are large enough.[87] Furthermore, the cellular uptake can be visualized using confocal laser scanning microscopy after staining the cell membrane. This is especially useful for distinguishing between cellular uptake and attachment of nanocarriers on the outer cell membranes. From the results, first conclusions on the in vivo behavior of the nanocarrier can be drawn.

4 Results and discussion

4.1 Preservation of the soft protein corona in distinct flow allows identification of weakly bound proteins

The work presented in this chapter is in parts already published in the journal *Acta Biomaterialia* **2018**, vol. 76, pp. 217-224.

Commonly, the protein corona is considered to consist of a hard and a soft protein corona. Proteins with high binding affinities and therefore low exchange rates are directly attached to the surface of the nanocarrier and therefore form the 'hard' protein corona. Around this hard corona, further proteins adsorb and form the highly dynamic 'soft' protein corona, consisting of those proteins with low binding affinities and high exchange rates.[7, 117] In practice, the hard corona consists of all the proteins, that are still attached to the nanocarrier after separating it from the free plasma proteins by centrifugation.[9] To identify the amount and types of proteins this separation is required and is usually followed by several washing steps. Even though centrifugation is an easy method to apply, it has some limitations. Proteins like human serum albumin (HSA), that are highly abundant can be overestimated if not washed off properly, as well as protein aggregates might be found in the pellet and accidentally found to be part of the protein corona.[19] When comparing the protein coronas after separation from free plasma proteins by different methods, e.g. centrifugation vs. magnetic separation, the resulting protein patterns differ significantly, indicating the importance of the preparation procedure on the outcome of the protein corona.[36, 118] However, recent analysis in the field of nanomedicine revealed that the *in vivo* efficacy of nanotechnologies is much lower than expected.[119] The reason for this failure in nanomedicine is, at least in part, related to the several hidden factors and incomplete declaration of the essential information at the nano-bio interfaces.[120]

At the same time, still little is known about the 'soft' protein corona, its composition and its function. So far, the soft protein corona is only accessible by *in situ* measurements, which means that the measurement is executed in the protein solution itself with no separation step. The size of the soft protein corona for example can be measured with dynamic light scattering (DLS) in concentrated blood plasma as shown by Rausch *et al.*[79, 92] Additionally, binding parameters of weakly associated proteins can be determined by isothermal titration calorimetry, allowing to distinguish between soft and hard corona proteins.[25] However, the exact composition of the soft protein corona, its biological relevance and impact on cellular uptake are still unknown. To

determine these parameters a method to preserve the soft protein corona after separation from free proteins has to be found.

Therefore, as a new approach to isolate the entire nanocarrier-protein complex including the soft protein corona, the asymmetric flow field-flow fractionation was used (AF4). It is a chromatography-like technique with a separation mechanism based on diffusion coefficient and subsequently size.[54, 56, 93] Thereby the separation itself takes place in a flow channel and is based on the stronger retention of larger particles by an applied cross flow. Since no stationary phase is present, the method exerts lowest shear forces on the sample and therefore is a very mild separation method.[53, 121] Due to the low shear force also weakly bound proteins stay associated with the nanocarriers and thus it offers the possibility of preserving the soft protein corona.

The main problem to overcome when applying the AF4 technique to separate a mixture of proteins and polymer-based nanocarriers are the different separation conditions that the two species require due to their different chemical nature.[122] Ashby et al. showed that a co-elution of proteins and nanocarriers in principle is possible.[61] Their elugrams even more show a large void peak, which could correspond to free proteins, while the flow rate conditions were selected with a focus on retaining only the NPs. Furthermore, Tsai et al. already separated free bovine serum albumin (BSA) from BSA-gold nanoparticle-conjugates.[80] However, both mentioned studies did not aim at applying this technique for more complex systems and to further analyze protein corona compositions. For magnetic nanoparticles parts of a soft corona could already be isolated and analyzed as done by Bonvin *et al*.[50] However, up to now no separation from free proteins was achieved for non-magnetic nanoparticle systems.

Therefore, herein we show a separation of free plasma proteins from the nanocarrier-protein complex with the hard and soft protein corona by AF4, which allows further analysis of biological implications. For the first time, it was possible to perform this separation for non-magnetic nanocarriers without disturbing the weak interaction forces of low affinity proteins. The resulting protein pattern was compared to the one obtained by centrifugation and subsequent washing. Both isolated corona forms were then subjected to cellular uptake experiments to determine their biological relevance and impact.

4.1.1 Characterization of the used polystyrene-nanoparticles

Polystyrene nanoparticles (PS-NPs), synthesized by Katja Klein (MPIP Mainz, Germany), were chosen as a model nanocarrier system. They provide a very good stability over time in contrast to many other more hydrophilic or biocompatible materials, so that a maximum

experimental reproducibility was ensured and the provided nanocarrier surface stayed the same throughout the experiments. In addition, they show a very narrow size distribution (Figure 4.1 and Figure 4.2A).

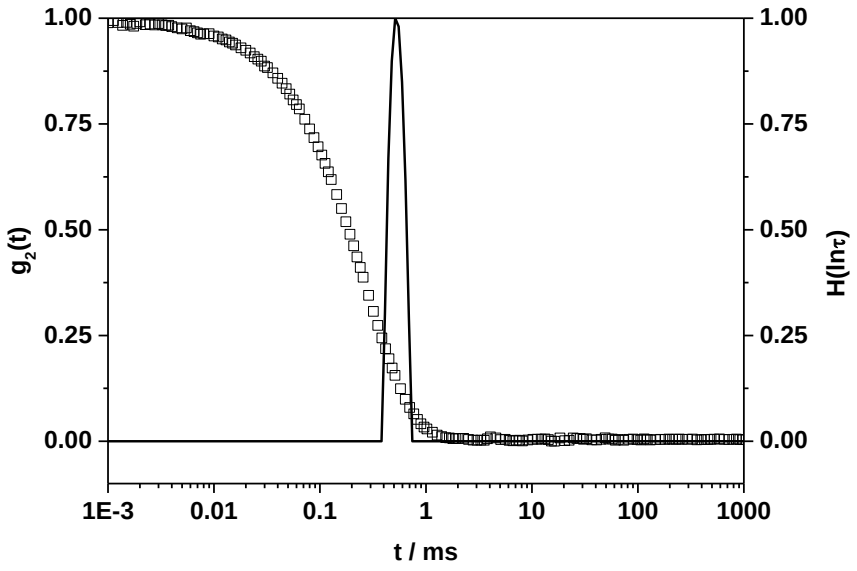

Figure 4.1: Autocorrelation function and distribution function of relaxation times determined via a CONTIN algorithm from DLS at an exemplary scattering angle of 90°. The polydispersity (PDI) was determined via a cumulant analysis and found to be 0.0427.

Furthermore, the surfactant used for ensuring the dispersion stability is Lutensol AT50, which has a polyethylene glycol (PEG) based hydrophilic part. This means that the protein adsorption pattern is mainly governed by the PEG functionalization.[42, 123] Thus, we consider the described PS-NPs as a suitable model system for protein corona studies. All main features of the used particles can be found in Figure 4.2B.

A

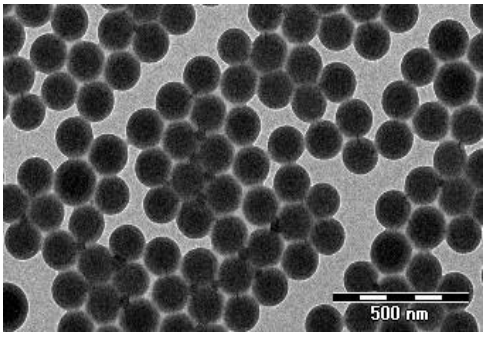

B

Material	**Polystyrene**
Surfactant	**Lutensol AT50 (PEG-based)**
Dye for fluorescence detection	**Bodipy (ex 523 nm / em 536 nm)**
R_h / nm	**67 ± 7**
ζ-Potential / mV	**-13 ± 1**

Figure 4.2: Physico-chemical properties of PS-NP. (A) shows the TEM micrograph while (B) shows the zeta potential and the size obtained by angular dependent dynamic light scattering.

4.1.2 Protein corona separation by AF4

PS-NPs were incubated with human citrate plasma for 1 h at 37 °C to allow protein corona formation. Subsequently, we applied two different methods – centrifugation vs. asymmetrical flow field-flow fractionation (AF4) – to separate free plasma proteins from the formed nanoparticle-protein complex. For obtaining the strongly bound proteins, the hard protein corona, the commonly exercised centrifugation and washing technique was applied.[9, 25, 124] For a preservation of weakly associated proteins in the soft protein corona, the mixtures were separated via AF4. In principle, components of the mixture are separated according to their size, meaning that the smaller free proteins elute first and later on the nanoparticles with the protein corona.

Accordingly, the elugram of PS-NPs incubated with plasma is shown by the red line in Figure 4.3A. Plasma (blue) and pristine PS-NPs (green) are also plotted as a reference. Free plasma proteins were eluted from the separation channel between 5 and 15 min elution time. This was also shown for the mixture of plasma and polymer nanoparticles. Therefore, free proteins were successfully separated from the nanoparticle-protein complexes. Between 20 and 30 min pure polymer nanoparticles were eluting. The incubated particles also showed a peak at this elution time, which corresponds to the polymer nanoparticles. Offline fluorescence measurements at 536 nm confirmed that this signal is originated from the nanoparticle (Figure 4.3B). The elugram shows the comparison of the fluorescence signal originating from the mixture to the signal of pure PS-NPs. The peak maximum related to the incubated particles is shifted to slightly higher elution times in comparison to the pure PS-NPs.

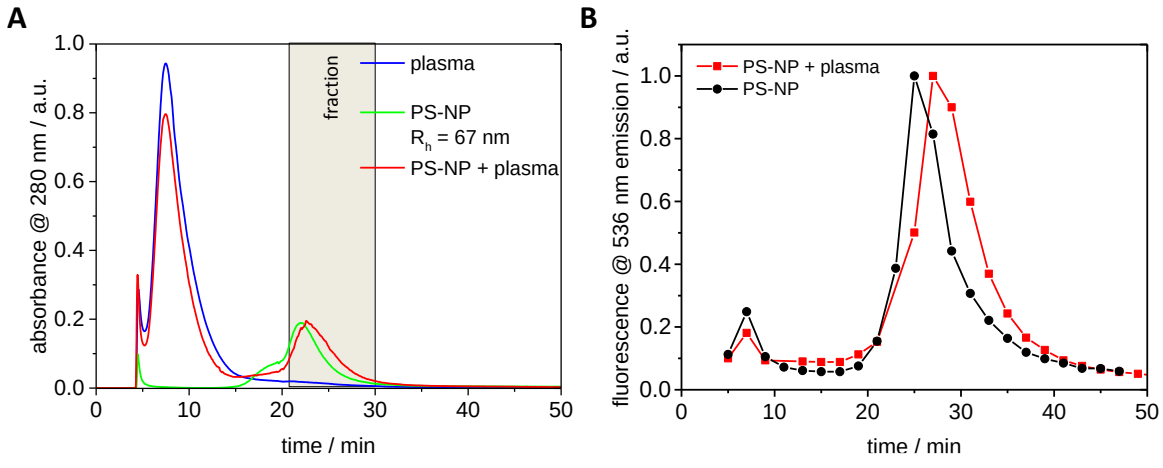

Figure 4.3: (A) AF4 elugrams of PS-NP (green), human plasma (blue) and the incubated mixture of both (red) as detected by UV absorbance at 280 nm. The fraction collected after injection of the mixture is indicated by the grey box. Separation was performed at 37 °C. (B) Elugram corresponding to the offline fluorescence signal of the respective runs in A. Fractions were collected every 2 minutes and fluorescence arising from the dye in polymer nanoparticles was measured at 536 nm.

As AF4 is a size dependent separation technique, we conclude, that the size increase is attributed to the protein corona formation. This highlights the successful separation of free plasma proteins from corona coated polymer nanoparticles by AF4.

Before proceeding with further experiments, it was investigated, weather the chosen carrier liquid for the AF4 separation was suitable for the proteins in the separation channel, without denaturing them. Therefore, differential scanning fluorimetry (Nano-DSF) experiments were executed with two exemplary proteins: HSA and transferrin. Nano-DSF measures the intrinsic fluorescence of proteins emitted by tryptophan and tyrosin. By increasing the temperature, the proteins denature, changing their conformation and consequently the emitted fluorescence is changing so that the melting point of the protein can be determined.[125] Consequently, the protein stability of HSA and transferring in 10 mM phosphate buffer (carrier liquid) was compared to the one in phosphate buffered saline (PBS), which served as a reference. The fluorescence slightly changed, but still in both cases a definite melting temperature (T_m) could be determined (Figure 4.4). The presence of a melding point implies that the proteins are mostly in their native and the used carrier liquid is suitable for the here described separation as it does not alter the protein conformation.

For further analysis of the components after AF4 separation, a fraction was collected from the nanoparticle-plasma mixture as indicated by the grey box in Figure 4.3A. This fraction was characterized regarding its size distribution using multi-angle dynamic light scattering (DLS) and regarding its protein composition with SDS-PAGE and LS-MS.

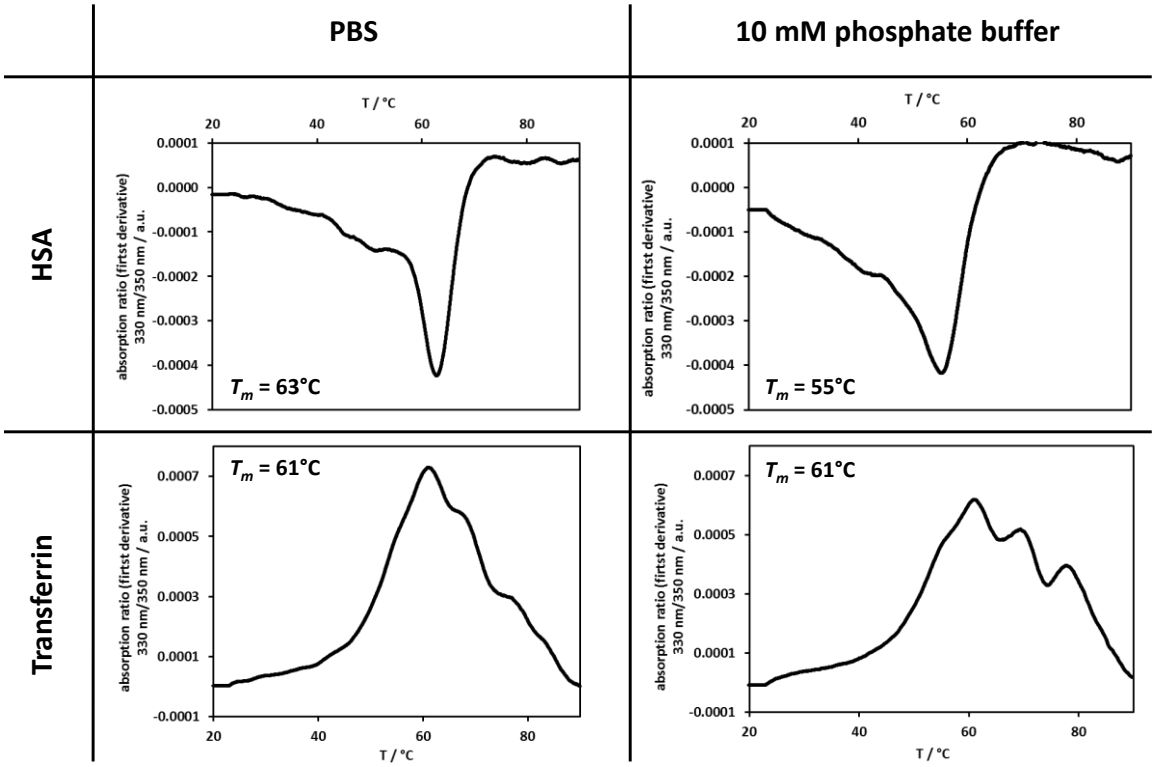

Figure 4.4: Nano-Differential scanning fluorimetry (DSF) results to check the stability in the chosen carrier liquid. Human serum albumin (HSA) and transferrin were chosen as exemplary proteins and measured in PBS and 10 mM phosphate buffer. Intrinsic Fluorescence at 330 nm and 350 nm was measured and the derivative of the ratio was plotted to determine the melting points.

4.1.3 Evaluation of the protein corona by dynamic light scattering

DLS measurements were evaluated using the method established by Rausch et al. with which the hydrodynamic radius of an aggregate in a complex mixture can be calculated.[79, 92] An aggregate is defined as a newly formed species that is larger than the original particle. The evaluated autocorrelation functions of all samples are summarized in

Figure 4.5.

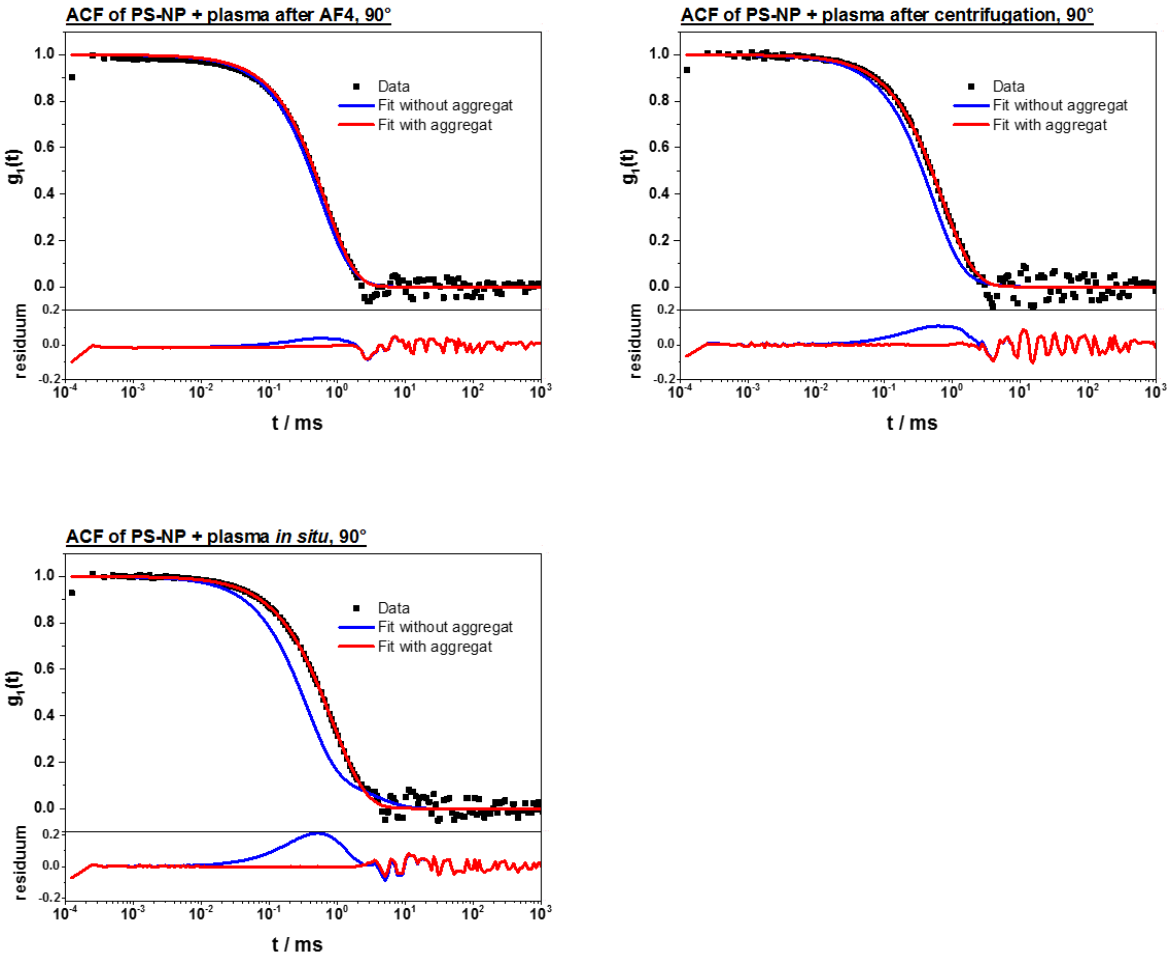

Figure 4.5: Upper part of each graph shows the autocorrelation function (ACF) $g_1(t)$ of the PS-NPs incubated with plasma at an exemplary scattering angle of 90°. The forced fit composed of the sum of the individual components is represented by the blue line. The red line represents the fit with an additional aggregation function. The residuals result from differences between the data and the fits are shown in the lower part of each graph.

Also the intensity of the scattered light can be differentiated into the different species: free protein, free PS-NPs and aggregate, so that the intensity fraction of each species in the sample can be determined.[79, 92]

After separation by AF4 the sample mainly consists of the newly formed aggregate that does not correspond to free proteins or free nanoparticles (Figure 4.6A). We attributed this to protein corona coated nanoparticles. Small amounts of free nanoparticles can also be found.

As a comparison, we introduced nanoparticles directly into plasma without further separation as it is a well-studied method to investigate protein-nanoparticle interactions *in situ*, attributed as soft protein corona.[92] As expected all three species were identified. Additionally, this was compared to the classical preparation of nanoparticles coated with the hard protein corona. Therefore, the

protein-particle complex is centrifuged to remove free proteins.[9, 25, 124] This sample contains almost no free protein, since it was washed off during the preparation. (Figure 4.6A)

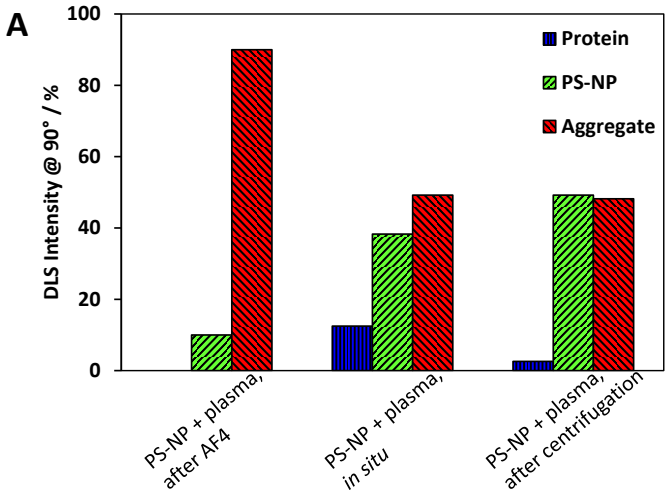

B

R_h PS-NP / nm	67 ± 7
R_h (after AF4) aggregate / nm	84 ± 8
R_h (after centrifugation) aggregate / nm	103 ± 10
R_h (*in situ*) aggregate / nm	136 ± 14

Figure 4.6: DLS data of PS-NPs incubated with plasma and subjected to different sample preparation: AF4 fraction as indicated in Figure 4.3A, mixture without separation of free proteins (*in situ*) and mixture after centrifugation and resuspension. (A) shows the scattering intensity of each species, which corresponds to the amount of this species in the sample. (B) sums up the hydrodynamic radii of the PS-NPs and aggregates from the mixtures as presented in A, obtained from extrapolation to scattering angle q→0 over all measured scattering angles. The error represents the experimental error of the light scattering experiment.

Looking at the hydrodynamic radii of the aggregate in Figure 4.6B, an increase in size from the free nanoparticles to the particles incubated with plasma isolated by AF4 is seen. As the size increase is not twice the size of one nanoparticle, we can exclude that the identified aggregate after AF4 is originating from particle-particle aggregates. Consequently, it is the protein layer that surrounds the particles which is responsible for the size increase.

The hydrodynamic radius of the aggregates determined after the separation by centrifugation is slightly higher than after AF4. In this case, the size increase can, however, be attributed to the centrifugation procedure itself. As this can also be observed for pure nanoparticles being centrifuged, we can conclude that a certain amount of nanoparticle-protein complexes cannot entirely be redispersed again, resulting in an overall higher average radius. Therefore, the size is not only depending on the protein corona formation but rather also on the sample preparation. The *in situ* DLS measurement reveals an overall size increase of around 70 nm, which is significantly higher compared to the corona coated nanoparticles after separation from free proteins. This is most probably the entire soft corona with additionally associated proteins being adsorbed in clusters or groups, since no outer influence was applied to the system. (Figure 4.6B)

4.1.4 Identification of the proteins of the different protein coronas

The protein corona compositions after isolation by centrifugation and AF4 were further analyzed by SDS-PAGE (Figure 4.7) and LC-MS (Figure 4.8). Already at first glance, the protein coronas after AF4 and after centrifutaion differ from each other. While the corona after AF4 shows a strong band at around 67 kDa, this band is weaker after centrifugation, therefore, the variety of observed proteins is higher for the corona after centrifugation.

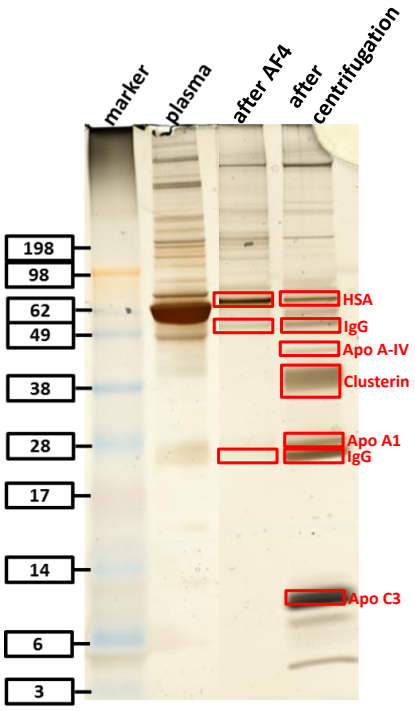

Figure 4.7: SDS-PAGE of the different fractions of the PS-NP sample incubated with plasma and isolated by the AF4. © 2018 Acta Materialia Inc. Published by Elsevier Ltd. All rights reserved.

The LC-MS experiments were preformed by Dr. Johanna Simon (MPIP Mainz, Germany) to gain a more detailed insight into the protein corona composition and to identify the proteins. All proteins identified by LC-MS were grouped according to their function (Figure 4.8A).

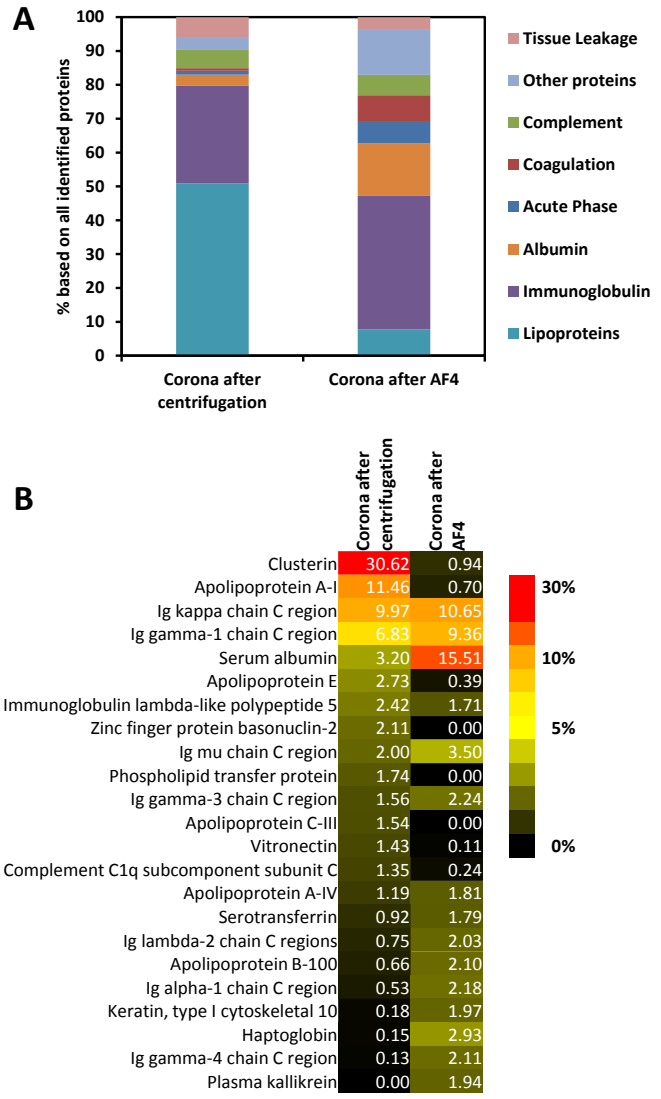

Figure 4.8: (A) Protein composition of the differently obtained protein coronas, analyzed by LC-MS. Proteins were grouped according to function. (B) LC-MS heat map showing the abundance of individual proteins in obtained protein coronas after centrifugation vs. AF4. The 15 most abundant proteins of each protein corona are displayed. Values are expressed as mean of three technical replicates.

The general protein composition highly differed for corona proteins isolated after centrifugation compared to AF4. Especially lipoproteins were enriched in the protein corona after centrifugation. In contrast, human serum albumin (HSA) was identified as abundant corona protein after AF4 and also the amount of immunoglobulins was increased. This leads to the conclusion that the composition of the protein corona differs depending on separation technique. In general, it is described, that HSA has a low binding affinity and a high exchange rate on the different material surfaces.[25, 126] As a consequence, HSA is considered to be associated as a soft corona protein. This is in line for the here investigated system as we found low amounts of HSA in the hard protein

corona after centrifugation. In contrast, HSA was identified as corona protein after AF4 separation, which in turn indicates that much more of the soft protein corona can be preserved during the separation in comparison to centrifugation.

Previous studies showed that apolipoprotein J - known as clusterin - is strongly enriched in the hard protein corona of PEGylated nanoparticles[42, 127]. For the here investigated nanoparticle system we also identified clusterin as the most abundant corona protein after centrifugation. Interestingly, LC-MS measurements indicate a remarkably lower relative amount of clusterin (0.94%) and apolipoprotein A-I (0.70%, Apo AI) in the protein corona obtained after AF4 (Figure 4.8B). However, it has to be noted that LC-MS only reflects the relative abundance of each corona protein. Thus, it is possible that the same total amount of clusterin and other hard corona proteins is still present after AF4 separation and that additionally a high amount of soft corona proteins is adsorbed 'on top'.

From the LC-MS data it could be argued that the protein coronas after both separation methods simply are different and that HSA replaces apolipoproteins due to the difference in sample handling. As a consequence, we wanted to clarify whether HSA and probably other soft corona proteins were adsorbed additionally and the hard protein corona was still present beneath the soft corona or the hard corona proteins were actually replaced by the proteins found after AF4. To answer this question, we performed two independent experiments. First, we verified that the proteins found in the sample after AF4 were indeed attached to the nanoparticles and are not an artefact of co-eluting plasma proteins. Therefore, we added a fluorescence-labeled antibody, which binds to the according protein on the nanoparticle's surface. This complex can only be measured by flow cytometry, if the protein that corresponds to the antibody is adsorbed to the nanoparticles. Since IgG was a very abundant protein in both protein coronas, we chose Zenon Alexa Fluor 647 human IgG labelling reagent. It is a fluorescence-labeled Fab fragment that will bind to the Fc part of the available IgG in the sample, but only if the IgG is adsorbed to the nanoparticle the fluorescence signal of the complex can be detected. In Figure 4.9, the percentage of nanoparticles positive for the labelling reagent is shown. Since the signal is positive for the labelling reagent in both protein coronas, IgG must be adsorbed to the particle and therefore it must be part of the protein corona after both separation methods. Furthermore, the amount of IgG-positive nanoparticles after AF4 is significantly higher than after centrifugation so that we conclude that most of the IgG is indeed part of the soft protein corona. The results of the protein pattern in Figure 4.8, where we see a higher amount of IgG in the protein corona after AF4 than after centrifugation are confirmed by this antibody-adsorption experiment where also more IgG can be found on the nanoparticle's surface after AF4.

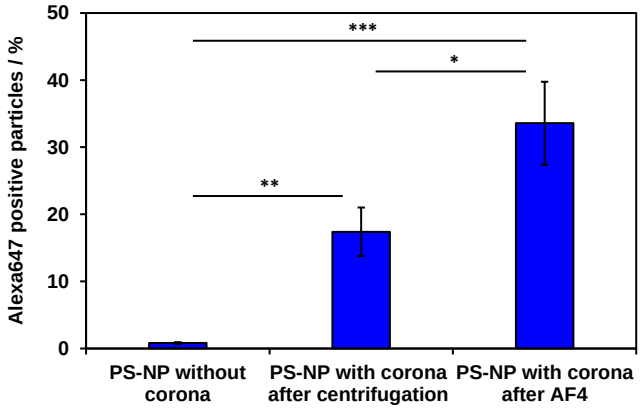

Figure 4.9: Detection of corona proteins (IgG) on the nanoparticle surface by flow cytometry. The used reagent only binds to IgG and can only be detected by flow cytometry if IgG is attached to the nanoparticle. In both protein coronas the found IgG is part of the protein corona, but the amount of IgG is enriched in the protein corona after AF4. Values are expressed as mean ± SD of three technical replicates. The experiment was carried out in two biological replicates by Dr. Johanna Simon (MPIP, Germany).

*p < 0.05, **p < 0.01, ***p < 0.001.

To further study protein corona formation after AF4, the particles were first incubated with plasma, then centrifuged one time to remove the excess of free proteins and some of the loosely bound soft corona proteins. Afterwards, the mixture was injected in the AF4, a fraction collected at the elution time as shown in Figure 4.3 and this fraction was then analyzed by SDS-PAGE to identify the adsorbed proteins. The resulting protein pattern is shown in Figure 4.10. Again, we identified HSA (~ 60 kDa) as the most abundant corona protein. However, there are two prominent additional protein bands (38 kDa and 28 kDa) visible. They can be seen now, because a significant amount of HSA was already removed by the centrifugation step. Comparing this protein pattern to the protein composition after centrifugation, Figure 4.10 reveals that the indicated bands correspond to clusterin (38 kDa) and immunoglobulin G (IgG, light chain, 25 kDa). This leads to the conclusion that the hard protein corona is still present underneath the soft protein corona that is isolated by AF4. From these results it can be concluded that the hard protein corona is the same for both separation techniques. Hence, with AF4 we could additionally identify loosely bound proteins and hereby show that a significant part of the soft corona can be preserved. In principle, it is likely that still not the complete soft corona can be isolated here due to the dilution during the separation process. However, in our opinion this is the closest one can get right now to obtain useful information about the loosely associated proteins.

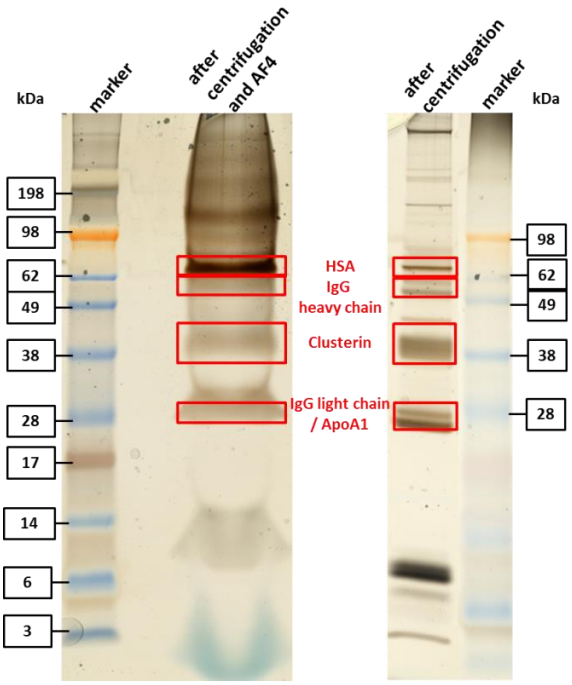

Figure 4.10: SDS-PAGE of the PS-NP protein corona after centrifugation and subsequent separation of the sample in AF4. On the left side the SDS-PAGE of the first centrifuged and subsequently by AF4 separated PS-NP is pictured. In comparison on the left side, there is the protein corona of the as usual centrifuged particle.

4.1.5 Cellular uptake behavior of the different protein coronas

The preservation of the soft protein corona now allowed comparing the biological impact of differently obtained protein coronas. Therefore, cellular uptake towards HeLa cells for nanoparticles without corona was compared to soft (AF4) and hard (centrifugation) protein corona coated polymer nanoparticles. The described cell experiments were preformed by Dr. Johanna Simon (MPIP Mainz, Germany). Cellular interactions were significantly reduced for protein corona coated nanoparticles compared to pristine polymer nanoparticles (Figure 4.11, cLSM results Figure 4.12). Interestingly, cellular uptake behavior of PS-NPs coated with the hard protein corona is comparable to soft corona coated polymer nanoparticles. This indicates that for the here investigated system proteins of the soft corona did not alter the biological behavior. We are aware that this may also depend on the cell type, nanoparticle system or additional factors as protein-protein interactions within the protein corona.

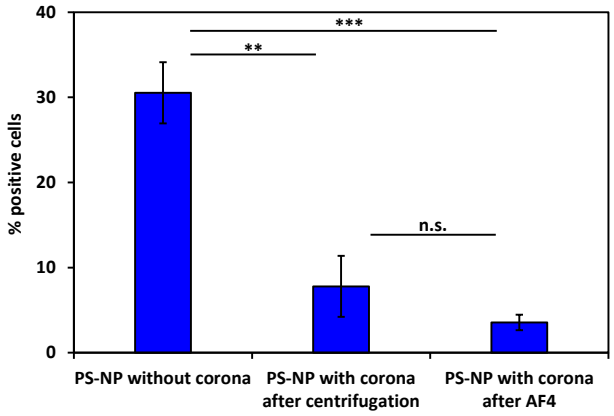

Figure 4.11: Flow cytometry results on the cellular uptake by HeLa cells after 2 h of incubation. Compared are the PS-NPs without protein corona and the PS-NPs with the different protein coronas obtained after centrifugation or AF4. Values are expressed as mean ± SD of three biological replicates. *p < 0.05, **p < 0.01, ***p < 0.001.

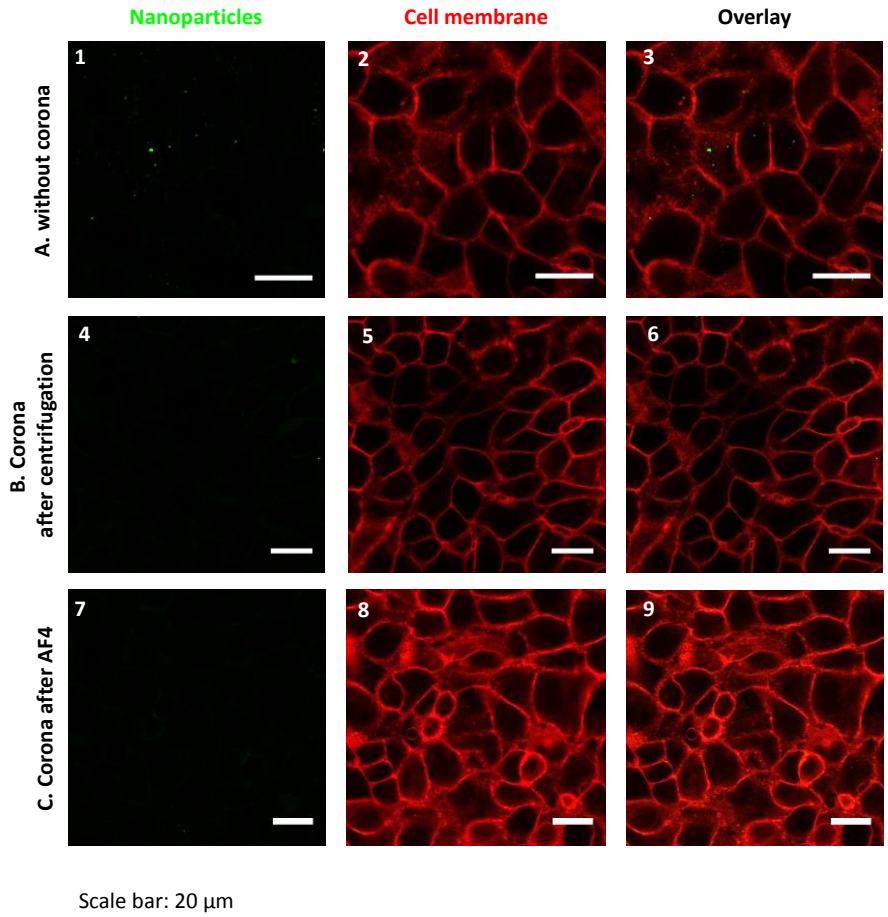

Figure 4.12: cLSM pictures of cellular uptake in HeLa cells after 2 h. The first row shows the PS-NPs without any protein corona. Line B shows the cellular uptake of the PS-NPs with the protein corona after centrifugation, so the hard protein corona. Line C shows the PS-NPs with the protein corona obtained after AF4.

4.1.6 Conclusion

In our experiments we showed that nanocarriers including their soft protein corona were isolated by AF4 for the first time. Since the AF4 has low shear forces, proteins with low affinities such as HSA and IgG could still be identified within the soft protein corona. Removing the excess of HSA indicated that the underlying hard protein corona is comparable for AF4 separated and centrifuged nanoparticles. On top of this, we found that cell uptake behavior of the particle with soft or hard protein corona was not significantly altered for our system. In general, preservation of the soft protein corona by AF4 now allows for conducting broader studies to elucidate the cellular interactions at the nano-bio-interface for nanocarriers systems where this has not been studied up to now, e.g. due to technical limitations.

4.2 Functionalization of liposomes with hyperbranched polyglycerol results in biological identity independent of the protein corona

Among nanocarrier systems, liposomes are an interesting material class for several reasons. They are spherical vesicles composed of one or more phospholipid bilayers. Because of the amphiphilic character of the phospholipids, the membrane bilayer displays an aqueous core and a hydrophilic outer surface as well as a lipophilic membrane interspace. Therefore, depending on their polarity, a high variety of lipophilic and hydrophilic drugs can be encapsulated, either in the membrane or in the core, respectively. Additionally, liposomes can disintegrade and are potentially biocompatible, because they consist of either natural or synthetic phospholipids. These factors make liposomes promising drugcarriers.[128-130] Moreover, they already found their way into the market, e.g. as the formulation Doxil®, which contains the chemotherapeutic drug doxorubicin encapsulated in a PEGylated liposome[131, 132], as well as in a non-PEGylated liposome formulation called Myocet® [133] and many others.[134]

To predict the behavior of potential nanocarriers in a biological system, it is necessary to consider and analyze the protein adsorption on the surface of the nanomaterial.[9, 25] Liposomes are no exception here, as they also adsorb proteins on their surface as shown by Caracciolo *et al.*[14] This adsorption process occurs as soon as the nanomaterial enters the body, e.g. via intravenous injection. The drug carrier is confronted with a high number of proteins and other biomolecules, which adsorb onto the material's surface and form the so-called protein corona.[7, 17, 19, 20, 135] Thereby, the adsorbed proteins cover the synthetic surface of the material giving it a new biological identity. For many other colloidal nanomaterials, it has been shown that this biological identity determines the organism's response towards the nanocarrier, influencing cell-uptake, clearance and body distribution.[8]

Even if liposomes are formed from natural phospholipids, they are still recognized as foreign objects by the immune system and therefore are rapidly cleared out of the body by the mononuclear phagocytic system.[128] To prevent this rapid clearance, hydrophilic long-chain polymers can be attached to the liposome's surface, with the most prominent being poly(ethylene glycol) (PEG).[130] The attachment of these polymers potentially decreases the unspecific protein adsorption and forms "stealth" liposomes, which show a longer blood circulation time and less clearance by the immune system.[136-140]

Caracciolo *et al.* already investigated the protein corona of PEGylated liposomes and lipoplexes as well as the ability of different PEG chain lengths to decrease cell uptake.[14, 123, 141, 142] However, the potential stealth effect of liposomes functionalized with polymers exhibiting a different structure

such as hyperbranched polyglycerol (*hb*PG) was not analyzed in regard to the protein corona to this point. This polymer with its tree-like structure provides a hydroxyl group on each branch end, leading to a high hydrophilicity comparable to PEG, but with more possible functionalization sites for targeted delivery (Figure 4.13).[143]

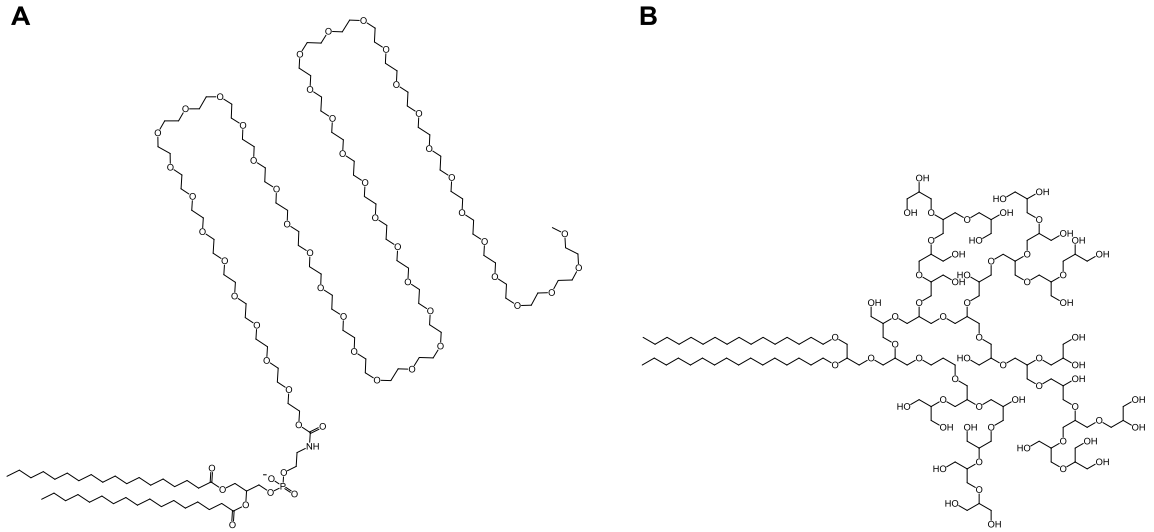

Figure 4.13: Structure of (A) linear poly(ethylene glycol) (PEG) and (B) hyperbranched polyglycerol (hbPG).

So far, Frey et al. compared the *in vivo* fate of *hb*PG functionalized liposomes to PEGylated ones by PET-imaging in mice, finding a comparable bio-distribution,[144] but the protein corona, which might influence the biological behavior, was not analyzed yet. Therefore, in this paper we analyzed the influence of different surface functionalizations of liposomes on the protein corona and investigated whether the protein corona or the intrinsic property of the stealth material itself has a greater impact on cellular uptake and accordingly on the biological identity. Consequently, we chose unfunctionalized liposomes, PEGylated ones and those with *hb*PG on the surface for comparison. We evaluated separation by asymmetric flow field-flow fractionation (AF4) compared to the usually applied centrifugation to isolate the protein corona.[25, 63] By combining these two techniques, a comparison between soft and hard protein corona is possible and the influence of the surface functionalization of liposomes on the soft and the hard protein corona was investigated. Moreover, we investigated the influence of the different surface functionalities with different protein concentrations on the biological response by executing cell-uptake experiments in macrophages.

4.2.1 Formulation and characterization of the used liposomes

Liposomes were formulated by Matthias Voigt (Department of Pharmacy, Johannes Gutenberg-Univeristy Mainz, Germany) via dual centrifugation, a rather new and easy to use "in-vial" homogenization technique for fast and reproducible liposome formulation within the single digit milligram range of total lipid (principle see Figure 4.14A).[145, 146] This makes the method suitable for screening of liposomes containing cost-intensive experimental materials only available in small amounts like *hb*PG, thus allowing aseptic formulation of up to 90 individual liposome samples within 30 min. High encapsulation efficiencies of hydrophilic cargo of around 50% and gentle preparation conditions are further advantages. For the following experiments, three different liposomes were chosen. Besides investigating a conventional, unfunctionalized liposome sample (L-un) with the same lipid composition as Myocet®, also two liposome samples with potential stealth functionalizations were analyzed: liposomes exhibiting PEG chains (L-PEG) as in Doxil® as well as a liposome with hyperbranched polyglycerol (L-*hb*PG) on the surface linked to the headgroup of DSPE or the hydroxyl group of a 1,2-bis-*n*-hexadecyl glyceryl ether, respectively. The liposome structure, individual components, composition and physico-chemical characteristics of all liposome samples are shown in Figure 4.14B and Table 4.1.

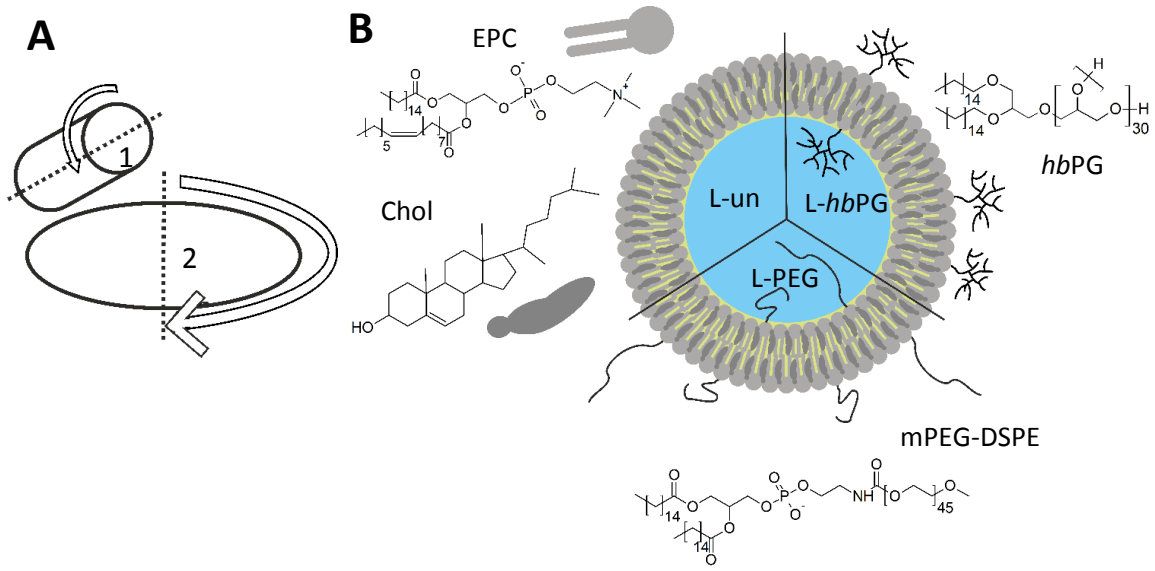

Figure 4.14: (A) Principle of dual centrifugation. The sample is subjected to the sample holder 1, which rotates contrary to the main axis 2. (B) The schematic structure of each liposomal composition together with the chemical structures of the used components egg phosphatidyl choline (EPC), cholesterol (Chol), hyperbranched polyglycerol (hbPG) and 1,2-distearoyl-sn-glycero-3-phosphoethanolamine-N-[methoxy(polyethylene glycol)-3000] (mPEG-DSPE).

Table 4.1: Composition and physico-chemical characteristics of all used liposomes.

Sample	Composition[a]	R_h / nm	R_g / nm	ρ-ratio[b] R_g/R_h	PDI[c]	ζ-potential / mV
L-un	55 mol% EPC 45 mol% Chol	86 ± 9	81 ± 8	0.94	0.08 ± 0.03	-20 ± 1
L-PEG	50 mol% EPC 45 mol% Chol 5 mol% mPEG-DSPE	61 ± 6	68 ± 7	1.15	0.10 ± 0.03	-26 ± 1
L-*hb*PG	50 mol% EPC 45 mol% Chol 5 mol% *hb*PG	91 ± 9	94 ± 9	1.03	0.13 ± 0.06	-21 ± 1

[a] *Abbreviations see figure 1*

[b] *ρ-ratio equals 1 for hollow spheres*

[c] *The cumulant analysis of the autocorrelation function reveals the given PDIs*

4.2.2 Separation of differently functionalized liposomes by AF4

The liposomes were incubated with 5 vol% citrate plasma to form the protein corona. 5 vol% plasma was chosen to not overload the AF4 channel with proteins, but still provide an excess of free proteins. The newly formed liposome-protein corona complexes were then separated from the medium by AF4 or by centrifugation. The former is used for the analysis of the whole complex including most of the soft protein corona, while the latter represents the standard analysis of the hard protein corona. AF4 was used because it is suitable also for fragile and self-assembled systems (e.g. liposomes or micelles), which cannot be separated from free proteins by other means. In our case, the liposome samples were stable enough to be centrifuged because of their high cholesterol content. Hence, we were able to compare the protein corona after AF4 with the one obtained after centrifugation.

The AF4 elugrams of all liposomes are displayed in Figure 4.15. The green line represents the elution of the pristine liposomes. Noticeably, all liposomes show a different elution profile depending on their surface functionalization. In theory, no interaction between the sample and the AF4 membrane should take place. However, in practice for some surface functionalizations the liposomes seem to interact preferably with the regenerated cellulose membrane. L-un and L-PEG demonstrate defined elution peaks, even though the L-PEG peak is tailing slightly more, whereas L-*hb*PG interacts strongly with the membrane, which is retarding the elution and results in a constant elution of the sample over the remaining separation time. The high number of hydroxyl endgroups introduced by the hyperbranched polyglycerol most probably causes the strong interaction with the membrane. Interestingly, also after plasma incubation (red line) the strong

interactions with the membrane still occur. This indicates that the proteins do not cover the surface functionalization completely and a significant amount of the hydroxyl endgroups is still accessible for membrane interactions.

The shoulder in all elugrams at 62 min does not correspond to another separated species of the sample, but corresponds to the time, at which the crossflow is stopped. Afterwards, no retention force is acting on the sample anymore and the remaining species that are left in the channel at that moment are eluting at once. Thus, no further analysis was performed on this last fraction. Free proteins should elute first from the separation channel, since according to the AF4 principle, the smallest components in a sample have the shortest retention time. In agreement with this the plasma protein elution takes place in the first 25 min as seen in the reference elugram of pure plasma (blue line, Figure 4.15). The red line represents the incubated mixture of pristine liposomes and blood plasma. The signal of the mixed sample nicely correlates with the pure components. The successful separation of incubated liposomes from free plasma proteins was confirmed by the distinct elution time. Indeed, free plasma proteins present in the mixture were eluting until 25 min, while the liposome signal just starts at that time. With only the UV detector the origin of the signal cannot be identified, so a fluorescence signal was recorded to verify that the second peak was generated by the fluorescently labeled liposomes and not by protein artefacts or else. Thereby, the second peak between 25 and 50 min was identified as the corresponding liposomes – presumably with proteins bound. The AF4 results indicate that an interaction between the proteins and the liposomes must have taken place, since the peak shape of the liposomes slightly changed in all cases after incubation with plasma. For further analysis of the liposome-protein complexes, fractions were collected as indicated by the grey boxes in each elugram.

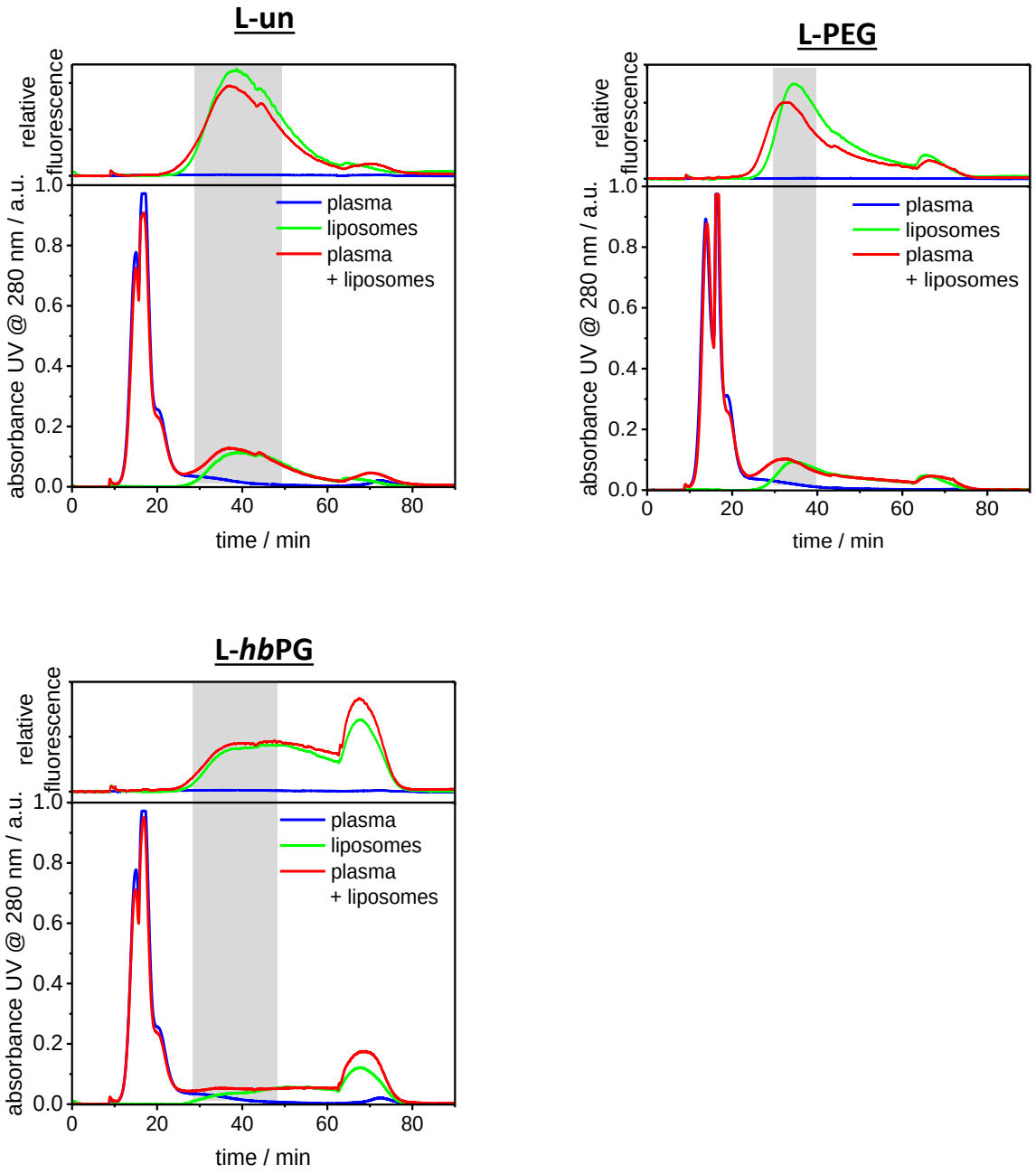

Figure 4.15: AF4 elugrams of all liposomes incubated with 5% plasma are shown in red. The individual elugrams are given as a reference, pure plasma in blue and pristine liposomes in green. The lower graph always represents the UV detector signal at 280 nm, while the upper one shows the fluorescence intensity. The fractions that were collected for further analysis are indicated by the grey box.

4.2.3 Analysis of the protein corona of the differently obtained protein coronas and the different functionalizations

To compare the protein corona after AF4, the sample was also separated via centrifugation. Therefore, the sample was centrifuged at 4 °C for 1 h at 20 000 g to pellet the liposome-protein

complex and remove the free proteins with the supernatant. Subsequently, the sample was washed for another three times with PBS and resuspended. The stability of the structure of the liposomes was confirmed first by TEM by Dr. Maria Kokkinopoulou (MPIP Mainz, Germany). The resulting micrographs in Figure 4.16 prove that the used liposomes were stable enough and centrifugation could be used as a technique for the classical hard corona separation as well. The protein compositions of the coronas obtained after AF4 and centrifugation were determined by Dr. Johanna Simon (MPIP Mainz, Germany) via liquid chromatography-mass spectrometry (LC-MS), as shown in Figure 4.17, where also a plasma reference is given. According to our procedure the detected protein amounts were below the limit of quantification, but no further sample concentration was possible.

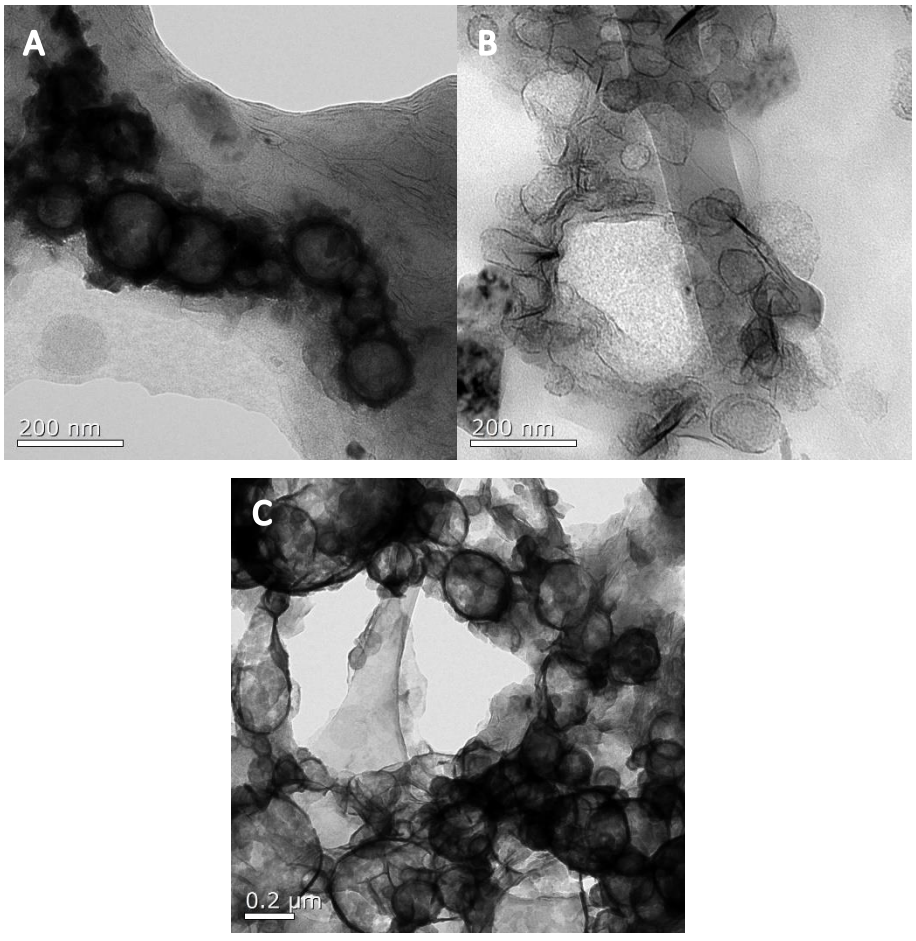

Figure 4.16: TEM micrographs of A) L-un, B) L-PEG and C) C-*hb*PG. The samples were centrifuged one time for 1 h at 20 000 g to check their stability during the centrifugation process.

The identified proteins were grouped according to their function to represent the most abundant protein types. Proteins that showed the most significant differences are displayed individually. A detailed list with all identified proteins can be found in the Appendix B.2.2.

Interestingly, when comparing the protein corona patterns between the differently functionalized liposomes, the identified proteins varied to some extent. Compared to pure plasma, the relative amount of albumin was lower in all cases, but still enough to constitute the main protein in the corona. This increase of albumin was the most dominant for L-*hb*PG after centrifugation and for L-un after AF4. Also, the amount of Apolipoprotein AI (Apo AI) increased for all samples and especially for L-*hb*PG after AF4. Depending on the preparation of the corona, however, differences that are more significant were obtained concerning the protein fractions. Most prominent are the changes regarding coagulation and tissue leakage proteins, which were significantly increased after centrifugation compared to AF4. Two proteins, which stand out are the histidine-rich glycoprotein and coagulation factor XII which are tremendously enriched after centrifugation for L-*hb*PG. On the other hand, immunoglobulins, albumin and acute phase proteins were more abundant after AF4. In general, immunoglobulins and albumin are mostly known as proteins with lower binding affinities and therefore part of the soft protein corona, which is supported by our data. Previously, for different kinds of PEGylated nanomaterials an enrichment of lipoproteins was reported,[42, 147] which surprisingly was not the case for the PEGylated liposome samples. Also, the functionalization with *hb*PG did not result in an attraction of apolipoproteins besides Apo AI although the monomer building blocks are in principle similar to PEG. It seems that for the here introduced liposomal system, the different surface functionalizations did not significantly change the properties of the surface with regard to the protein interaction. Instead, the hydrophilic base material forming the membranes (phospholipids and cholesterol) apparently was mainly responsible for determining the biological identity.

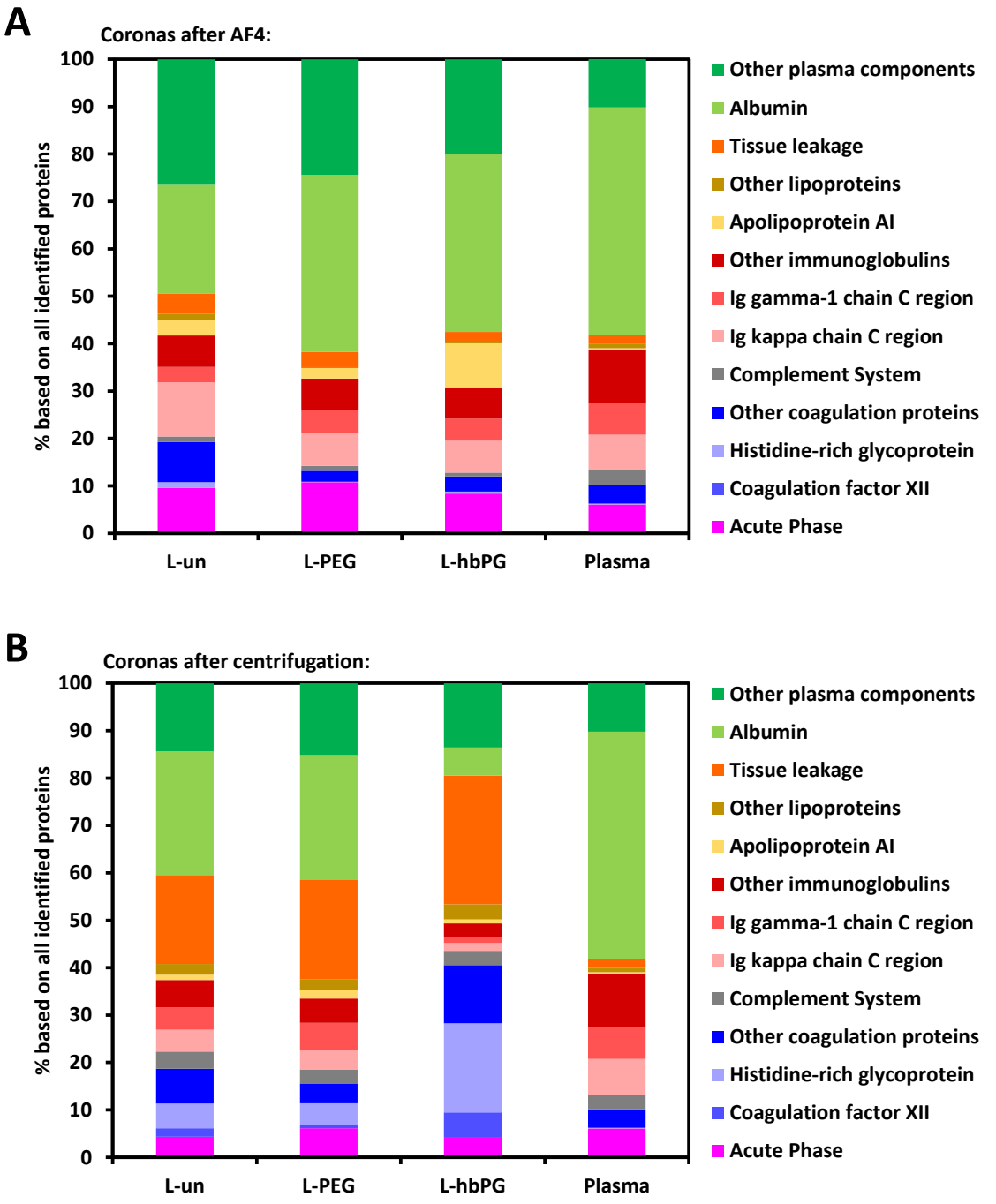

Figure 4.17: MS data of the protein corona. A shows the coronas of the different liposomes after AF4, compared to plasma and B shows the same for the coronas after centrifugation. Significant proteins are displayed individually.

To make sure that the corona obtained after AF4 can indeed be compared with the one obtained after centrifugation, it is important to exclude the chance that the observed corona proteins are just coeluting with the liposomes. In this respect, an assay was conducted, in which a fluorescently labeled Fab fragment selective for the Fc part of Immunoglobulin G (IgG) was incubated with the liposome-protein mixtures after AF4 and after centrifugation to form complexes with a specific

protein of the protein corona. Only if the selected proteins are actually attached on the liposome's surface, the formed complex of liposome, protein and labeling agent is large enough to then be detected by flow cytometry (Figure 4.18A). For this test, executed by Dr. Johanna Simon (MPIP Mainz, Germany), IgG was chosen as the to be tested protein, since it was found as a highly abundant component in all coronas. The results are demonstrated in Figure 4.18B. The fluorescence signal of the fluorescently labeled anti-IgG-antibody fragment is directly proportional to the number of liposomes with IgG in the corona. From the results it can be confirmed that the investigated proteins were constituents of the corona after centrifugation and AF4, but also that the amount of the immunoglobulins after AF4 was significantly higher. This is in good agreement with the results of the LC-MS experiment (Figure 4.17). Therefore, we conclude that the Immunoglobulin G were indeed part of the liposomal protein corona for all samples and that the obtained protein pattern is not a result of a coelution effect.

Additionally, the corona formation around the liposomes was visualized with TEM by Dr. Maria Kokkinopoulou (MPIP Mainz, Germany) as previously described by Kokkinopoulou *et al*,[124] see Figure 4.18C. The spherical liposome structure was preserved during the centrifugation process, which is not universally valid for all liposomes. The here used liposomes were comparably stable because of the high amount of cholesterol that was incorporated into the lipid membrane. When zoomed-in into the sample, even the protein corona itself could be observed as indicated by the red arrows.

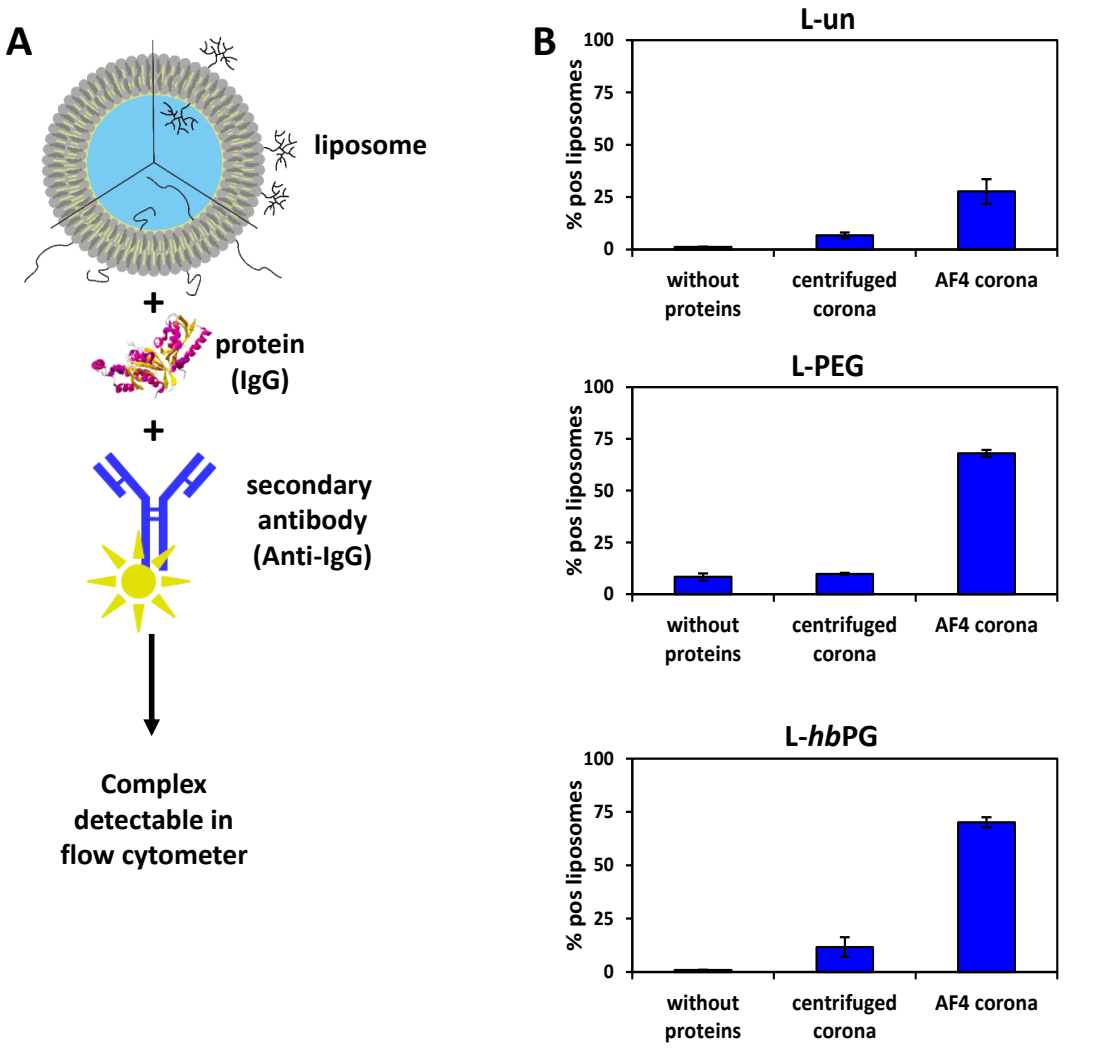

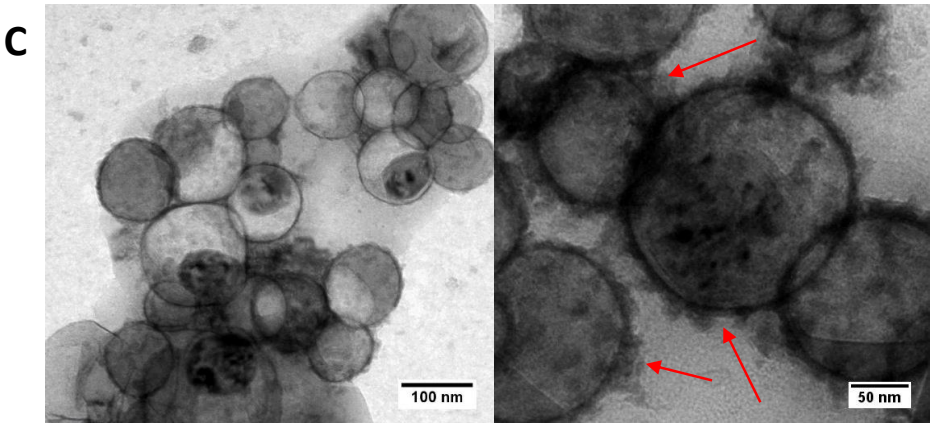

Figure 4.18: (A) Schematic illustration of the experimental design. (B) Liposomes were incubated with human plasma for 1 h. Protein coated liposomes were either centrifuged to remove unbound proteins or applied to AF4. Secondary fluorescent labeled anti-human IgG antibodies were incubated with liposomes for 30 min in the dark. The fluorescence intensity of secondary fluorescently labeled antibodies, which were bound to liposomes, was detected by flow cytometry. (C) TEM micrograph with two magnifications of liposomes incubated with plasma after centrifugation. Arrows indicate protein corona formation.

4.2.4 Cellular uptake and stealth behavior of differently functionalized liposomes

Since the protein coronas were quite similar for all liposome samples with only L-*hb*PG showing slight deviations, the influence of the different surface functionalizations on the cellular uptake by macrophages (RAW264.7) was investigated. When the macrophage uptake decreases, the drug carrier will not be cleared out as rapidly by the immune system and therefore potentially has a longer blood circulation time, making it more probable that the drug carrier reaches its target location in the body.[148, 149]

In Figure 4.19A, the cell uptake results, obtained from flow cytometry measurements, performed by Dr. Johanna Simon (MPIP Mainz, Germany), after 2 and 24 h incubation for all liposome samples (7.5 µg mL^{-1}) are represented. For the formation of the protein corona, different plasma concentrations (0, 5 and 100%) were chosen to detect any concentration dependency, as it was already observed by Monopoli *et al.* for different systems.[150] Interestingly, when first comparing the liposome uptake behavior with and without protein corona, there is no significant change visible. After 2 h incubation time, the number of positive cells was generally very low (<10%). Liposomes functionalized with PEG-chains (L-PEG) showed an even lower cellular uptake than the other two samples, even though their protein corona composition did only differ slightly. After 24 h, the uptake was increased for all samples, but most prominently for L-*hb*PG. Additional cell experiments using a higher liposome concentration (75 µg mL^{-1}, Figure 4.19B) confirmed the presented results (Figure 4.19A) and confocal laser scanning microscopy images verified the intracellular localization of the liposomes with protein corona (Figure 4.19C). To sum up, the hyperbranched polyglycerol did not lead to a reduced cell uptake even though the attached chains are very hydrophilic. In contrast to the PEG functionalization, which ends with methoxy endgroups, the endgroups of the *hb*PG chains are hydroxyl groups, which in this system seem to mediate a stronger cellular internalization into macrophages. The observed reduction in cellular uptake for L-PEG is generally in line with other reports for reduced unspecific uptake of PEGylated materials, but is in this case clearly not a result of the protein corona composition. Thus, we conclude that even though protein adsorption takes place on the liposomes the underlying material still plays a crucial role in the biological response. This might be due to the fact that the base material is composed of hydrophilic, biocompatible molecules and that the general amount of proteins adsorbed is very low compared to other nanomaterials.

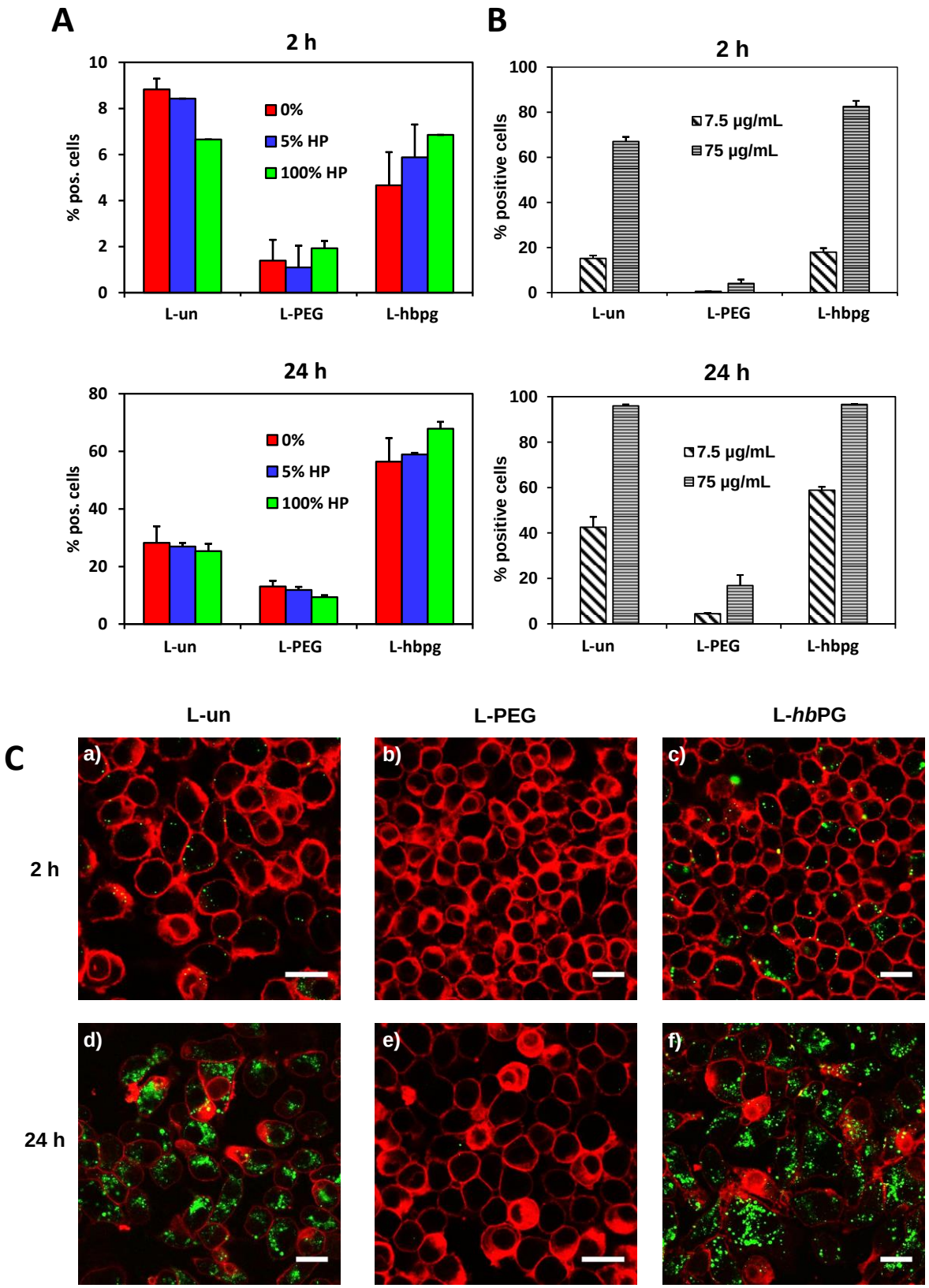

Figure 4.19: (A) Influence of protein corona formation on the cellular uptake behavior of liposomes. Liposomes were either directly incubated with RAW 264.7 cells (referred to as 0%) or pre-incubated with human plasma (5% or 100%) and further added to cells at a concentration 7.5 µg mL^{-1}. Cellular interaction was analyzed by flow cytometry after 2 h and 24 h. The amount of fluorescent positive cells (%) is shown. (B) Cellular uptake of differently functionalized

liposomes in different concentrations into RAW 264.7 cells. The overall trend of the cell uptake is the same for different concentrations. (C) Representative confocal laser scanning microscopy images. Liposomes were treated with 100% human plasma and incubated with RAW 264.7 cells for 2 h or 24 h at a concentration of 75 µg mL^{-1}. The cell membrane was stained with CellMask Deep Red and is pseudo-colored in red. Liposomes are pseudo-colored in green. Scale bar: 20 µm.

4.2.5 Conclusion

As the investigation of the protein corona is important in the context of using liposomes in nanomedicine, we focused our work on the analysis of different separation techniques and the biological response. The used liposomes were synthesized via dual centrifugation, which appears to be an easy and reproducible way for monodisperse liposome synthesis. We could confirm that AF4 is a valuable method to analyze the soft protein corona for liposomes, but also that the presence of proteins for the tested system has no influence on the cellular uptake. The protein corona composition differed only slightly for different surface functionalizations, but those different functional groups, PEG and *hb*PG, did change the uptake behavior in macrophages. The ‘stealth’ effect valid for PEG could not be confimed for *hb*PG in this work.

4.3 Evaluation of the “negative” biomolecule corona

According to the standard procedure of investigating the protein corona, proteins that are actually attached to nanocarriers are analyzed.[37, 38] However, with that approach, the influence of the nanomaterial on the unbound proteins and other biomolecules remains unclear. The contact to the nanomaterial might alter the nature of proteins, even if they do not adsorb to the nanocarriers and lead to aggregation, denaturation or rearrangement of biomolecules. Since the supernatant containing all molecules that did not adsorb to the nanocarriers is usually discarded in the normal protein corona analysis, this information was inaccessible so far. Moreover, protein corona formation should lead to a depletion of individual components in the plasma after being adsorbed to the nanocarriers and consequently the remaining protein composition in the supernatant could be analyzed to elucidate whether this depletion is significant. However, this is only possible, if the concentration decrease of certain proteins is significant and not covered by the plasma excess. Therefore, a method is needed to investigate the biological impact of nanomaterials from a different perspective, focusing on the characterization of the biological medium itself after the interaction with nanomaterials. Thus, the nanocarriers with their formed protein corona have to be removed from the medium so that subsequently the remaining supernatant is analyzed. Theoretically, the main proteins (and other biomolecules) that remain attached to the nanocarriers could then be identified by investigating the composition of the supernatant: the “negative” of the protein corona. However, when it comes to blood plasma, due to its complexity and usually the large excess of biomolecules, analyzing the whole supernatant solution at once is extremely difficult.

A potential approach to separate the complex biomolecule mixture according to hydrodynamic size of the different blood plasma fractions is the use of AF4.[53] The separation of plasma was already executed by AF4, however with a focus on specific protein groups (especially lipoproteins) only.[151-154] With this separation step prior to analysis, a better insight in the protein composition is enabled since every size fraction can be analyzed individually. A crucial factor for a successful separation by AF4 is the choice of the right separation parameters like the carrier liquid, the used membrane, etc. When species of different chemical nature (e.g. polymeric nanomaterials and proteins, see chapter 4.1) are analyzed, determining the optimum parameters is not trivial and usually a compromise must be found. By first removing the nanocarrier-protein complexes from the medium, all the remaining species for the separation are biomolecules, which facilitates the method optimization tremendously. The separation and fractionation by AF4 then enable a detailed investigation of the “negative” biomolecule corona components.

4.3.1 Characterization of the used silica nanocapsules

In this study, the aim was to analyze the plasma supernatant after incubation with nanocarriers and thereby to gain information about proteins adsorbed to the nanocarrier and changes occurring to the free proteins. Silica nanocapsules (SiNCs) stabilized with the poly(ethylene glycol) (PEG)-based surfactant Lutensol AT50 synthesized by Dr. Shuai Jiang (MPIP Mainz, Germany) were used for this purpose, since they offer several advantages as drug carriers: (i) Their interior cavity offers a larger loading capacity for cargo, (ii) their shell can be designed to have a tunable permeability for a controlled cargo release, and (iii) further grafting of functional ligands due to the versatile silica chemistry is possible. The nanocapsule morphology was confirmed by electron microscopy (see Figure 4.20A and B) as well as by the ρ-ratio value (R_g/R_h) of 1.1 obtained from static and dynamic light scattering experiments (Table 4.2, a ρ-ratio of 1 represents a hollow sphere). In Figure 4.20C an exemplary autocorrelation function together with the distribution of relaxation times is shown for a scattering angle of 90°. Further physico-chemical characteristics of the NCs are given in Table 4.2.

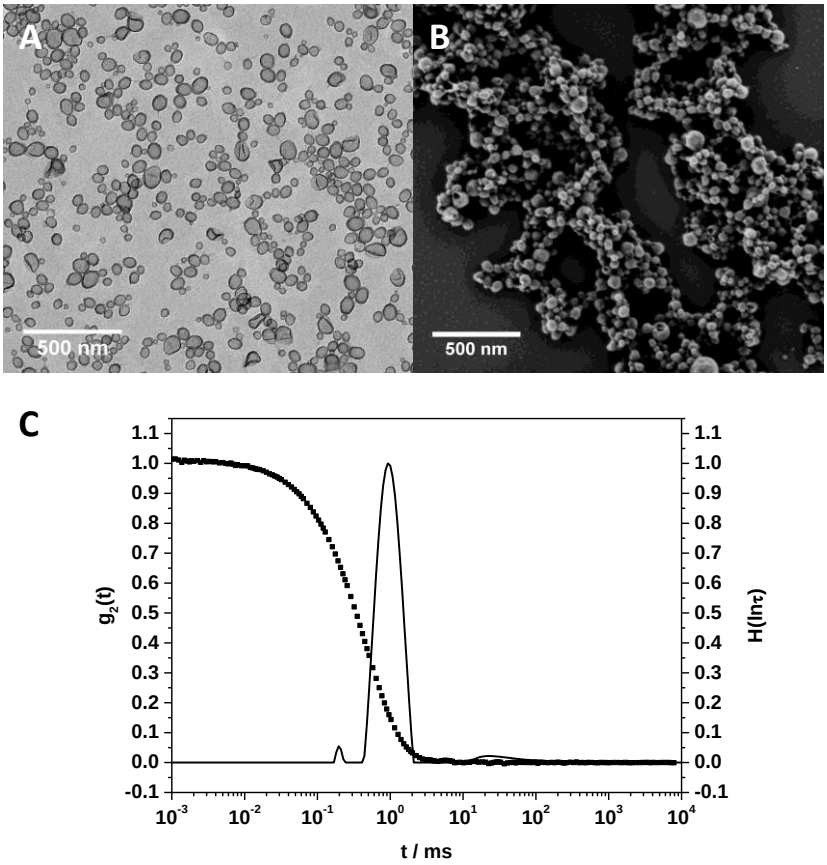

Figure 4.20: TEM (A) and SEM (B) micrographs of the used SiNCs. DLS measurement (C), displaying the autocorrelation function of the SiNCs and the distribution function of the decay time. The results were obtained with the CONTIN algorithm and are displayed exemplary for the scattering angle of 90°.

Table 4.2: Physico-chemical characteristics of SiNCs.

Shell material	silica
Core	aqueous
Surfactant	Lutensol AT50
R_h / nm	85 ± 9
R_g / nm	99 ± 10
ρ-ratio	1.1
PDI[a]	0.229
ζ-potential	-3 ± 1

[a] *The cumulant analysis of the autocorrelation function at a scattering angle of 90° reveals the given PDI*

4.3.2 Analyis of the protein corona and its supernatant

To form the protein corona, SiNCs were incubated in plasma, which was diluted in phosphate buffered saline (PBS) to obtain a final plasma concentration of 5 vol%. For the characterization of the supernatant it was important to choose a low protein concentration, because only then small differences in the composition generated by the removal of the protein corona will be detectable. Moreover, the quality of the subsequent separation by AF4 cannot be guaranteed for an overloaded system. After the incubation in plasma, the SiNCs with the adsorbed protein corona were separated by one centrifugation step. These supernatants were used in later measurements. First, the normal protein corona was prepared and analyzed after three subsequent washing steps of the pellet. The protein corona composition, as well as the supernatant containing unbound proteins and the supernatant after the first washing step were analyzed by SDS-PAGE (Figure 4.21A). As a control, the same procedure was applied to the pristine plasma without any NCs (“protein corona plasma” = washing off the proteins adsorbed only to the vial walls, Figure 4.21B). This has to be taken into account to ensure that protein adsorption in the vials does not lead to an altered “negative” corona pattern. The proteins found in the corona of the particle should generally be depleted in the supernatant. The prominent band in the supernatant at around 67 kDa representing human serum albumin (HSA) was only present in the protein corona in small amounts (red square, Figure 4.21A). In contrast, the bands at ca. 28 kDa and 49 kDa (green squares) represent proteins enriched in the protein corona compared to the supernatant. However, when looking at the supernatant, it becomes clear that the resolution of the SDS-PAGE was too low to evaluate the protein pattern in a meaningful way. The washing steps for the sample and the control show HSA as the main protein. Interestingly, for the plasma control, some protein adsorption at the vial walls was detected, which resulted in the occurrence of mainly HSA as well as some other proteins after washing the empty

vial with PBS (Figure 4.21B). However, this adsorption seems to unspecifically resemble the overall plasma protein pattern so that an interference with the negative corona could be excluded.

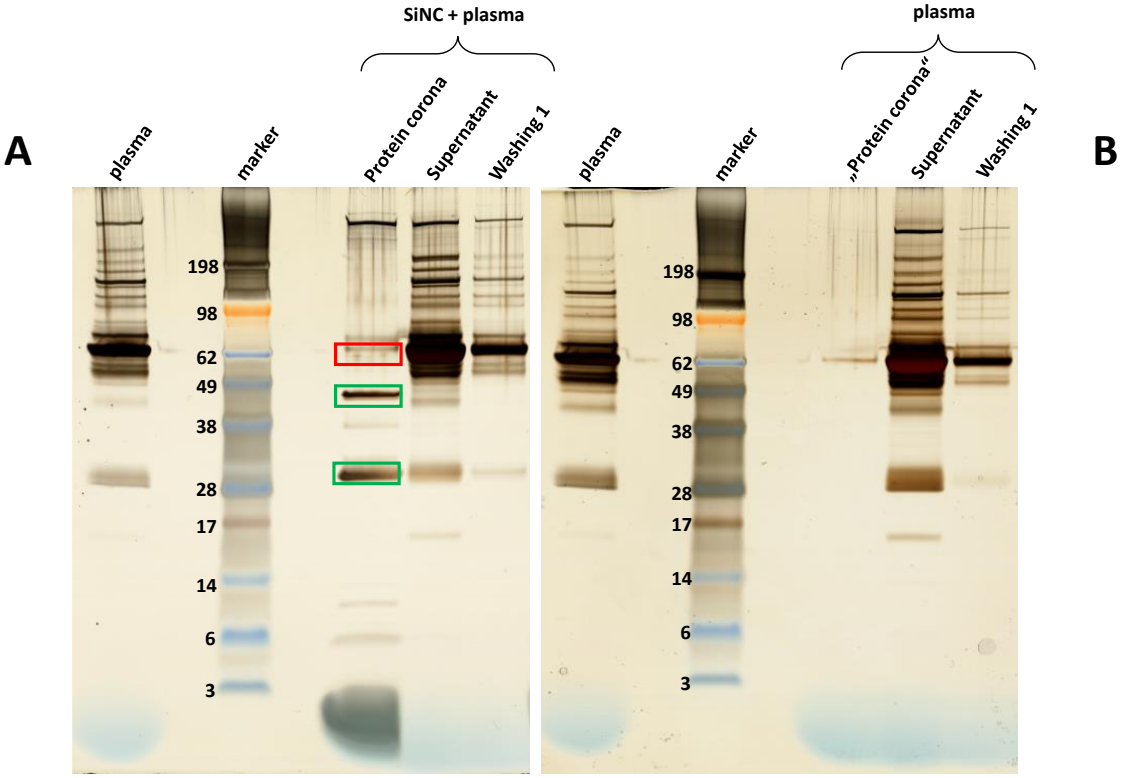

Figure 4.21: SDS-PAGE gels: (A) SiNC protein corona, the supernatant after centrifugation without separation by AF4 and the supernatant of the first washing step. Red square indicate protein which are enriched in the plasma control, while the green squares refer to proteins enriched in the protein corona. (B) Respective plasma control after centrifugation.

Since the resolution of the SDS-PAGE was very low and individual proteins could not be identified, the samples were additionally analyzed by liquid chromatography-mass spectrometry (LC-MS, Figure 4.22 and Figure 4.23). The detailed analysis of the composition of the protein corona and the plasma control after centrifugation are displayed in Figure 4.22. The LC-MS results are in good agreement with the results already obtained by SDS-PAGE, but also provide some more detailed information. The following LC-MS experiemtns were performed by Dr. Johanna Simon (MPIP Mainz, Germany). As already suggested, the main protein of the corona was identified to be apolipoprotein A-I (Apo AI), which corresponds to the 28 kDa band seen in the SDS-PAGE. In general, apolipoproteins seem the be enriched in the corona with apolipoprotein A-IV being another prominent protein, while HSA is only present with about 6%. In contrast, in the corresponding plasma control (protein corona preparation without NCs), only unspecific adsorption to the vial occurred, as it was already determined via SDS-PAGE. It has to be noted that the LC-MS data are normalized to 100%.

Protein class	Description	Protein corona after centrifugation	
		SiNC + plasma	Plasma control
Acute Phase	Alpha-1-acid glycoprotein 1	0.15	0.56
Acute Phase	Alpha-1-antitrypsin	0.70	0.47
Acute Phase	Haptoglobin	0.54	0.80
Acute Phase	Haptoglobin-related protein	2.52	5.73
Acute Phase	Lipopolysaccharide-binding protein	0.74	0.02
Coagulation	Fibrinogen alpha chain	0.15	1.15
Coagulation	Fibrinogen beta chain	0.24	0.60
Coagulation	Fibrinogen gamma chain	0.22	0.63
Coagulation	Histidine-rich glycoprotein	6.50	0.60
Complement system	Complement C3	0.79	1.34
Immunoglobulins	Ig alpha-1 chain C region	0.66	0.29
Immunoglobulins	Ig gamma-1 chain C region	1.32	2.09
Immunoglobulins	Ig gamma-2 chain C region	0.65	0.43
Immunoglobulins	Ig kappa chain C region	3.40	2.92
Immunoglobulins	Ig lambda-2 chain C regions	1.04	0.81
Immunoglobulins	Ig mu chain C region	2.49	0.70
Immunoglobulins	Immunoglobulin J chain	1.33	7.54
Lipoproteins	Apolipoprotein A-I	29.32	1.18
Lipoproteins	Apolipoprotein A-II	0.63	0.09
Lipoproteins	Apolipoprotein A-IV	8.46	2.14
Lipoproteins	Apolipoprotein B-100	2.09	0.18
Lipoproteins	Apolipoprotein D	1.04	0.06
Lipoproteins	Apolipoprotein E	9.93	1.03
Lipoproteins	Apolipoprotein L1	4.77	1.06
Lipoproteins	Clusterin	0.57	0.73
Lipoproteins	Serum paraoxonase/arylesterase 1	2.00	0.24
Other Plasma components	Cathepsin L2	0.08	1.25
Other Plasma components	Complement C1q tumor necrosis factor-related protein 4	0.05	0.78
Other Plasma components	Dynein regulatory complex protein 1	0.34	0.64
Other Plasma components	FGFR1 oncogene partner 2	0.35	2.98
Other Plasma components	Myristoylated alanine-rich C-kinase substrate	1.18	0.18
Other Plasma components	Protein MEMO1	0.10	0.86
Other Plasma components	Ras-related protein Rab-32	0.14	0.56
Other Plasma components	RNA binding motif protein, X-linked-like-1	0.12	0.54
Other Plasma components	Serotransferrin	0.31	1.11
Other Plasma components	Serum albumin	6.36	38.10
Other Plasma components	Talanin	1.62	13.84
Other Plasma components	Uncharacterized protein C16orf46	1.14	0.01
Other Plasma components	Uncharacterized protein C19orf43	0.13	0.80

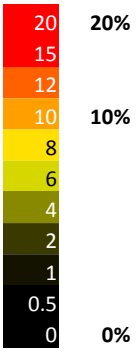

Figure 4.22: LC-MS heat map showing the abundance of individual proteins of the protein corona of SiNCs and the corresponding plasma control (same preparation without SiNCs). All proteins with an abundance above 0.5% are displayed.

The LC-MS analysis of the supernatants after protein corona formation together with the plasma control are shown in Figure 4.23. In this case, the most obvious difference in the protein composition also concerns the presence of HSA. Only 11% of the plasma control were HSA, because a significant fraction of the protein was attached to the surface of the vial, as observed for the protein corona control in Figure 4.22. In contrast, high amounts of HSA were found in the plasma supernatant of the SiNCs (28%, Figure 4.23). This high amount in the supernatant indicates, that probably low amounts of HSA adsorbed to the nanocapsules. Most of the other differences in the composition of the supernatant are rather small. The data evaluation was again difficult, because

the displayed heat maps give relative protein amounts, which refer to the sum of all identified proteins.

Protein class	Description	Supernatant after centrifugation	
		SiNC + plasma	Plasma control
Acute Phase	Alpha-1-acid glycoprotein 1	0.82	0.93
Acute Phase	Alpha-1-antichymotrypsin	0.53	0.76
Acute Phase	Alpha-1-antitrypsin	1.72	0.74
Acute Phase	Alpha-2-macroglobulin	1.62	2.39
Acute Phase	Ceruloplasmin	0.56	0.64
Acute Phase	Fibronectin	0.48	0.62
Acute Phase	Haptoglobin	1.53	1.23
Coagulation	Fibrinogen alpha chain	1.25	1.30
Coagulation	Fibrinogen beta chain	3.58	3.94
Coagulation	Fibrinogen gamma chain	1.31	0.78
Coagulation	Histidine-rich glycoprotein	0.40	0.87
Coagulation	Kininogen-1	0.75	0.64
Complement system	Complement C3	2.78	3.34
Complement system	Complement C4-B	0.56	0.66
Complement system	Complement factor H	0.48	0.51
Immunoglobulins	Ig alpha-1 chain C region	0.95	1.11
Immunoglobulins	Ig gamma-1 chain C region	6.33	8.25
Immunoglobulins	Ig gamma-2 chain C region	1.50	1.05
Immunoglobulins	Ig gamma-3 chain C region	0.52	0.49
Immunoglobulins	Ig gamma-4 chain C region	0.67	0.66
Immunoglobulins	Ig kappa chain C region	8.37	9.87
Immunoglobulins	Ig mu chain C region	1.78	2.74
Immunoglobulins	Immunoglobulin lambda-like polypeptide 5	1.10	1.51
Lipoproteins	Apolipoprotein A-I	0.50	0.71
Lipoproteins	Apolipoprotein A-IV	2.31	2.87
Lipoproteins	Apolipoprotein B-100	1.28	1.54
Lipoproteins	Beta-2-glycoprotein 1	0.49	0.52
Lipoproteins	Clusterin	0.57	0.54
Other Plasma components	3 beta-hydroxysteroid dehydrogenase/Delta 5-->4-isomerase type 1	0.45	0.58
Other Plasma components	Alpha-2-HS-glycoprotein	0.97	1.00
Other Plasma components	Angiotensinogen	0.51	0.55
Other Plasma components	Bifunctional 3'-phosphoadenosine 5'-phosphosulfate synthase 1	1.60	0.53
Other Plasma components	Carbonic anhydrase 3	0.56	0.75
Other Plasma components	Cytosolic 5'-nucleotidase 1A	0.67	1.25
Other Plasma components	Hemopexin	0.63	0.79
Other Plasma components	Interleukin-18	1.61	1.23
Other Plasma components	Kin of IRRE-like protein 3	3.09	6.30
Other Plasma components	Negative elongation factor E	0.50	0.50
Other Plasma components	Pre-mRNA 3'-end-processing factor FIP1	0.71	0.69
Other Plasma components	Protein FAM122A	0.59	0.80
Other Plasma components	Putative cancer susceptibility gene HEPN1 protein	0.55	1.19
Other Plasma components	Reticulocalbin-2	0.06	0.50
Other Plasma components	Selenoprotein M	0.45	5.49
Other Plasma components	Serotransferrin	1.79	1.61
Other Plasma components	Serum albumin	27.93	10.99
Other Plasma components	Tetratricopeptide repeat protein 1	1.91	2.32
Other Plasma components	Uncharacterized protein C15orf53	0.31	0.56
Other Plasma components	Vitamin D-binding protein	2.41	2.38
Other Plasma components	Zinc-alpha-2-glycoprotein	0.42	0.58

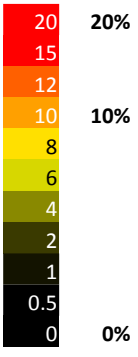

Figure 4.23: LC-MS heat map showing the abundance of individual proteins of supernatant of the sample and the corresponding plasma control (same preparation without SiNCs). All proteins with an abundance above 0.5% are displayed.

4.3.3 Separation of the “negative corona” into smaller entities by AF4

Subsequently, the obtained plasma supernatant (after protein corona formation and removal of the NC-protein complexes) was injected into the AF4 separation channel and the plasma components were separated according to their hydrodynamic volume. As a control measurement, the same preparation was applied to pristine plasma (incubation and centrifugation without NCs) and the obtained sample separated by AF4 for comparison. In both cases, the separation was performed in PBS, which represents the ideal separation conditions for proteins because of a salt composition similar to blood plasma.

In Figure 4.24A, the UV and RI signals of the two corresponding AF4 chromatograms are displayed together with an indication of seven fractions (grey boxes) collected for further analysis. In fraction 1, 2, 3, and 6 a reproducible difference in the elution profiles of the supernatant after incubation with the SiNCs compared to the plasma control was observed. Comparing the UV signal to the RI elugram of the same run, differences in the elution profile were visible. This is due to the fact that the UV signal is not only proportional to the concentration of the analyte, but also to the UV activity. Different proteins show different UV activities and additionally to the proteins, other biomolecules are being detected as well. The presence of lipids, cholesterol, etc. also explains why the protein amount of the fractions (see Figure 4.24B) does not fully correspond to the signal intensity in the respective AF4 elugrams. Comparing the protein amounts of the different collected fractions, no significant changes between the plasma control and the supernatant after incubation can be detected. Only in fraction 3 a reduced protein amount in the supernatant can be detected, which however could also be a result of the overall very low protein amount and cannot be interpreted reliably. Most likely, the amount of proteins contributing to the corona only constitutes a small part of the entire protein amount of the sample. The overall protein recovery after AF4 for the runs displayed in figure 5 was 72% for the plasma control and 63% for the supernatant of SiNC incubated with plasma.

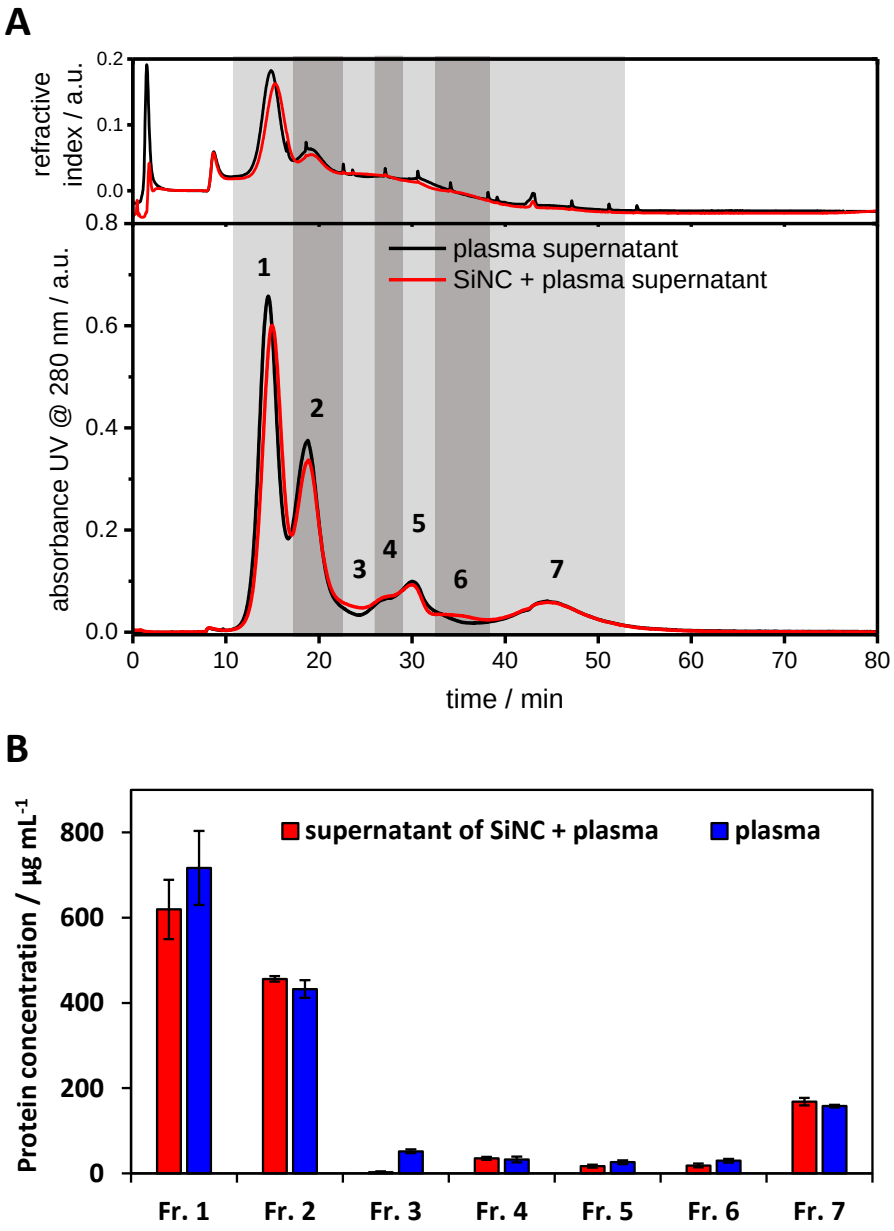

Figure 4.24: (A) AF4 elugrams of the separation of the supernatant of SiNCs incubated with plasma (red) and the plasma control (black). The top graph shows the RI signal and the lower graph the UV signal. The collected fractions are indicated by the grey boxes. (B) Protein concentration determined for the corresponding fractions collected after AF4.

From the AF4 elugrams the question arises, how strictly different proteins could be separated from each other and to which extent changes in the protein pattern could be identified after removal of the protein corona proteins. Therefore, the next step was the SDS-PAGE analysis of the proteins in the collected fractions (Figure 4.25). Some differences for the "negative" corona sample and the plasma control were observed: The bands at 17 kDa, 28 kDa and 49 kDa in fraction 2-4 are more prominent in the plasma control while the band at 28 kDa, corresponding to Apo AI, is even completely missing in fraction 3 of the sample and seems to be shifted to fraction 4. Fraction 7

shows a more complex composition for the plasma control, but also fraction 5 and 6 display a broader variety of different proteins in the high molecular range than the sample of plasma after SiNC contact. The proteins of the corona should in principle correspond to those missing in the supernatant after centrifugation and AF4 separation. Additionally, the proteins found in the supernatant after centrifugation (Figure 4.23) should be the sum of all proteins detected in the fractions after AF4 (Figure 4.25). Generally, for SDS-PAGE analysis 1 µg of protein is applied to the gel, however, in fraction 3, 5 and 6 of the “negative” corona and fraction 3-6 of the plasma control the final amount of 1 µg could not be achieved due to the volume limitation of the pockets in the gel.

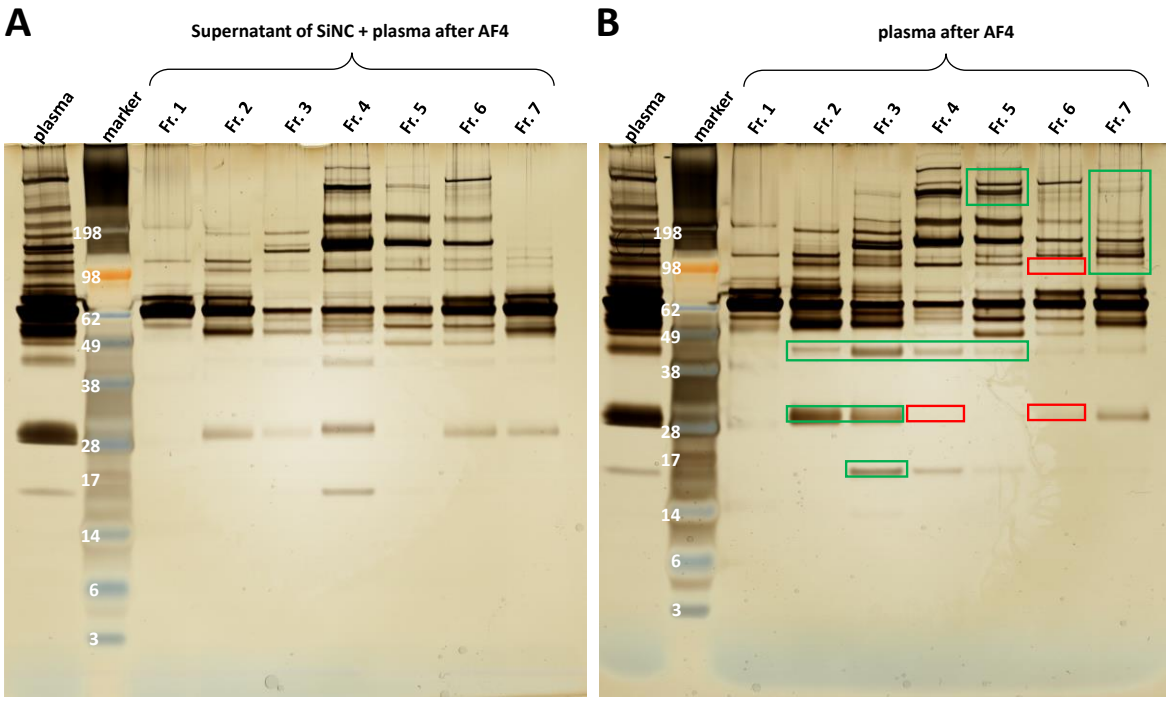

Figure 4.25: SDS-PAGE gels of the fractions (Fr. 1-7) collected during AF4 separation. (A) Supernatant of SiNCs incubated with plasma, (B) plasma control. Pure plasma is shown in the first lane as a reference in both cases.

To obtain further insight into the detailed protein compositions of each fraction, again LC-MS measurements were conducted (Figure 4.26). Similar to the SDS-PAGE analysis, distinct differences between the injected supernatant of the SiNCs and the plasma control were found. Certain proteins were enriched in the supernatant after removal of the protein corona, while others were depleted. The proteins with the strongest enrichment were complement C3, immunoglobulin mu chain C region, Apo AI and apolipoprotein A-II, while haptoglobin, immunoglobulin lambda-like polypeptide 5, HSA and zinc-alpha-2-glycoprotein were enriched in the plasma control. Since Apo AI was found as the main component in the SiNC protein corona, it seems surprising at a first glance that there should be an enrichment of Apo AI in the supernatant, too. Here again, the relative

protein amounts given (normalized to 100%) complicate the data evaluation and therefore, care must be taken when interpreting the data.

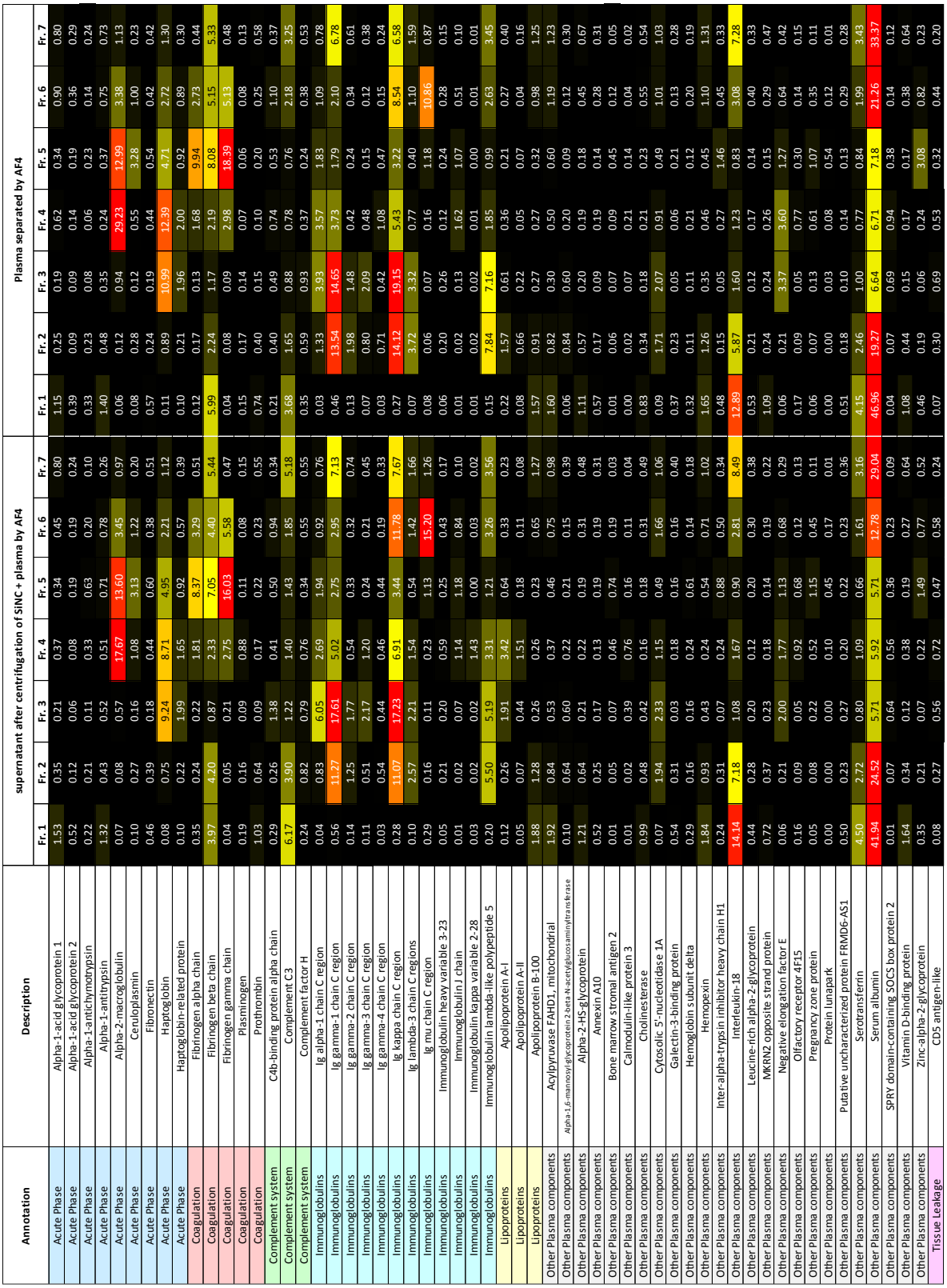

Annotation	Description	supernatant after centrifugation of SiNC + plasma by AF4							Plasma separated by AF4						
		Fr. 1	Fr. 2	Fr. 3	Fr. 4	Fr. 5	Fr. 6	Fr. 7	Fr. 1	Fr. 2	Fr. 3	Fr. 4	Fr. 5	Fr. 6	Fr. 7
Acute Phase	Alpha-1-acid glycoprotein 1	1.53	0.35	0.21	0.37	0.34	0.45	0.80	1.15	0.25	0.19	0.62	0.34	0.90	0.80
Acute Phase	Alpha-1-acid glycoprotein 2	0.52	0.12	0.06	0.08	0.19	0.19	0.24	0.39	0.09	0.09	0.14	0.19	0.36	0.29
Acute Phase	Alpha-1-antichymotrypsin	0.22	0.21	0.11	0.33	0.63	0.20	0.10	0.33	0.23	0.08	0.06	0.23	0.14	0.24
Acute Phase	Alpha-1-antitrypsin	1.32	0.43	0.52	0.51	0.71	0.78	0.26	1.40	0.48	0.35	0.24	0.37	0.75	0.73
Acute Phase	Alpha-2-macroglobulin	0.07	0.08	0.57	17.67	13.60	3.45	0.97	0.06	0.12	0.94	29.23	12.99	3.38	1.13
Acute Phase	Ceruloplasmin	0.10	0.27	0.16	1.08	3.13	1.22	0.20	0.08	0.28	0.12	0.55	3.28	1.00	0.23
Acute Phase	Fibronectin	0.46	0.39	0.18	0.44	0.60	0.38	0.51	0.57	0.24	0.19	0.44	0.54	0.42	0.42
Acute Phase	Haptoglobin	0.08	0.75	9.24	8.71	4.95	2.21	1.12	0.11	0.89	10.99	12.39	4.71	2.72	1.30
Acute Phase	Haptoglobin-related protein	0.10	0.22	1.99	1.65	0.92	0.57	0.39	0.10	0.21	1.96	2.00	0.92	0.89	0.30
Coagulation	Fibrinogen alpha chain	0.35	0.24	0.22	1.81	8.37	3.29	0.51	0.12	0.17	0.13	1.68	9.94	2.73	0.44
Coagulation	Fibrinogen beta chain	3.97	4.20	0.87	2.33	7.05	4.40	5.44	5.99	2.24	1.17	2.19	8.08	5.15	5.33
Coagulation	Fibrinogen gamma chain	0.04	0.05	0.21	2.75	16.03	5.58	0.47	0.04	0.08	0.09	2.98	18.39	5.13	0.48
Coagulation	Plasminogen	0.19	0.16	0.09	0.88	0.11	0.08	0.15	0.15	0.17	0.14	0.07	0.06	0.08	0.13
Coagulation	Prothrombin	1.03	0.64	0.09	0.17	0.22	0.23	0.55	0.74	0.40	0.15	0.10	0.20	0.25	0.58
Complement system	C4b-binding protein alpha chain	0.29	0.26	1.38	0.41	0.50	0.94	0.34	0.21	0.40	0.49	0.74	0.53	1.10	0.37
Complement system	Complement C3	6.17	3.90	1.22	1.40	1.43	1.85	5.18	3.68	1.65	0.88	0.78	0.76	2.18	3.25
Complement system	Complement factor H	0.24	0.82	0.79	0.76	0.34	0.55	0.55	0.35	0.59	0.93	0.37	0.24	0.38	0.53
Immunoglobulins	Ig alpha-1 chain C region	0.04	0.83	6.05	2.69	1.94	0.92	0.76	0.03	1.33	3.93	3.57	1.83	1.09	0.78
Immunoglobulins	Ig gamma-1 chain C region	0.56	11.27	17.61	5.02	2.75	2.95	7.13	0.46	13.54	14.65	3.73	1.79	2.10	6.78
Immunoglobulins	Ig gamma-2 chain C region	0.14	1.25	1.77	0.54	0.33	0.32	0.74	0.13	1.98	1.48	0.42	0.24	0.34	0.61
Immunoglobulins	Ig gamma-3 chain C region	0.11	0.51	2.17	1.20	0.24	0.21	0.45	0.07	0.80	2.09	0.48	0.15	0.12	0.38
Immunoglobulins	Ig gamma-4 chain C region	0.03	0.54	0.44	0.46	0.44	0.19	0.33	0.03	0.71	0.42	1.08	0.47	0.15	0.24
Immunoglobulins	Ig kappa chain C region	0.28	11.07	17.23	6.91	3.44	11.78	7.67	0.27	14.12	19.15	5.43	3.22	8.54	6.58
Immunoglobulins	Ig lambda-3 chain C regions	0.10	2.57	2.21	1.54	0.54	1.42	1.66	0.07	3.72	3.32	0.77	0.40	1.10	1.59
Immunoglobulins	Ig mu chain C region	0.29	0.16	0.11	0.23	1.13	15.20	1.26	0.08	0.06	0.07	0.16	1.18	10.86	0.87
Immunoglobulins	Immunoglobulin heavy variable 3-23	0.05	0.21	0.20	0.59	0.25	0.43	0.17	0.06	0.20	0.26	0.12	0.24	0.28	0.15
Immunoglobulins	Immunoglobulin J chain	0.01	0.02	0.07	1.14	1.18	0.84	0.10	0.01	0.02	0.13	1.62	1.07	0.51	0.10
Immunoglobulins	Immunoglobulin kappa variable 2-28	0.03	0.02	0.02	1.43	0.00	0.03	0.02	0.01	0.02	0.02	0.01	0.00	0.01	0.01
Immunoglobulins	Immunoglobulin lambda-like polypeptide 5	0.20	5.50	5.19	3.31	1.21	3.26	3.56	0.15	7.84	7.16	1.85	0.99	2.63	3.45
Lipoproteins	Apolipoprotein A-I	0.12	0.26	1.91	3.42	0.64	0.33	0.23	0.22	1.57	0.61	0.36	0.21	0.27	0.40
Lipoproteins	Apolipoprotein A-II	0.05	0.07	0.44	1.51	0.18	0.11	0.08	0.08	0.66	0.22	0.05	0.07	0.04	0.16
Lipoproteins	Apolipoprotein B-100	1.88	1.28	0.26	0.26	0.23	0.65	1.27	1.57	0.91	0.27	0.27	0.32	0.98	1.25
Other Plasma components	Acylpyruvase FAHD1, mitochondrial	1.92	0.84	0.53	0.37	0.46	0.75	0.98	1.60	0.82	0.30	0.50	0.60	1.19	1.23
Other Plasma components	Alpha-1,6-mannosyl-glycoprotein 2-beta-N-acetylglucosaminyltransferase	0.10	0.64	0.60	0.22	0.21	0.15	0.39	0.06	0.84	0.60	0.20	0.09	0.12	0.30
Other Plasma components	Alpha-2-HS-glycoprotein	1.21	0.64	0.21	0.22	0.19	0.31	0.48	1.11	0.57	0.20	0.19	0.18	0.45	0.67
Other Plasma components	Annexin A10	0.52	0.25	0.17	0.13	0.19	0.19	0.31	0.57	0.17	0.09	0.19	0.14	0.28	0.31
Other Plasma components	Bone marrow stromal antigen 2	0.01	0.05	0.07	0.46	0.76	0.74	0.19	0.03	0.01	0.06	0.07	0.09	0.45	0.12	0.05
Other Plasma components	Calmodulin-like protein 3	0.01	0.02	0.39	0.76	0.16	0.16	0.11	0.04	0.00	0.02	0.07	0.21	0.14	0.04	0.02
Other Plasma components	Cholinesterase	0.99	0.48	0.42	0.16	0.18	0.31	0.49	0.83	0.34	0.18	0.21	0.21	0.23	0.55	0.54
Other Plasma components	Cytosolic 5'-nucleotidase 1A	0.07	1.94	2.33	1.15	0.49	1.66	1.06	0.09	1.71	2.07	0.91	0.49	1.01	1.03
Other Plasma components	Galectin-3-binding protein	0.54	0.31	0.03	0.18	0.16	0.16	0.40	0.37	0.23	0.05	0.06	0.21	0.13	0.28
Other Plasma components	Hemoglobin subunit delta	0.29	0.16	0.16	0.24	0.61	0.14	0.18	0.32	0.11	0.11	0.21	0.12	0.20	0.19
Other Plasma components	Hemopexin	1.84	0.93	0.43	0.24	0.54	0.71	1.02	1.65	1.26	0.35	0.46	0.45	1.10	1.31
Other Plasma components	Inter-alpha-trypsin inhibitor heavy chain H1	0.24	0.31	0.07	0.24	0.88	0.50	0.34	0.48	0.15	0.05	0.27	1.46	0.45	0.33
Other Plasma components	Interleukin-18	14.14	7.18	1.08	1.67	0.90	2.81	8.49	12.89	5.87	1.60	1.23	0.83	3.08	7.28
Other Plasma components	Leucine-rich alpha-2-glycoprotein	0.44	0.28	0.20	0.12	0.20	0.30	0.38	0.53	0.21	0.12	0.17	0.14	0.40	0.33
Other Plasma components	MKRN2 opposite strand protein	0.72	0.37	0.23	0.18	0.14	0.19	0.22	1.09	0.24	0.24	0.26	0.15	0.29	0.47
Other Plasma components	Negative elongation factor E	0.06	0.21	2.00	1.77	1.13	0.68	0.29	0.06	0.21	3.37	3.60	1.27	0.64	0.42
Other Plasma components	Olfactory receptor 4F15	0.16	0.09	0.05	0.92	0.68	0.12	0.13	0.17	0.09	0.05	0.77	0.30	0.14	0.15
Other Plasma components	Pregnancy zone protein	0.05	0.08	0.22	0.52	1.15	0.45	0.11	0.06	0.07	0.13	0.61	1.07	0.35	0.11
Other Plasma components	Protein lunapark	0.00	0.00	0.00	0.10	0.45	0.17	0.01	0.00	0.00	0.03	0.08	0.54	0.12	0.01
Other Plasma components	Putative uncharacterized protein FRMD6-AS1	0.50	0.23	0.27	0.20	0.22	0.23	0.36	0.51	0.18	0.10	0.14	0.13	0.29	0.28
Other Plasma components	Serotransferrin	4.50	2.72	0.80	1.09	0.66	1.61	3.16	4.15	2.46	1.00	0.77	0.84	1.99	3.43
Other Plasma components	Serum albumin	41.94	24.52	5.71	5.92	5.71	12.78	29.04	46.96	19.27	6.64	6.71	7.18	21.26	33.37
Other Plasma components	SPRY domain-containing SOCS box protein 2	0.01	0.07	0.64	0.56	0.36	0.23	0.09	0.04	0.07	0.69	0.94	0.38	0.14	0.12
Other Plasma components	Vitamin D-binding protein	1.64	0.34	0.12	0.38	0.19	0.27	0.64	1.08	0.44	0.15	0.17	0.17	0.38	0.64
Other Plasma components	Zinc-alpha-2-glycoprotein	0.35	0.21	0.07	0.22	1.49	0.77	0.52	0.46	0.19	0.06	0.24	3.08	0.82	0.23
Tissue Leakage	CD5 antigen-like	0.08	0.27	0.56	0.72	0.47	0.58	0.24	0.07	0.30	0.69	0.53	0.32	0.44	0.20

Figure 4.26: LC-MS heat map showing the abundance of individual proteins of the supernatant after separation by AF4 and the corresponding plasma control after AF4 (collected fractions 1-7). All proteins with an abundance above 0.5% are displayed.

Hence, it is more meaningful to take a closer look at shifts in the AF4 retention time of certain proteins. Four of the identified proteins changed their elution time most prominently: C4b-binding protein alpha chain (changes from fraction 6 in the plasma control to fraction 3 after SiNC contact), Apo AI (changes from fraction 2 in the plasma control to fraction 3 and 4 after SiNC contact), Interleukin-18 (changes from fraction 3 in the plasma control to fraction 4 after SiNC contact). Consequently, the contact to the nanomaterial must have changed certain characteristics of the proteins, like the structure, the aggregation state, or else. For the here executed experiments the protein concentration was too low to record a potential protein denaturation by methods like differential scanning fluorimetry or else. In case of the apolipoproteins, the formation of complexes or aggregates with other biomolecules, leading to different sizes and to a higher retention time, could also be possible. Upon contact to the nanomaterial, the original lipoprotein complexes might be disturbed, and the newly formed ones show a different composition, indicating the importance of other biomolecules like cholesterol or lipids. As it has already been shown that also lipid molecules from lipoproteins can be adsorbed to nanomaterials,[155] it will be interesting for further experiments, to analyze the collected fractions also regarding the content of other biomolecules.

Since the absolute interpretation of the data is difficult from the heat map representation (Figure 4.26), the displayed data is normalized by the absolute protein mass (Figure 4.27), which was detected in the corresponding fractions (Figure 4.24B). For clarity, proteins are grouped according to function with only HSA and Apo AI shown individually. Fraction 1, 2 and 7 showed the highest protein amount (represented in the upper graphs in Figure 4.27) and only small differences in the composition of the plasma control and the supernatant after removal of the protein corona components are visible: Fraction 1 showed a decrease of proteins from the complement system group and an increase of albumin for the plasma control, while the amount of albumin, complement system, coagulation and acute phase proteins was lower in fraction 2 for the plasma control. The above-mentioned Apo AI was found in fraction 2 for the plasma control, while it was only present in very small amounts in the same fraction in the negative corona. Fraction 7 showed an overall smaller amount of proteins for the plasma control. Looking at fractions 3-6, which showed a lower protein amount (displayed in more detail in the lower graph, Figure 4.27), Apo AI was found in fraction 4 after contact with the SiNCs. Generally, fraction 4 of the negative corona was enriched with apolipoproteins. Fraction 4 also contained more complement and coagulation proteins and more immunoglobulins after SiNC contact. In contrast, the plasma control contained more coagulation proteins in fraction 5. Fraction 6 was rather similar for both samples, but the plasma control contained more lipoproteins in comparison to the negative corona. A detailed description of fraction 3 cannot be given, since it contained only very low amounts of protein after SiNC contact.

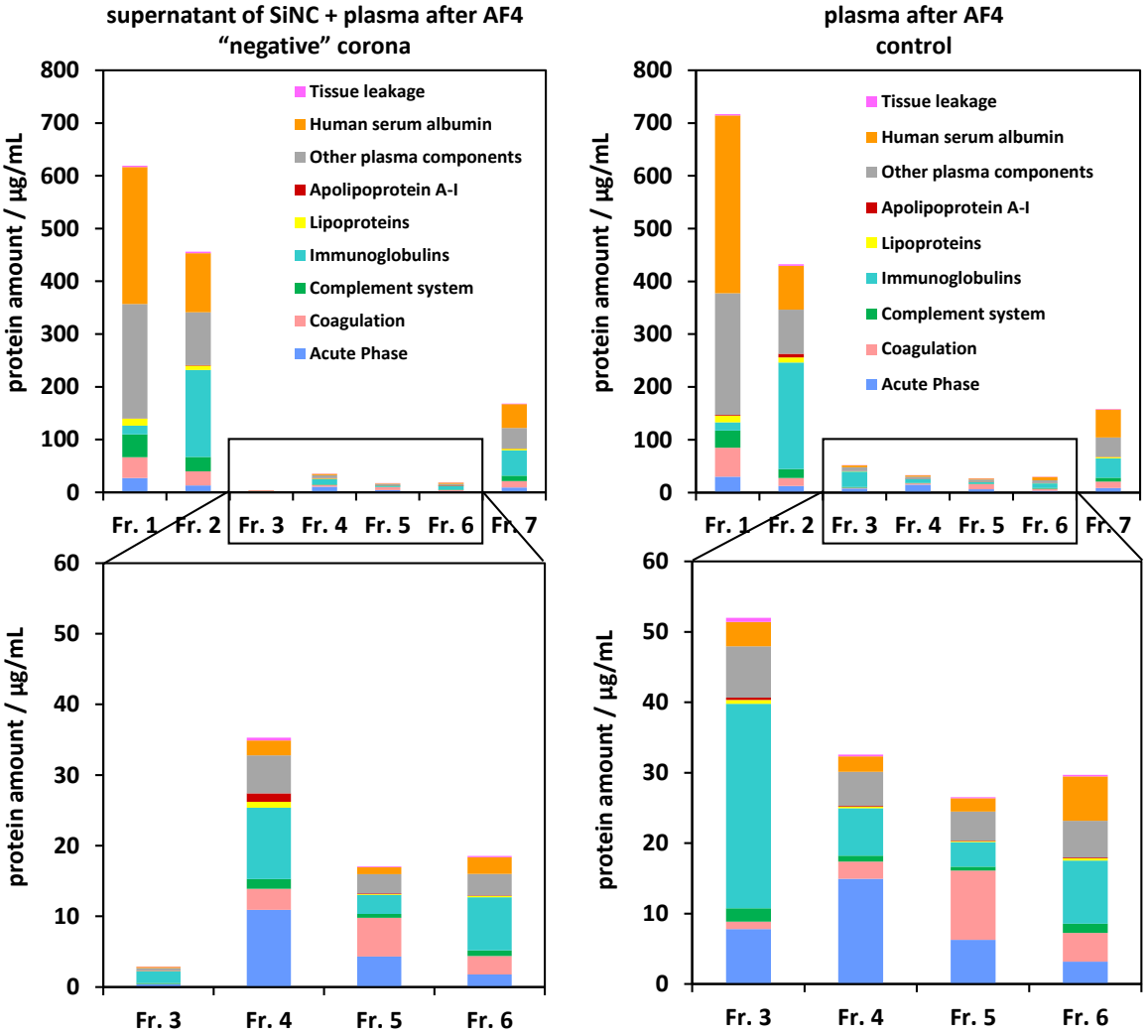

Figure 4.27: Bar diagram representation of LC-MS data obtained after AF4 separation and fraction collection related to the absolute amount of protein found in each fraction. The proteins were grouped according to their function with only HSA and Apo AI shown individually.

Special attention was payed to Apo AI as it was the main protein compound of the protein corona itself. From the LC-MS data, it was already evaluated that Apo AI was present in fraction 2 for the plasma control and in fraction 4 for the sample separated by AF4. Consequently, as described above, some structural changes must have happened to the excess free Apo AI upon contact to the nanomaterial. Additionally, the total amount of Apo AI was larger in fraction 2 of the plasma control, than in fraction 4 of the sample. This indicates that some of the total amount of Apo AI was missing in the investigated supernatant due to protein adsorption onto the nanomaterial. A calculation of the Apo AI removed from the plasma supernatant due to protein corona formation was done by correcting the protein mass obtained from the pierce assay by the Apo AI fraction identified by LC-MS and can be found in Table 4.3.

Table 4.3: Data of the amounts of adsorbed Apo AI and calculation of the absolute decrease of Apo AI amount due to protein corona formation, referred to 1 mL of sample.

Total protein in negative corona *m(protein) / µg*	**Apo AI in protein corona** *m(Apo AI) / µg*	**Apo AI in plasma control** *m(Apo AI) / µg*
2777.50	11.25	19.72
Apo AI decrease in negative corona		**57%**
AF4 fraction number	**Supernatant of SiNC + plasma after AF4** *m(Apo AI) / µg*	**Plasma control after AF4** *m(Apo AI) / µg*
1	0.72	1.06
2	**1.20**	**6.78**
3	0.06	0.32
4	**1.21**	**0.12**
5	0.11	0.06
6	0.06	0.08
7	0.62	0.63
sum	3.97	9.59
Apo AI decrease in negative corona after AF4 separation		**41%**

From the evaluation of the Apo AI amounts in the plasma and after formation and removal of the protein corona, the decrease of Apo AI from the plasma is around 57% after centrifugation and 41% after additional separation by AF4. The difference of the Apo AI loss after the different methods is most likely caused by the protein recovery after AF4 and other influences of the sample preparation. However, in both cases, the amounts show a significant decrease of Apo AI from the plasma due to protein corona formation. Thereby, we can conclude that it must be part of the protein corona, which was confirmed by the direct analysis of it (Figure 4.22).

This is the first time that indeed a significant depletion of one protein that constitutes a large fraction of the protein corona can be detected in the plasma supernatant. Additionally, the protein fraction remaining in the supernatant apparently changed after contact with the nanocarriers, as the elution time in AF4 was changed. This means that with this kind of analysis also possible size or structure alterations of the proteins in the medium could be assessed. In the specific case of apolipoproteins, these changes might be related to their occurrence in the form of lipoproteins, meaning that other molecules than just proteins might be involved in the ongoing processes. With AF4 as a separation tool, the plasma fractions containing these lipoprotein complexes could now even be further analyzed.

4.3.4 Conclusion

By applying AF4 as a separation method, the plasma was successfully separated into smaller entities. Some proteins, like HSA and IgG, elute over the entire run, because they are very abundant, but other proteins like alpha-2-macroglobulin (fraction 4-6), ceruloplasmin (fraction 5), Ig mu chain C region (fraction 6), Apolipoprotein B-100 (fraction 1) were enriched in specific fractions, which could be useful for other experiments.

Moreover, the evaluation of the plasma supernatant after corona removal has been reported in this chapter. It was possible to identify the depletion of Apo AI in the supernatant, which was the main protein of the protein corona. Additionally, other changes of the proteins in the supernatant after corona removal became visible. This might lead to completely new insights, because usually only the adsorbed proteins are analyzed. Other proteins, especially the apolipoproteins changed their retention time, which must be originated in for example structural alterations of the proteins themselves after contact to the nanocarriers. Therefore, it is clear that also other biomolecules play a role in the protein corona formation and it is important to additionally focus on these other biomolecules like cholesterol, lipids and else. Additionally, the stability and conformation of the proteins after nanocarrier contact should be further analyzed.

To make the analysis of the negative corona as straightforward as possible, for future investigations it would be advisable to analyze simpler media such as an artificial plasma with defined proteins, e.g. individual lipoprotein fractions. Thereby, the evaluation of the plasma upon contact with nanocarriers becomes a promising field, in which more possibilities for research are open.

4.3.5 Repetition of experiment – excursion to membrane fouling

Additionally, in the context of the experiments of this chapter, we investigated whether any signs of membrane fouling could be detected in our AF4 system. For this, the same sample (supernatant of plasma after incubation with SiNCs and removal of the NC-protein complexes) was injected with a difference of 3 and 4 weeks to the first measurement and the elugrams were recorded (see Figure 4.28). Between each measurement the system was used for other measurements, however, the system was always rinsed with water and 20% ethanol solution and stored in the latter according to the recommendation of the manufacturer.

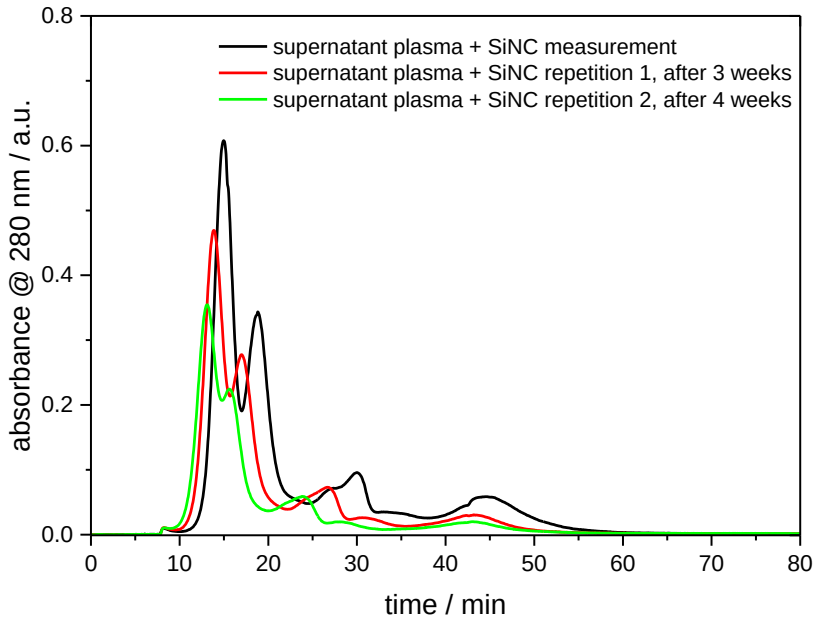

Figure 4.28: AF4 UV elugram of the plasma supernatant after removal of SiNC including the protein corona, displaying the used measurement (black), the first repetition after 3 weeks (red) and the second repetition after 4 weeks (green).

During these different measurements, the retention time shifted and the signal intensity decreased. This indicates that an adsorption of proteins and likely also other molecules to the membrane must have taken place after injection. Therefore, it was important to determine if specific proteins adsorbed or if the attachment happened in an unspecific manner. To analyze this, the fractions were collected according the previous chapter and analyzed by LC-MS. Even though no interactions of the samples with the membrane should occur, over time more and more proteins attach to that membrane. Once this protein adsorption is induced, the attached proteins attract even more proteins. Resulting from this effect, the signal of the sample eluting from the channel is constantly decreasing. Moreover, the channel height might decrease due to the formed protein layer, which has the same effect on the flow profile as a decreased cross flow and thereby leads to a reduction of the retention time. The same procedure as for the negative corona experiment was executed after 4 weeks and the fractions indicated by the grey boxes (Figure 4.29A) were collected at the same retention times as already shown in Figure 4.24A. The protein amounts of the plasma fractions were determined and compared to the values of the first measurement. As displayed in Figure 4.29B, a general decrease of the detected protein concentration could be observed for the measurement after 4 weeks.

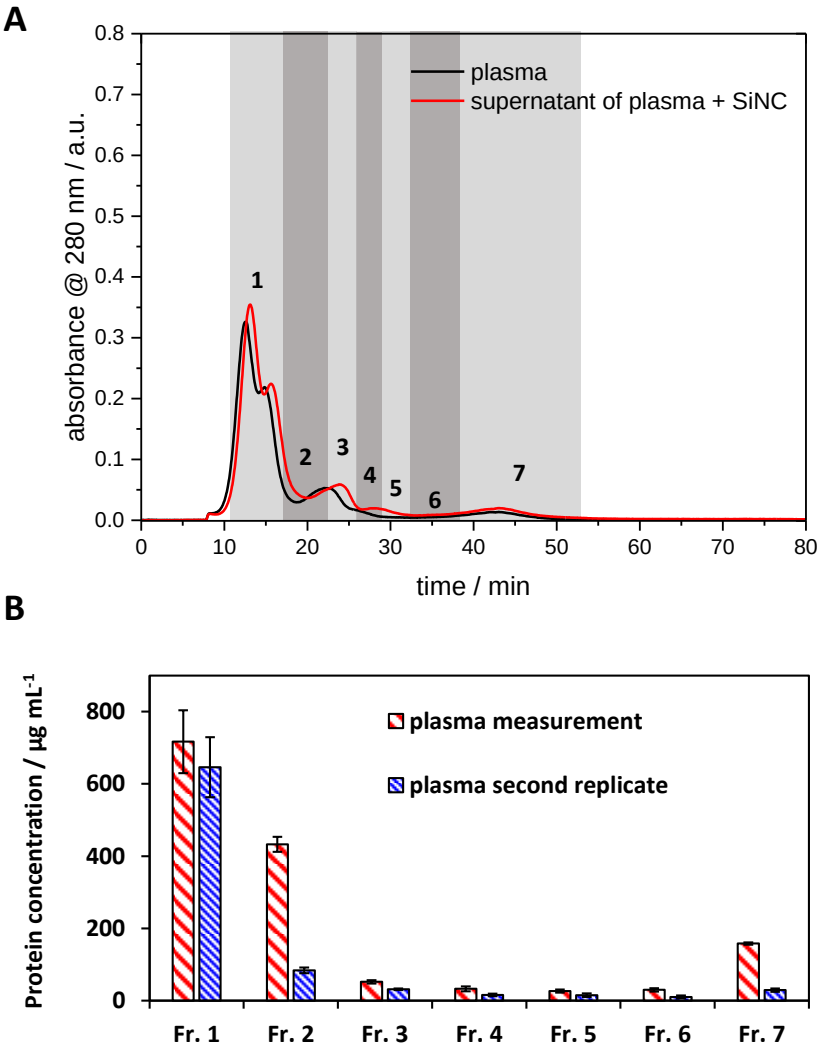

Figure 4.29: (A) AF4 elugram of the plasma supernatant after removal of SiNC including the protein corona and the corresponding plasma control 4 weeks after the first measurement. Fractions were collected as indicated by the grey boxes. (B) The protein amount was determined for the collected fractions after AF4 separation of the plasma controls, comparing the first measurement and the second repetition after 4 weeks.

Additionally, the protein composition of the taken fractions was compared to the original data by LC-MS (Figure 4.30). However, since the fractionation times were kept constant while the elution profile changed over time, a direct comparison of the data was difficult. From the different fractionation, the proteins were detected in different AF4 fractions compared to the initial measurement. Generally, the abundance of the individual proteins identified by LC-MS decreased, however, abundant proteins from the first run were also more abundant in the displayed repetition. Hence the protein adsorption to the membrane seemed to be unspecific.

Annotation	Description	plasma measurement							plasma second replicate						
		Fr. 1	Fr. 2	Fr. 3	Fr. 4	Fr. 5	Fr. 6	Fr. 7	Fr. 1	Fr. 2	Fr. 3	Fr. 4	Fr. 5	Fr. 6	Fr. 7
Acute Phase	Alpha-1-acid glycoprotein 1	1.15	0.25	0.19	0.62	0.34	0.90	0.80	0.79	0.23	0.28	0.23	0.13	0.98	0.57
Acute Phase	Alpha-1-antitrypsin	1.40	0.48	0.35	0.24	0.37	0.75	0.73	1.03	0.32	0.31	0.48	1.72	0.92	0.89
Acute Phase	Alpha-2-macroglobulin	0.06	0.12	0.94	29.23	12.99	3.38	1.13	0.07	5.16	17.11	4.56	0.87	0.50	2.30
Acute Phase	Ceruloplasmin	0.08	0.28	0.12	0.55	3.28	1.00	0.23	0.18	0.30	2.99	1.28	0.44	0.26	0.31
Acute Phase	Fibronectin	0.57	0.24	0.19	0.44	0.54	0.42	0.42	0.41	0.25	0.51	0.37	0.78	0.60	0.40
Acute Phase	Haptoglobin	0.11	0.89	10.99	12.39	4.71	2.72	1.30	0.43	6.61	6.54	3.15	2.21	1.29	2.32
Acute Phase	Haptoglobin-related protein	0.10	0.21	1.96	2.00	0.92	0.89	0.30	0.12	1.21	1.04	1.20	16.99	10.08	0.66
Coagulation	Fibrinogen alpha chain	0.12	0.17	0.13	1.68	9.94	2.73	0.44	0.08	0.49	9.25	4.15	1.17	0.61	0.48
Coagulation	Fibrinogen beta chain	5.99	2.24	1.17	2.19	8.08	5.15	5.33	3.56	1.76	7.15	3.80	1.65	3.07	3.28
Coagulation	Fibrinogen gamma chain	0.04	0.08	0.09	2.98	18.39	5.13	0.48	0.07	0.63	17.90	7.39	1.02	0.49	0.59
Coagulation	Prothrombin	0.74	0.40	0.15	0.10	0.20	0.25	0.58	0.52	0.21	0.12	0.10	0.03	0.02	0.51
Complement system	C4b-binding protein alpha chain	0.21	0.40	0.49	0.74	0.53	1.10	0.37	0.35	0.44	0.60	1.44	13.67	11.14	0.68
Complement system	Complement C3	3.68	1.65	0.88	0.78	0.76	2.18	3.25	2.01	1.07	0.38	0.57	5.77	3.18	2.66
Complement system	Complement factor H	0.35	0.59	0.93	0.37	0.24	0.38	0.53	0.41	0.66	0.23	0.81	0.07	0.08	0.82
Immunoglobulins	Ig alpha-1 chain C region	0.03	1.33	3.93	3.57	1.83	1.09	0.78	0.57	3.13	1.97	1.04	0.36	1.29	1.20
Immunoglobulins	Ig delta chain C region	0.13	0.08	0.09	0.09	0.08	0.18	0.09	0.14	0.09	0.06	0.17	3.15	2.05	0.15
Immunoglobulins	Ig gamma-1 chain C region	0.46	13.54	14.65	3.73	1.79	2.10	6.78	7.11	12.55	2.74	2.06	2.13	3.99	12.96
Immunoglobulins	Ig gamma-2 chain C region	0.13	1.98	1.48	0.42	0.24	0.34	0.61	0.86	1.49	0.32	0.23	0.19	0.39	1.00
Immunoglobulins	Ig gamma-3 chain C region	0.07	0.80	2.09	0.48	0.15	0.12	0.38	0.39	1.94	0.29	0.19	0.01	0.06	0.53
Immunoglobulins	Ig gamma-4 chain C region	0.03	0.71	0.42	1.08	0.47	0.15	0.24	0.35	0.77	0.57	0.29	0.00	0.04	0.46
Immunoglobulins	Ig kappa chain C region	0.27	14.12	19.15	5.43	3.22	8.54	6.58	5.01	16.92	4.51	16.37	5.51	4.86	11.50
Immunoglobulins	Ig lambda-3 chain C regions	0.07	3.72	3.32	0.77	0.40	1.10	1.59	1.57	3.94	0.70	1.41	0.36	0.32	1.45
Immunoglobulins	Ig mu chain C region	0.08	0.06	0.07	0.16	1.18	10.86	0.87	0.07	0.09	1.53	15.39	4.11	2.64	1.20
Immunoglobulins	Immunoglobulin heavy variable 3-66	0.03	0.27	0.43	0.23	0.16	0.39	0.18	0.12	0.44	0.19	0.74	1.19	1.21	0.29
Immunoglobulins	Immunoglobulin J chain	0.01	0.02	0.13	1.62	1.07	0.51	0.10	0.01	0.35	1.11	1.05	0.24	0.12	0.21
Immunoglobulins	Immunoglobulin kappa variable 3-11	0.01	0.26	0.34	0.13	0.21	0.25	0.14	0.11	0.27	0.27	0.52	0.90	0.48	0.24
Immunoglobulins	Immunoglobulin kappa variable 4-1	0.05	0.18	0.12	0.07	0.06	0.18	0.12	0.07	0.16	0.08	0.30	0.38	0.58	0.14
Immunoglobulins	Immunoglobulin lambda-like polypeptide 5	0.15	7.84	7.16	1.85	0.99	2.63	3.45	3.30	8.24	1.64	3.58	0.72	0.67	3.51
Lipoproteins	Apolipoprotein A-I	0.22	1.57	0.61	0.36	0.21	0.27	0.40	0.47	1.20	0.48	0.36	0.37	0.32	0.69
Lipoproteins	Apolipoprotein B-100	1.57	0.91	0.27	0.27	0.32	0.98	1.25	1.21	0.44	0.15	0.26	0.19	0.65	1.23
Other Plasma components	Acylpyruvase FAHD1, mitochondrial	1.60	0.82	0.30	0.50	0.60	1.19	1.23	1.02	0.35	0.32	0.45	1.58	1.81	1.35
Other Plasma components	Alpha-1,6-mannosyl-glycoprotein 2-beta-N-acetylglucosaminyltransferase	0.06	0.84	0.60	0.20	0.09	0.12	0.30	0.36	0.73	0.15	0.09	0.01	0.05	0.52
Other Plasma components	Alpha-2-HS-glycoprotein	1.11	0.57	0.20	0.19	0.18	0.45	0.67	1.05	0.24	0.10	0.20	0.45	0.42	0.50
Other Plasma components	Annexin A10	0.57	0.17	0.09	0.19	0.14	0.28	0.31	0.38	0.09	0.09	0.12	0.00	0.17	0.28
Other Plasma components	Cholinesterase	0.83	0.34	0.18	0.21	0.23	0.55	0.54	0.65	0.21	0.11	0.20	0.19	0.29	0.47
Other Plasma components	Cytosolic 5'-nucleotidase 1A	0.09	1.71	2.07	0.91	0.49	1.01	1.03	0.74	1.91	0.73	3.35	0.61	0.15	1.80
Other Plasma components	Hemopexin	1.65	1.26	0.35	0.46	0.45	1.10	1.31	1.70	0.52	0.23	0.33	0.11	1.00	1.48
Other Plasma components	Inter-alpha-trypsin inhibitor heavy chain H1	0.48	0.15	0.05	0.27	1.46	0.45	0.33	0.22	0.12	1.39	0.69	0.20	0.27	0.19
Other Plasma components	Interleukin-18	12.89	5.87	1.60	1.23	0.83	3.08	7.28	10.80	2.31	0.25	0.64	1.21	3.66	2.87
Other Plasma components	MKRN2 opposite strand protein	1.09	0.24	0.24	0.26	0.15	0.29	0.47	1.01	0.23	0.13	0.62	0.12	1.30	0.49
Other Plasma components	Negative elongation factor E	0.06	0.21	3.37	3.60	1.27	0.64	0.42	0.13	1.28	1.05	0.93	0.94	0.23	0.93
Other Plasma components	Olfactory receptor 4F15	0.17	0.09	0.05	0.77	0.30	0.14	0.15	0.14	0.16	0.40	0.08	0.03	0.08	0.17
Other Plasma components	Pregnancy zone protein	0.06	0.07	0.13	0.61	1.07	0.35	0.11	0.07	0.16	1.27	0.77	1.88	1.60	0.19
Other Plasma components	Protein lunapark	0.00	0.00	0.03	0.08	0.54	0.12	0.01	0.00	0.02	0.55	0.23	0.00	0.00	0.01
Other Plasma components	Putative uncharacterized protein FRMD6-AS1	0.51	0.18	0.10	0.14	0.13	0.29	0.28	0.30	0.10	0.12	0.19	1.73	1.25	0.29
Other Plasma components	RNA 3'-terminal phosphate cyclase	0.00	0.18	0.37	0.02	0.01	0.00	0.19	0.36	0.38	0.01	0.00	0.00	0.00	0.13
Other Plasma components	RWD domain-containing protein 2A	0.09	0.07	0.08	0.19	0.15	0.27	0.08	0.08	0.07	0.13	0.29	4.03	3.68	0.23
Other Plasma components	Serotransferrin	4.15	2.46	1.00	0.77	0.84	1.99	3.43	3.62	1.11	0.39	0.67	0.70	1.95	3.36
Other Plasma components	Serum albumin	46.96	19.27	6.64	6.71	7.18	21.26	33.37	36.39	8.38	2.13	4.48	7.74	17.58	21.44
Other Plasma components	Solute carrier family 52, riboflavin transporter, member 1	0.04	0.02	0.04	0.12	0.11	0.20	0.03	0.01	0.02	0.09	0.14	1.46	2.96	0.04
Other Plasma components	SPRY domain-containing SOCS box protein 2	0.04	0.07	0.69	0.94	0.38	0.14	0.12	0.05	0.55	0.45	0.17	0.06	0.07	0.28
Other Plasma components	Transcription elongation factor A N-terminal and central domain-containing protein	0.00	0.00	0.00	0.01	0.01	0.03	0.00	0.00	0.00	0.01	0.05	0.68	0.35	0.01
Other Plasma components	Vitamin D-binding protein	1.08	0.44	0.15	0.17	0.17	0.38	0.64	1.08	0.23	0.19	0.25	0.13	0.29	0.35
Other Plasma components	Zinc-alpha-2-glycoprotein	0.46	0.19	0.06	0.24	3.08	0.82	0.23	0.38	0.12	1.71	1.31	0.07	0.01	0.21
Tissue Leakage	CD5 antigen-like	0.07	0.30	0.69	0.53	0.32	0.44	0.20	0.14	0.56	0.43	1.02	0.15	0.10	0.26

Figure 4.30: LC-MS heat map showing the abundance of individual proteins of the AF4 fractions of the first measurement of the plasma control and the second repetition after 4 weeks. All proteins with an abundance above 0.5% are displayed.

The observed fouling highlights the importance of evaluation of the used equipment and method. The attachment of protein to the membrane was changing the composition of the sample, and therefore making it unfeasible for further analysis. Additionally, the fouling changes the membrane surface and consequently, the separation system interacts differently with the sample itself, leading to abnormal conditions. These results indicate the importance of checking the reproducibility of the data, before unwanted effects like membrane fouling might change the outcome of the results and induce a wrong data interpretation. By the right choice of the membrane material, this effect can be minimized, but unfortunately never fully prevented. Therefore, the system must be regularly rinsed and the membrane exchanged after either a certain time or a certain number of measurements.

4.4 Analysis of the influence of flow on the protein corona formation – evaluation of light scattering measurements in the flow

In the previous chapters, the extensive characterization of the protein corona to predict the physiological response of nanocarriers was described.[7] However, all these analyses neglect a crucial factor of a biological system, which is the flow. As soon as a nanocarrier is injected into a blood vessel, it is not only confronted with an excess of biomolecules, but also with the blood flow itself. This flow is most likely influencing the protein corona formation, the aggregation state and the distribution in the body. Therefore, it is important to consider the influence of the flow on the interactions of the nanocarriers with a biological system.

Combining the knowledge of the importance of the blood flow in biological systems with the protein corona analysis, the group of Prof. Caracciolo already addressed this challenge. For this purpose, they applied a dynamic incubation of liposomes in fetal bovine serum under constant movement, mimicking the blood flow; then they collected the samples and compared the resulting corona to the one obtained after static incubation via characterization by dynamic light scattering and liquid chromatography-mass spectrometry. They found that the protein corona composition differed depending on the applied incubation method.[26, 156] Generally, light scattering is a powerful tool for the analysis of the aggregation state of a nanocarrier or the size of the protein corona after incubation of the nanomaterial in a biological fluid.[78] However, the characterization techniques for the protein corona analysis used by Caracciolo *et al.* were applied as offline measurements. In the case of offline measurements, the protein corona is collected after the incubation and analyzed under static conditions. This means that the actual state of the corona might already change from the incubation to the actual measurement depending on the time needed for equilibrium formation.

To overcome the deficit of offline analysis for the protein corona, a light scattering cuvette was built according to the advice of Prof. Schmidt (Johannes Gutenberg University Mainz, Germany) to possibly characterize the aggregation behavior and size increase due to protein adsorption online under flow conditions. In the following, the cuvette is presented and the used set-up is introduced. After simulations of the flow conditions, first measurements of model nanoparticles in human blood plasma were performed. The measurements were executed first without flow and subsequently different flow rates were applied to investigate their influence on the nanoparticles in a biological medium.

4.4.1 General cuvette set-up

To mimic natural conditions of the flow in blood vessels and its influence on potential nanocarriers, a light scattering cuvette was assembled, which can be integrated in a commercially available multi-angle light scattering set-up. The designed cuvette (Figure 4.31A) consisted of a quartz glass part as the actual optical cuvette connected to the flow system by capillaries with exchangeable diameters, to mimic different flow conditions. The cuvette was geometrically adjusted to match the light scattering set-up by the combination with teflon and brass parts and sealed with rubber O-rings. The final cuvette is shown in Figure 4.31B as produced by the in-house fine mechanics workshop (MPIP Mainz, Germany).

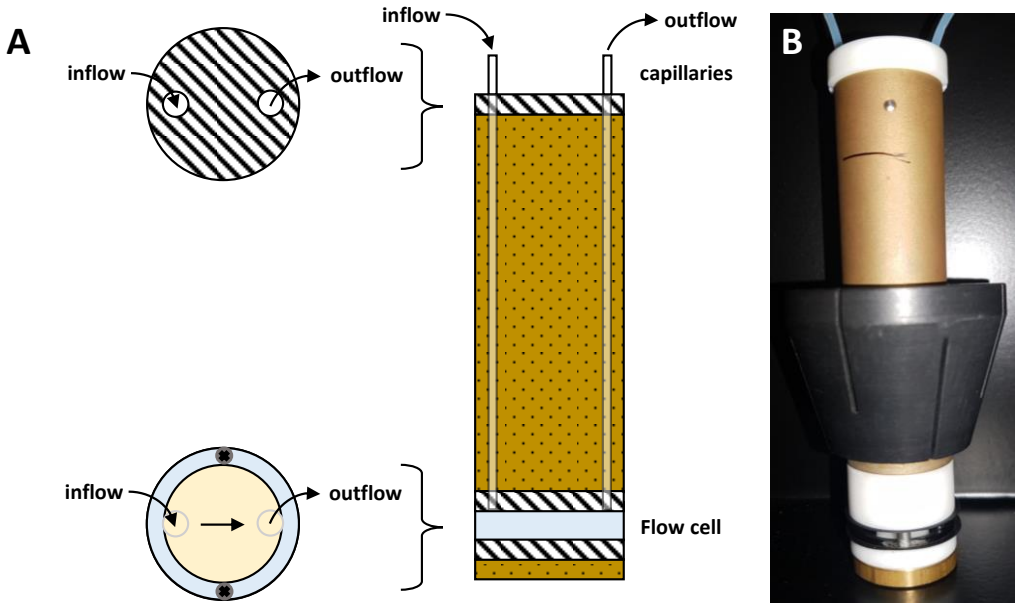

Figure 4.31: (A) Schematic construction and (B) image of the built light scattering cuvette.

4.4.2 Simulations of the flow inside the cuvette

Prior to the actual measurements, simulations of the flow in the flow cell were performed by Srinath Lakshman (Group of Prof. Detlef Lohse, University of Twente, Netherlands). The aim of the simulations was to obtain information about the flow profile and the flow velocities. Since high flow rates can potentially introduce more disorder or turbulences, the simulations were conducted for the highest flow rate to be applied in the upcoming experiments of 5 mL min^{-1}. The simulations were executed with the COSMOL Multiphysics® 5.3a CFD software and the parameters used as input for the simulation process are displayed in Table 4.4. For better visualization, the geometric

flow cell parameters are shown in Figure 4.32. The simulations were performed representatively for water and also for full blood plasma. Since the experiments were performed with 50 vol% plasma, the true flow profiles must lie between both representations.

Table 4.4: Parameters, assumptions and boundaries defined for the simulation of the flow inside the cell.

Geometric parameters	Radius of the cell	5 mm
	Height of the cell	3 mm
	Height of the cell capillaries	20 mm
	Radius of the cell capillaries	0.5 mm
Flow physics	3 dimensions	
	Steady state	
	Laminar flow	
	Incompressible liquid	
	Gravity included	
Fluid	Water	
	ρ	998.7 kg m^{-3}
	μ	0.00089 Pa s
	Blood plasma	
	ρ	1025 kg m^{-3}
	μ	0.00195 Pa s
Boundaries	Inflow $\dot{v}$	5 mL min^{-1}
	Outflow	
	Outer boundaries, no-slip wall	

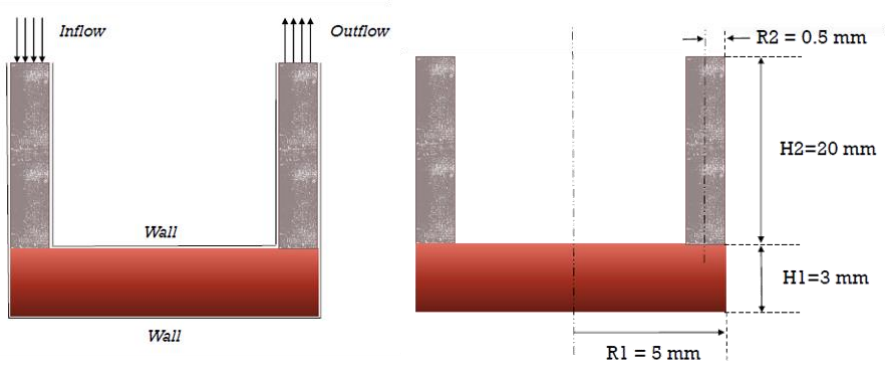

Figure 4.32: Cell and flow parameters of the cuvette measurement volume, which were applied for the simulation.

The resulting velocity profile with flow streamlines are displayed in Figure 4.33 corresponding to water as a carrier liquid.

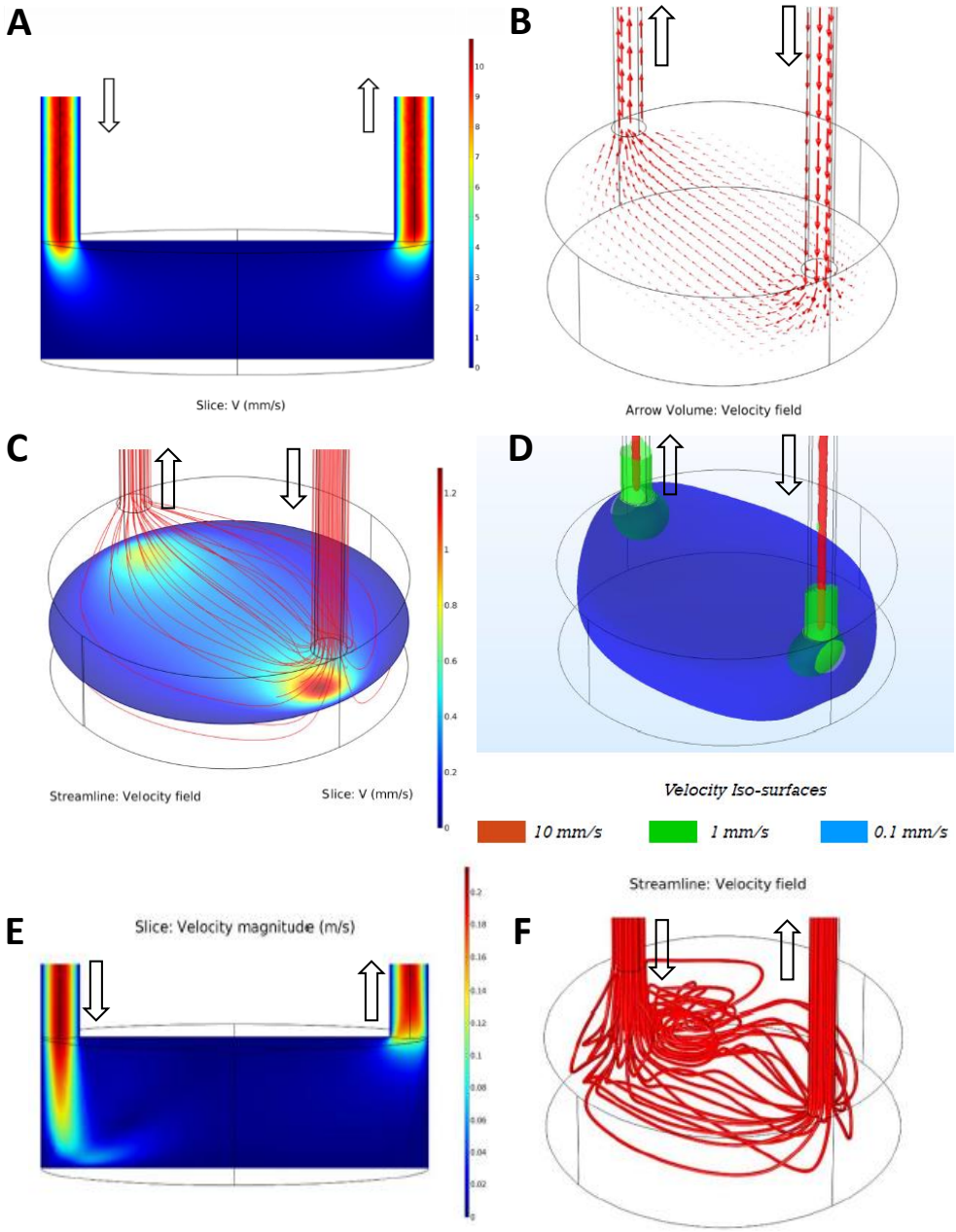

Figure 4.33: Flow velocity and stream lines of the liquid flow at a flow rate of 5 mL min^{-1}. The four upper plots represent the flow velocity of water (at the cross section (A) and in the entire volume (C)), the corresponding stream lines (B) and the velocity iso-surfaces (D). The two lower plots represent the flow velocity of water at the cross section (E) and the stream lines of plasma (F).

The simulations demonstrate that the flow velocity in the center of the capillaries is relatively high (> 10 mm s^{-1}). However, after entering the larger volume of the cuvette, the flow velocity decreases significantly (to about 0.1 mm s^{-1}) due to the expansion. Because of the limitations of the set-up (round scattering cuvette for multiangle measurements), this change of volume was unavoidable. Depending on the duration of the equilibrium formation of the protein adsorption or the aggregate formation, the effects of the blood flow simulated in the capillaries should still be observable in the

measurement volume. This is valid as long as the equilibrium formation takes longer than a few seconds, which is the time the sample needs to pass through the cuvette. Looking at the flow lines, only minor or no turbulences could be observed at the flow rate of 5 mL min^{-1}. This finding was very important to continue with the actual light scattering experiments. A turbulent flow would have complicated the situation, because additionally to the Brownian motion and the longitudinal flow, other flow components would have to be considered.

4.4.3 Set-up of the system

Via the attached pump, different flow rates could be adjusted, depending on the desired flow conditions. The entire set-up is represented in Figure 4.34. The sample was pumped from a sample reservoir into the cuvette, where it was directly measured without stopping the flow. To mimic flow of the nanoparticles in a blood vessel, the sample reservoir was filled with human blood plasma (diluted to 50 vol% plasma with PBS). Then polystyrene nanoparticles stabilized with CTMA-Cl were added and the solution was incubated before the flow was started. For this experiment, CTMA-Cl stabilized NPs were chosen because their overall cationic charge (here ζ-potential = (36 ± 3) mV) is known to induce aggregation in blood plasma.[92] Like this, the effect of flow on possible aggregate formation could be evaluated. Dynamic and static light scattering measurements were then carried out without flow and under different flow rates. Before measuring the mixture, the pristine components were analyzed as a reference.

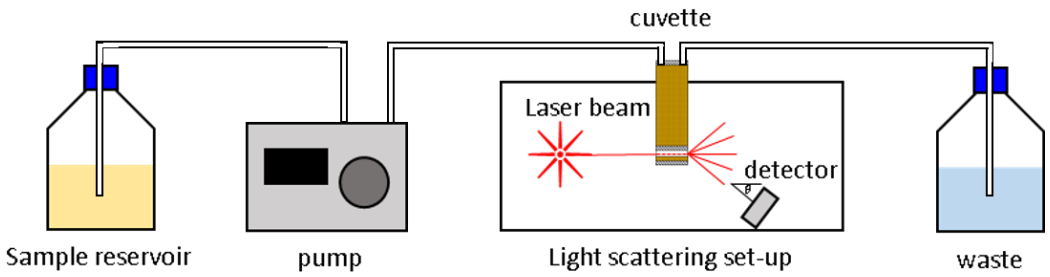

Figure 4.34: Schematic set-up of the used light scattering in the flow experiments. From the sample reservoir the sample was pumped into the cuvette, which was embedded into the commercially available ALV spectrometer. The detector was attached to a goniometer to measure the scattering intensity at different scattering angles.

4.4.4 Dynamic light scattering in the flow

Dynamic light scattering (DLS) data were recorded for pristine plasma, the pure nanoparticles and for the mixture of both. In Figure 4.35, an overlay of the exemplary autocorrelation functions (ACFs) of pristine nanoparticles dispersed in water at different flow rates at a scattering angle of 30° are shown. The ACFs obtained from measurements of the pristine nanoparticles under static conditions were fitted according to the CONTIN algorithm[157, 158] and yielded a hydrodynamic radius of 60 nm after extrapolation to the scattering vector → 0. The average hydrodynamic radius for the measurements of plasma under static conditions was calculated as well. However, a triexponential fit was used for the data evaluation (equation (3.33), chapter 3.2.3), and afterwards, the average hydrodynamic radius was calculated.

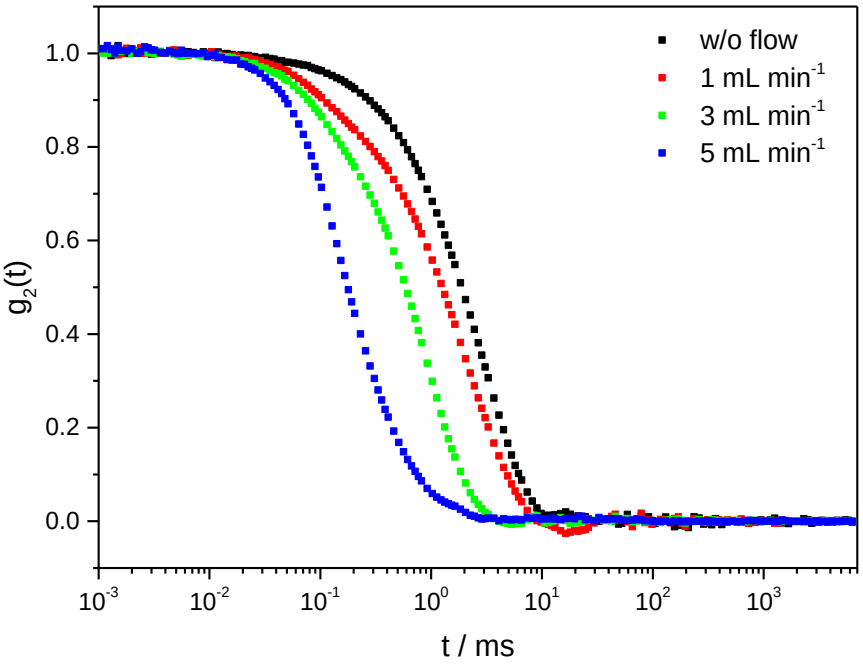

Figure 4.35: Normalized autocorrelation functions $g_2(t)$ of the pristine polystyrene nanoparticle solution at different flow rates shown for an exemplary scattering angle of 30°.

When comparing the ACFs before and after starting the flow, the average relaxation time decreased with the increase of the flow rate. Generally, a shorter relaxation time is originated from smaller species in the sample when only diffusive motions occur. Since the flow was additionally moving the nanoparticles through the measurement volume, an additional flow component was added to the Brownian motion of the nanoparticles, so that the faster nanoparticle movement was no

consequence of a higher diffusion coefficient due to a smaller size. Consequently, the nanoparticles appeared smaller from the ACFs under flow than they actually were.

Interestingly, for in the flow the ACFs were not only shifted, but additionally showed a different decay behavior. This becomes especially visible for the two ACFs at 1 and 3 mL min^{-1}. The decays seem to consist of a biexponential function, which indicates the presence of two or more processes in the measurement volume. When trying to describe the function with a biexponential decay fit, this was only possible for the nanoparticles without applied flow. For 1 mL min^{-1}, the fit was theoretically still possible, however, for higher flow rates, the fit functions did not describe the data points appropriately. For the observed decays of the ACFs, no accordance of the individual decays could be observed. The results indicate that the changed decay behavior of the ACFs originated from the flow itself, leading to artefacts. In case the ACFs cannot be described with one or more exponential decays, the resulting apparent relaxation times cannot originate from diffusive motion. For further analysis, it should be determined, whether the observed relaxation times and thus diffusion coefficients are changing the dependency on the scattering vector q in the flow. Additionally, by turning the flow plane compared to the q-plane, it could be observed, whether the detected effects are changing if the flow is parallel or perpendicular to the scattering angle. Because more than one decay are observed and because the ACF is shifted to lower relaxation times by the flow, a reliable and correct calculation of the hydrodynamic radius of the nanocarriers in flow cannot be done.

The decay functions of the plasma, the nanoparticles and the mixture of the particles incubated with plasma are overlaid for the different flow rates in Figure 4.36.

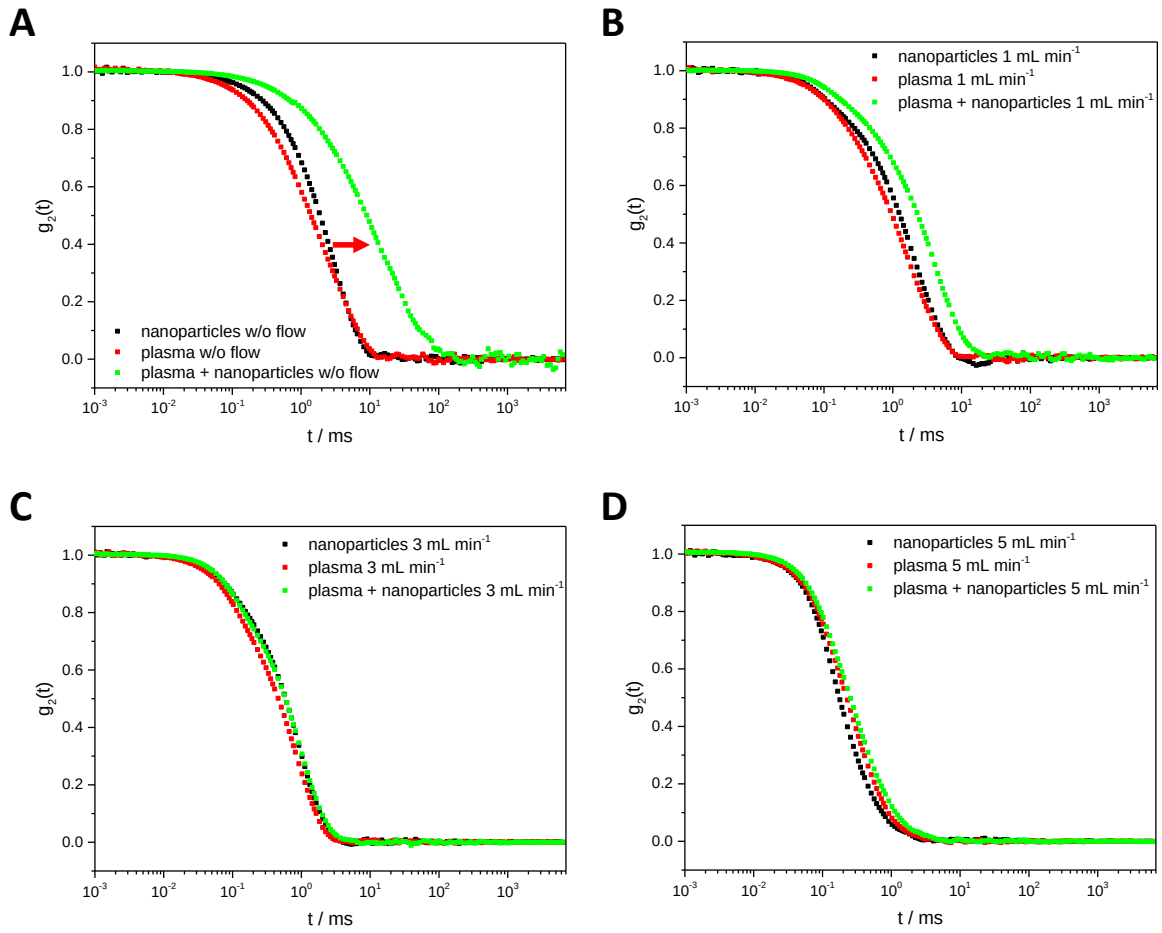

Figure 4.36: Normalized autocorrelation functions of plasma (red), nanoparticles (black) and the mixture of both (green) in each graph. The different graphs display the overlay of the different species at flow rates of (A) 0 mL min^{-1}, (B) 1 mL min^{-1}, (C) 3 mL min^{-1} and (D) 5 mL min^{-1} at 30°.

The sizes of the different species were nicely represented by the autocorrelation functions without flow (Figure 4.36A). The nanoparticles showed a single exponential decay of the ACF, while the plasma as a more complex system is characterized by a combination of several exponential decays (typically three as described in chapter 3.2.3). Upon exposure of the nanoparticles to plasma, aggregation took place in the sample as expected, which was observed by the shift of the ACF corresponding to the mixture as indicated by the arrow in Figure 4.36A. Comparing the ACFs of all components for a flow of 1 mL min^{-1}, a different behavior of the species was observed (Figure 4.36B). The ACF of the plasma-nanoparticle mixture is shifted less with regard to the pure components and the decay of the ACF is similar to the nanoparticle and plasma ACFs. At first glance, this might lead to the conclusion that the aggregate size decreased due to the applied flow. However, care must be taken during the data evaluation because of the effects already described above for the measurement of pristine nanoparticles. The flow might also just move the aggregates through the cuvette faster, which is simply simulating a smaller size. Looking at the ACFs at an applied flow of 3 mL min^{-1} (Figure 4.36C) the influence of the flow already overshadowed the self-

diffusion completely. The ACFs of all species were stacked and shifted to shorter lag times. For the sample measured at 5 mL min^{-1} this effect was observed as well, but additionally, the ACF decay became steeper again (Figure 4.36D). The only conclusion, which could be drawn from these results was that the flow influences the measurements of the nanoparticle-plasma mixture in the same way as for the pristine nanoparticles. Since mostly the flow components of the scattered light were visible in the measurements, the size of the diffusing species could not be determined and in the given set-up no further data analysis could be executed for DLS.

4.4.5 Static light scattering in the flow

Further static light scattering (SLS) experiments were conducted since the overall scattering intensities should not be influenced by the applied flow. Thus, for all samples shown above the corresponding measurements were performed and corrected for the scattering intensities of the solvent (water) and the standard (toluene) according to equation (3.15) in chapter 3.2.1. When analyzing the data of an SLS experiment, different presentations of the data can be displayed. In Figure 4.37 the results of all SLS measurements are shown. On the left side, the absolute scattering intensity $R(q)$ against the scattering vector q is displayed and on the right side of Figure 4.37 a simplified Zimm-plot is presented (plot of $1/R(q)$ against q^2).

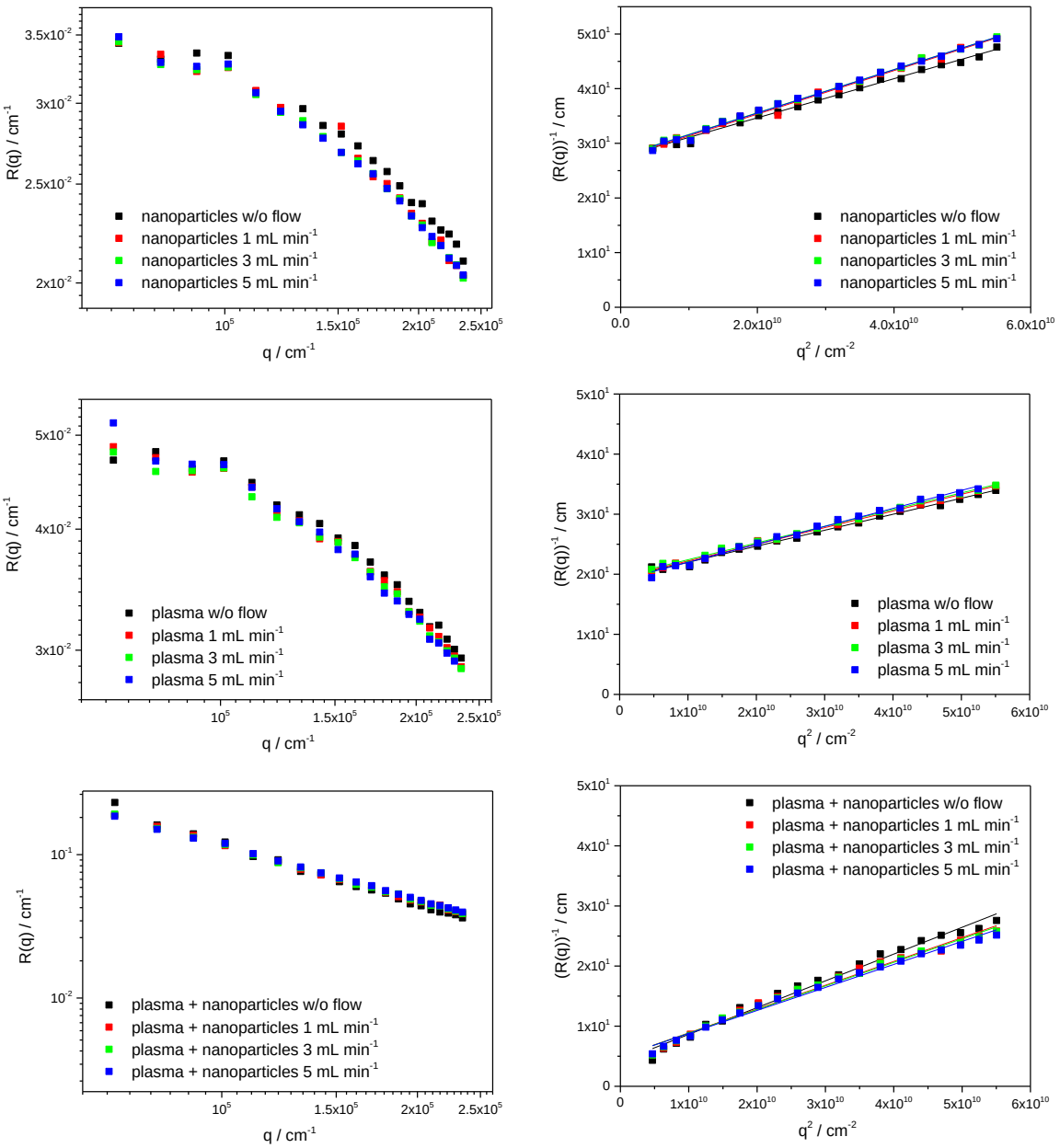

Figure 4.37: Absolute scattering intensity *R* plotted against scattering vector *q* of the individual species on the left side and a simplified Zimm-plot of the different species on the right side together with a linear regression of each dataset.

For the mixture of nanoparticles with plasma, the absolute scattering intensity was the highest, while for the pristine nanoparticles themselves it was the lowest (Figure 4.37, left). This increase of scattering intensity is proportional to the number of scattering centers (i.e. concentration), as well as to the size of the molecules, which was both the highest for the mixture because of the aggregation. Interestingly, there was no visible influence of the flow on the overall scattering intensity as it can be seen from all three plots on the left side of Figure 4.37. A potential explanation is that even if the sample was flowing through the measurement volume, on average there was always the same number of nanoparticles and proteins in the cuvette. The data representation in a

Zimm-plot gives the chance to perform an evaluation procedure, which can yield several sample characteristics. Normally, for this representation $\frac{K \cdot c}{R(q)}$ is plotted against q^2 (see equation (3.18), chapter 3.2.1). Since in this set-up K is not known, because the refractive index increment was not determined, in the simplified version $1/R(q)$ was plotted against q^2. As it can be seen in Figure 4.37, the scattering curves also in this representation are very similar to each other and it appears that the applied flow did not influence the overall shape and mass of the diffusing species.

To get a more quantitative description of the measured data, linear regressions were applied. From the representations in Figure 4.37 on the right, only the radius of gyration and not the total apparent molar mass could be determined. For all samples, the averaged radius of gyration R_g was determined according to the Zimm equation (equation 3.18, chapter 3.2.1), in which the slope of the linear regression is given by:

$$slope = \frac{{R_g}^2}{3M_w} \tag{4.1}$$

with $\frac{1}{M_w}$ = intercept of the y-axis of the Zimm-plot. Transformation of equation (4.1) gives the radius gyration to obtain information about the influence of the flow:

$$R_g = \sqrt{3 \cdot slope \cdot M_w} = \sqrt{\frac{3 \cdot slope}{intercept}} \tag{4.2}$$

The results are displayed in Table 4.5.

Table 4.5: Hydrodynamic radii and radii of gyration for pristine polystyrene nanoparticles (PS-NPs), pristine plasma and the mixture of both with and without applied flow.

Sample	**Flow / mL min^{-1}**	**R_h / nm**
PS-NPs	None	60
plasma	None	29
Sample	**Flow /mL min^{-1}**	**R_g / nm**
PS-NPs	None	62
	1	66
	3	66
	5	66
plasma	None	64
	1	65
	3	65
	5	69
plasma + PS-NPs	None	153
	1	155
	3	155
	5	152

Calculating the ρ-ratio (R_g/R_h) of the nanoparticles under static conditions, a value of 1 was obtained, which is usually attributed to a hollow sphere. Since the nanoparticles were not filtered prior to analysis, the value is most likely influenced by polydispersities of the sample. However, the system was checked for dust and thoroughly rinsed before use. For the plasma measurement under static conditions, the ρ-ratio resulted in a high value of 2.2 due to the high polydispersity of the plasma sample. Usually, SLS experiments cannot be evaluated for complex samples like mixtures, e.g. plasma, and therefore, the calculated radius of gyration is an average value, which is biased by the larger species in the mixture, since the results are intensity weighted. The same is valid for the mixture of the nanoparticles in plasma, the R_g and the ρ-ratio, so that they cannot be used as absolute values.

Even if the absolute values of the SLS experiments cannot be evaluated reliably, the relative radii of gyration can be compared to each other for the same sample in different flow conditions (Table 4.5). When comparing the R_g of the nanoparticles at different flow rates, no influence of the flow can be observed. Also for plasma, and moreover for the mixture of nanoparticles incubated in plasma, no different R_g values were observed at different flow rates. In this case, where R_g was not altered by the applied flow, the radius of gyration can be used as a measure of the compactness of the scattering species. Especially for the mixture, the results indicate that the structure was not changed in the flow and the protein layer or aggregate was neither compressed nor looser structures were formed. In addition to the radius of gyration, the Zimm-plot can give information about the apparent molar mass via the y-intercept of the linear regression. In the displayed data (Figure 4.37, left), the intercept is still proportional to the apparent molar mass and approximately the same for all used flow rates. Consequently, the apparent molar mass of the mixture does not change under higher flow conditions.

From the results of the SLS experiments, no influence or effect of the applied flow could be observed for the used system. However, the reproducibility of this conclusion still needs to be verified with a higher number of samples.

4.4.6 Conclusion

In this chapter it was demonstrated how a newly built light scattering set-up was successfully established for the measurement of light scattering in an applied flow. The measurements of the DLS experiments showed a change of the autocorrelation functions due to the increasing flow rates, so that the data evaluation was not possible yet and no conclusions on the concrete effect of the flow on the protein corona could be drawn so far. On the other hand, the performed SLS experiments could be used for the comparison of different flow rates for nanoparticles incubated in

plasma for the first time. Surprisingly, no influence of the flow rate on the tested system could be observed. In future experiments, the reproducibility of the results must be verified with other nanocarrier systems, while the effect of the flow on the DLS must be evaluated in more detail still. In summary, the presented data show that the investigation of the protein corona under flow conditions is a promising, new field with a lot of potential.

5 Experimental

5.1 Materials

Phosphate buffered saline (PBS), human serum albumin (HSA) and transferrin were purchased from Sigma-Aldrich (USA). Monosodium phosphate (H_2NaPO_4, Sigma Aldrich, USA) and disodium phosphate (HNa_2PO_4, Fisher Scientific, UK) were used for the 10 mM phosphate buffer at pH 7.4. For the protein desorption a 62 mM Tris-Cl buffer (Sigma Aldrich, USA) containing 2% sodium dodecyl sulfate (Carl Roth GmbH, Germany) was used. Demineralized water was received from a MilliQ device (Merck Millipore, Germany). Freshly distilled styrene (Acros Organics, USA), 2,2'-azobis(2-methylbutyronitrile) (V59, Wako, ≥98.0%), hexadecane (Sigma-Aldrich, 99%) and Lutensol AT50 (BASF, Germany) were used for the nanoparticle synthesis. Sephacryl S500-HR was purchased from Sigma-Aldrich (USA), while ethanol (99.5%) and cholesterol were acquired from Carl Roth, Germany. Egg phosphatidyl choline (EPC) and mPEG-DSPE (both Lipoid, Germany) were used for liposome formulation. The membrane dye DiI (1,1'-dioctadecyl-3,3,3',3'-tetramethylindocarbocyanine perchlorate) was purchased from Thermo Fisher Scientific. Tetraethylsilane (Alfa Aesar, 98%), chloroform (Sigma-Aldrich ≥99%) and cetyltrimethylammonium chloride (CTMA-Cl, Acros Organics, 99%) were used for the SiNC synthesis. Phosphate buffered saline PBS was used from Sigma-Aldrich (USA) for all experiment, except as a carrier liquid, where 10x concentrated PBS diluted to 1x was used from Roche (Switzerland).

5.2 Methods and instrumentation

5.2.1 Human blood plasma

Human blood plasma was obtained from ten healthy donors at the Transfusion Center of the University Clinic of Mainz, Germany, according to standard guidelines. It was pooled and stored at -20 °C. Before use, it was centrifuged at 20 000 g and 4 °C for 1 h (Sigma 3-30K, Germany) to remove cell fragments and additional protein precipitates.

5.2.2 Transmission electron microscopy (TEM)

TEM measurements were executed with a JEOL JEM1400 electron microscope operating at an acceleration voltage of 120 kV. The samples were prepared by diluting the 1 wt% nanoparticle dispersion 1:50 with water. Each droplet was placed on a 300 mesh carbon-coated copper grid and dried overnight.

5.2.3 Zeta-potential measurements

The zeta-potential (ζ-potential) was determined using a Malvern Zetasizer Nano series (UK). If not stated otherwise 20 µL of the respective dispersion were diluted in 2 mL 1 mM KCl. The samples were measured in a disposable folded capillary cell. The measurement was executed in triplet.

5.2.4 Light scattering (LS)

All LS experiments were carried out with an ALV spectrometer (ALV-GmbH, Germany) consisting of a goniometer and an ALV/LSE-5004 multiple-tau full-digital correlator with 320 channels. A He-Ne laser was used as the light source operating at a wavelength of 632.8 nm. A thermostat (Julabo, Germany) enables temperature-controlled measu rements. Protein samples as well as plasma were filtered through a Millex GS 0.22 µm syringe filter (Merck, Germany). Other samples were filtered respectively to their size into cylindrical quartz cuvettes (18 mm diameter, Hellma, Germany) after cleaning them in an acetone fountain to remove dust.

5.2.5 Separation of nanoparticles with protein corona by asymmetric flow field-flow fractionation (AF4)

A Postnova AF2000 system was used equipped with a degasser, TIP- and focus-pump, auto sampler, smart stream splitter and fraction collector. The separation channel was equipped with a stainless steel frit, a 500 µm spacer and a membrane with a molecular cut-off of 10 kDa. As detectors, a refractive index detector (PN3152 RI Detector, Postnova, Germany), a fluorescence detector (1260 Infinity, Agilent Technologies, USA) at 549/565 nm and a UV-detector (SPD-20A, Polstnova, Germany) at 280 nm were used. The data was evaluated with the AF2000Control 2.0.8.0 (Postnova, Germany).

5.2.6 SDS polyacrylamide gel electrophoresis (SDS-PAGE)

For the preparation of the SDS-PAGE 16.25 µL of the sample containing 1 µg of protein was mixed with 6.25 µL NuPAGE LDS sample buffer and 2.5 µL NuPAGE sample reducing agent and incubated for 10 min at 70 °C. This mixture was applied on a NuPAGE 10% Bis Tris Protein Gel (Novex, Thermo Fisher Scientific, USA). SeeBlue Plus2 Pre-Stained Standard (Invitrogen, USA) was used as a molecular ladder. The electrophoresis was carried out in NuPAGE MES SDS running buffer at 100 V for 1.5 h.

The gel was stained with the SilverQuest Silver Staining Kit (Thermo Fischer Scientific, USA).

5.2.7 Liquid chromatography – mass spectrometry (LC-MS)

In solution digestion and LC-MS analysis were performed as previously described[42, 159]. Briefly, proteins were precipitated using Proteo Extract protein precipitation kit (Merck Millipore, Germany) according the manufacturer's instruction. The isolated protein pellet was resuspended with 0.1% RapiGest SF (50 mM ammonium bicarbonate solution, Waters, USA) and incubated at 80 °C for 15 min. Dithiothreitol (DTT, Sigma-Aldrich, USA, 5 mM, 45 min, 56 °C) and Iodoacetamide (IAA, Sigma-Aldrich, USA, 15 mM, 1 h) were added to the protein solution. Proteins were digested overnight with protein ratio of 1:50. Hydrochloric acid (2 µL, Sigma-Aldrich, USA) was added to stop the digestion the next day. Peptide samples were diluted with 0.1% formic acid (Thermo Fischer, USA) and 50 fmol μL^{-1} Hi3 *E.coli* Standard (Waters, USA) for absolute quantification. A Synapt G2 Si mass spectrometer coupled to NanoACQUITY with a C18 analytical reversed-phase column (1.7 µm, 75 µm x 150 mm) and a C18 nanoACQUITY Trap Column (5 µm, 180 µm x 20 mm, both Waters, USA) were used for proteomic measurements. Mobile phase A 0.1% (v/v) formic water and mobile phase B of 0.1% (v/v) formic acetonitrile (both Biosolve, Netherlands) were used. A flow rate of 0.3 µL min^{-1} over a gradient from 2% to 40% from mobile phase A to B was applied. Glu-Fibrinopeptide and Leucine Enkephaline (both Sigma-Aldrich, USA) served as reference component infused at a flow rate of 0.5 µL min^{-1}. Electrospray ionization (ESI) was performed with a NanoLockSpray in positive ion mode and data-independent acquisition (MSe) experiments were carried out.

Peptides and proteins were identified by Progenesis QI software. The following criteria were set for analysis: energy (120 counts), high energy (25 counts) and peptide intensity (750 counts) were set and continuum LC-MS data was post acquisition lock mass corrected. A protein false discovery rate of 4% for all samples was applied. Peptides were searched against a human reviewed database from Uniprot. The data base was spiked with the sequence of Hi3 *E.coli* standard and procine

trypsin. The final criteria were chosen: 1 peptide = 3 fragments; 1 protein = 2 peptides and 5 fragments. The Top/Hi3 approach the amount of each protein in fmol was obtained.[160] Relative amounts of each protein were calculated based on the total amount of all identified proteins.

5.2.8 Cellular uptake

Cells were cultured in Dulbecco Modified Eagle Medium (DMEM, Gibco, USA) supplemented with 10% fetal bovine serum (FBS), 100 U mL^{-1} penicillin, 100 mg mL^{-1} streptomycin and 2 mM glutamine (all Invitrogen, Germany).

The cells were splitted at 80% confluency and after detaching, the cells were seeded out in 24-well plates (100 000 cells/well) in cell culture medium. After 24 h the medium was changed to serum-free medium. Nanocarriers were added and incubated with cells. For flow cytometry analysis, cells were detached with 2.5% trypsin (Gibco, Germany). Measurements were performed on an Attune NxT flow cytometer (Thermo Fisher, USA) with a 488 nm laser to excite Bodipy.

5.2.9 Confocal laser scanning microscopy (CLSM)

50 x 10^4 cells were seeded in Ibidi iTreat µ-dishes (IBIDI, Germany) for 24 h, washed with PBS and kept in DMEM without additional proteins for 2 h. Subsequently, nanocarriers with and without corona were added to cells. Afterwards, cells were washed with PBS and fixed with Roti-Histofix 4% (Carl Roth GmbH, Germany) for 15 min. The cell membrane was stained with CellMask Orange (CMO, stock solution: 5 mg mL^{-1} in DMSO, dilution 1:5000, Thermo Fisher, USA). Images were taken on a Leica TCS SP5 II microscope with an HC PL APO CS 63x/1.4 oil objective using the LAS AF 3000 software. The fluorescence signals of CMO (561 nm) were pseudo colored in red and nanoparticles in green. Detection was carried out in a serial scan mode.

5.2.10 Detection of corona proteins (IgG) on the nanoparticle surface by flow cytometry

Nanocarriers (1 µg) were incubated with 5 µL Zenon Alexa Fluor 647 human IgG labelling reagent (200 µg mL^{-1} as provided by Thermo Fisher, USA) for 30 min at room temperature. The solution was further filled up to 1 mL with PBS and measured using an Attune NxT flow cytometer (Thermo Fisher, USA). Nanoparticles were displayed in a dot plot (SSC vs FL1 channel in logarithmical

scale). The negative control was defined as nanoparticles without corona and set to 1% of Alexa Fluor 647 positive nanocarriers.

5.3 Preservation of the soft protein corona in distinct flow allows identification of weakly bound proteins

5.3.1 Synthesis of polystyrene nanoparticles

The nanoparticles were synthesized by direct miniemulsion as described elsewhere. [161, 162] Briefly, after dissolving 300 mg of the initiator V59 and 750 mg hexadecane in 18 g styrene and 1.8 g Lutensol AT50 in 72 mL demineralized water both phases were combined and stirred for one hour to achieve a pre-emulsification. Subsequently, the miniemulsion was prepared with the microfluidizer (Microfluidics, USA) at 15 000 psi for 60 s. The polymerization took place at 72 °C over night. Purification was achieved by centrifugation at 14 000 rpm for 2 h (Sigma 3-30K, Germany) and resuspension in water for 4 times. For the fluorescence labeled particle the procedure was the same with the addition of 18 mg Bodipy 523/535 into the disperse phase. Bodipy 523/535 was synthesized according to literature.[163] The solid content of the nanoparticle suspension was determined by drying and weighing a defined volume of the sample.

5.3.2 Dynamic light scattering (DLS)

Concentrations of the measured samples where adjusted to obtain the same concentration as samples had after separation by AF4 and filtered through Millex LCR 0.45 µm syringe filters (Merck, Germany). All experiments were performed as a triplet measurement at 37 °C. Data analysis was performed according to the procedure described in literature by Rausch et al.[79, 92]

5.3.3 Protein corona preparation

The nanoparticles were diluted with demineralized water to a constant particle surface concentration: 0.05 m^2 particle surface in 300 µL. The surface of the nanoparticle was calculated based on its solid content, its hydrodynamic radius and its density. This diluted dispersion was incubated with 1 mL of concentrated human blood plasma at 37 °C for 1 h under constant agitation.

After obtaining the nanoparticle-protein complexes (see 5.3.4 and 5.3.5), the proteins were desorbed by dissolving the pellet in 100 µL SDS-Tris buffer (2% SDS, 62.5 mM Tris-HCl). The SDS was removed from the protein solution using Pierce Detergent Removal Spin Columns, 0.5 mL (Thermo Scientific, Germany). Protein quantification was done using a Pierce 660 nm Protein Assay (Thermo Scientific, Germany) according to the manufacturer's instruction.

5.3.4 Separation of nanoparticles with protein corona by centrifugation

Unbound proteins were removed by centrifugation at 20 000 g at 4 °C for 1 h (Sigma 3-30K, Germany). The pellet consisting of nanoparticles with adsorbed proteins was resuspended in 10 mM phosphate buffer like in AF4 and washed by three subsequent centrifugation steps at 20 000 g and 4 °C for 1 h.

5.3.5 Separation of nanoparticles with protein corona by asymmetric flow field-flow fractionation (AF4)

A cellulose triacetate membrane was used and the channel was kept at a temperature of 37 °C. As detectors a RI-detector and a UV-detector at 280 nm were used. Additionally, the fluorescence signal was recorded offline with a platereader (infinite M1000, Tecan) at excitation 523 nm / emission 536 nm.

For the separation of the mixture of nanoparticles and proteins the channel flow was split to result in a channel flow of 0.25 mL min^{-1}. The initial crossflow was 1 mL min^{-1}, decreased exponential over 15 min and was kept at 0 mL min^{-1} for the remainder of the separation. The carrier liquid was a 10 mM phosphate buffer at pH 7.4.

The samples were prepared as described above and 20 µL of the sample were injected and measurements were repeated four to eight times, depending on the measured sample.

5.3.6 Cellular uptake

HeLa cells (obtained by BSMZ, Germany) were used for the cellular uptake experiments.

After changing to serum-free medium, nanoparticles were added to achieve a final concentration in the cell culture medium of 2 µg mL^{-1} and incubated with cells for 2 h at 37 °C.

5.3.7 Confocal laser scanning microscopy (CLSM)

Nanoparticles with and without corona were added to HeLa cells for 2 h at a concentration of 2 μg mL^{-1}.

5.3.8 Differential scanning fluorimetry (Nano-DSF)

A Prometheus NT.48 (NanoTemper technologies GmbH, Germany) was used to determine the protein stability in 10 mM phosphate buffer used in the AF4. HSA and transferrin solutions were prepared with a concentration of 1 mg mL^{-1} in PBS and 10 mM phosphate buffer and the change of the intrinsic fluorescence was measured at 330 nm and 350 nm between 20 °C and 90 °C.

5.3.9 Statistical analysis

An unpaired student´s t-test assuming equal variances was performed for the experiments concerning detection of IgG in the corona and cellular uptake. The p-values were defined as followed: *$p < 0.05$, **$p < 0.01$, ***$p < 0.001$. Not significant differences are labelled as n.s.

5.4 Functionalization of liposomes with hyperbranched polyglycerol results in biological identity independent of the protein corona

5.4.1 Liposome formulation by dual centrifugation

All lipids and amphiphilic polymers were dissolved in ethanol and stored at -20 °C. After thawing at room temperature, stock solutions of cholesterol (20 mg mL^{-1}), EPC (50 mg mL^{-1}) and amphiphilic polymer (20 mg mL^{-1}) were combined in a PCR tube (Kisker Biotech, Steinfurt, Germany) to yield the intended compositions. The unfunctionalized bare liposomes L-un consisted of 55:45 mol% for EPC:cholesterol. For liposomes functionalized with PEG or *hb*PG, 5 mol% of EPC were substituted with either mPEG-DSPE (2750 g mol^{-1}) or amphiphilic dialkyl-based *hb*PG polymer (2750 g mol^{-1}), resulting in a composition of 55:40:5 mol% for EPC:cholesterol:PEG/*hb*PG. 0.2 mol% of the membrane dye DiI was added to each composition. The combined lipid solutions with a total lipid mass of 5 mg were dried in a SpeedVac® vacuum centrifuge (Eppendorf, Hamburg, Germany) at 30 °C for at least 6 h and then in a lyophilisation

unit (Alpha 2-4 LD Christ, Osterode am Harz, Germany) for at least 24 h. 9.3 µL of PBS were added to the dry lipids and incubated for 10 min at room temperature. After adding 71 mg of ceramic beads (SiLiBeads® ZY, 0.3 – 0.4 mm, Sigmund Lindner, Warmensteinach, Germany), the PCR tube was subjected to the dual centrifuge (Rotanta 400 with a prototype DC-rotor, Hettich, Tuttlingen, Germany) in 3D-printed insets for PCR tubes (Helm Group, Johannes Gutenberg University Mainz, Germany) for 20 min at 2500 rpm. The obtained vesicular phospholipid gel was then diluted with 28.5 µL PBS and subjected again to dual centrifugation for 2 x 2 minutes at 2500 rpm, while turning the reaction tube by 180° in between. The highly concentrated resulting liposome suspension was stored at 4 °C until usage.

5.4.2 Liposome purification

Preparative size exclusion chromatography was performed via an Agilent 1100 System (Agilent, Germany) to remove non-encapsulated cargo and free lipids from the nanocarrier solution. 60 µL of the liposome suspension as obtained after dual centrifugation were injected into the system running with PBS at a flowrate of 1 mL min^{-1}. A BioRad UNO Q1 column (BioRad, Munich, Germany) filled with Sephacryl S500-HR was used for separation. A multiwavelength detector (G1365A Agilent 1100 Series, Germany) was used for detection of the absorption of DiI-labeled liposomes at 550 nm. An automated fraction collector collected the resulting purified liposome solution with a volume of 600 µL.

5.4.3 Light scattering (LS)

Liposomes samples were prepared in a concentration of 0.001 mg mL^{-1} in PBS and filtered through Millex LCR 0.45 µm syringe filters (Merck, Germany). All experiments were performed as a triplet measurement. Data analysis was performed with the CONTIN algorithm.[157, 158]

5.4.4 Protein corona preparation

The liposomes were diluted in PBS containing 5% human blood plasma to give a final concentration of 2 mg mL^{-1}. This dispersion was incubated at 37 °C for 1 h under constant agitation.

After obtaining the liposome-protein complexes (see 5.4.5 and 5.4.6), the sample was resuspended in the according solvent. Protein quantification was done using a Pierce 660 nm Protein Assay (Thermo Scientific, Germany) according to the manufacturer's instruction.

5.4.5 Separation of liposomes with protein corona by centrifugation

Unbound proteins were removed by centrifugation at 20 000 g at 4 °C for 1 h (Sigma 3-30K, Germany). The pellet consisting of liposomes with adsorbed proteins was resuspended in 1 mL PBS and washed by three subsequent centrifugation steps at 20 000 g and 4 °C for 1 h each. After the last centrifugation step, the sample was resuspended in 200 µL PBS. Samples were dried by a SpeedVac Concentrator (Savant DNA120, Thermo Scientific, USA) and resuspended again to align sample preparation to the AF4 procedure.

5.4.6 Separation of liposomes with protein corona by asymmetric flow field-flow fractionation (AF4)

For the separation of the mixture of liposomes and proteins the channel flow was split to result in a detector flow of 0.2 mL min^{-1}. The initial crossflow was 1 mL min^{-1} and kept constant for 7.2 min, then it was decreased exponentially over 20 min to a crossflow of 0.05 mL min^{-1}, which was kept constant for another 7 min. A second exponential decrease was used to lower the crossflow to 0 mL min^{-1} for the remainder of the separation. PBS was used as a carrier liquid.

The samples were prepared as described above and 50 µL of the sample were injected. After collection of the fractions by the fraction collector, they were dried in a SpeedVac and then resuspended in 350 µL H_2O for further analysis.

5.4.7 Transmission electron microscopy (TEM)

2 µL of the corresponding liposome sample were placed on a lacey grid and embedded in 1% trehalose with 4% uranyl acetate. Measurements were executed on a FEI Tecnai F20 transmission electron microscope with a working voltage of 200 kV. An Ultrascan 1000 (Gatan) charge-coupled device camera took the electron micrographs and the images were collected with the Digital Mictrograph software (Gatan).

5.4.8 Cellular uptake

RAW264.7 cells (obtained from ATCC ® TIB-71™) were used for the cellular uptake experiments. After changing to serum-free medium, liposomes were added to achieve a final concentration in the cell culture medium of 7.5 μg mL^{-1} or and 75 μg mL^{-1} incubated with cells for 2 h or 24 h at 37 °C.

5.4.9 Confocal Laser Scanning Microscopy (CLSM)

Liposomes with and without corona were added to RAW264.7 cells for 2 h or 24 h at a concentration of 7.5 μg mL^{-1} or 75 μg mL^{-1}.

5.5 Evaluation of the “negative” biomolecule corona

5.5.1 Synthesis of silica nanocapsules

The synthesis of the silica nanocapsules (SiNCs) via miniemulsion was executed by Dr. Shuai Jiang (MPIP Mainz, Germany) using a modified procedure adapted to literature.[164] In short, 2.0 g tetraethoxylsilane were mixed with 125 mg of hexadecane and 1 mL chloroform. Afterwards, the hydrophobic mixture was added to 30 mL of a 0.77 mg mL^{-1} aqueous solution of cetyltrimethylammonium chloride (CTMA-Cl) under constant stirring. After pre-emulsification by stirring at 1000 rpm for 1 h, the emulsion was sonicated (Branson 450 W sonifier) for 180 s under ice-cooling with a ½’’ tip at 70% amplitude in a pulse regime (30 s sonification, 10 s pause). The resulting miniemulsion was stirred at 1000 rpm for 12 h at room temperature to obtain silica nanocapsules. The dispersion was further stirred at 1000 rpm for 12 h at air, during which the chloroform in the core evaporates leading to an aqueous core. To substitute the CTMA-Cl, which was used during the synthesis, 40 mg Lutensol AT50 was added to the nanocapsules dispersion and the solution was dialyzed against water in a 1000 Da cut-off cellulose membrane (Spectrum Laboratories, Inc., USA) to remove the CTMA-Cl.

5.5.2 Light Scattering

Before measuring the samples in triplicate with a concentration of 0.3 mg mL^{-1}, the samples were filtered (Millex LCR 0.45 µm syringe filter, Merck, Germany). The data was analyzed using the CONTIN algorithm.[157, 158]

5.5.3 Scanning electron microscopy

The morphology of nanocapsules was examined with a Gemini 1530 scanning electron microscope (SEM, Carl Zeiss AG, Oberkochen, Germany) operating at 0.35 kV. Silica nanocapsules were prepared by casting the diluted nanocapsule dispersion on silicon wafers.

5.5.4 Protein corona preparation and collection of plasma supernatant

An aqueous SiNC dispersion was added to 5 vol% human blood plasma (diluted in phosphate buffered saline (PBS, Sigma-Aldrich, USA)) to obtain a final NC concentration of 2.5 mg mL^{-1}. The dispersion was incubated at 37 °C for 1 h under constant agitation. As a plasma control sample, plasma diluted to 5 vol% in PBS was incubated for 1 h at 37 °C as well.

Subsequently, the mixture and the control were centrifuged for 1 h at 20 000 g and 4 °C (Sigma 3-30K, Germany). After the first centrifugation step the supernatant was collected for further separation and analysis. The remaining pellet and the "pseudo-pellet" of the plasma control were subjected to the established protein corona preparation method. Accordingly, the pellet was resuspended in 1 mL PBS and washed by three subsequent centrifugation steps at 20 000 g and 4 °C for 1 h each. After the last centrifugation step, the sample was resuspended in 100 µL 62.5 mM Tris buffer containing 2 wt% SDS. To detach the proteins from the nanocarriers, the sample was heated to 95 °C for 5 minutes and centrifuged for one more time. The resulting supernatant contained the proteins, which formed the protein corona. Protein quantification was done using a Pierce 660 nm Protein Assay (Thermo Scientific, Germany) according to the manufacturer's instruction.

5.5.5 Separation of the plasma supernatant (negative corona) by asymmetric flow field-flow fractionation (AF4)

For the separation 50 µL of the plasma supernatant as obtained after centrifugation (either with or without incubation with NCs) were injected and the detector flow was set to 0.25 mL min^{-1}. The initial crossflow was set to 1.5 mL min^{-1} and kept constant for 15 min. Then it was decreased linearly over 20 min to a crossflow of 0 mL min^{-1}, which was kept constant for another 40 min. PBS (1x) was used as a carrier liquid.

The separated samples were collected in different fractions and afterwards concentrated with centrifugal filter units (Amicon Ultra-4, Ultracel, 3 K, Merck, Germany) according to the manufacturer's protocol.

5.6 Analysis of the influence of flow on the protein corona formation – evaluation of light scattering measurements in the flow

5.6.1 Synthesis of polystyrene particles

The nanoparticles were synthesized by direct miniemulsion by Katja Klein (MPIP, Mainz) as described elsewhere.[161, 162] Briefly, after dissolving 100 mg of the initiator V59 and 150 mg hexadecane in 5.82 g styrene and 500 mg cetyltrimethylammonium chloride (CTMA-Cl) with 18 mg 2-aminoethyl methacrylate hydrochloride in 23.32 mL demineralized water both phases were combined and stirred for one hour to achieve a pre-emulsification. Subsequently, the miniemulsion was sonicated (Branson 450W sonifier) for 2 min under ice-cooling with a ½" tip at 90% aplitude. The polymerization took place at 72 °C over night. Purification was achieved by centrifugation at 13200 RZB for 2 h and resuspension in water for 3 times.

5.6.2 Light scattering set-up

An ALV spectrometer (ALV-GmbH, Germany) was used for light scattering experiments. It consists of a goniometer, an ALV/LSE-5004 multiple-tau full-digital correlator with 320 channels and a He-Ne laser at a wavelength of 632.8 nm. A single-piston pump (Series I Pump, Scientific Systems, Inc., USA) with polyether ether ketone (PEEK) pump head was used to move the liquid

through the system with different flow rates (0, 1, 3, 5 mL min^{-1}). The assembled cuvette consists of a custom-made quartz glass part (inner diameter 10 mm, High Precision Cell, Hellma Analytics, Germany) through which the sample flows, connected by polytetrafluoroethylene (PTFE) capillaries (Bola, Germany) with an inner diameter of 1 mm. The flow direction was fixed from ~ 45° to ~ -135°, while the measuring angle was variable between 30° and 125°. Human blood plasma, diluted to a plasma concentration of 50 vol% with phosphate buffered saline (PBS, Sigma-Aldrich, USA), filtered through a Millex GS 0.22 µm GS syringe filter (Merck, Germany) as well as the polystyrene nanoparticle solution (50 µg mL^{-1} in water) were measured individually. To measure the mixture of both components and to mimic the injection of the nanocarrier in the blood, the nanoparticles were added to the reservoir containing 50 vol% plasma to result in a final nanoparticle concentration of 50 µg mL^{-1}. After 5 min incubation under constant agitation, the mixture was pumped through the system with the flow rates mentioned above. For 5 min the flowing fluid was directed to the waste to rinse the system. Afterwards the flow was directed to the incubation reservoir again to save material and measurements were started. For static light scattering, the scattering intensity was recorded every 5° between scattering angles of 30° and 125° (higher angles could not be measured, because of the cuvette's geometry) for 5 s in triplicates. For dynamic light scattering experiments the intensity was recorded every 10° between 30° and 120° for 30 seconds each. The temperature was kept at 20 °C for all measurements.

6 Summary and outlook

The objective of this thesis was to gain new insights into the interactions of nanocarriers with biological systems. To understand the phenomena involved in the interactions is crucial for the development of effective drug delivery systems. However, there is a deficit of analytical methods for the protein corona close to mimic realistic physiological conditions. The here described projects advance the currently available characterization methods by introducing the asymmetric flow field-flow fractionation as a new separation technique for the isolation of the protein corona prior to analysis. Thus, the impact of the separation method on the protein corona outcome was investigated. The main focus was put on the analysis of the soft protein corona and its influence on cellular uptake. Furthermore, the influence of the nanocarriers on free proteins and the measurement of light scattering in the flow were investigated.

As a model system, polystyrene nanoparticles incubated in human blood plasma were used in the first section of the thesis and the resulting nanoparticle-protein complexes were isolated from free proteins successfully by AF4. By comparing the protein corona isolated by AF4 and by centrifugation, it was possible to confirm the presence of a soft corona. Hence, the influence of the soft and hard corona on the cellular uptake in HeLa cells could be compared. Interestingly it was found that for this system mainly the hard corona was influencing the interaction with cells.

After the proof of concept using model polystyrene nanoparticles, a potential carrier system (liposomes), was investigated in the second section. The used liposomes were functionalized with hyperbranched polyglycerol, which was tested for its potential stealth effect. After discovering that all investigated liposomes adsorbed less proteins than many other nanomaterials, the potential stealth liposomes were compared to PEGylated (known to expose a stealth effect) and unfunctionalized liposomes. Separation of the liposomes from the biological medium was conducted by AF4 as well as by centrifugation. The separation by AF4 was shown to be successful even for self-assembled systems, which now allows the characterization of nanomaterials that cannot be centrifuged for separation from the medium. We found that the protein adsorption of the *hb*PG-liposomes slightly differed from the other systems, but no decrease in the uptake in macrophages was observed. Therefore, no general stealth effect could be attributed to the functionalization by *hb*PG. Rather, the results indicated that also the material underlying the surface functionalization plays an important role for the biological identity. Combining the knowledge gained in section one and two of this thesis, the variety of information gained by the additional use of the AF4 separation showed the importance to combine several methods for the protein corona analysis. For future works, the AF4 method should be adopted for the analysis of other carrier systems as well to enable a general conclusion of the impact of loosely bound proteins.

In the third section, the focus was shifted from the analysis of the protein corona to the investigation of the influence of the nanocarrier contact on free proteins and biomolecules. Therefore, silica nanocapsules were incubated with plasma and subsequently removed from the mixture including their formed protein corona by centrifugation. The remaining plasma supernatant was separated into smaller fractions for a simplified evaluation of such a complex protein mixture. During these experiments, AF4 proved to be a valuable separation tool. Different size fractions of the plasma containing different protein classes were obtained, which could be further used for other projects. Additionally, it was demonstrated that the contact to the nanocarriers influenced also unbound proteins, resulting in a changed retention behavior of some proteins after incubation with the nanomaterial. Moreover, the most dominant protein (Apo AI) of the protein corona on silica nanocapsules was depleted in the supernatant. The results demonstrate that not only the protein corona should be investigated, but also the influence of the nanomaterial on the surrounding biological media. In future experiments, the aggregation and denaturation phenome occurring in the plasma medium should also be evaluated with regards to other biomolecules such as lipids and lipoproteins.

In the last section of the thesis, our experiments aimed at the comprehension of the aggregation and stability of a formed nanocarrier-protein complex influenced by the blood flow. For this purpose, a light scattering cuvette was built, which enabled the measurement during an applied flow. First experiments in the new set-up were performed, evaluating the influence of the blood flow on the aggregation behavior. For this purpose, polystyrene nanoparticles that exhibit significant aggregation during static incubation with plasma were subjected to different flow conditions. Interestingly, no obvious changes were visible when comparing the aggregation states under static and dynamic conditions. In future experiments, the light scattering measurements will focus on a deeper understanding of directed flow vs. diffusion induced effects. Subsequently, a broader variety of nanomaterials needs to be investigated to confirm the effect of flow on protein-nanomaterial interactions.

In the presented thesis, the potential of the AF4 in the field of protein corona research was demonstrated. Generally, the influence of the applied separation method on the outcome of the protein corona analysis was confirmed and the separation by AF4 should be included in the protein corona analysis of different materials. By the investigation of the protein corona in flow and by the analysis of the consequence of the nanocarrier contact on the free proteins, the awareness on the parameters influencing the protein corona was broadened. In this regard, it was possible to introduce tools enabling a characterization closer to physiological conditions. In summary, the knowledge on the protein corona was deepened and neglected areas in the protein corona analysis were investigated, bringing us one step closer to make drug delivery successful.

7 References

1. T. Helleday. *Annals of Oncology*. 2017; **28(9)**, 2054.
2. I.H. Plenderleith. *Can Fam Physician*. 1990; **36**, 1827.
3. Cancer - Key Facts: World Health Organization; 2018 [Available from: http://www.who.int/en/news-room/fact-sheets/detail/cancer. Accessed on: 15 Oct 2018
4. V. Jain, S. Jain, S.C. Mahajan. *Current drug delivery*. 2015; **12(2)**, 177.
5. S. Tran, P.J. DeGiovanni, B. Piel, P. Rai. *Clin Transl Med*. 2017; **6(1)**, 44.
6. R.R. Wakaskar. *Journal of drug targeting*. 2018; **26(4)**, 319.
7. C.D. Walkey, W.C. Chan. *Chem Soc Rev*. 2012; **41(7)**, 2780.
8. D. Walczyk, F.B. Bombelli, M.P. Monopoli, I. Lynch, K.A. Dawson. *J Am Chem Soc*. 2010; **132(16)**, 5761.
9. M. Lundqvist, J. Stigler, G. Elia, I. Lynch, T. Cedervall, K.A. Dawson. *Proc Natl Acad Sci U S A*. 2008; **105(38)**, 14265.
10. G.J. Tortora, D.B. H. The Cardiovascular System: The Blood. Principles of Anatomy and Physiology. 15: John Wiley & Sons; 2016.
11. K.S. Soppimath, T.M. Aminabhavi, A.R. Kulkarni, W.E. Rudzinski. *J Controlled Release*. 2001; **70(1-2)**, 1.
12. M. Rahman, S. Laurent, N. Tawil, L.H. Yahia, M. Mahmoudi. Protein-Nanoparticle Interactions: Springer-Verlag Berlin Heidelberg; 2013.
13. R. Singh, J.W. Lillard, Jr. *Experimental and molecular pathology*. 2009; **86(3)**, 215.
14. G. Caracciolo. *Nanomedicine*. 2015; **11(3)**, 543.
15. M. Tonigold, J. Simon, D. Estupinan, M. Kokkinopoulou, J. Reinholz, U. Kintzel, et al. *Nat Nanotechnol*. 2018.
16. H. Maeda, J. Wu, T. Sawa, Y. Matsumura, K. Hori. *J Controlled Release*. 2000; **65(1-2)**, 271.
17. M.P. Monopoli, C. Aberg, A. Salvati, K.A. Dawson. *Nat Nanotechnol*. 2012; **7(12)**, 779.
18. D. Nierenberg, A.R. Khaled, O. Flores. *Rep Pract Oncol Radiother*. 2018; **23(4)**, 300.
19. P. Aggarwal, J.B. Hall, C.B. McLeland, M.A. Dobrovolskaia, S.E. McNeil. *Adv Drug Deliv Rev*. 2009; **61(6)**, 428.
20. R.M. Pearson, V.V. Juettner, S. Hong. *Frontiers in chemistry*. 2014; **2**, 108.
21. L. Vroman, A.L. Adams, G.C. Fischer, P.C. Munoz. *Blood*. 1980; **55(1)**, 156.
22. H. Noh, E.A. Vogler. *Biomaterials*. 2007; **28(3)**, 405.
23. M. Lundqvist, J. Stigler, T. Cedervall, T. Berggard, M.B. Flanagan, I. Lynch, et al. *ACS Nano*. 2011; **5(9)**, 7503.
24. K. Cai, A.Z. Wang, L. Yin, J. Cheng. *J Controlled Release*. 2017.
25. S. Winzen, S. Schoettler, G. Baier, C. Rosenauer, V. Mailaender, K. Landfester, et al. *Nanoscale*. 2015; **7(7)**, 2992.
26. D. Pozzi, G. Caracciolo, L. Digiacomo, V. Colapicchioni, S. Palchetti, A.L. Capriotti, et al. *Nanoscale*. 2015; **7(33)**, 13958.
27. T.G. Papaioannou, C. Stefanadis. *Hellenic journal of cardiology : HJC = Hellenike kardiologike epitheorese*. 2005; **46(1)**, 9.
28. Y.C. Fung. Chapter 8: Mechanical Properties of Blood Vessels. Biomechanics. New York: Springer-Verlag; 1981.
29. P.R. Painter, P. Edén, H.-U.J.T.B. Bengtsson, M. Modelling. *Theor Biol Med Model*. 2006; **3(1)**, 31.
30. W.V. Potters, H.A. Marquering, E. VanBavel, A.J. Nederveen. *Curr Cardiovasc Imaging Rep*. 2014; **7(4)**, 9257.
31. F. Pederzoli, G. Tosi, M.A. Vandelli, D. Belletti, F. Forni, B. Ruozi. *Wiley interdisciplinary reviews Nanomedicine and nanobiotechnology*. 2017.
32. S. Morsbach, G. Gonella, V. Mailänder, S. Wegner, S. Wu, T. Weidner, et al. *Angew Chem, Int Ed*. 2018; **57(39)**, 12626.
33. H. Zhang, J. Peng, X. Li, S. Liu, Z. Hu, G. Xu, et al. *Colloids Surf, B*. 2018; **167**, 220.

34. C. Carrillo-Carrion, M. Carril, W.J. Parak. *Current Opinion in Biotechnology*. 2017; **46**, 106.
35. L. Li, Q. Mu, B. Zhang, B. Yan. *Analyst*. 2010; **135(7)**, 1519.
36. T. Cedervall, I. Lynch, S. Lindman, T. Berggard, E. Thulin, H. Nilsson, et al. *Proc Natl Acad Sci U S A*. 2007; **104(7)**, 2050.
37. T. Cedervall, I. Lynch, M. Foy, T. Berggard, S.C. Donnelly, G. Cagney, et al. *Angew Chem Int Ed Engl*. 2007; **46(30)**, 5754.
38. S. Tenzer, D. Docter, J. Kuharev, A. Musyanovych, V. Fetz, R. Hecht, et al. *Nat Nanotechnol*. 2013; **8(10)**, 772.
39. D. Docter, U. Distler, W. Storck, J. Kuharev, D. Wunsch, A. Hahlbrock, et al. *Nat Protoc*. 2014; **9(9)**, 2030.
40. S. Tenzer, D. Docter, S. Rosfa, A. Wlodarski, J. Kuharev, A. Rekik, et al. *ACS Nano*. 2011; **5(9)**, 7155.
41. L.K. Muller, J. Simon, S. Schottler, K. Landfester, V. Mailander, K. Mohr. *RSC Advances*. 2016; **6(99)**, 96495.
42. S. Schottler, G. Becker, S. Winzen, T. Steinbach, K. Mohr, K. Landfester, et al. *Nat Nanotechnol*. 2016; **11(4)**, 372.
43. A.S. Lubbe, C. Bergemann, H. Riess, F. Schriever, P. Reichardt, K. Possinger, et al. *Cancer Res*. 1996; **56(20)**, 4686.
44. A.S. Lubbe, C. Bergemann, W. Huhnt, T. Fricke, H. Riess, J.W. Brock, et al. *Cancer Res*. 1996; **56(20)**, 4694.
45. A.J. Lemke, M.I. Senfft von Pilsach, A. Lübbe, C. Bergemann, H. Riess, R. Felix. *Eur J Radiol*. 2004; **14(11)**, 1949.
46. M. Kettering, J. Winter, M. Zeisberger, S. Bremer-Streck, H. Oehring, C. Bergemann, et al. *Nanotechnology*. 2007; **18(17)**, 9.
47. Z. Iszaly, K. Lovasz, I. Nagy, I.G. Marian, J. Racz, I.A. Szabo, et al. *J Magn Magn Mater*. 2018; **466**, 452.
48. Z.Y. Hu, H.Y. Zhang, Y. Zhang, R.A. Wu, H.F. Zou. *Colloid Surf B-Biointerfaces*. 2014; **121**, 354.
49. S.S. Raesch, S. Tenzer, W. Storck, A. Rurainski, D. Selzer, C.A. Ruge, et al. *ACS Nano*. 2015; **9(12)**, 11872.
50. D. Bonvin, D. Chiappe, M. Moniatte, H. Hofmann, M. Mionic Ebersold. *Analyst*. 2017; **142(20)**, 3805.
51. U. Sakulkhu, L. Maurizi, M. Mahmoudi, M. Motazacker, M. Vries, A. Gramoun, et al. *Nanoscale*. 2014; **6(19)**, 11439.
52. U. Sakulkhu, M. Mahmoudi, L. Maurizi, G. Coullerez, M. Hofmann-Amtenbrink, M. Vries, et al. *Biomaterials science*. 2015; **3(2)**, 265.
53. M. Wagner, S. Holzschuh, A. Traeger, A. Fahr, U.S. Schubert. *Anal Chem*. 2014; **86(11)**, 5201.
54. F.A. Messaud, R.D. Sanderson, J.R. Runyon, T. Otte, H. Pasch, S.K.R. Williams. *Progress in Polymer Science*. 2009; **34(4)**, 351.
55. C.R.M. Bria, S.K.R. Williams. *J Chromatogr A*. 2016; **1465**, 155.
56. M.I. Malik, H. Pasch. *Prog Polym Sci*. 2016; **63**, 42.
57. U. Hansen, A.F. Thunemann. *Langmuir*. 2015; **31(24)**, 6842.
58. P. Wimuktiwan, J. Shiowatana, A. Siripinyanond. *J Anal At Spectrom*. 2015; **30(1)**, 245.
59. C. Bantz, O. Koshkina, T. Lang, H.J. Galla, C.J. Kirkpatrick, R.H. Stauber, et al. *Beilstein J Nanotechnol*. 2014; **5**, 1774.
60. O. Koshkina, D. Westmeier, T. Lang, C. Bantz, A. Hahlbrock, C. Würth, et al. *Macromol Biosci*. 2016; **16(9)**, 1287.
61. J. Ashby, S. Schachermeyer, S. Pan, W. Zhong. *Anal Chem*. 2013; **85(15)**, 7494.
62. J. Ashby, S. Pan, W. Zhong. *ACS Appl Mater Interfaces*. 2014; **6(17)**, 15412.
63. C. Weber, J. Simon, V. Mailander, S. Morsbach, K. Landfester. *Acta Biomater*. 2018; **76**, 217.
64. A.M. Striegel, A.K. Brewer. *Annual review of analytical chemistry (Palo Alto, Calif)*. 2012; **5**, 15.

65. A.K. Brewer, A.M. Striegel. *J Sep Sci*. 2010; **33(22)**, 3555.
66. M. Roman, C. Rigo, H. Castillo-Michel, I. Munivrana, V. Vindigni, I. Mičetić, et al. *Anal Bioanal Chem*. 2016; **408(19)**, 5109.
67. R.R. Burgess. *Protein Expression and Purif*. 2018; **150**, 81.
68. B. Bobály, S. Fleury-Souverain, A. Beck, J.-L. Veuthey, D. Guillarme, S. Fekete. *Journal of pharmaceutical and biomedical analysis*. 2018; **147**, 493.
69. G. Brusotti, E. Calleri, R. Colombo, G. Massolini, F. Rinaldi, C. Temporini. *Chromatographia*. 2018; **81(1)**, 3.
70. J. Klein. *Proc Natl Acad Sci U S A*. 2007; **104(7)**, 2029.
71. W. Liu, J. Rose, S. Plantevin, M. Auffan, J.Y. Bottero, C. Vidaud. *Nanoscale*. 2013; **5(4)**, 1658.
72. A.J. Chetwynd, E.J. Guggenheim, S.M. Briffa, J.A. Thorn, I. Lynch, E. Valsami-Jones. *Nanomaterials*. 2018; **8(2)**, 29.
73. L. Trapiella-Alfonso, G. Ramírez-García, F. d'Orlyé, A. Varenne. *TrAC, Trends Anal Chem*. 2016; **84**, 121.
74. M. Matczuk, J. Legat, F. Scaletti, L. Messori, A.R. Timerbaev, M. Jarosz. *J Chromatogr A*. 2017; **1499**, 222.
75. J. Legat, M. Matczuk, A. Timerbaev, M. Jarosz. *Chromatographia*. 2017; **80(11)**, 1695.
76. M. Matczuk, K. Anecka, F. Scaletti, L. Messori, B.K. Keppler, A.R. Timerbaev, et al. *Metallomics*. 2015; **7(9)**, 1364.
77. W. Schärtl. Light Scattering from Polymer Solutions and Nanoparticle Dispersions. Heidelberg Germany: Springer-Verlag Berlin; 2007.
78. L. Nuhn, S. Gietzen, K. Mohr, K. Fischer, K. Toh, K. Miyata, et al. *Biomacromolecules*. 2014; **15(4)**, 1526.
79. K. Rausch, A. Reuter, K. Fischer, M. Schmidt. *Biomacromolecules*. 2010; **11**, 2836.
80. D.-H. Tsai, F.W. DelRio, A.M. Keene, K.M. Tyner, R.I. MacCuspie, T.J. Cho, et al. *Langmuir*. 2011; **27(6)**, 2464.
81. K. Oleg, B. Grégoire. *Reports on Progress in Physics*. 2002; **65(2)**, 251.
82. L. Shang, G.U. Nienhaus. *Acc Chem Res*. 2017; **50(2)**, 387.
83. H.X. Wang, Y.H. Lin, K. Nienhaus, G.U. Nienhaus. *Wiley Interdiscip Rev-Nanomed Nanobiotechnol*. 2018; **10(4)**, 9.
84. R. Frost, C. Wadell, A. Hellman, S. Molander, S. Svedhem, M. Persson, et al. *ACS Sens*. 2016; **1(6)**, 798.
85. R. Frost, C. Langhammer, T. Cedervall. *Nanoscale*. 2017; **9(10)**, 3620.
86. M. Carril, D. Padro, P. del Pino, C. Carrillo-Carrion, M. Gallego, W.J. Parak. *Nat Commun*. 2017; **8**, 5.
87. M.C. Lo Giudice, L.M. Herda, E. Polo, K.A. Dawson. *Nat Commun*. 2016; **7**, 10.
88. T. Miclaus, V.E. Bochenkov, R. Ogaki, K.A. Howard, D.S. Sutherland. *Nano Lett*. 2014; **14(4)**, 2086.
89. S. Lara, F. Alnasser, E. Polo, D. Garry, M.C. Lo Giudice, D.R. Hristov, et al. *ACS Nano*. 2017; **11(2)**, 1884.
90. O. Vilanova, J.J. Mittag, P.M. Kelly, S. Milani, K.A. Dawson, J.O. Radler, et al. *ACS Nano*. 2016; **10(12)**, 10842.
91. A.S. Pitek, D. O'Connell, E. Mahon, M.P. Monopoli, F. Baldelli Bombelli, K.A. Dawson. *PloS one*. 2012; **7(7)**, e40685.
92. K. Mohr, M. Sommer, G. Baier, S. Schöttler, P. Okwieka, S. Tenzer, et al. *J Nanomed Nanotechnol*. 2014; **05(02)**.
93. J.C. Giddings. *Science*. 1993; **260**, 1456.
94. K.G. Wahlund, J.C. Giddings. *Anal Chem*. 1987; **59**, 1332.
95. S.K.R. Williams, J.R. Runyon, A.A. Ashames. *Anal Chem*. 2011; **83(3)**, 634.
96. K.-G. Wahlund, L. Nilsson. Flow FFF – Basics and Key Applications. In: Williams SKR, Caldwell KD, editors. Field-Flow Fractionation in Biopolymer Analysis. Vienna: Springer Vienna; 2012. p. 1.
97. M. v Smoluchowski. *Annalen der Physik*. 1908; **25**, 205.
98. A. Einstein. *Annalen der Physik*. 1910; **338(16)**, 1275.

99. P. Kratochvíl. Classical light scattering from polymer solutions: Elsevier; 1987.
100. B.H. Zimm. *Journal of Physical and Colloid Chemistry*. 1948; **52**.
101. M.M. Bradford. *Anal Biochem*. 1976; **72**, 248.
102. S.J. Compton, C.G. Jones. *Anal Biochem*. 1985; **151(2)**, 369.
103. T. Zor, Z. Selinger. *Anal Biochem*. 1996; **236(2)**, 302.
104. J.M. Berg, L. Stryer, J.L. Tymoczko. Stryer Biochemie. Heidelberg: Springer Spektrum; 2013.
105. K. Weber, M. Osborn. *The Journal of biological chemistry*. 1969; **244(16)**, 4406.
106. A.L. Shapiro, E. Vinuela, J.V. Maizel, Jr. *Biochem Biophys Res Commun*. 1967; **28(5)**, 815.
107. J.A. Reynolds, C. Tanford. *The Journal of biological chemistry*. 1970; **245(19)**, 5161.
108. W.F. Patton. *Journal of chromatography B, Analytical technologies in the biomedical and life sciences*. 2002; **771(1-2)**, 3.
109. J. Sasse, S.R. Gallagher. *Current protocols in molecular biology*. 2003; **Chapter 10**, Unit 10.6.
110. L. Monaci, A. Visconti. *Trac-Trends Anal Chem*. 2009; **28(5)**, 581.
111. W. Bittremieux, D.L. Tabb, F. Impens, A. Staes, E. Timmerman, L. Martens, et al. *Mass Spectrom Rev*. 2018; **37(5)**, 697.
112. J.M. Burkhart, C. Schumbrutzki, S. Wortelkamp, A. Sickmann, R.P. Zahedi. *J Proteomics*. 2012; **75(4)**, 1454.
113. : iProteoToul; 2018 [Available from: http://proteomique.ipbs.fr/front-page/waters-synapt-g2-si/. Accessed on: 10 Oct 2018
114. R.J. Hunter. Chapter 3 - The Calculation of Zeta Potential. In: Hunter RJ, editor. Zeta Potential in Colloid Science: Academic Press; 1981. p. 59.
115. V. Mailander, K. Landfester. *Biomacromolecules*. 2009; **10(9)**, 2379.
116. H.R. Hulett, W.A. Bonner, J. Barrett, L.A. Herzenberg. *Science*. 1969; **166(3906)**, 747.
117. S. Milani, F.B. Bombelli, A.S. Pitek, K.A. Dawson, J. Rädler. *ACS Nano*. 2012; **6(3)**, 2532.
118. C. Pisani, J.C. Gaillard, C. Dorandeu, C. Charnay, Y. Guari, J. Chopineau, et al. *Nanoscale*. 2017; **9(18)**, 5769.
119. S. Wilhelm, A.J. Tavares, Q. Dai, S. Ohta, J. Audet, H.F. Dvorak, et al. *Nat Rev Mater*. 2016; **1**, 16014.
120. M. Mahmoudi. *Trends in biotechnology*. 2018.
121. S. Podzimek. Light Scattering, Size Exclusion Chromatography and Asymmetric Flow Field Flow Fractionation. Hoboken, New Jersey: John Wiley & Sons, Inc.; 2011.
122. S. Schachermeyer, J. Ashby, M. Kwon, W. Zhong. *J Chromatogr A*. 2012; **1264**, 72.
123. D. Pozzi, V. Colapicchioni, G. Caracciolo, S. Piovesana, A.L. Capriotti, S. Palchetti, et al. *Nanoscale*. 2014; **6(5)**, 2782.
124. M. Kokkinopoulou, J. Simon, K. Landfester, V. Mailander, I. Lieberwirth. *Nanoscale*. 2017; **9(25)**, 8858.
125. G. Senisterra, I. Chau, M. Vedadi. *Assay Drug Dev Technol*. 2012; **10(2)**, 128.
126. S. Winzen, J.C. Schwabacher, J. Müller, K. Landfester, K. Mohr. *Biomacromolecules*. 2016; **17(11)**, 3845.
127. J. Müller, K.N. Bauer, D. Prozeller, J. Simon, V. Mailänder, F.R. Wurm, et al. *Biomaterials*. 2017; **115**, 1.
128. A. Akbarzadeh, R. Rezaei-Sadabady, S. Davaran, S. Woo Joo, N. Zarghami, Y. Hanifehpour, et al. *Nanoscale Research Letters*. 2013; **8(102)**.
129. T. Lian, R.J. Ho. *J Pharm Sci*. 2001; **90(6)**, 667.
130. A. Sharma, U.S. Sharma. *Int J Pharm*. 1997; **154(2)**, 123.
131. A. Gabizon, R. Catane, B. Uziely, B. Kaufman, T. Safra, R. Cohen, et al. *Cancer Research*. 1994; **54(4)**, 987.
132. A.A. Gabizon. *Cancer Investigation*. 2001; **19(4)**, 424.
133. C.E. Swenson, W.R. Perkins, P. Roberts, A.S. Janoff. *The Breast*. 2001; **10**, 1.
134. D. Bobo, K.J. Robinson, J. Islam, K.J. Thurecht, S.R. Corrie. *Pharm Res*. 2016; **33(10)**, 2373.
135. B. Kharazian, N.L. Hadipour, M.R. Ejtehadi. *Int J Biochem Cell Biol*. 2016; **75**, 162.
136. T. Shehata, K. Ogawara, K. Higaki, T. Kimura. *Int J Pharm*. 2008; **359(1-2)**, 272.

137. L.K. Muller, K. Landfester. *Biochem Biophys Res Commun*. 2015; **468(3)**, 411.
138. M.C. Woodle, K.K. Matthay, M.S. Newman, J.E. Hidayat, L.R. Collins, C. Redemann, et al. *Biochim Biophys Acta, Biomembr*. 1992; **1105(2)**, 193.
139. C. Siegers, M. Biesalski, R. Haag. *Chemistry – A European Journal*. 2004; **10(11)**, 2831.
140. D. Papahadjopoulos, T.M. Allen, A. Gabizon, E. Mayhew, K. Matthay, S.K. Huang, et al. *Proc Natl Acad Sci U S A*. 1991; **88(24)**, 11460.
141. A. Bigdeli, S. Palchetti, D. Pozzi, M.R. Hormozi-Nezhad, F. Baldelli Bombelli, G. Caracciolo, et al. *ACS Nano*. 2016; **10(3)**, 3723.
142. G. Caracciolo, D. Pozzi, A.L. Capriotti, C. Cavaliere, S. Piovesana, G. La Barbera, et al. *J Mater Chem B*. 2014; **2(42)**, 7419.
143. T. Fritz, M. Hirsch, F.C. Richter, S.S. Müller, A.M. Hofmann, K.A.K. Rusitzka, et al. *Biomacromolecules*. 2014; **15(7)**, 2440.
144. K. Wagener, M. Worm, S. Pektor, M. Schinnerer, R. Thiermann, M. Miederer, et al. *Biomacromolecules*. 2018; **19(7)**, 2506.
145. U. Massing, S. Cicko, V. Ziroli. *J Controlled Release*. 2008; **125(1)**, 16.
146. U. Massing, S.G. Ingebrigtsen, N. Skalko-Basnet, A.M. Holsoeter. Dual Centrifugation - A Novel "in-vial" Liposome Processing Technique. In: Catala A, editor. Liposomes: IntechOpen; 2017. p. 3.
147. R. Gref, M. Luck, P. Quellec, M. Marchand, E. Dellacherie, S. Harnisch, et al. *Colloids Surf, B*. 2000; **18(3-4)**, 301.
148. M.L. Immordino, F. Dosio, L. Cattel. *Int J Nanomed*. 2006; **1(3)**, 297.
149. J.S. Suk, Q. Xu, N. Kim, J. Hanes, L.M. Ensign. *Adv Drug Delivery Rev*. 2016; **99(Pt A)**, 28.
150. M.P. Monopoli, D. Walczyk, A. Campbell, G. Elia, I. Lynch, F.B. Bombelli, et al. *J Am Chem Soc*. 2011; **133(8)**, 2525.
151. R.N. Qureshi, W.T. Kok, P.J. Schoenmakers. *Anal Chim Acta*. 2009; **654(1)**, 85.
152. Z.G. Kuklenyik, M.S.; Parks, B.A.; Schieltz, D.M.; Rees, J.C.; McWilliams, L.G.; Williamson, Y.M.; Pirkle, J.L.; Barr, J.R. *Chromatography*. 2015; **2**, 96.
153. M. Madorin, P. van Hoogevest, R. Hilfiker, B. Langwost, G.M. Kresbach, M. Ehrat, et al. *Pharm Res*. 1997; **14(12)**, 1706.
154. I. Park, K.J. Paeng, Y. Yoon, J.H. Song, M.H. Moon. *Journal of chromatography B, Analytical technologies in the biomedical and life sciences*. 2002; **780(2)**, 415.
155. J. Müller, D. Prozeller, A. Ghazaryan, M. Kokkinopoulou, V. Mailänder, S. Morsbach, et al. *Acta Biomater*. 2018; **71**, 420.
156. S. Palchetti, V. Colapicchioni, L. Digiacomo, G. Caracciolo, D. Pozzi, A.L. Capriotti, et al. *Biochim Biophys Acta*. 2016; **1858(2)**, 189.
157. S.W. Provencher. *Comput Phys Commun*. 1982; **27(3)**, 213.
158. S.W. Provencher. *Die Makromolekulare Chemie*. 1979; **180(1)**, 201.
159. D. Hofmann, S. Tenzer, M.B. Bannwarth, C. Messerschmidt, S.-F. Glaser, H. Schild, et al. *ACS Nano*. 2014; **8(10)**, 10077.
160. J.C. Silva, M.V. Gorenstein, G.Z. Li, J.P. Vissers, S.J. Geromanos. *Molecular & cellular proteomics : MCP*. 2006; **5(1)**, 144.
161. K. Landfester, N. Bechthold, F. Tiarks, M. Antonietti. *Macromolecules*. 1999; **32(8)**, 2679.
162. L.L. Hecht, A. Schoth, R. Muñoz-Espí, A. Javadi, K. Köhler, R. Miller, et al. *Macromol Chem Phys*. 2013; **214(7)**, 812.
163. I. García-Moreno, A. Costela, L. Campo, R. Sastre, F. Amat-Guerri, M. Liras, et al. *J Phys Chem A*. 2004; **108(16)**, 3315.
164. S. Jiang, B.C. Ma, J. Reinholz, Q. Li, J. Wang, K.A. Zhang, et al. *ACS Appl Mater Interfaces*. 2016; **8(44)**, 29915.

Appendix

A Abbreviations/Symbols

A	area of the accumulation wall
A_2	second Virial coefficient
ACF	autocorrelation function
AF4	asymmetric flow field-flow fractionation
API	active pharmaceutical ingredient
Apo AI	apolipoprotein A-I
b_0	channel width at the inlet
b_L	channel width at the outlet
BSA	bovine serum albumin
c	concentration
CE	capillary electrophoresis
Chol	cholesterol
cLSM	confocal laser scanning microscopy
CTMA-Cl	cetyltrimethylammonium chloride
D	diffusion coefficient
D_{app}	apparent diffusion coefficient
D_s	self-diffusion coefficient
DLS	dynamic light scattering
E_0	incoming energy
EPC	egg phosphatidyl choline
EPR	enhanced permeability and retention
E_s	emitted energy
ESI	electrospray ionization
f	friction
FACS	fluorescence activated cell sorting
FBS	fetal bovine serum
F_{cross}	cross flow
FCS	fluorescence correlation spectrometry
F_{out}	detector flow
Fr.	fraction
F_s	dynamic scattering factor

G_s	Self-correlation function of the intensity fluctuation
*hb*PG	hyperbranched polyglycerol
HDC	hydrodynamic chromatography
HSA	human serum albumin
IgG	immunoglobulin G
I_{solution}	scattering intensity of the solution
I_{solvent}	scattering intensity of the solvent
$I_{\text{std,abs}}$	scattering intensity of the standard
K	contrast factor
L	channel length
l	distance of the center of concentration of the sample to the wall
LC-MS	liquid chromatorgraphy – mass spectrometry
L-*hb*PG	liposomes functionalized with hbPG
L-PEG	PEGylated liposomes
L-un	unfunctionalized liposomes
M	molar mass
mPEG-DSPE	1,2-distearoyl-sn-glycero-3-phosphoethanolamine-N-[methoxy(polyethylene glycol)-3000]
n	partible number density
n_{D}	refractive index of the solute
$n_{\text{D,0}}$	refractive index of the solvent
N_L	nanoparticle number
$P(D_{\text{s}})$	distribution function
$P(q)$	particle form factor
$P(R_{\text{h}})$	size distribution
PBS	phosphate buffered saline
PDI	polydispersity index
PEG	polyethylene glycol
PS-NP	polystyrene nanoparticles
$\vec{q}$	scattering vector
R	Rayleigh ratio
r_{D}	distance of the scattering sample to the detector
R_{g}	radius of gyration
R_{h}	hydrodynamic radius
RI	refractive index
RL	retention level

R_s	resolution
SDS	sodium dodecyl sulfate
SDS-PAGE	sodium dodecyl sulfate – polyacrylamide gel electrophoresis
SEC	size exclusion chromatography
SEM	scanning electron microscopy
SiNC	Silica-nanocapsules
SLS	static light scattering
T	temperature
t^0	void time
TEM	transmission electron microscopy
TOF	time of flight
t_r	retention time
u_0	speed of the cross flow on the membrane surface
V	scattering volume
V^0	void volume
w	channel height
$\overline{w}_b$	width of the signal on its basis
y	spare area at the channel inlet
z'	channel width at the injection point
α	polarizability
$\frac{\partial n_D}{\partial c}$	refractive index increment
θ	scattering angle
κ_1	diffusion coefficient
κ_2	quantitative measurement of the polydispersity
λ^*	retention parameter
ν	frequency
σ_D	diffusion coefficient distribution function
σ_R	the size polydispersity
η	viscosity
τ	time shift

B Data

B.1 Preservation of the soft protein corona in distinct flow allows identification of weakly bound proteins

B.1.1 Complete LC-MS data

Accession	Annotation	Description	fmol		%	
			AF4	Centri-fuged	AF4	Centri-fuged
P02763	Acute Phase	Alpha-1-acid glycoprotein 1	27.77	0.00	0.24	0.00
P19652	Acute Phase	Alpha-1-acid glycoprotein 2	5.68	0.00	0.05	0.00
P01011	Acute Phase	Alpha-1-antichymotrypsin	25.71	0.00	0.22	0.00
P01009	Acute Phase	Alpha-1-antitrypsin	120.27	1.83	1.03	0.23
P01023	Acute Phase	Alpha-2-macroglobulin	116.42	0.25	0.99	0.03
P00450	Acute Phase	Ceruloplasmin	34.71	0.00	0.30	0.00
P02751	Acute Phase	Fibronectin	30.05	4.99	0.26	0.63
P00738	Acute Phase	Haptoglobin	343.91	1.16	2.93	0.15
P00739	Acute Phase	Haptoglobin-related protein	46.19	0.17	0.40	0.02
P18428	Acute Phase	Lipopolysaccharide-binding protein	0.00	0.07	0.00	0.01
P0DJI8; P0DJI9	Acute Phase	Serum amyloid A-1 protein	0.00	0.53	0.00	0.07
P02743	Acute Phase	Serum amyloid P-component	20.58	0.00	0.18	0.00
P08697	Coagulation	Alpha-2-antiplasmin	3.37	0.00	0.03	0.00
P01008	Coagulation	Antithrombin-III	13.62	0.44	0.12	0.06
P00742	Coagulation	Coagulation factor X	0.07	0.00	0.00	0.00
P02671	Coagulation	Fibrinogen alpha chain	55.81	0.46	0.48	0.06
P02675	Coagulation	Fibrinogen beta chain	199.45	1.09	1.67	0.14
P02679	Coagulation	Fibrinogen gamma chain	88.51	1.36	0.75	0.17
P23142	Coagulation	Fibulin-1	0.00	2.15	0.00	0.27
P04196	Coagulation	Histidine-rich glycoprotein	11.66	0.00	0.10	0.00
P08514	Coagulation	Integrin alpha-IIb O	0.00	0.29	0.00	0.04
P01042	Coagulation	Kininogen-1	73.25	0.00	0.63	0.00
P03952	Coagulation	Plasma kallikrein	225.28	0.00	1.94	0.00
P00747	Coagulation	Plasminogen	57.50	0.00	0.49	0.00
P00734	Coagulation	Prothrombin	165.04	0.00	1.39	0.00
P02730	Complement system	Band 3 anion transport protein	0.00	2.15	0.00	0.27
P04003	Complement system	C4b-binding protein alpha chain	69.87	1.32	0.60	0.17
P02745	Complement system	Complement C1q subcomponent subunit A	0.00	4.15	0.00	0.53
P02746	Complement system	Complement C1q subcomponent subunit B	59.47	3.54	0.51	0.45
P02747	Complement system	Complement C1q subcomponent subunit C	28.54	10.61	0.24	1.35
P00736	Complement system	Complement C1r subcomponent	16.79	1.59	0.15	0.20
P09871	Complement system	Complement C1s subcomponent	9.30	2.26	0.08	0.29
P01024	Complement system	Complement C3	154.79	3.56	1.32	0.45
P0C0L4	Complement system	Complement C4-A	78.63	3.50	0.67	0.45

P0C0L5	Complement system	Complement C4-B	77.89	2.42	0.67	0.31
P01031	Complement system	Complement C5	8.49	0.00	0.07	0.00
P07357	Complement system	Complement component C8 alpha chain	19.61	0.00	0.17	0.00
P07358	Complement system	Complement component C8 beta chain	12.41	0.00	0.11	0.00
P07360	Complement system	Complement component C8 gamma chain	10.81	0.37	0.10	0.05
P02748	Complement system	Complement component C9	0.00	0.95	0.00	0.12
P00751	Complement system	Complement factor B	55.50	0.00	0.48	0.00
P08603; Q02985; Q03591	Complement system	Complement factor H	65.71	0.00	0.57	0.00
P08603	Complement system	Complement factor H	0.00	5.00	0.00	0.64
Q03591; P36980	Complement system	Complement factor H-related protein 1	0.00	0.78	0.00	0.10
O75636	Complement system	Ficolin-3	0.57	0.00	0.01	0.00
P05155	Complement system	Plasma protease C1 inhibitor	37.43	0.52	0.32	0.07
P27918	Complement system	Properdin	0.00	1.18	0.00	0.15
P01876	Immunoglobulins	Ig alpha-1 chain C region	255.47	4.16	2.18	0.53
P01877	Immunoglobulins	Ig alpha-2 chain C region	50.11	0.32	0.43	0.04
P01880	Immunoglobulins	Ig delta chain C region	1.22	0.49	0.01	0.06
P01857	Immunoglobulins	Ig gamma-1 chain C region	1102.98	53.70	9.36	6.83
P01859	Immunoglobulins	Ig gamma-2 chain C region	88.25	6.14	0.76	0.78
P01860	Immunoglobulins	Ig gamma-3 chain C region	262.40	12.26	2.24	1.56
P01861	Immunoglobulins	Ig gamma-4 chain C region	246.32	1.04	2.11	0.13
P06331	Immunoglobulins	Ig heavy chain V-II region ARH-77	23.52	0.00	0.20	0.00
P06331; P01825	Immunoglobulins	Ig heavy chain V-II region ARH-77	0.00	1.18	0.00	0.15
P01766; P01777	Immunoglobulins	Ig heavy chain V-III region BRO	0.00	6.99	0.00	0.89
P01766; P01771; P01777	Immunoglobulins	Ig heavy chain V-III region BRO	84.58	0.00	0.73	0.00
P01767	Immunoglobulins	Ig heavy chain V-III region BUT	14.16	0.00	0.12	0.00
P01781	Immunoglobulins	Ig heavy chain V-III region GAL	0.66	0.00	0.01	0.00
P01765; P01767; P01774	Immunoglobulins	Ig heavy chain V-III region TIL	0.00	0.34	0.00	0.04
P01765	Immunoglobulins	Ig heavy chain V-III region TIL	0.53	0.00	0.00	0.00
P01779	Immunoglobulins	Ig heavy chain V-III region TUR	0.00	1.53	0.00	0.19
P01779; P01774	Immunoglobulins	Ig heavy chain V-III region TUR	0.00	0.00	0.00	0.00
P01764	Immunoglobulins	Ig heavy chain V-III region VH26	50.88	0.93	0.44	0.12
P01776	Immunoglobulins	Ig heavy chain V-III region WAS	1.79	0.00	0.02	0.00
P01763	Immunoglobulins	Ig heavy chain V-III region WEA	2.05	0.99	0.02	0.13
P01834	Immunoglobulins	Ig kappa chain C region	1250.58	78.31	10.65	9.97
P01593	Immunoglobulins	Ig kappa chain V-I region AG	11.35	0.00	0.10	0.00
P01593; P01609	Immunoglobulins	Ig kappa chain V-I region AG	0.00	0.00	0.00	0.00
P01598	Immunoglobulins	Ig kappa chain V-I region EU	5.84	0.00	0.05	0.00
P01600; P01594; P01599; P01607; P01609; P01610; P80362	Immunoglobulins	Ig kappa chain V-I region Hau	0.00	0.00	0.00	0.00

P01602	Immunoglobulins	Ig kappa chain V-I region HK102 (Fragment)	7.18	0.00	0.06	0.00
P01608	Immunoglobulins	Ig kappa chain V-I region Roy	2.58	0.00	0.02	0.00
P01614	Immunoglobulins	Ig kappa chain V-II region Cum	5.19	0.00	0.04	0.00
P06309	Immunoglobulins	Ig kappa chain V-II region GM607 (Fragment)	0.00	2.03	0.00	0.26
P01617; P06310	Immunoglobulins	Ig kappa chain V-II region TEW	0.00	1.29	0.00	0.16
P01617	Immunoglobulins	Ig kappa chain V-II region TEW	8.78	0.00	0.08	0.00
P18135; P18136	Immunoglobulins	Ig kappa chain V-III region HAH	0.01	0.00	0.00	0.00
P18136; P18135	Immunoglobulins	Ig kappa chain V-III region HIC	0.00	0.00	0.00	0.00
P01621	Immunoglobulins	Ig kappa chain V-III region NG9 (Fragment)	10.97	1.78	0.10	0.23
P01620; P01622; P01623; P04206	Immunoglobulins	Ig kappa chain V-III region SIE	39.75	0.26	0.34	0.03
P04433	Immunoglobulins	Ig kappa chain V-III region VG (Fragment)	0.32	1.89	0.00	0.24
P01625	Immunoglobulins	Ig kappa chain V-IV region Len	5.05	0.00	0.05	0.00
P83593; P06312; P06313	Immunoglobulins	Ig kappa chain V-IV region STH (Fragment)	0.00	0.00	0.00	0.00
P04208	Immunoglobulins	Ig lambda chain V-I region WAH	9.88	0.00	0.09	0.00
P04208; P01700	Immunoglobulins	Ig lambda chain V-I region WAH	0.00	1.77	0.00	0.23
P80748	Immunoglobulins	Ig lambda chain V-III region	14.85	0.00	0.13	0.00
P01714	Immunoglobulins	Ig lambda chain V-III region SH	13.86	0.36	0.12	0.05
P01717	Immunoglobulins	Ig lambda chain V-IV region Hil	4.92	0.00	0.04	0.00
P0CG05; P0CF74; P0CG06	Immunoglobulins	Ig lambda-2 chain C regions	238.61	5.92	2.03	0.75
A0M8Q6	Immunoglobulins	Ig lambda-7 chain C region	158.67	2.96	1.36	0.38
P01871	Immunoglobulins	Ig mu chain C region	410.28	15.73	3.50	2.00
P04220	Immunoglobulins	Ig mu heavy chain disease protein	29.59	5.47	0.25	0.70
P01591	Immunoglobulins	Immunoglobulin J chain	13.68	0.48	0.12	0.06
B9A064; P0CG04	Immunoglobulins	Immunoglobulin lambda-like polypeptide 5	197.99	18.95	1.71	2.42
P02647	Lipoproteins	Apolipoprotein A-I	82.16	90.21	0.70	11.46
P02652	Lipoproteins	Apolipoprotein A-II	1.95	1.71	0.02	0.22
P06727	Lipoproteins	Apolipoprotein A-IV	209.96	9.36	1.81	1.19
Q6Q788	Lipoproteins	Apolipoprotein A-V	0.00	0.24	0.00	0.03
P04114	Lipoproteins	Apolipoprotein B-100	243.16	5.19	2.10	0.66
P02655	Lipoproteins	Apolipoprotein C-II	0.00	0.24	0.00	0.03
P02656	Lipoproteins	Apolipoprotein C-III	0.00	12.12	0.00	1.54
P05090	Lipoproteins	Apolipoprotein D	4.23	0.00	0.04	0.00
P02649	Lipoproteins	Apolipoprotein E	45.52	21.45	0.39	2.73
O14791	Lipoproteins	Apolipoprotein L1	0.00	0.34	0.00	0.04
O95445	Lipoproteins	Apolipoprotein M	0.00	1.28	0.00	0.16
P02749	Lipoproteins	Beta-2-glycoprotein 1	185.72	1.42	1.57	0.18
P10909	Lipoproteins	Clusterin	102.90	240.78	0.94	30.62
P55058	Lipoproteins	Phospholipid transfer protein	0.00	13.66	0.00	1.74
P27169	Lipoproteins	Serum paraoxonase/arylesterase 1	20.60	2.08	0.18	0.26
Q13639	Other Plasma components	5-hydroxytryptamine receptor 4	0.00	0.00	0.00	0.00

P62736	Other Plasma components	Actin, aortic smooth muscle	0.00	0.03	0.00	0.00
P63261; P60709; P63267; P68032; P68133; Q562R1	Other Plasma components	Actin, cytoplasmic 2	0.00	1.43	0.00	0.18
O15144	Other Plasma components	Actin-related protein 2/3 complex subunit 2	0.00	1.33	0.00	0.17
Q10469	Other Plasma components	Alpha-1,6-mannosyl-glycoprotein 2-beta-N-acetylglucosaminyltransferase	10.10	0.00	0.09	0.00
P19652; P02763	Other Plasma components	Alpha-1-acid glycoprotein 2	0.00	0.37	0.00	0.05
P04217	Other Plasma components	Alpha-1B-glycoprotein	18.18	0.00	0.15	0.00
P02765	Other Plasma components	Alpha-2-HS-glycoprotein	14.18	0.16	0.12	0.02
P01019	Other Plasma components	Angiotensinogen	16.45	0.00	0.14	0.00
P10415	Other Plasma components	Apoptosis regulator Bcl-2	0.00	0.69	0.00	0.09
Q96CX2	Other Plasma components	BTB/POZ domain-containing protein KCTD12	149.70	0.00	1.28	0.00
Q9HA72	Other Plasma components	Calcium homeostasis modulator protein 2	1.22	0.00	0.01	0.00
Q9NZU7	Other Plasma components	Calcium-binding protein 1	16.32	0.00	0.14	0.00
Q9NPB3	Other Plasma components	Calcium-binding protein 2	0.00	0.25	0.00	0.03
Q9BXU9	Other Plasma components	Calcium-binding protein 8	10.01	0.00	0.09	0.00
P22792	Other Plasma components	Carboxypeptidase N subunit 2	0.83	0.00	0.01	0.00
P13688	Other Plasma components	Carcinoembryonic antigen-related cell adhesion molecule 1	3.78	0.00	0.03	0.00
P55212	Other Plasma components	Caspase-6	0.00	0.00	0.00	0.00
P11597	Other Plasma components	Cholesteryl ester transfer protein	0.00	0.08	0.00	0.01
O15335	Other Plasma components	Chondroadherin	0.00	0.16	0.00	0.02
A2IDD5	Other Plasma components	Coiled-coil domain-containing protein 78	4.55	0.00	0.04	0.00
O43639	Other Plasma components	Cytoplasmic protein NCK2	1.47	0.00	0.01	0.00
Q5VU92	Other Plasma components	DDB1- and CUL4-associated factor 12-like protein 1	0.00	1.88	0.00	0.24
Q92874	Other Plasma components	Deoxyribonuclease-1-like 2	0.00	0.00	0.00	0.00
Q96KS0	Other Plasma components	Egl nine homolog 2	0.00	0.00	0.00	0.00
Q9UHV8	Other Plasma components	Galactoside-binding soluble lectin 13	0.00	0.00	0.00	0.00
Q08380	Other Plasma components	Galectin-3-binding protein	3.65	0.00	0.03	0.00
Q86X53	Other Plasma components	Glutamate-rich protein 1	0.00	0.38	0.00	0.05
O14653	Other Plasma components	Golgi SNAP receptor complex member 2	0.94	0.00	0.01	0.00
P69905	Other Plasma components	Hemoglobin subunit alpha	3.03	0.00	0.03	0.00
P68871; P02042; P02100; P69891; P69892	Other Plasma components	Hemoglobin subunit beta	10.35	0.00	0.09	0.00
P02790	Other Plasma components	Hemopexin	73.88	0.34	0.63	0.04
P30512	Other Plasma components	HLA class I histocompatibility antigen, A-29 alpha chain	0.00	0.33	0.00	0.04
Q86UW8	Other Plasma components	Hyaluronan and proteoglycan link protein 4	7.83	0.00	0.07	0.00
P01624; P01605	Other Plasma components	Ig kappa chain V-III region POM	0.00	0.00	0.00	0.00
P19827	Other Plasma components	Inter-alpha-trypsin inhibitor heavy chain H1	25.64	0.00	0.22	0.00
P19823	Other Plasma components	Inter-alpha-trypsin inhibitor heavy chain H2	108.65	0.26	0.94	0.03
Q14624	Other Plasma components	Inter-alpha-trypsin inhibitor heavy chain H4	4.58	0.00	0.04	0.00
Q14116	Other Plasma components	Interleukin-18	0.09	0.00	0.00	0.00

Q14532	Other Plasma components	Keratin, type I	19.78	0.42	0.17	0.05
Q15323	Other Plasma components	Keratin, type I cuticular Ha1	0.00	0.00	0.00	0.00
Q14525	Other Plasma components	Keratin, type I cuticular Ha3-II	0.00	0.13	0.00	0.02
O76015; O76014	Other Plasma components	Keratin, type I cuticular Ha8	35.90	0.00	0.31	0.00
P13645; O76013; O76014; P13646; Q7Z3Y7; Q92764	Other Plasma components	Keratin, type I cytoskeletal 10	0.00	1.38	0.00	0.18
P13645; O76013; P13646; Q14525; Q15323; Q2M2I5; Q7Z3Y7; Q7Z3Z0; Q92764; Q99456	Other Plasma components	Keratin, type I cytoskeletal 10	228.80	0.00	1.97	0.00
Q99456	Other Plasma components	Keratin, type I cytoskeletal 12	0.00	0.46	0.00	0.06
P02533; P08727; P19012; Q04695	Other Plasma components	Keratin, type I cytoskeletal 14	29.76	0.00	0.26	0.00
P02533	Other Plasma components	Keratin, type I cytoskeletal 14	0.00	0.05	0.00	0.01
P19012	Other Plasma components	Keratin, type I cytoskeletal 15	0.00	0.26	0.00	0.03
P08779	Other Plasma components	Keratin, type I cytoskeletal 16	6.06	0.11	0.06	0.01
Q04695	Other Plasma components	Keratin, type I cytoskeletal 17	0.00	0.14	0.00	0.02
P05783	Other Plasma components	Keratin, type I cytoskeletal 18	0.00	2.67	0.00	0.34
P08727	Other Plasma components	Keratin, type I cytoskeletal 19	0.00	0.95	0.00	0.12
Q2M2I5	Other Plasma components	Keratin, type I cytoskeletal 24	0.00	3.23	0.00	0.41
Q7Z3Y8	Other Plasma components	Keratin, type I cytoskeletal 27	0.00	0.00	0.00	0.00
P35527	Other Plasma components	Keratin, type I cytoskeletal 9	39.61	1.14	0.34	0.15
P04264	Other Plasma components	Keratin, type II cytoskeletal 1	109.67	1.94	0.98	0.25
Q7Z794	Other Plasma components	Keratin, type II cytoskeletal 1b	0.00	0.25	0.00	0.03
P35908; O95678; P12035	Other Plasma components	Keratin, type II cytoskeletal 2 epidermal	105.70	0.00	0.93	0.00
P35908	Other Plasma components	Keratin, type II cytoskeletal 2 epidermal	0.00	0.60	0.00	0.08
Q01546	Other Plasma components	Keratin, type II cytoskeletal 2 oral	11.42	0.23	0.10	0.03
P12035	Other Plasma components	Keratin, type II cytoskeletal 3	0.00	0.00	0.00	0.00
P19013	Other Plasma components	Keratin, type II cytoskeletal 4	20.54	0.00	0.17	0.00
P13647	Other Plasma components	Keratin, type II cytoskeletal 5	5.44	1.55	0.05	0.20
P02538; P04259; P48668; Q14CN4; Q3SY84; Q7RTS7	Other Plasma components	Keratin, type II cytoskeletal 6A	0.00	0.00	0.00	0.00
P04259; P02538; P48668	Other Plasma components	Keratin, type II cytoskeletal 6B	0.00	0.49	0.00	0.06
Q86Y46	Other Plasma components	Keratin, type II cytoskeletal 73	0.00	0.00	0.00	0.00
Q5XKE5	Other Plasma components	Keratin, type II cytoskeletal 79	60.24	0.00	0.52	0.00
P05787	Other Plasma components	Keratin, type II cytoskeletal 8	11.62	0.00	0.10	0.00
Q6PIL6	Other Plasma components	Kv channel-interacting protein 4	0.06	0.00	0.00	0.00

P20700	Other Plasma components	Lamin-B1	38.83	0.00	0.34	0.00
Q8TCA0	Other Plasma components	Leucine-rich repeat-containing protein 20	33.26	0.00	0.28	0.00
Q1X8D7	Other Plasma components	Leucine-rich repeat-containing protein 36	178.99	0.00	1.54	0.00
Q8N8R3	Other Plasma components	Mitochondrial basic amino acids transporter	1.51	0.00	0.01	0.00
P60660	Other Plasma components	Myosin light polypeptide 6	0.00	0.37	0.00	0.05
P29966	Other Plasma components	Myristoylated alanine-rich C-kinase substrate	0.00	2.83	0.00	0.36
P18615	Other Plasma components	Negative elongation factor E	0.22	0.00	0.00	0.00
Q8ND90	Other Plasma components	Paraneoplastic antigen	16.64	0.00	0.14	0.00
P36955	Other Plasma components	Pigment epithelium-derived factor	6.72	0.00	0.06	0.00
Q6S8J3; P0CG38; P0CG39	Other Plasma components	POTE ankyrin domain family member E	0.00	0.14	0.00	0.02
P20742	Other Plasma components	Pregnancy zone protein	21.17	0.00	0.17	0.00
P02760	Other Plasma components	Protein AMBP	21.30	0.06	0.19	0.01
Q96NH3	Other Plasma components	Protein broad-minded OS=Homo sapiens GN=TBC1D32 PE=2 SV=4	1.90	0.00	0.02	0.00
Q7Z7L7	Other Plasma components	Protein zer-1 homolog	4.37	0.00	0.04	0.00
P61224; A6NIZ1; P62834	Other Plasma components	Ras-related protein Rap-1b	0.00	0.40	0.00	0.05
Q6UW15	Other Plasma components	Regenerating islet-derived protein 3-gamma	55.84	0.00	0.48	0.00
P12271	Other Plasma components	Retinaldehyde-binding protein 1	9.52	0.00	0.08	0.00
P38159; Q96E39	Other Plasma components	RNA-binding motif protein, X chromosome	12.72	0.00	0.11	0.00
Q9NY27	Other Plasma components	Serine/threonine-protein phosphatase 4 regulatory subunit 2	0.81	0.00	0.01	0.00
P02787	Other Plasma components	Serotransferrin	207.48	7.20	1.79	0.92
P02768	Other Plasma components	Serum albumin	1824.54	25.10	15.51	3.20
Q99469	Other Plasma components	SH3 and cysteine-rich domain-containing protein	0.00	0.53	0.00	0.07
P11166	Other Plasma components	Solute carrier family 2, facilitated glucose transporter member 1	0.00	0.95	0.00	0.12
P02549	Other Plasma components	Spectrin alpha chain, erythrocytic 1	0.00	1.11	0.00	0.14
Q96QR8	Other Plasma components	Transcriptional activator protein Pur-beta	23.92	0.00	0.20	0.00
Q9BVX2	Other Plasma components	Transmembrane protein 106C	1.22	0.00	0.01	0.00
P02766	Other Plasma components	Transthyretin	12.46	1.42	0.11	0.18
P04350	Other Plasma components	Tubulin beta-4A chain	0.00	0.56	0.00	0.07
Q8NHH1	Other Plasma components	Tubulin polyglutamylase TTLL11	0.00	0.50	0.00	0.06
Q16763	Other Plasma components	Ubiquitin-conjugating enzyme E2 S	0.00	0.00	0.00	0.00
Q9H9H4	Other Plasma components	Vacuolar protein sorting-associated protein 37B	0.00	0.00	0.00	0.00
P02774	Other Plasma components	Vitamin D-binding protein	6.87	0.00	0.06	0.00
P21796	Other Plasma components	Voltage-dependent anion-selective channel protein 1	0.43	0.00	0.00	0.00
P25311	Other Plasma components	Zinc-alpha-2-glycoprotein	15.17	0.00	0.13	0.00
P49747	Tissue Leakage	Cartilage oligomeric matrix protein	17.28	0.00	0.16	0.00
O43866	Tissue Leakage	CD5 antigen-like	21.51	1.06	0.18	0.13
Q2M243	Tissue Leakage	Coiled-coil domain-containing protein 27	0.00	0.22	0.00	0.03
P27105	Tissue Leakage	Erythrocyte band 7 integral membrane protein	0.00	0.38	0.00	0.05
P04406	Tissue Leakage	Glyceraldehyde-3-phosphate dehydrogenase	0.00	0.59	0.00	0.07
P51884	Tissue Leakage	Lumican	76.35	0.00	0.64	0.00

Q99733	Tissue Leakage	Nucleosome assembly protein 1-like 4	1.49	0.00	0.01	0.00
A5A3E0	Tissue Leakage	POTE ankyrin domain family member F	0.00	0.24	0.00	0.03
Q96TC7	Tissue Leakage	Regulator of microtubule dynamics protein 3	3.68	0.00	0.03	0.00
Q5W0B1	Tissue Leakage	RING finger protein 219	0.00	4.39	0.00	0.56
Q9H2S5	Tissue Leakage	RING finger protein 39	0.00	0.30	0.00	0.04
P04004	Tissue Leakage	Vitronectin	12.44	11.20	0.11	1.43
Q6ZN30	Tissue Leakage	Zinc finger protein basonuclin-2	0.00	16.55	0.00	2.11

B.2 Functionalization of liposomes with hyperbranched polyglycerol results in biological identity independent of the protein corona

B.2.1 Characterization of dialkyl-based hyperbranched polyglycerol amphiphiles (*hb*PG)

*hb*PG was synthesized and characterized form Ulrike Kemmer-Jonas and Dr. Matthias Worm (AG Frey, Johannes Gutenberg University Mainz, Germany).

Table B1: Properties of the synthesized BisHD-*hb*PG_{30}.

#	Composition	M_n^{th} g mol^{-1}	M_n^{NMR} g mol^{-1}	$M_n^{SEC, a}$ g mol^{-1}	$M_w/M_n^{SEC, a}$
1	BisHD-*hb*PG_{30}	3500	2760	2100	1.30

[a] obtained from SEC measurement in DMF using PEG standards.

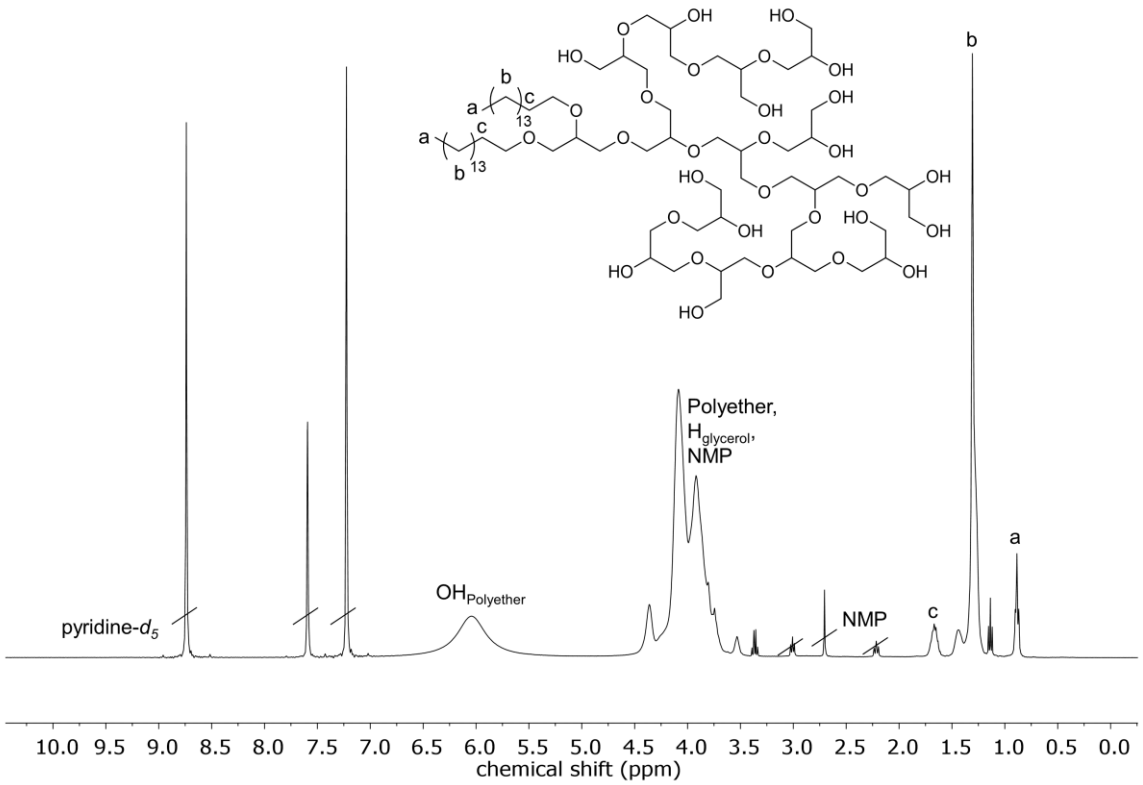

Figure B1: ^{1}H NMR (pyridine-d_5, 400 MHz) of BisOD-*hb*PG_{30}.

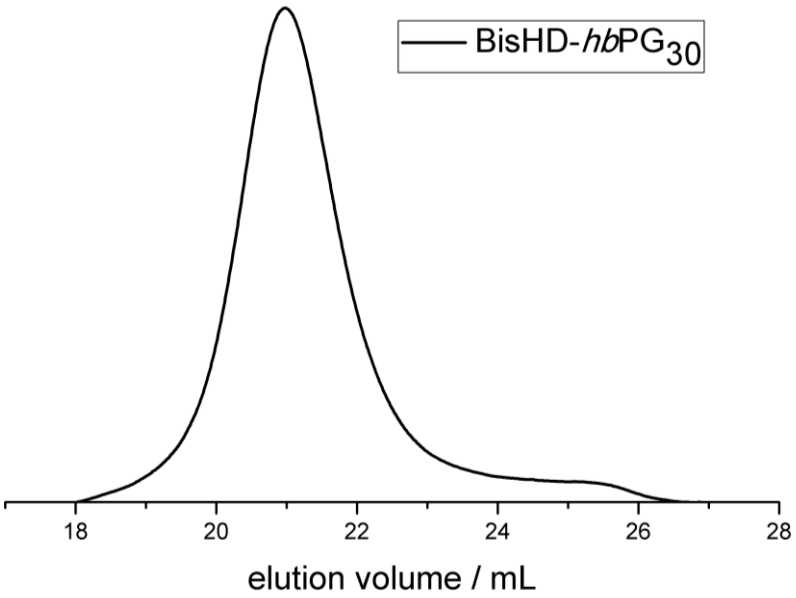

Figure B2: SEC trace (DMF, PEG standard, RI signal) of BisOD-*hb*PG_{30}.

B.2.2 Complete LC-MS data

Samples after centrifugation:

Annotation	Accession	Description	% based on all identified proteins			mol		
			L-un	L-PEG	L-*hb*PG	L-un	L-PEG	L-*hb*PG
Acute Phase	P02763	Alpha-1-acid glycoprotein 1	0.32	0.28	0.13	0.35	0.55	0.16
Acute Phase	P19652	Alpha-1-acid glycoprotein 2	0.12	0.03	0.03	0.14	0.05	0.04
Acute Phase	P01011	Alpha-1-antichymotrypsin	0.18	0.16	0.04	0.20	0.31	0.05
Acute Phase	P01009	Alpha-1-antitrypsin	0.80	2.43	0.37	0.87	4.78	0.44
Acute Phase	P01023	Alpha-2-macroglobulin	0.72	0.43	1.72	0.79	0.85	2.04
Acute Phase	P00450	Ceruloplasmin	0.43	0.16	0.20	0.47	0.32	0.24
Acute Phase	P02751	Fibronectin	0.13	0.25	0.13	0.14	0.49	0.16
Acute Phase	P00738	Haptoglobin	0.83	0.88	0.56	0.91	1.73	0.66
Acute Phase	P00739	Haptoglobin-related protein	0.69	1.49	0.93	0.76	2.93	1.10
Acute Phase	P18428	Lipopolysaccharide-binding protein	0.10	0.04	0.19	0.11	0.08	0.23
Acute Phase	P02743	Serum amyloid P-component	0.03	0.01	0.01	0.03	0.01	0.01
Coagulation	P08697	Alpha-2-antiplasmin	0.06	0.02	0.05	0.07	0.05	0.06
Coagulation	P01008	Antithrombin-III	0.06	0.04	0.03	0.07	0.08	0.04
Coagulation	P03951	Coagulation factor XI	0.33	0.20	0.34	0.36	0.39	0.40
Coagulation	P00748	Coagulation factor XII	1.78	0.59	5.15	1.95	1.17	6.11
Coagulation	P02671	Fibrinogen alpha chain	1.21	0.87	1.78	1.33	1.71	2.11
Coagulation	P02675	Fibrinogen beta chain	1.33	0.99	0.96	1.46	1.94	1.15
Coagulation	P02679	Fibrinogen gamma chain	1.73	0.73	1.31	1.89	1.43	1.56
Coagulation	P04196	Histidine-rich glycoprotein	5.20	4.66	18.81	5.69	9.18	22.34
Coagulation	Q14520	Hyaluronan-binding protein 2	0.05	0.01	0.42	0.06	0.02	0.50
Coagulation	P01042	Kininogen-1	0.50	0.33	1.51	0.55	0.66	1.79
Coagulation	P03952	Plasma kallikrein	0.72	0.14	3.04	0.79	0.27	3.62
Coagulation	P00747	Plasminogen	1.08	0.54	2.54	1.18	1.05	3.02
Coagulation	P00734	Prothrombin	0.14	0.04	0.19	0.15	0.07	0.23
Coagulation	P07996	Thrombospondin-1	0.15	0.27	0.12	0.16	0.54	0.14
Complement system	P04003	C4b-binding protein alpha chain	0.24	0.19	0.27	0.26	0.38	0.33
Complement system	P02746	Complement C1q subcomponent subunit B	0.03	0.02	0.02	0.03	0.04	0.02
Complement system	P02747	Complement C1q subcomponent subunit C	0.08	0.04	0.06	0.09	0.08	0.07
Complement system	P01024	Complement C3	1.84	1.61	1.08	2.02	3.17	1.28
Complement system	P0C0L4	Complement C4-A	0.20	0.29	0.24	0.22	0.57	0.28
Complement system	P0C0L5	Complement C4-B	0.18	0.25	0.21	0.19	0.50	0.24
Complement system	P02748	Complement component C9	0.09	0.09	0.11	0.10	0.18	0.13
Complement system	P00751	Complement factor B	0.10	0.05	0.05	0.11	0.10	0.06
Complement system	P08603	Complement factor H	0.18	0.18	0.13	0.20	0.35	0.16
Complement system	P36980	Complement factor H-related protein 2	0.00	0.00	0.03	0.00	0.00	0.03
Complement system	P05155	Plasma protease C1 inhibitor	0.31	0.11	0.49	0.34	0.21	0.59
Complement system	P27918	Properdin	0.31	0.10	0.31	0.34	0.20	0.37
Complement system	P08670	Vimentin	0.03	0.02	0.01	0.03	0.05	0.02

Immunoglobulins	P01876; P01877	Ig alpha-1 chain C region	1.02	0.85	0.31	1.12	1.68	0.36
Immunoglobulins	P01857	Ig gamma-1 chain C region	4.78	5.82	1.32	5.23	11.47	1.56
Immunoglobulins	P01859	Ig gamma-2 chain C region	0.34	0.36	0.11	0.37	0.70	0.13
Immunoglobulins	P01860	Ig gamma-3 chain C region	0.31	0.26	0.11	0.34	0.51	0.13
Immunoglobulins	P01861	Ig gamma-4 chain C region	0.25	0.27	0.12	0.27	0.54	0.14
Immunoglobulins	P01834	Ig kappa chain C region	4.61	4.03	1.64	5.05	7.94	1.95
Immunoglobulins	P0CG05; A0M8Q6; P0CF74; P0CG04; P0CG06	Ig lambda-2 chain C regions	1.46	1.25	0.42	1.60	2.47	0.50
Immunoglobulins	P01871	Ig mu chain C region	1.00	0.92	0.86	1.09	1.82	1.02
Immunoglobulins	P04220	Ig mu heavy chain disease protein	0.26	0.33	0.25	0.29	0.64	0.30
Immunoglobulins	P01764; P01768	Immunoglobulin heavy variable 3-23	0.08	0.05	0.04	0.08	0.10	0.05
Immunoglobulins	A0A075 B6Q5	Immunoglobulin heavy variable 3-64	0.15	0.09	0.19	0.16	0.17	0.23
Immunoglobulins	P01782	Immunoglobulin heavy variable 3-9	0.00	0.00	0.00	0.00	0.00	0.00
Immunoglobulins	P01824; A0A075 B6R2; A0A0C4 DH41; P01825; P06331	Immunoglobulin heavy variable 4-39	0.06	0.07	0.07	0.07	0.14	0.08
Immunoglobulins	A0A07 5B6S5	Immunoglobulin kappa variable 1-27	0.07	0.03	0.03	0.07	0.06	0.03
Immunoglobulins	P01597; P04432	Immunoglobulin kappa variable 1-39	0.04	0.04	0.02	0.05	0.08	0.02
Immunoglobulins	P04433	Immunoglobulin kappa variable 3-11	0.13	0.12	0.07	0.15	0.23	0.09
Immunoglobulins	P01624	Immunoglobulin kappa variable 3-15	0.02	0.02	0.02	0.02	0.03	0.02
Immunoglobulins	P01619	Immunoglobulin kappa variable 3-20	0.02	0.00	0.00	0.02	0.00	0.00
Immunoglobulins	A0A0C 4DH25	Immunoglobulin kappa variable 3-20	0.00	0.00	0.01	0.00	0.00	0.01
Immunoglobulins	P01700	Immunoglobulin lambda variable 1-47	0.10	0.10	0.05	0.11	0.19	0.06
Immunoglobulins	B9A064	Immunoglobulin lambda-like polypeptide 5	0.43	0.34	0.13	0.47	0.67	0.16
Lipoproteins	P02647	Apolipoprotein A-I	1.12	1.85	0.84	1.23	3.64	0.99
Lipoproteins	P02652	Apolipoprotein A-II	0.06	0.01	0.08	0.07	0.01	0.09
Lipoproteins	P06727	Apolipoprotein A-IV	0.26	0.12	0.34	0.29	0.25	0.40
Lipoproteins	P04114	Apolipoprotein B-100	0.40	0.36	0.49	0.44	0.70	0.58
Lipoproteins	P02656	Apolipoprotein C-III	0.04	0.01	0.08	0.04	0.03	0.10
Lipoproteins	P05090	Apolipoprotein D	0.10	0.04	0.05	0.11	0.07	0.06
Lipoproteins	P02649	Apolipoprotein E	0.36	0.55	1.24	0.39	1.09	1.47
Lipoproteins	P02749	Beta-2-glycoprotein 1	0.25	0.19	0.30	0.27	0.38	0.36
Lipoproteins	P10909	Clusterin	0.61	0.86	0.52	0.67	1.70	0.62
Lipoproteins	P27169	Serum paraoxonase/arylesterase 1	0.16	0.14	0.13	0.17	0.28	0.16
Other Plasma components	Q5TCS8	Adenylate kinase 9	0.54	0.53	0.71	0.59	1.04	0.85
Other Plasma components	P43652	Afamin	0.05	0.01	0.10	0.06	0.03	0.11
Other Plasma components	P04217	Alpha-1B-glycoprotein	0.42	0.26	0.43	0.46	0.51	0.51
Other Plasma components	P02765	Alpha-2-HS-glycoprotein	0.38	0.39	0.24	0.42	0.76	0.28
Other Plasma components	Q9C0B1	Alpha-ketoglutarate-dependent dioxygenase FTO	1.01	2.07	0.78	1.10	4.08	0.92

Other Plasma components	P01019	Angiotensinogen	0.05	0.06	0.05	0.06	0.11	0.06
Other Plasma components	B4E2M5	Ankyrin repeat domain-containing protein 66	0.08	0.05	0.11	0.09	0.11	0.14
Other Plasma components	P07355; A6NMY6	Annexin A2	0.01	0.00	0.01	0.01	0.00	0.01
Other Plasma components	Q99856	AT-rich interactive domain-containing protein 3A	0.89	0.59	0.30	0.98	1.17	0.36
Other Plasma components	Q13867	Bleomycin hydrolase	0.01	0.00	0.00	0.01	0.00	0.00
Other Plasma components	Q9P1Z2	Calcium-binding and coiled-coil domain-containing protein 1	0.15	0.05	0.17	0.17	0.10	0.21
Other Plasma components	P27482	Calmodulin-like protein 3 2	0.00	0.00	0.00	0.00	0.00	0.00
Other Plasma components	P31944	Caspase-14	0.02	0.01	0.12	0.03	0.01	0.14
Other Plasma components	Q14781	Chromobox protein homolog 2	0.39	0.68	0.35	0.43	1.34	0.42
Other Plasma components	Q03591; Q9BXR6	Complement factor H-related protein 1	0.03	0.01	0.10	0.03	0.02	0.12
Other Plasma components	Q15517	Corneodesmosin	0.10	0.05	0.01	0.11	0.10	0.01
Other Plasma components	P35321	Cornifin-A	0.04	0.00	0.08	0.04	0.00	0.09
Other Plasma components	P01040	Cystatin-A	0.05	0.04	0.09	0.05	0.07	0.10
Other Plasma components	Q08554	Desmocollin-1	0.16	0.07	0.31	0.18	0.13	0.36
Other Plasma components	Q02413	Desmoglein-1	0.11	0.06	0.15	0.12	0.13	0.18
Other Plasma components	P15924	Desmoplakin	0.22	0.12	0.21	0.24	0.24	0.24
Other Plasma components	P49917	DNA ligase 4	0.10	0.18	0.13	0.11	0.36	0.15
Other Plasma components	Q01469; A8MUU1	Fatty acid-binding protein, epidermal	0.02	0.03	0.03	0.02	0.06	0.04
Other Plasma components	Q5D862	Filaggrin-2	0.04	0.04	0.05	0.04	0.07	0.06
Other Plasma components	P47929	Galectin-7	0.00	0.01	0.02	0.00	0.02	0.02
Other Plasma components	O75223	Gamma-glutamylcyclotransferase	0.00	0.00	0.01	0.00	0.00	0.01
Other Plasma components	A6NH11	Glycolipid transfer protein domain-containing protein 2	0.77	0.76	0.25	0.85	1.49	0.29
Other Plasma components	P02790	Hemopexin	1.04	0.40	0.27	1.14	0.80	0.32
Other Plasma components	Q9NQG7	Hermansky-Pudlak syndrome 4 protein	0.06	0.04	0.06	0.06	0.09	0.07
Other Plasma components	Q92826	Homeobox protein Hox-B13	0.09	0.04	0.09	0.10	0.08	0.11
Other Plasma components	Q6YN16	Hydroxysteroid dehydrogenase-like protein 2	0.06	0.01	0.02	0.07	0.02	0.02
Other Plasma components	P17936	Insulin-like growth factor-binding protein 3	0.03	0.00	0.11	0.03	0.01	0.13
Other Plasma components	O43736	Integral membrane protein 2A	0.02	0.00	0.02	0.02	0.00	0.02
Other Plasma components	P19827	Inter-alpha-trypsin inhibitor heavy chain H1	0.91	0.14	0.58	0.99	0.28	0.69
Other Plasma components	P19823	Inter-alpha-trypsin inhibitor heavy chain H2	0.06	0.07	0.04	0.07	0.13	0.05
Other Plasma components	Q14624	Inter-alpha-trypsin inhibitor heavy chain H4	0.37	0.40	0.58	0.40	0.79	0.69
Other Plasma components	P14923	Junction plakoglobin	0.15	0.32	0.18	0.17	0.63	0.22
Other Plasma components	P61626	Lysozyme C	0.01	0.00	0.02	0.01	0.00	0.02
Other Plasma components	Q96NY8	Nectin-4	0.11	0.00	0.24	0.12	0.00	0.29
Other Plasma components	Q8N4E4	Phosducin-like protein 2	0.53	0.74	0.83	0.58	1.45	0.98
Other Plasma components	Q9H814	Phosphorylated adapter RNA export protein	0.12	0.01	0.02	0.13	0.01	0.02
Other Plasma components	Q13835	Plakophilin-1	0.00	0.00	0.07	0.00	0.00	0.08
Other Plasma components	P02776; P10720	Platelet factor 4	0.23	0.13	0.64	0.25	0.26	0.76
Other Plasma components	A5A3E0; Q6S8J3; Q9BYX7	POTE ankyrin domain family member F	0.59	2.00	0.87	0.65	3.94	1.04

Other Plasma components	P20742	Pregnancy zone protein	0.04	0.02	0.04	0.05	0.04	0.05
Other Plasma components	P02760	Protein AMBP	0.08	0.08	0.07	0.09	0.16	0.08
Other Plasma components	Q96NT3	Protein GUCD1	0.22	0.20	0.06	0.25	0.39	0.07
Other Plasma components	Q8WVV4	Protein POF1B	0.25	0.14	0.33	0.27	0.27	0.39
Other Plasma components	Q9NVS9	Pyridoxine-5'-phosphate oxidase	0.07	0.01	0.06	0.08	0.02	0.07
Other Plasma components	P49908	Selenoprotein P	0.19	0.05	0.39	0.21	0.09	0.46
Other Plasma components	P02787	Serotransferrin	1.58	1.98	1.04	1.73	3.90	1.24
Other Plasma components	P02768	Serum albumin	26.10	26.23	5.92	28.60	51.69	7.03
Other Plasma components	Q9BXU3	Testis-expressed protein 13A	0.01	0.04	0.02	0.01	0.08	0.02
Other Plasma components	Q9H1E5	Thioredoxin-related transmembrane protein 4	0.32	1.19	0.54	0.35	2.35	0.65
Other Plasma components	P02766	Transthyretin	0.15	0.13	0.06	0.16	0.25	0.08
Other Plasma components	P07477	Trypsin-1	0.01	0.00	0.04	0.01	0.01	0.05
Other Plasma components	P62979; P0CG47; P0CG48	Ubiquitin-40S ribosomal protein S27a	0.04	0.07	0.06	0.04	0.13	0.07
Other Plasma components	Q6ZVL6	UPF0606 protein KIAA1549L	0.14	0.02	0.03	0.15	0.05	0.03
Other Plasma components	Q12981	Vesicle transport protein SEC20	0.27	0.28	0.47	0.30	0.56	0.56
Other Plasma components	P02774	Vitamin D-binding protein	0.26	0.11	0.43	0.28	0.22	0.51
Other Plasma components	P25311	Zinc-alpha-2-glycoprotein	0.68	0.46	0.52	0.74	0.90	0.62
Tissue Leakage	P62736; P63267; P68032; P68133; Q562R1	Actin, aortic smooth muscle	0.12	0.03	0.14	0.13	0.06	0.17
Tissue Leakage	P60709; P63261	Actin, cytoplasmic 1	0.04	0.01	0.02	0.04	0.02	0.02
Tissue Leakage	P03950	Angiogenin	0.05	0.02	0.13	0.05	0.04	0.16
Tissue Leakage	O43866	CD5 antigen-like	0.22	0.19	0.27	0.24	0.36	0.32
Tissue Leakage	P81605	Dermcidin	0.07	0.13	0.22	0.07	0.25	0.26
Tissue Leakage	P04406	Glyceraldehyde-3-phosphate dehydrogenase	0.05	0.04	0.06	0.06	0.08	0.08
Tissue Leakage	A0A0C4DH42; A0A0B4J1X5; P01767; P01772	Immunoglobulin heavy variable 3-66	0.16	0.15	0.07	0.18	0.30	0.08
Tissue Leakage	Q15323; Q14525	Keratin, type I cuticular Ha1	0.03	0.04	0.05	0.03	0.09	0.05
Tissue Leakage	Q14532	Keratin, type I cuticular Ha2	0.14	0.02	0.05	0.16	0.04	0.05
Tissue Leakage	Q92764	Keratin, type I cuticular Ha5	0.09	0.06	0.04	0.09	0.12	0.05
Tissue Leakage	O76014; O76015	Keratin, type I cuticular Ha7	0.08	0.04	0.11	0.09	0.09	0.13
Tissue Leakage	P13645; Q7Z3Y8; Q7Z3Y9; Q7Z3Z0; Q99456	Keratin, type I cytoskeletal 10	2.54	4.04	3.86	2.78	7.95	4.59
Tissue Leakage	P13646	Keratin, type I cytoskeletal 13	0.03	0.06	0.02	0.04	0.11	0.03
Tissue Leakage	P02533	Keratin, type I cytoskeletal 14	0.76	1.30	0.55	0.84	2.56	0.65
Tissue Leakage	P19012	Keratin, type I cytoskeletal 15	0.06	0.19	0.09	0.07	0.38	0.11
Tissue Leakage	P08779	Keratin, type I cytoskeletal 16	0.35	1.28	0.22	0.38	2.53	0.26
Tissue Leakage	Q04695	Keratin, type I cytoskeletal 17	0.14	0.18	0.08	0.15	0.36	0.09

Tissue Leakage	P05783	Keratin, type I cytoskeletal 18	0.12	0.13	0.05	0.13	0.25	0.06
Tissue Leakage	P08727	Keratin, type I cytoskeletal 19	0.01	0.02	0.04	0.02	0.03	0.05
Tissue Leakage	Q2M2I5	Keratin, type I cytoskeletal 24	0.29	0.89	0.48	0.32	1.75	0.57
Tissue Leakage	Q7Z3Y7	Keratin, type I cytoskeletal 28	0.00	0.00	0.00	0.00	0.00	0.00
Tissue Leakage	P35527	Keratin, type I cytoskeletal 9	1.97	0.88	4.98	2.16	1.73	5.91
Tissue Leakage	Q9NSB2; O43790; P78385; Q14533	Keratin, type II cuticular Hb4	0.01	0.01	0.02	0.01	0.01	0.02
Tissue Leakage	P04264	Keratin, type II cytoskeletal 1	3.67	3.62	7.56	4.02	7.12	8.98
Tissue Leakage	Q7Z794	Keratin, type II cytoskeletal 1b	0.34	0.50	0.39	0.37	0.99	0.46
Tissue Leakage	P35908	Keratin, type II cytoskeletal 2 epidermal	1.42	0.69	1.93	1.56	1.37	2.29
Tissue Leakage	Q01546	Keratin, type II cytoskeletal 2 oral	0.20	0.32	0.21	0.22	0.64	0.25
Tissue Leakage	P12035	Keratin, type II cytoskeletal 3	0.05	0.03	0.05	0.05	0.07	0.06
Tissue Leakage	P13647	Keratin, type II cytoskeletal 5	0.28	0.37	0.39	0.30	0.73	0.46
Tissue Leakage	P02538	Keratin, type II cytoskeletal 6A	0.19	0.23	0.11	0.21	0.44	0.13
Tissue Leakage	P04259	Keratin, type II cytoskeletal 6B	0.12	0.13	0.32	0.13	0.26	0.39
Tissue Leakage	P08729	Keratin, type II cytoskeletal 7	0.07	0.11	0.13	0.07	0.21	0.16
Tissue Leakage	Q14CN4	Keratin, type II cytoskeletal 72	2.44	1.42	0.48	2.68	2.80	0.57
Tissue Leakage	Q86Y46	Keratin, type II cytoskeletal 73	0.07	0.02	0.12	0.07	0.04	0.14
Tissue Leakage	Q8N1N4	Keratin, type II cytoskeletal 78	0.13	0.04	0.09	0.14	0.08	0.10
Tissue Leakage	Q5XKE5	Keratin, type II cytoskeletal 79	0.05	0.09	0.10	0.05	0.18	0.11
Tissue Leakage	P05787	Keratin, type II cytoskeletal 8	0.02	0.00	0.05	0.02	0.01	0.06
Tissue Leakage	Q6KB66	Keratin, type II cytoskeletal 80	0.32	0.52	0.44	0.35	1.02	0.52
Tissue Leakage	Q8N1A0	Keratin-like protein KRT222	0.06	0.04	0.13	0.06	0.09	0.15
Tissue Leakage	Q5T749	Keratinocyte proline-rich protein	0.04	0.02	0.01	0.05	0.04	0.02
Tissue Leakage	P02788	Lactotransferrin	0.46	0.23	0.25	0.50	0.45	0.30
Tissue Leakage	P12036	Neurofilament heavy polypeptide	0.12	0.11	0.11	0.13	0.21	0.13
Tissue Leakage	P12273	Prolactin-inducible protein	0.02	0.02	0.03	0.02	0.04	0.04
Tissue Leakage	Q8NHM4; P07478	Putative trypsin-6	0.03	0.11	0.05	0.04	0.21	0.05
Tissue Leakage	P05452	Tetranectin	0.04	0.01	0.22	0.04	0.02	0.26
Tissue Leakage	P04004	Vitronectin	0.58	0.33	1.19	0.63	0.64	1.42
Tissue Leakage	Q9UGR2	Zinc finger CCCH domain-containing protein 7B	0.73	2.35	1.20	0.80	4.63	1.43

Samples after AF4:

Annotation	Accession	Description	%basedn on all identified proteins			fmol		
			L-un	L-PEG	L-*hb*PG	L-un	L-PEG	L-*hb*PG
Acute Phase	P02763	Alpha-1-acid glycoprotein 1	0.31	0.27	0.27	0.84	0.89	0.81
Acute Phase	P19652	Alpha-1-acid glycoprotein 2	0.17	0.01	0.02	0.46	0.03	0.07
Acute Phase	P01011	Alpha-1-antichymotrypsin	0.15	0.20	0.04	0.40	0.68	0.14
Acute Phase	P01009	Alpha-1-antitrypsin	1.57	4.86	3.66	4.21	16.11	11.13
Acute Phase	P01023	Alpha-2-macroglobulin	1.83	0.22	0.49	4.92	0.73	1.48
Acute Phase	P00450	Ceruloplasmin	1.10	0.74	0.38	2.96	2.46	1.16

Acute Phase	P02751	Fibronectin	1.93	0.01	0.12	5.17	0.03	0.36
Acute Phase	P00738	Haptoglobin	1.07	4.11	3.25	2.88	13.65	9.88
Acute Phase	P00739	Haptoglobin-related protein	1.38	0.31	0.11	3.70	1.04	0.35
Acute Phase	P02743	Serum amyloid P-component	0.02	0.01	0.01	0.06	0.04	0.03
Coagulation	P08697	Alpha-2-antiplasmin	0.01	0.01	0.00	0.02	0.02	0.00
Coagulation	P01008	Antithrombin-III	0.56	0.31	0.19	1.50	1.02	0.58
Coagulation	P02671	Fibrinogen alpha chain	1.08	0.48	0.57	2.90	1.59	1.72
Coagulation	P02675	Fibrinogen beta chain	3.77	0.77	1.63	10.11	2.57	4.96
Coagulation	P02679	Fibrinogen gamma chain	0.10	0.10	0.02	0.26	0.32	0.07
Coagulation	P04196	Histidine-rich glycoprotein	1.25	0.11	0.44	3.36	0.38	1.33
Coagulation	P01042	Kininogen-1	1.28	0.08	0.09	3.42	0.26	0.27
Coagulation	P00747	Plasminogen	0.97	0.10	0.36	2.61	0.32	1.09
Coagulation	P00734	Prothrombin	0.71	0.48	0.35	1.91	1.59	1.07
Complement system	P01024	Complement C3	0.34	0.30	0.21	0.92	1.00	0.64
Complement system	P0C0L4	Complement C4-A	0.03	0.06	0.04	0.08	0.20	0.12
Complement system	P0C0L5	Complement C4-B	0.15	0.33	0.21	0.41	1.11	0.64
Complement system	P13671	Complement component C6	0.02	0.00	0.00	0.06	0.00	0.00
Complement system	P02748	Complement component C9	0.14	0.07	0.07	0.37	0.24	0.22
Complement system	P00751	Complement factor B	0.07	0.03	0.01	0.20	0.09	0.03
Complement system	P08603	Complement factor H	0.05	0.00	0.00	0.12	0.00	0.00
Complement system	P05155	Plasma protease C1 inhibitor	0.35	0.21	0.24	0.94	0.68	0.74
Immunoglobulins	Q9NQZ3; Q13117; Q86SG3; Q9NR90	Deleted in azoospermia protein 1	0.00	0.00	0.00	0.00	0.00	0.00
Immunoglobulins	P01876	Ig alpha-1 chain C region	2.16	0.89	1.86	5.79	2.96	5.64
Immunoglobulins	P01877	Ig alpha-2 chain C region	0.03	0.00	0.00	0.08	0.01	0.01
Immunoglobulins	P01857	Ig gamma-1 chain C region	3.25	4.82	4.62	8.71	15.99	14.06
Immunoglobulins	P01859	Ig gamma-2 chain C region	1.03	1.67	1.49	2.77	5.55	4.55
Immunoglobulins	P01860	Ig gamma-3 chain C region	0.07	0.10	0.12	0.18	0.32	0.37
Immunoglobulins	P01861	Ig gamma-4 chain C region	0.34	0.33	0.36	0.92	1.08	1.08
Immunoglobulins	P01834	Ig kappa chain C region	11.40	7.02	6.76	30.59	23.28	20.58
Immunoglobulins	P0CG05; P0CF74; P0CG06	Ig lambda-2 chain C regions	0.14	0.20	0.17	0.38	0.65	0.53
Immunoglobulins	A0M8Q6	Ig lambda-7 chain C region	0.42	0.50	0.47	1.12	1.65	1.44
Immunoglobulins	P01871	Ig mu chain C region	1.13	1.79	0.74	3.04	5.95	2.25
Immunoglobulins	P04220	Ig mu heavy chain disease protein	0.00	0.00	0.00	0.01	0.00	0.01
Immunoglobulins	P01762	Immunoglobulin heavy variable 3-11	0.00	0.00	0.00	0.00	0.00	0.00
Immunoglobulins	P01768; P01764	Immunoglobulin heavy variable 3-30	0.00	0.00	0.00	0.00	0.00	0.00
Immunoglobulins	P01780	Immunoglobulin heavy variable 3-7	0.11	0.03	0.01	0.29	0.09	0.03
Immunoglobulins	P01591	Immunoglobulin J chain	0.05	0.03	0.03	0.14	0.09	0.08
Immunoglobulins	P01602; A0A0C4 DH72	Immunoglobulin kappa variable 1-5	0.00	0.00	0.00	0.00	0.00	0.00

Immunoglobulins	A0A0C4DH67; A0A075B6S5	Immunoglobulin kappa variable 1-8	0.06	0.05	0.00	0.16	0.15	0.00
Immunoglobulins	A0A075B6S2; A0A0A0MRZ7	Immunoglobulin kappa variable 2D-29	0.03	0.02	0.00	0.09	0.06	0.01
Immunoglobulins	A0A075B6S6	Immunoglobulin kappa variable 2D-30	0.00	0.00	0.00	0.00	0.00	0.00
Immunoglobulins	P04433	Immunoglobulin kappa variable 3-11	0.04	0.07	0.07	0.10	0.22	0.20
Immunoglobulins	P01624	Immunoglobulin kappa variable 3-15	0.00	0.00	0.00	0.00	0.00	0.01
Immunoglobulins	A0A0C4DH25	Immunoglobulin kappa variable 3-20	0.62	0.44	0.68	1.67	1.45	2.07
Immunoglobulins	P01699	Immunoglobulin lambda variable 1-44	0.04	0.00	0.00	0.11	0.00	0.00
Immunoglobulins	B9A064; P0CG04	Immunoglobulin lambda-like polypeptide 5	0.38	0.52	0.46	1.01	1.73	1.40
Lipoproteins	P02647	Apolipoprotein A-I	3.32	2.21	9.45	8.91	7.34	28.75
Lipoproteins	P02652	Apolipoprotein A-II	0.09	0.02	0.12	0.23	0.08	0.36
Lipoproteins	P06727	Apolipoprotein A-IV	0.09	0.04	0.05	0.23	0.14	0.15
Lipoproteins	P02749	Beta-2-glycoprotein 1	0.12	0.00	0.00	0.33	0.00	0.01
Lipoproteins	P10909	Clusterin	0.97	0.13	0.12	2.60	0.43	0.37
Lipoproteins	P27169	Serum paraoxonase/arylesterase 1	0.03	0.00	0.03	0.07	0.00	0.08
Other Plasma components	P43652	Afamin	0.21	0.07	0.07	0.56	0.24	0.20
Other Plasma components	Q10469	Alpha-1,6-mannosyl-glycoprotein 2-beta-N-acetylglucosaminyltransferase	0.75	0.00	0.02	2.00	0.00	0.06
Other Plasma components	P04217	Alpha-1B-glycoprotein	1.06	0.09	0.27	2.85	0.28	0.83
Other Plasma components	P02765	Alpha-2-HS-glycoprotein	0.47	0.93	0.91	1.27	3.08	2.78
Other Plasma components	P01019	Angiotensinogen	0.73	0.64	0.25	1.97	2.13	0.75
Other Plasma components	O15296	Arachidonate 15-lipoxygenase B	0.02	0.00	0.00	0.05	0.01	0.00
Other Plasma components	Q6P093	Arylacetamide deacetylase-like 2	0.62	1.37	1.02	1.67	4.54	3.11
Other Plasma components	Q99856	AT-rich interactive domain-containing protein 3A	1.34	0.73	0.20	3.60	2.42	0.60
Other Plasma components	P31939	Bifunctional purine biosynthesis protein PURH	0.07	0.05	0.00	0.19	0.15	0.01
Other Plasma components	P27482	Calmodulin-like protein 3 2	0.00	0.00	0.00	0.00	0.00	0.00
Other Plasma components	P22792	Carboxypeptidase N subunit 2	0.01	0.00	0.01	0.03	0.01	0.02
Other Plasma components	P25774	Cathepsin S	0.00	0.00	0.00	0.01	0.00	0.00
Other Plasma components	Q16739	Ceramide glucosyltransferase	0.10	0.02	0.02	0.27	0.06	0.05
Other Plasma components	P51160	Cone cGMP-specific 3',5'-cyclic phosphodiesterase subunit alpha'	0.28	1.04	0.50	0.75	3.44	1.52
Other Plasma components	Q69YN2	CWF19-like protein 1	0.03	0.13	0.15	0.09	0.43	0.45
Other Plasma components	O43639	Cytoplasmic protein NCK2	0.02	0.02	0.02	0.05	0.05	0.06
Other Plasma components	O95376	E3 ubiquitin-protein ligase ARIH2	1.64	0.60	1.56	4.41	2.01	4.75
Other Plasma components	P63241	Eukaryotic translation initiation factor 5A-1	0.23	0.00	0.08	0.62	0.00	0.25
Other Plasma components	Q9UK97	F-box only protein 9	0.06	0.20	0.12	0.15	0.66	0.36
Other Plasma components	Q12841	Follistatin-related protein 1	0.18	0.40	0.30	0.47	1.33	0.90
Other Plasma components	O95954	Formimidoyltransferase-cyclodeaminase	0.23	0.27	0.19	0.61	0.90	0.59
Other Plasma components	Q6IB77	Glycine N-acyltransferase	0.00	0.00	0.00	0.00	0.00	0.00
Other Plasma components	O60760	Hematopoietic prostaglandin D synthase	0.00	0.00	0.00	0.00	0.00	0.00
Other Plasma components	P69905	Hemoglobin subunit alpha	0.00	0.00	0.00	0.00	0.00	0.00

Other Plasma components	P68871; P02042; P69891; P69892	Hemoglobin subunit beta	0.35	0.26	1.05	0.94	0.87	3.21
Other Plasma components	P02790	Hemopexin	0.58	0.95	0.39	1.55	3.14	1.19
Other Plasma components	P35858	Insulin-like growth factor-binding protein complex acid labile subunit	0.00	0.00	0.00	0.00	0.00	0.00
Other Plasma components	P19827	Inter-alpha-trypsin inhibitor heavy chain H1	0.02	0.01	0.00	0.05	0.02	0.00
Other Plasma components	P19823	Inter-alpha-trypsin inhibitor heavy chain H2	0.54	0.03	0.01	1.46	0.10	0.02
Other Plasma components	Q14624	Inter-alpha-trypsin inhibitor heavy chain H4	0.32	0.36	0.42	0.85	1.19	1.27
Other Plasma components	Q14116	Interleukin-18	0.06	0.34	0.27	0.16	1.12	0.81
Other Plasma components	O95760	Interleukin-33	0.01	0.04	0.02	0.03	0.13	0.06
Other Plasma components	P05231	Interleukin-6	0.02	0.00	0.00	0.05	0.01	0.00
Other Plasma components	P02750	Leucine-rich alpha-2-glycoprotein	0.31	0.21	0.17	0.83	0.70	0.52
Other Plasma components	Q9Y4U1	Methylmalonic aciduria and homocystinuria type C protein	0.03	0.00	0.01	0.07	0.01	0.03
Other Plasma components	Q29980	MHC class I polypeptide-related sequence B	0.01	0.00	0.00	0.02	0.00	0.00
Other Plasma components	H3BPM6	MKRN2 opposite strand protein	0.00	0.00	0.00	0.01	0.01	0.00
Other Plasma components	Q9UMX5	Neudesin	0.00	0.00	0.00	0.00	0.00	0.00
Other Plasma components	P36955	Pigment epithelium-derived factor	4.24	0.55	0.42	11.37	1.81	1.29
Other Plasma components	P20742	Pregnancy zone protein	0.05	0.00	0.00	0.14	0.02	0.00
Other Plasma components	Q8N8N7	Prostaglandin reductase 2	0.00	0.00	0.00	0.00	0.00	0.00
Other Plasma components	P02760	Protein AMBP	0.58	0.09	0.20	1.56	0.28	0.61
Other Plasma components	P0C7A2	Protein FAM153B	0.00	0.00	0.00	0.00	0.00	0.00
Other Plasma components	Q8N6L0	Protein KASH5	0.02	0.00	0.00	0.04	0.00	0.00
Other Plasma components	Q8IWL2	Pulmonary surfactant-associated protein A1	0.00	0.00	0.00	0.00	0.00	0.00
Other Plasma components	Q6WQI6	Putative cancer susceptibility gene HEPN1 protein	0.00	0.00	0.00	0.00	0.00	0.00
Other Plasma components	P02753	Retinol-binding protein 4	0.25	0.14	0.02	0.68	0.45	0.08
Other Plasma components	Q13228	Selenium-binding protein	0.00	0.00	0.00	0.00	0.00	0.00
Other Plasma components	Q9NY27	Serine/threonine-protein phosphatase 4 regulatory subunit 2	1.63	0.40	0.18	4.36	1.33	0.56
Other Plasma components	P02787	Serotransferrin	1.20	1.70	0.99	3.23	5.63	3.00
Other Plasma components	P02768	Serum albumin	23.02	37.37	37.43	61.78	123.99	113.87
Other Plasma components	P04278	Sex hormone-binding globulin OS=Homo sapiens GN=SHBG PE=1 SV=2	0.00	0.00	0.00	0.00	0.00	0.00
Other Plasma components	Q5VSL9	Striatin-interacting protein 1	0.70	4.22	2.54	1.89	14.00	7.71
Other Plasma components	O75558	Syntaxin-11	0.11	0.01	0.01	0.28	0.02	0.02
Other Plasma components	Q9Y4I5	Tesmin	0.00	0.00	0.00	0.00	0.00	0.00
Other Plasma components	Q9H3H9	Transcription elongation factor A protein-like 2	0.00	0.00	0.00	0.00	0.00	0.00
Other Plasma components	Q16514	Transcription initiation factor TFIID subunit 12	0.00	0.00	0.00	0.00	0.00	0.00
Other Plasma components	Q6ZMR5	Transmembrane protease serine 11A	0.04	0.22	0.20	0.10	0.72	0.60
Other Plasma components	Q9BVX2	Transmembrane protein 106C	0.08	0.63	0.33	0.22	2.09	1.01
Other Plasma components	P02766	Transthyretin	1.34	0.56	0.49	3.60	1.85	1.48
Other Plasma components	P08621	U1 small nuclear ribonucleoprotein 70 kDa	0.62	1.50	0.55	1.67	4.98	1.68

Other Plasma components	P36537; Q9BY64	UDP-glucuronosyltransferase 2B10	0.20	0.52	0.26	0.55	1.74	0.79
Other Plasma components	Q96K31	Uncharacterized protein C8orf76	0.01	0.00	0.00	0.01	0.00	0.00
Other Plasma components	Q13336	Urea transporter 1	3.32	2.37	3.18	8.90	7.87	9.69
Other Plasma components	P02774	Vitamin D-binding protein	0.43	0.19	0.18	1.17	0.63	0.56
Other Plasma components	P54284	Voltage-dependent L-type calcium channel subunit beta-3	0.34	0.09	0.87	0.91	0.31	2.66
Other Plasma components	P25311	Zinc-alpha-2-glycoprotein	1.02	2.44	1.64	2.73	8.09	5.00
Tissue Leakage	P63261; P60709	Actin, cytoplasmic 2	0.07	0.00	0.00	0.18	0.00	0.00
Tissue Leakage	O43866	CD5 antigen-like	0.00	0.00	0.00	0.01	0.01	0.01
Tissue Leakage	P47755	F-actin-capping protein subunit alpha-2	0.00	0.00	0.00	0.00	0.00	0.00
Tissue Leakage	P13645	Keratin, type I cytoskeletal 10	0.42	0.14	0.09	1.13	0.45	0.27
Tissue Leakage	P02533	Keratin, type I cytoskeletal 14	0.07	0.44	0.26	0.19	1.46	0.79
Tissue Leakage	P35527	Keratin, type I cytoskeletal 9	1.67	0.60	0.41	4.49	1.98	1.24
Tissue Leakage	P78385	Keratin, type II cuticular Hb3	0.02	0.10	0.06	0.07	0.33	0.18
Tissue Leakage	P04264; Q7Z794	Keratin, type II cytoskeletal 1	1.31	0.75	0.58	3.52	2.48	1.78
Tissue Leakage	P35908	Keratin, type II cytoskeletal 2 epidermal	0.29	0.86	0.48	0.77	2.84	1.47
Tissue Leakage	P13647	Keratin, type II cytoskeletal 5	0.25	0.18	0.19	0.68	0.61	0.57
Tissue Leakage	P04259; P02538; P48668	Keratin, type II cytoskeletal 6B	0.01	0.02	0.00	0.02	0.06	0.01
Tissue Leakage	P51884	Lumican	0.00	0.00	0.00	0.00	0.00	0.00
Tissue Leakage	Q96PD5	N-acetylmuramoyl-L-alanine amidase	0.02	0.04	0.00	0.05	0.15	0.00
Tissue Leakage	Q96EI5	Transcription elongation factor A protein-like 4	0.01	0.09	0.00	0.02	0.28	0.00
Tissue Leakage	P04004	Vitronectin	0.00	0.00	0.00	0.01	0.01	0.00

Citrate plasma:

Annotation	Accession	Description	%based on all identified proteins		
			1	2	3
Acute Phase	P01023	Alpha-2-macroglobulin	1.43	1.47	1.45
Acute Phase	P00738	Haptoglobin	1.39	1.41	1.52
Acute Phase	P01009	Alpha-1-antitrypsin	1.23	1.09	1.05
Acute Phase	P02763	Alpha-1-acid glycoprotein 1	0.74	0.72	0.73
Acute Phase	P01011	Alpha-1-antichymotrypsin	0.40	0.39	0.39
Acute Phase	P19652	Alpha-1-acid glycoprotein 2	0.35	0.36	0.35
Acute Phase	P00450	Ceruloplasmin	0.30	0.30	0.31
Acute Phase	P02751	Fibronectin	0.26	0.27	0.29
Acute Phase	P00739	Haptoglobin-related protein	0.02	0.02	0.03
Coagulation	P02679	Fibrinogen gamma chain	1.44	1.41	1.51
Coagulation	P02671	Fibrinogen alpha chain	1.08	0.99	1.07
Coagulation	P02675	Fibrinogen beta chain	0.87	0.86	0.91
Coagulation	P01042	Kininogen-1	0.26	0.23	0.23

Coagulation	P00734	Prothrombin	0.19	0.19	0.18
Coagulation	P04196	Histidine-rich glycoprotein	0.17	0.15	0.15
Coagulation	P00747	Plasminogen	0.09	0.09	0.10
Complement system	P01024	Complement C3	0.92	0.98	0.99
Complement system	P0C0L4	Complement C4-A	0.76	0.76	0.70
Complement system	P0C0L5	Complement C4-B	0.57	0.57	0.53
Complement system	P05155	Plasma protease C1 inhibitor	0.33	0.35	0.38
Complement system	P08603	Complement factor H	0.21	0.21	0.21
Complement system	P00751	Complement factor B	0.19	0.17	0.18
Complement system	P04003	C4b-binding protein alpha chain	0.10	0.10	0.10
Immunoglobulins	P01834	Ig kappa chain C region	7.44	7.46	7.67
Immunoglobulins	P01857	Ig gamma-1 chain C region	6.38	6.60	6.69
Immunoglobulins	P0CG05; A0M8Q6; P0CF74; P0CG06	Ig lambda-2 chain C regions	3.89	4.23	4.25
Immunoglobulins	B9A064; P0CG04	Immunoglobulin lambda-like polypeptide 5	1.88	2.05	2.06
Immunoglobulins	P01876	Ig alpha-1 chain C region	1.34	1.33	1.46
Immunoglobulins	P01859	Ig gamma-2 chain C region	0.90	0.98	0.97
Immunoglobulins	P01860	Ig gamma-3 chain C region	0.91	0.79	0.80
Immunoglobulins	P01871; P04220	Ig mu chain C region	0.75	0.82	0.81
Immunoglobulins	P01861	Ig gamma-4 chain C region	0.60	0.68	0.66
Immunoglobulins	P01619	Immunoglobulin kappa variable 3-20	0.28	0.27	0.29
Immunoglobulins	P01768; A0A0B4J1X5; P01764	Immunoglobulin heavy variable 3-30	0.20	0.18	0.20
Immunoglobulins	P01624; A0A0C4DH55	Immunoglobulin kappa variable 3-15	0.07	0.08	0.06
Immunoglobulins	P01877	Ig alpha-2 chain C region	0.07	0.06	0.06
Immunoglobulins	A0A075B6S6; P06310	Immunoglobulin kappa variable 2D-30	0.01	0.00	0.00
Lipoproteins	P04114	Apolipoprotein B-100	0.61	0.58	0.60
Lipoproteins	P02647	Apolipoprotein A-I	0.43	0.36	0.37
Lipoproteins	P02749	Beta-2-glycoprotein 1	0.27	0.26	0.28
Lipoproteins	P27169	Serum paraoxonase/arylesterase 1	0.08	0.08	0.07
Other Plasma components	P02768	Serum albumin	48.30	48.09	47.60
Other Plasma components	P02787	Serotransferrin	4.23	3.61	3.59
Other Plasma components	P19827	Inter-alpha-trypsin inhibitor heavy chain H1	1.78	1.72	1.66
Other Plasma components	P02790	Hemopexin	1.37	1.37	1.33
Other Plasma components	P02774	Vitamin D-binding protein	0.78	0.82	0.78
Other Plasma components	P02765	Alpha-2-HS-glycoprotein	0.60	0.78	0.72
Other Plasma components	P25311	Zinc-alpha-2-glycoprotein	0.38	0.34	0.35
Other Plasma components	P01019	Angiotensinogen	0.22	0.28	0.25

Other Plasma components	P04217	Alpha-1B-glycoprotein	0.24	0.25	0.24
Other Plasma components	Q14964	Ras-related protein Rab-39A	0.19	0.23	0.27
Other Plasma components	P02766	Transthyretin	0.17	0.18	0.19
Other Plasma components	Q5VSP4	Putative lipocalin 1-like protein 1	0.19	0.13	0.14
Other Plasma components	Q14624	Inter-alpha-trypsin inhibitor heavy chain H4	0.14	0.14	0.13
Other Plasma components	P02760	Protein AMBP	0.12	0.13	0.14
Other Plasma components	P19823	Inter-alpha-trypsin inhibitor heavy chain H2	0.11	0.11	0.12
Other Plasma components	P20742	Pregnancy zone protein	0.04	0.03	0.02
Other Plasma components	P04278	Sex hormone-binding globulin	0.01	0.01	0.01
Tissue Leakage	P35527	Keratin, type I cytoskeletal 9	1.04	1.11	1.03
Tissue Leakage	P04004	Vitronectin	0.24	0.26	0.26
Tissue Leakage	P13645	Keratin, type I cytoskeletal 10	0.14	0.18	0.16
Tissue Leakage	P04264	Keratin, type II cytoskeletal 1	0.12	0.12	0.12
Tissue Leakage	O43866	CD5 antigen-like	0.07	0.08	0.09
Tissue Leakage	Q96PD5	N-acetylmuramoyl-L-alanine amidase	0.07	0.07	0.07
Tissue Leakage	P06396	Gelsolin	0.07	0.07	0.07

B.3 Evaluation of the “negative” biomolecule corona

B.3.1 Polystyrene nanoparticles with iron oxide core in AF4 after removal of the nanocarriers including the protein corona

To see, if the evaluation of the “negative”corona can be adopted to other nanocarrier systems, the procedure was repeated with polystyrene-nanoparticles containing an iron core (PS-FeO). These magnetic nanoparticles were chosen, since they can be isolated via magnetic separation additionally to centrifugation and AF4 separation. Therefore, after incubation of the PS-FeOs in 5 vol% plasma, a magnet was put into close vicinity of the vial. After the PS-FeOs including their protein corona concentrated close the the magnet, the supernatant was removed. The same procedure was applied to pure plasma as well, and both supernatants were injected in the AF4 and separated (Figure B3). The collected fractions were further analyzed by SDS-PAGE (Figure B4). To compare the results, the protein corona and supernatant of the PS-FeOs incubated in plasma were obtained via centrifutaion and via magnetic separation. The results are displayed in Figure B4.

The results indicate that the concept of the analysis of the supernatant after removal of the protein corona can be transferred to other nanocarrier systems. Even more, for the PS-FeOs three different separation methods could be compared and the influence of the separation on the protein corona formation can be further investigated with the presented system.

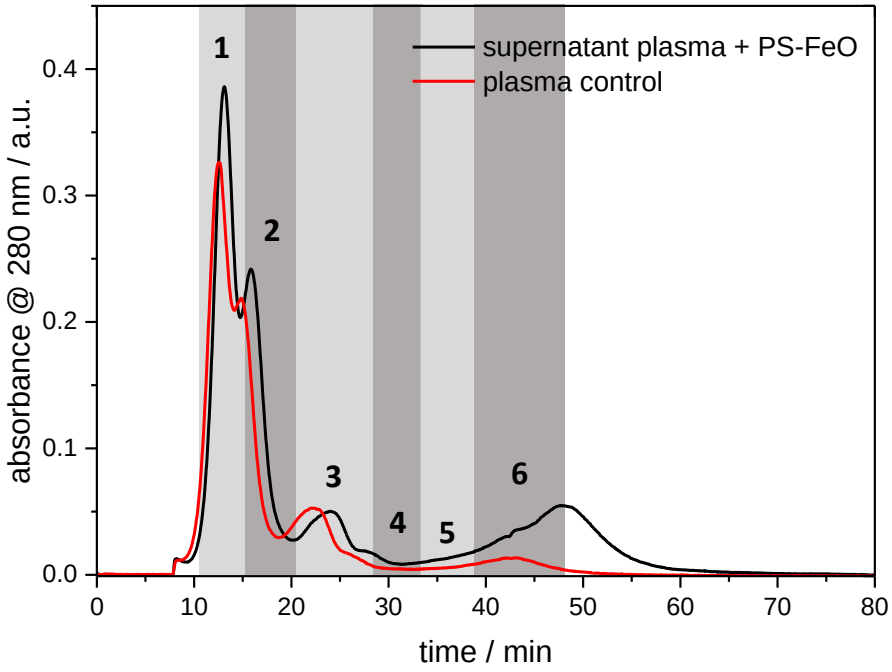

Figure B3: AF4 elugram of the supernatant of polysyrene-nanoparticles containing an iron oxide core, incubated with 5 vol% human blood plasma, after removal of the protein corona via magnetic separation (black). A reference elugram of plasma after the same treatment is given in black (red). Fractions for further analysis were collected at the retention times indicated by the grey boxes. The experiments were done to transfer the methods from chapter 4.3 on another nanocarrier system

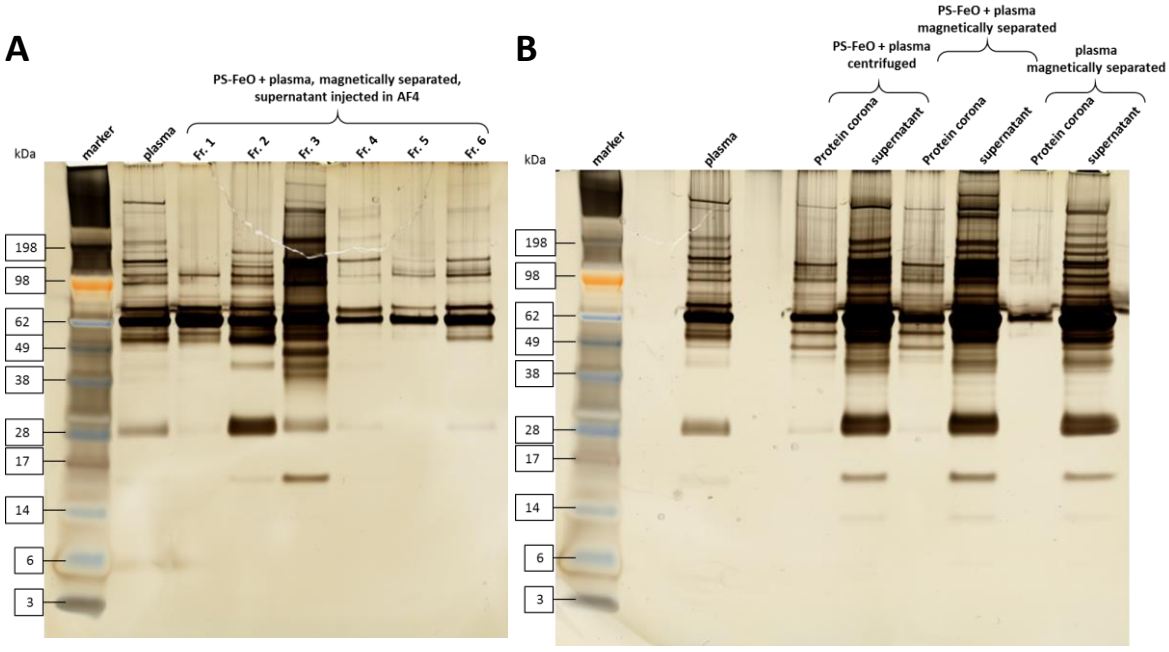

Figure B4: SDS-PAGE of the collected fractions of the AF4 elugram (Figure B3) of the supernatant of polystyrene-nanoparticles containing an iron oxide core, incubated with 5 vol% human blood plasma after removal of the protein corona (A). The protein corona and supernatant of polystyrene-nanoparticles containing an iron core incubated with 5 vol% plasma and isolated either by classic centrifugation or by magnetic separation (B). Plasma after the magnetic separation is given as a reference (B).

B.3.2 Complete LC-MS data

Protein corona:

Accession	Annotation	Description	% based on all identified proteins	
			PC SiNC + plasma	plasma control
P00739	Acute Phase	Haptoglobin-related protein	2.52	5.73
P18428	Acute Phase	Lipopolysaccharide-binding protein	0.74	0.02
P01009	Acute Phase	Alpha-1-antitrypsin	0.70	0.47
P00738	Acute Phase	Haptoglobin	0.54	0.80
P19652	Acute Phase	Alpha-1-acid glycoprotein 2	0.37	0.19
P02763	Acute Phase	Alpha-1-acid glycoprotein 1	0.15	0.56
P01023	Acute Phase	Alpha-2-macroglobulin	0.13	0.12
P04196	Coagulation	Histidine-rich glycoprotein	6.50	0.60
P02675	Coagulation	Fibrinogen beta chain	0.24	0.60
P02679	Coagulation	Fibrinogen gamma chain	0.22	0.63
P02671	Coagulation	Fibrinogen alpha chain	0.15	1.15
P01042	Coagulation	Kininogen-1	0.14	0.11
P01024	Complement system	Complement C3	0.79	1.34
P0C0L4; P0C0L5	Complement system	Complement C4-A	0.11	0.22
P01834	Immunoglobulins	Ig kappa chain C region	3.40	2.92
P01871	Immunoglobulins	Ig mu chain C region	2.49	0.70
P01591	Immunoglobulins	Immunoglobulin J chain	1.33	7.54
P01857	Immunoglobulins	Ig gamma-1 chain C region	1.32	2.09
P0CG05; A0M8Q6; B9A064; P0CF74; P0CG04; P0CG06	Immunoglobulins	Ig lambda-2 chain C regions	1.04	0.81
P01876; P01877	Immunoglobulins	Ig alpha-1 chain C region	0.66	0.29
P01859	Immunoglobulins	Ig gamma-2 chain C region	0.65	0.43
P01619	Immunoglobulins	Immunoglobulin kappa variable 3-20	0.40	0.28
P01767; A0A0C4 DH42; P01772	Immunoglobulins	Immunoglobulin heavy variable 3-53	0.26	0.39
P01861	Immunoglobulins	Ig gamma-4 chain C region	0.16	0.17
P04220	Immunoglobulins	Ig mu heavy chain disease protein	0.14	0.04
P01780; A0A0B4 J1V1; A0A0B4 J1X5; P01762; P01763	Immunoglobulins	Immunoglobulin heavy variable 3-7	0.12	0.04
P01860	Immunoglobulins	Ig gamma-3 chain C region	0.04	0.08
A6NJ69	Immunoglobulins	IgA-inducing protein homolog	0.03	0.49
P02647	Lipoproteins	Apolipoprotein A-I	29.32	1.18
P02649	Lipoproteins	Apolipoprotein E	9.93	1.03
P06727	Lipoproteins	Apolipoprotein A-IV	8.46	2.14

O14791	Lipoproteins	Apolipoprotein L1	4.77	1.06
P04114	Lipoproteins	Apolipoprotein B-100	2.09	0.18
P27169	Lipoproteins	Serum paraoxonase/arylesterase 1	2.00	0.24
P05090	Lipoproteins	Apolipoprotein D	1.04	0.06
P02652	Lipoproteins	Apolipoprotein A-II	0.63	0.09
P10909	Lipoproteins	Clusterin	0.57	0.73
P02656	Lipoproteins	Apolipoprotein C-III	0.47	0.17
O95445	Lipoproteins	Apolipoprotein M	0.17	0.03
P02768	Other Plasma components	Serum albumin	6.36	38.10
Q70YC4	Other Plasma components	Talanin	1.62	13.84
P29966	Other Plasma components	Myristoylated alanine-rich C-kinase substrate	1.18	0.18
Q6P387	Other Plasma components	Uncharacterized protein C16orf46	1.14	0.01
Q96HR3	Other Plasma components	Mediator of RNA polymerase II transcription subunit 30	0.46	0.00
A8K554	Other Plasma components	Putative protein ZNF815	0.36	0.01
Q9NVK5	Other Plasma components	FGFR1 oncogene partner 2	0.35	2.98
Q96MC2	Other Plasma components	Dynein regulatory complex protein 1	0.34	0.64
P02787	Other Plasma components	Serotransferrin	0.31	1.11
P01019	Other Plasma components	Angiotensinogen	0.29	0.01
P11597	Other Plasma components	Cholesteryl ester transfer protein	0.18	0.00
Q9UHR4	Other Plasma components	Brain-specific angiogenesis inhibitor 1-associated protein 2-like protein 1	0.15	0.07
Q13637	Other Plasma components	Ras-related protein Rab-32	0.14	0.56
Q9BQ61	Other Plasma components	Uncharacterized protein C19orf43	0.13	0.80
Q96I13	Other Plasma components	Protein ABHD8	0.12	0.00
Q5TA50	Other Plasma components	Ceramide-1-phosphate transfer protein	0.12	0.28
Q96E39	Other Plasma components	RNA binding motif protein, X-linked-like-1	0.12	0.54
P68871	Other Plasma components	Hemoglobin subunit beta	0.10	0.00
Q9Y316	Other Plasma components	Protein MEMO1	0.10	0.86
P35858	Other Plasma components	Insulin-like growth factor-binding protein complex acid labile subunit	0.10	0.04
P02790	Other Plasma components	Hemopexin	0.08	0.37
Q15761	Other Plasma components	Neuropeptide Y receptor type 5	0.08	0.11
O60911	Other Plasma components	Cathepsin L2	0.08	1.25
Q15800	Other Plasma components	Methylsterol monooxygenase 1	0.07	0.00
Q8N6D5	Other Plasma components	Ankyrin repeat domain-containing protein 29	0.06	0.02
P0DJI9; P0DJI8	Other Plasma components	Serum amyloid A-2 protein	0.06	0.04
Q9BXJ3	Other Plasma components	Complement C1q tumor necrosis factor-related protein 4	0.05	0.78
Q8TCZ2	Other Plasma components	CD99 antigen-like protein 2	0.05	0.00
Q6P3W2	Other Plasma components	DnaJ homolog subfamily C member 24	0.05	0.32
Q5T5N4	Other Plasma components	Uncharacterized protein C6orf118	0.04	0.00
P68032	Other Plasma components	Actin, alpha cardiac muscle 1	0.04	0.04
P18509	Other Plasma components	Pituitary adenylate cyclase-activating polypeptide	0.03	0.05
Q9UHF0	Other Plasma components	Tachykinin-3	0.03	0.23
Q5T749	Other Plasma components	Keratinocyte proline-rich protein	0.03	0.08

P18848	Other Plasma components	Cyclic AMP-dependent transcription factor ATF-4	0.02	0.17
Q9UBP8	Other Plasma components	Kidney-associated antigen 1	0.02	0.00
Q9BYD3	Other Plasma components	39S ribosomal protein L4, mitochondrial	0.01	0.03
Q9UNE0	Other Plasma components	Tumor necrosis factor receptor superfamily member EDAR	0.01	0.11
Q9BUY7	Other Plasma components	EF-hand calcium-binding domain-containing protein 11	0.00	0.20
O95971	Other Plasma components	CD160 antigen	0.00	0.02
P04004	Tissue Leakage	Vitronectin	0.28	0.18
O43866	Tissue Leakage	CD5 antigen-like	0.28	0.00
P81605	Tissue Leakage	Dermcidin	0.10	0.26
P12273	Tissue Leakage	Prolactin-inducible protein	0.08	0.04

Supernatant after centrifugation:

Accession	Annotation	Description	Super-natant plasma +SiNC	plasma control
P00738	Acute Phase	Haptoglobin	1.53	1.23
P01023	Acute Phase	Alpha-2-macroglobulin	1.62	2.39
P01009	Acute Phase	Alpha-1-antitrypsin	1.72	0.74
P02763	Acute Phase	Alpha-1-acid glycoprotein 1	0.82	0.93
P00450	Acute Phase	Ceruloplasmin	0.56	0.64
P02751	Acute Phase	Fibronectin	0.48	0.62
P01011	Acute Phase	Alpha-1-antichymotrypsin	0.53	0.76
P19652	Acute Phase	Alpha-1-acid glycoprotein 2	0.19	0.28
P02743	Acute Phase	Serum amyloid P-component	0.10	0.10
P00739	Acute Phase	Haptoglobin-related protein	0.04	0.01
P02675	Coagulation	Fibrinogen beta chain	3.58	3.94
P01042	Coagulation	Kininogen-1	0.75	0.64
P02679	Coagulation	Fibrinogen gamma chain	1.31	0.78
P02671	Coagulation	Fibrinogen alpha chain	1.25	1.30
P00734	Coagulation	Prothrombin	0.32	0.31
P04196	Coagulation	Histidine-rich glycoprotein	0.40	0.87
P00747	Coagulation	Plasminogen	0.11	0.11
P01008	Coagulation	Antithrombin-III	0.09	0.02
P08697	Coagulation	Alpha-2-antiplasmin	0.02	0.09
P01024	Complement system	Complement C3	2.78	3.34
P0C0L5	Complement system	Complement C4-B	0.56	0.66
P08603	Complement system	Complement factor H	0.48	0.51
P05155	Complement system	Plasma protease C1 inhibitor	0.20	0.29
P00751	Complement system	Complement factor B	0.28	0.28
P04003	Complement system	C4b-binding protein alpha chain	0.09	0.08
P02747	Complement system	Complement C1q subcomponent subunit C	0.02	0.03
P0C0L4	Complement system	Complement C4-A	0.00	0.00
P01834	Immunoglobulins	Ig kappa chain C region	8.37	9.87

P01857	Immunoglobulins	Ig gamma-1 chain C region	6.33	8.25
P01871	Immunoglobulins	Ig mu chain C region	1.78	2.74
P01876	Immunoglobulins	Ig alpha-1 chain C region	0.95	1.11
P01859	Immunoglobulins	Ig gamma-2 chain C region	1.50	1.05
B9A064; P0CG04	Immunoglobulins	Immunoglobulin lambda-like polypeptide 5	1.10	1.51
P01861	Immunoglobulins	Ig gamma-4 chain C region	0.67	0.66
P01860	Immunoglobulins	Ig gamma-3 chain C region	0.52	0.49
P01780	Immunoglobulins	Immunoglobulin heavy variable 3-7	0.37	0.31
P04220	Immunoglobulins	Ig mu heavy chain disease protein	0.24	0.19
P06312	Immunoglobulins	Immunoglobulin kappa variable 4-1	0.09	0.08
P01764; P01768	Immunoglobulins	Immunoglobulin heavy variable 3-23	0.19	0.21
A0A075 B6S5	Immunoglobulins	Immunoglobulin kappa variable 1-27	0.15	0.14
P01591	Immunoglobulins	Immunoglobulin J chain	0.10	0.09
P01700	Immunoglobulins	Immunoglobulin lambda variable 1-47	0.08	0.07
P04433	Immunoglobulins	Immunoglobulin kappa variable 3-11	0.02	0.01
P01619	Immunoglobulins	Immunoglobulin kappa variable 3-20	0.06	0.05
P01877	Immunoglobulins	Ig alpha-2 chain C region	0.06	0.06
A0M8Q6	Immunoglobulins	Ig lambda-7 chain C region	0.02	0.02
A0A0C4 DH72	Immunoglobulins	Immunoglobulin kappa variable 1-6	0.02	0.04
A0A075 B6S2; A0A075 B6P5; A0A075 B6S6; A0A0A0 MRZ7; P01615; P06310	Immunoglobulins	Immunoglobulin kappa variable 2D-29	0.04	0.03
P01767	Immunoglobulins	Immunoglobulin heavy variable 3-53	0.02	0.02
A0A0C4 DH42; A0A0B4 J1V1; A0A0B4 J1X5; P01762; P01763; P01772	Immunoglobulins	Immunoglobulin heavy variable 3-66	0.00	0.00
P01782	Immunoglobulins	Immunoglobulin heavy variable 3-9	0.00	0.00
P01624	Immunoglobulins	Immunoglobulin kappa variable 3-15	0.02	0.02
P06727	Lipoproteins	Apolipoprotein A-IV	2.31	2.87
P04114	Lipoproteins	Apolipoprotein B-100	1.28	1.54
P02647	Lipoproteins	Apolipoprotein A-I	0.50	0.71
P10909	Lipoproteins	Clusterin	0.57	0.54
O95445	Lipoproteins	Apolipoprotein M	0.02	0.01
P02749	Lipoproteins	Beta-2-glycoprotein 1	0.49	0.52
P02649	Lipoproteins	Apolipoprotein E	0.07	0.09
P02652	Lipoproteins	Apolipoprotein A-II	0.11	0.12
O14791	Lipoproteins	Apolipoprotein L1	0.01	0.01
P02768	Other Plasma components	Serum albumin	27.93	10.99

Q8IZU9	Other Plasma components	Kin of IRRE-like protein 3	3.09	6.30
Q14116	Other Plasma components	Interleukin-18	1.61	1.23
Q99614	Other Plasma components	Tetratricopeptide repeat protein 1	1.91	2.32
P02787	Other Plasma components	Serotransferrin	1.79	1.61
Q6UN15	Other Plasma components	Pre-mRNA 3'-end-processing factor FIP1	0.71	0.69
P02774	Other Plasma components	Vitamin D-binding protein	2.41	2.38
O43252	Other Plasma components	Bifunctional 3'-phosphoadenosine 5'-phosphosulfate synthase 1	1.60	0.53
P19827	Other Plasma components	Inter-alpha-trypsin inhibitor heavy chain H1	0.27	0.24
Q13123	Other Plasma components	Protein Red	0.34	0.33
P02790	Other Plasma components	Hemopexin	0.63	0.79
P02765	Other Plasma components	Alpha-2-HS-glycoprotein	0.97	1.00
P01019	Other Plasma components	Angiotensinogen	0.51	0.55
P18615	Other Plasma components	Negative elongation factor E	0.50	0.50
Q9BXI3	Other Plasma components	Cytosolic 5'-nucleotidase 1A	0.67	1.25
Q96E09	Other Plasma components	Protein FAM122A	0.59	0.80
P07451	Other Plasma components	Carbonic anhydrase 3	0.56	0.75
P25311	Other Plasma components	Zinc-alpha-2-glycoprotein	0.42	0.58
Q6WQI6	Other Plasma components	Putative cancer susceptibility gene HEPN1 protein	0.55	1.19
Q8WWX9	Other Plasma components	Selenoprotein M	0.45	5.49
P02766	Other Plasma components	Transthyretin	0.30	0.30
P04155	Other Plasma components	Trefoil factor 1	0.31	0.23
P04217	Other Plasma components	Alpha-1B-glycoprotein	0.36	0.38
Q5VZ03	Other Plasma components	Nucleoredoxin-like protein 2	0.23	0.31
Q8NAA6	Other Plasma components	Uncharacterized protein C15orf53	0.31	0.56
Q03252	Other Plasma components	Lamin-B2	0.28	0.32
P62068	Other Plasma components	Ubiquitin carboxyl-terminal hydrolase 46	0.07	0.13
A6NGD5	Other Plasma components	Putative zinc finger and SCAN domain-containing protein 5C	0.15	0.29
P14060	Other Plasma components	3 beta-hydroxysteroid dehydrogenase/Delta 5-->4-isomerase type 1	0.45	0.58
P82970	Other Plasma components	High mobility group nucleosome-binding domain-containing protein 5	0.03	0.01
Q13106	Other Plasma components	Zinc finger protein 154	0.03	0.03
Q12774; A5YM69	Other Plasma components	Rho guanine nucleotide exchange factor 5	0.19	0.17
P19823	Other Plasma components	Inter-alpha-trypsin inhibitor heavy chain H2	0.17	0.40
Q14624	Other Plasma components	Inter-alpha-trypsin inhibitor heavy chain H4	0.13	0.17
Q5T200	Other Plasma components	Zinc finger CCCH domain-containing protein 13	0.07	0.02
P20742	Other Plasma components	Pregnancy zone protein	0.05	0.10
P02760	Other Plasma components	Protein AMBP	0.09	0.13
P43652	Other Plasma components	Afamin	0.06	0.08
Q969V1	Other Plasma components	Melanin-concentrating hormone receptor 2	0.03	0.01
O95749	Other Plasma components	Geranylgeranyl pyrophosphate synthase	0.05	0.08
Q6NXT6	Other Plasma components	Transmembrane anterior posterior transformation protein 1 homolog	0.11	0.10

Q5SR53	Other Plasma components	Putative uncharacterized protein PIK3CD-AS1	0.10	0.00
Q155Q3	Other Plasma components	Dixin	0.12	0.07
Q14257	Other Plasma components	Reticulocalbin-2	0.06	0.50
P02753	Other Plasma components	Retinol-binding protein 4	0.09	0.08
O75449	Other Plasma components	Katanin p60 ATPase-containing subunit A1	0.07	0.01
Q6KCM7	Other Plasma components	Calcium-binding mitochondrial carrier protein SCaMC-2	0.06	0.07
Q96MU5	Other Plasma components	Uncharacterized protein C17orf77	0.04	0.05
Q9Y6A9	Other Plasma components	Signal peptidase complex subunit 1	0.04	0.12
O95972	Other Plasma components	Bone morphogenetic protein 15	0.04	0.05
P22792	Other Plasma components	Carboxypeptidase N subunit 2	0.05	0.07
P36955	Other Plasma components	Pigment epithelium-derived factor	0.03	0.04
P19971	Other Plasma components	Thymidine phosphorylase	0.01	0.02
Q9BUG6	Other Plasma components	Zinc finger and SCAN domain-containing protein 5A	0.04	0.04
Q9NXJ0	Other Plasma components	Membrane-spanning 4-domains subfamily A member 12	0.02	0.09
Q9NZZ3	Other Plasma components	Charged multivesicular body protein 5	0.01	0.01
P55822	Other Plasma components	SH3 domain-binding glutamic acid-rich protein	0.03	0.04
Q8NHM4	Other Plasma components	Putative trypsin-6	0.00	0.01
P0CG21	Other Plasma components	NHL-repeat-containing protein 4	0.01	0.02
Q9NQV5	Other Plasma components	PR domain-containing protein 11	0.01	0.02
P04004	Tissue Leakage	Vitronectin	0.15	0.21
P06396	Tissue Leakage	Gelsolin	0.08	0.16
O43866	Tissue Leakage	CD5 antigen-like	0.02	0.03

Supernatant of plasma + SiNC after AF4:

Accession	Annotation	Description	supernatant plasma + SiNC after AF4						
			Fr. 1	Fr. 2	Fr. 3	Fr. 4	Fr. 5	Fr. 6	Fr. 7
P02763	Acute Phase	Alpha-1-acid glycoprotein 1	1.53	0.35	0.21	0.37	0.34	0.45	0.80
P01009	Acute Phase	Alpha-1-antitrypsin	1.32	0.43	0.52	0.51	0.71	0.78	0.26
P19652	Acute Phase	Alpha-1-acid glycoprotein 2	0.52	0.12	0.06	0.08	0.19	0.19	0.24
P02751	Acute Phase	Fibronectin	0.46	0.39	0.18	0.44	0.60	0.38	0.51
P01011	Acute Phase	Alpha-1-antichymotrypsin	0.22	0.21	0.11	0.33	0.63	0.20	0.10
P00450	Acute Phase	Ceruloplasmin	0.10	0.27	0.16	1.08	3.13	1.22	0.20
P00739	Acute Phase	Haptoglobin-related protein	0.10	0.22	1.99	1.65	0.92	0.57	0.39
P00738	Acute Phase	Haptoglobin	0.08	0.75	9.24	8.71	4.95	2.21	1.12
P01023	Acute Phase	Alpha-2-macroglobulin	0.07	0.08	0.57	17.67	13.60	3.45	0.97
P02743	Acute Phase	Serum amyloid P-component	0.01	0.10	0.08	0.14	0.10	0.05	0.06
P02675	Coagulation	Fibrinogen beta chain	3.97	4.20	0.87	2.33	7.05	4.40	5.44
P00734	Coagulation	Prothrombin	1.03	0.64	0.09	0.17	0.22	0.23	0.55
P01042	Coagulation	Kininogen-1	0.42	0.28	0.23	0.18	0.21	0.21	0.33
P02671	Coagulation	Fibrinogen alpha chain	0.35	0.24	0.22	1.81	8.37	3.29	0.51
P00747	Coagulation	Plasminogen	0.19	0.16	0.09	0.88	0.11	0.08	0.15
P08697	Coagulation	Alpha-2-antiplasmin	0.13	0.09	0.00	0.02	0.01	0.03	0.07

P01008	Coagulation	Antithrombin-III	0.12	0.05	0.08	0.03	0.04	0.07	0.03
P03952	Coagulation	Plasma kallikrein	0.11	0.09	0.05	0.18	0.14	0.11	0.12
P02679	Coagulation	Fibrinogen gamma chain	0.04	0.05	0.21	2.75	16.03	5.58	0.47
P05160	Coagulation	Coagulation factor XIII B chain	0.00	0.00	0.01	0.03	0.04	0.02	0.00
P07225	Coagulation	Vitamin K-dependent protein S	0.00	0.00	0.01	0.00	0.00	0.06	0.00
P01024	Complement system	Complement C3	6.17	3.90	1.22	1.40	1.43	1.85	5.18
P04003	Complement system	C4b-binding protein alpha chain	0.29	0.26	1.38	0.41	0.50	0.94	0.34
P08603; Q02985; Q03591	Complement system	Complement factor H	0.24	0.82	0.79	0.76	0.34	0.55	0.55
P00751	Complement system	Complement factor B	0.20	0.23	0.25	0.31	0.37	0.17	0.24
P0C0L4	Complement system	Complement C4-A	0.03	0.30	0.42	0.35	0.13	0.20	0.12
P0C0L5	Complement system	Complement C4-B	0.01	0.14	0.20	0.17	0.06	0.10	0.06
P01031	Complement system	Complement C5	0.01	0.04	0.08	0.04	0.01	0.01	0.02
O75636	Complement system	Ficolin-3	0.01	0.01	0.03	0.14	0.20	0.09	0.03
P05155	Complement system	Plasma protease C1 inhibitor	0.01	0.25	0.39	0.16	0.06	0.05	0.15
P00736	Complement system	Complement C1r subcomponent	0.01	0.02	0.04	0.12	0.05	0.03	0.05
P20851	Complement system	C4b-binding protein beta chain	0.00	0.00	0.00	0.03	0.02	0.08	0.01
P02747	Complement system	Complement C1q subcomponent subunit C	0.00	0.00	0.00	0.02	0.01	0.23	0.01
P13671	Complement system	Complement component C6	0.00	0.02	0.00	0.00	0.01	0.00	0.01
P02746	Complement system	Complement C1q subcomponent subunit B	0.00	0.00	0.00	0.00	0.00	0.01	0.00
P01857	Immunoglobulins	Ig gamma-1 chain C region	0.56	11.27	17.61	5.02	2.75	2.95	7.13
P01871	Immunoglobulins	Ig mu chain C region	0.29	0.16	0.11	0.23	1.13	15.20	1.26
P01834	Immunoglobulins	Ig kappa chain C region	0.28	11.07	17.23	6.91	3.44	11.78	7.67
B9A064; P0CG04	Immunoglobulins	Immunoglobulin lambda-like polypeptide 5	0.20	5.50	5.19	3.31	1.21	3.26	3.56
A0A0B4J1V1; A0A0B4J1X8; P01762; P01763; P01766; P01780	Immunoglobulins	Immunoglobulin heavy variable 3-21	0.14	0.20	0.41	0.23	0.34	0.36	0.15
P01859	Immunoglobulins	Ig gamma-2 chain C region	0.14	1.25	1.77	0.54	0.33	0.32	0.74
P01860	Immunoglobulins	Ig gamma-3 chain C region	0.11	0.51	2.17	1.20	0.24	0.21	0.45
P01714	Immunoglobulins	Immunoglobulin lambda variable 3-19	0.10	0.24	0.15	1.11	0.15	0.13	0.19
P0CG06; P0CF74; P0CG05	Immunoglobulins	Ig lambda-3 chain C regions	0.10	2.57	2.21	1.54	0.54	1.42	1.66
A0A075B6S2; A0A0A0MRZ7	Immunoglobulins	Immunoglobulin kappa variable 2D-29	0.08	0.04	0.00	0.00	0.01	0.01	0.03
A0A0C4DH25	Immunoglobulins	Immunoglobulin kappa variable 3-20	0.07	0.07	0.07	0.07	0.05	0.06	0.09
P01619	Immunoglobulins	Immunoglobulin kappa variable 3-20	0.06	0.03	0.02	0.11	0.02	0.03	0.03
P01880	Immunoglobulins	Ig delta chain C region	0.06	0.06	0.26	0.16	0.12	0.10	0.08
A0A0B4J1X5	Immunoglobulins	Immunoglobulin heavy variable 3-74	0.06	0.06	0.04	0.06	0.03	0.06	0.07
P01764; P01768	Immunoglobulins	Immunoglobulin heavy variable 3-23	0.05	0.21	0.20	0.59	0.25	0.43	0.17
A0A0C4DH42	Immunoglobulins	Immunoglobulin heavy variable 3-66	0.04	0.27	0.48	0.32	0.33	0.49	0.28
P01876	Immunoglobulins	Ig alpha-1 chain C region	0.04	0.83	6.05	2.69	1.94	0.92	0.76
A0A0B4J1Y9	Immunoglobulins	Immunoglobulin heavy variable 3-72	0.04	0.06	0.04	0.09	0.06	0.08	0.05
P01861	Immunoglobulins	Ig gamma-4 chain C region	0.03	0.54	0.44	0.46	0.44	0.19	0.33

P06312	Immunoglobulins	Immunoglobulin kappa variable 4-1	0.03	0.14	0.19	0.26	0.09	0.23	0.11
P80748	Immunoglobulins	Immunoglobulin lambda variable 3-21	0.03	0.16	0.22	0.17	0.09	0.14	0.13
A0A0A0MRZ8	Immunoglobulins	Immunoglobulin kappa variable 3D-11	0.03	0.02	0.05	0.02	0.03	0.05	0.02
P01700	Immunoglobulins	Immunoglobulin lambda variable 1-47	0.03	0.08	0.19	0.16	0.28	0.25	0.06
A0A075B6P5; P01615	Immunoglobulins	Immunoglobulin kappa variable 2-28	0.03	0.02	0.02	1.43	0.00	0.03	0.02
P01624; A0A0C4DH55	Immunoglobulins	Immunoglobulin kappa variable 3-15	0.02	0.10	0.18	0.07	0.07	0.16	0.07
P01782	Immunoglobulins	Immunoglobulin heavy variable 3-9	0.02	0.01	0.02	0.01	0.01	0.01	0.01
A0A0C4DH41; A0A075B6R2; P01824; P01825; P06331	Immunoglobulins	Immunoglobulin heavy variable 4-61	0.02	0.15	0.22	0.22	0.13	0.25	0.11
P04433	Immunoglobulins	Immunoglobulin kappa variable 3-11	0.02	0.19	0.28	0.15	0.20	0.34	0.13
P01602	Immunoglobulins	Immunoglobulin kappa variable 1-5	0.01	0.09	0.08	0.12	0.11	0.12	0.07
P01591	Immunoglobulins	Immunoglobulin J chain	0.01	0.02	0.07	1.14	1.18	0.84	0.10
A0A075B6S5	Immunoglobulins	Immunoglobulin kappa variable 1-27	0.01	0.02	0.03	0.01	0.00	0.05	0.02
P01767; P01772	Immunoglobulins	Immunoglobulin heavy variable 3-53	0.01	0.02	0.02	0.03	0.02	0.04	0.02
A0M8Q6	Immunoglobulins	Ig lambda-7 chain C region	0.00	0.07	0.06	0.06	0.03	0.02	0.04
P01611; A0A0C4DH73	Immunoglobulins	Immunoglobulin kappa variable 1D-12	0.00	0.01	0.00	0.02	0.03	0.01	0.00
P01699	Immunoglobulins	Immunoglobulin lambda variable 1-44	0.00	0.01	0.02	0.02	0.01	0.04	0.01
P04220	Immunoglobulins	Ig mu heavy chain disease protein	0.00	0.00	0.00	0.00	0.01	0.06	0.01
P01877	Immunoglobulins	Ig alpha-2 chain C region	0.00	0.03	0.12	0.07	0.04	0.02	0.02
A0A0C4DH24	Immunoglobulins	Immunoglobulin kappa variable 6-21	0.00	0.01	0.00	0.00	0.00	0.01	0.01
A0A087WSY6	Immunoglobulins	Immunoglobulin kappa variable 3D-15	0.00	0.00	0.01	0.00	0.00	0.01	0.00
P04432; P01597	Immunoglobulins	Immunoglobulin kappa variable 1D-39	0.00	0.00	0.00	0.00	0.00	0.04	0.00
A0A087WW87; P01614	Immunoglobulins	Immunoglobulin kappa variable 2-40	0.00	0.00	0.00	0.00	0.00	0.00	0.01
P04114	Lipoproteins	Apolipoprotein B-100	1.88	1.28	0.26	0.26	0.23	0.65	1.27
P02647	Lipoproteins	Apolipoprotein A-I	0.12	0.26	1.91	3.42	0.64	0.33	0.23
P02749	Lipoproteins	Beta-2-glycoprotein 1	0.11	0.32	0.17	0.13	0.20	0.10	0.16
P02652	Lipoproteins	Apolipoprotein A-II	0.05	0.07	0.44	1.51	0.18	0.11	0.08
P10909	Lipoproteins	Clusterin	0.03	0.08	0.14	0.37	0.07	0.09	0.10
P06727	Lipoproteins	Apolipoprotein A-IV	0.01	0.02	0.03	0.07	0.02	0.02	0.02
P27169	Lipoproteins	Serum paraoxonase/arylesterase 1	0.00	0.00	0.00	0.01	0.00	0.01	0.00
P02768	Other Plasma components	Serum albumin	41.94	24.52	5.71	5.92	5.71	12.78	29.04
Q14116	Other Plasma components	Interleukin-18	14.14	7.18	1.08	1.67	0.90	2.81	8.49
P02787	Other Plasma components	Serotransferrin	4.50	2.72	0.80	1.09	0.66	1.61	3.16
Q6P587	Other Plasma components	Acylpyruvase FAHD1, mitochondrial	1.92	0.84	0.53	0.37	0.46	0.75	0.98
P02790	Other Plasma components	Hemopexin	1.84	0.93	0.43	0.24	0.54	0.71	1.02
P02774	Other Plasma components	Vitamin D-binding protein	1.64	0.34	0.12	0.38	0.19	0.27	0.64
P02765	Other Plasma components	Alpha-2-HS-glycoprotein	1.21	0.64	0.21	0.22	0.19	0.31	0.48
P06276	Other Plasma components	Cholinesterase	0.99	0.48	0.42	0.16	0.18	0.31	0.49
H3BPM6	Other Plasma components	MKRN2 opposite strand protein	0.72	0.37	0.23	0.18	0.14	0.19	0.22
Q08380	Other Plasma components	Galectin-3-binding protein	0.54	0.31	0.03	0.18	0.16	0.16	0.40

Q9UJ72	Other Plasma components	Annexin A10	0.52	0.25	0.17	0.13	0.19	0.19	0.31
P0C7T7	Other Plasma components	Putative uncharacterized protein FRMD6-AS1	0.50	0.23	0.27	0.20	0.22	0.23	0.36
P35218	Other Plasma components	Carbonic anhydrase 5A, mitochondrial	0.46	0.35	0.10	0.07	0.11	0.23	0.35
P01019	Other Plasma components	Angiotensinogen	0.44	0.19	0.12	0.10	0.12	0.10	0.18
P02750	Other Plasma components	Leucine-rich alpha-2-glycoprotein	0.44	0.28	0.20	0.12	0.20	0.30	0.38
Q9NY27	Other Plasma components	Serine/threonine-protein phosphatase 4 regulatory subunit 2	0.39	0.17	0.07	0.02	0.02	0.11	0.18
P25311	Other Plasma components	Zinc-alpha-2-glycoprotein	0.35	0.21	0.07	0.22	1.49	0.77	0.52
Q4JDL3	Other Plasma components	Tyrosine-protein phosphatase non-receptor type 20	0.32	0.18	0.02	0.04	0.03	0.06	0.18
P04217	Other Plasma components	Alpha-1B-glycoprotein	0.30	0.13	0.06	0.03	0.07	0.10	0.13
P02042; P68871; P69891; P69892	Other Plasma components	Hemoglobin subunit delta	0.29	0.16	0.16	0.24	0.61	0.14	0.18
Q86WP2	Other Plasma components	Vasculin	0.26	0.29	0.07	0.32	0.12	0.15	0.31
P19823	Other Plasma components	Inter-alpha-trypsin inhibitor heavy chain H2	0.25	0.19	0.29	0.13	0.06	0.14	0.18
P82970	Other Plasma components	High mobility group nucleosome-binding domain-containing protein 5	0.24	0.21	0.07	0.28	0.55	0.37	0.24
P19827	Other Plasma components	Inter-alpha-trypsin inhibitor heavy chain H1	0.24	0.31	0.07	0.24	0.88	0.50	0.34
Q96HR3	Other Plasma components	Mediator of RNA polymerase II transcription subunit 30	0.24	0.19	0.06	0.09	0.53	0.14	0.20
Q14624	Other Plasma components	Inter-alpha-trypsin inhibitor heavy chain H4	0.23	0.17	0.10	0.35	0.40	0.18	0.20
B4DZS4	Other Plasma components	T-complex protein 11 X-linked protein 1	0.21	0.14	0.08	0.04	0.03	0.10	0.06
P07098	Other Plasma components	Gastric triacylglycerol lipase	0.20	0.09	0.03	0.03	0.06	0.06	0.10
P02766	Other Plasma components	Transthyretin	0.19	0.12	0.24	0.14	0.15	0.26	0.35
Q8NGB8	Other Plasma components	Olfactory receptor 4F15	0.16	0.09	0.05	0.92	0.68	0.12	0.13
Q9NRM6	Other Plasma components	Interleukin-17 receptor B	0.12	0.04	0.00	0.02	0.01	0.02	0.03
Q9UIY3	Other Plasma components	RWD domain-containing protein 2A	0.10	0.10	0.50	0.11	0.20	0.20	0.18
Q10469	Other Plasma components	Alpha-1,6-mannosyl-glycoprotein 2-beta-N-acetylglucosaminyltransferase	0.10	0.64	0.60	0.22	0.21	0.15	0.39
P01583	Other Plasma components	Interleukin-1 alpha	0.09	0.11	0.02	0.01	0.02	0.09	0.07
Q16832	Other Plasma components	Discoidin domain-containing receptor 2	0.08	0.07	0.02	0.02	0.02	0.03	0.05
Q96IZ5	Other Plasma components	RNA-binding protein 41	0.08	0.03	0.03	0.23	0.02	0.07	0.01
Q9BXI3	Other Plasma components	Cytosolic 5'-nucleotidase 1A	0.07	1.94	2.33	1.15	0.49	1.66	1.06
P18615	Other Plasma components	Negative elongation factor E	0.06	0.21	2.00	1.77	1.13	0.68	0.29
P08185	Other Plasma components	Corticosteroid-binding globulin	0.06	0.05	0.03	0.02	0.01	0.02	0.04
P20742	Other Plasma components	Pregnancy zone protein	0.05	0.08	0.22	0.52	1.15	0.45	0.11
P02760	Other Plasma components	Protein AMBP	0.04	0.17	0.35	0.10	0.11	0.08	0.11
P43652	Other Plasma components	Afamin	0.04	0.04	0.01	0.02	0.02	0.12	0.03
P02753	Other Plasma components	Retinol-binding protein 4	0.04	0.03	0.01	0.22	0.04	0.03	0.03
Q86WK7	Other Plasma components	Amphoterin-induced protein 3	0.03	0.02	0.00	0.02	0.02	0.01	0.02
P36955	Other Plasma components	Pigment epithelium-derived factor	0.03	0.00	0.00	0.00	0.00	0.00	0.00
P55957	Other Plasma components	BH3-interacting domain death agonist	0.03	0.01	0.07	0.04	0.09	0.02	0.01
A8MT65	Other Plasma components	Zinc finger protein 891	0.02	0.01	0.00	0.00	0.00	0.00	0.01
Q6ZTU2; Q96L91	Other Plasma components	EP400 N-terminal-like protein	0.02	0.02	0.00	0.00	0.00	0.01	0.02
P69905	Other Plasma components	Hemoglobin subunit alpha	0.02	0.01	0.02	0.17	0.06	0.03	0.01
O94760	Other Plasma components	N(G),N(G)-dimethylarginine dimethylaminohydrolase 1	0.02	0.01	0.02	0.01	0.03	0.01	0.01
Q8N140	Other Plasma components	EP300-interacting inhibitor of differentiation 3	0.02	0.03	0.07	0.09	0.09	0.03	0.03
O75638	Other Plasma components	Cancer/testis antigen 2	0.01	0.00	0.00	0.00	0.00	0.00	0.00

Q99619	Other Plasma components	SPRY domain-containing SOCS box protein 2	0.01	0.07	0.64	0.56	0.36	0.23	0.09
Q9NWF4	Other Plasma components	Solute carrier family 52, riboflavin transporter, member 1	0.01	0.02	0.31	0.07	0.11	0.07	0.03
P16260	Other Plasma components	Graves disease carrier protein	0.01	0.00	0.00	0.00	0.01	0.00	0.00
Q96MC2	Other Plasma components	Dynein regulatory complex protein 1 OS=Homo sapiens GN=DRC1 PE=2 SV=2	0.01	0.02	0.14	0.03	0.08	0.04	0.03
Q8NHV9	Other Plasma components	Rhox homeobox family member 1	0.01	0.01	0.04	0.06	0.05	0.06	0.01
P22792	Other Plasma components	Carboxypeptidase N subunit 2	0.01	0.04	0.06	0.05	0.04	0.02	0.02
P27482	Other Plasma components	Calmodulin-like protein 3	0.01	0.02	0.39	0.76	0.16	0.11	0.04
Q10589	Other Plasma components	Bone marrow stromal antigen 2	0.01	0.05	0.07	0.46	0.74	0.19	0.03
Q8N8B7	Other Plasma components	Transcription elongation factor A N-terminal and central domain-containing protein	0.00	0.00	0.03	0.01	0.01	0.01	0.00
Q8NCY6	Other Plasma components	Myb/SANT-like DNA-binding domain-containing protein 4	0.00	0.00	0.00	0.00	0.00	0.01	0.01
Q9C0E8	Other Plasma components	Protein lunapark	0.00	0.00	0.00	0.10	0.45	0.17	0.01
Q9BX74	Other Plasma components	TM2 domain-containing protein 1	0.00	0.00	0.00	0.00	0.00	0.00	0.00
P04278	Other Plasma components	Sex hormone-binding globulin	0.00	0.01	0.00	0.00	0.00	0.00	0.00
P63261; P60709; Q6S8J3	Other Plasma components	Actin, cytoplasmic 2	0.00	0.00	0.00	0.02	0.01	0.00	0.00
Q16048	Other Plasma components	Putative pro-MCH-like protein 1	0.00	0.00	0.01	0.01	0.04	0.02	0.00
Q68G75	Other Plasma components	LEM domain-containing protein 1	0.00	0.02	0.02	0.02	0.02	0.04	0.01
Q13434	Other Plasma components	Putative E3 ubiquitin-protein ligase makorin-4	0.00	0.00	0.00	0.01	0.01	0.00	0.00
Q14376	Other Plasma components	UDP-glucose 4-epimerase	0.00	0.00	0.00	0.00	0.00	0.00	0.03
P10916	Other Plasma components	Myosin regulatory light chain 2, ventricular/cardiac muscle isoform	0.00	0.02	0.04	0.01	0.01	0.14	0.02
O00442	Other Plasma components	RNA 3'-terminal phosphate cyclase	0.00	0.26	0.09	0.07	0.01	0.01	0.12
E7EML9	Other Plasma components	Serine protease 44	0.00	0.00	0.00	0.00	0.06	0.14	0.01
A6NGD5	Other Plasma components	Putative zinc finger and SCAN domain-containing protein 5C	0.00	0.00	0.01	0.01	0.00	0.02	0.00
Q96E09	Other Plasma components	Protein FAM122A	0.00	0.00	0.00	0.01	0.00	0.00	0.00
Q9BUG6	Other Plasma components	Zinc finger and SCAN domain-containing protein 5A	0.00	0.00	0.00	0.00	0.00	0.00	0.01
P25788	Other Plasma components	Proteasome subunit alpha type-3	0.00	0.01	0.00	0.00	0.00	0.01	0.00
Q14954	Other Plasma components	Killer cell immunoglobulin-like receptor 2DS1	0.00	0.00	0.00	0.01	0.01	0.00	0.00
A6NMT0	Other Plasma components	Homeobox protein DBX1	0.00	0.00	0.00	0.00	0.00	0.03	0.00
Q9HAJ7	Other Plasma components	Histone deacetylase complex subunit SAP30L	0.00	0.00	0.00	0.02	0.00	0.00	0.00
Q96A32	Other Plasma components	Myosin regulatory light chain 2, skeletal muscle isoform	0.00	0.01	0.01	0.03	0.01	0.00	0.00
P04004	Tissue Leakage	Vitronectin	0.17	0.23	0.20	0.29	0.15	0.17	0.20
P49662	Tissue Leakage	Caspase-4	0.09	0.04	0.01	0.01	0.01	0.02	0.04
O43866	Tissue Leakage	CD5 antigen-like	0.08	0.27	0.56	0.72	0.47	0.58	0.24
P06396	Tissue Leakage	Gelsolin	0.07	0.04	0.03	0.01	0.03	0.02	0.02
Q9UPQ4	Tissue Leakage	Tripartite motif-containing protein 35	0.03	0.03	0.01	0.01	0.02	0.05	0.04
Q96A61	Tissue Leakage	Tripartite motif-containing protein 52	0.01	0.01	0.00	0.01	0.00	0.00	0.01
P53672	Tissue Leakage	Beta-crystallin A2	0.00	0.01	0.12	0.11	0.05	0.03	0.01
Q96PD5	Tissue Leakage	N-acetylmuramoyl-L-alanine amidase	0.00	0.01	0.00	0.00	0.00	0.00	0.00
P12273	Tissue Leakage	Prolactin-inducible protein	0.00	0.00	0.00	0.00	0.00	0.00	0.00

Supernatant of plasma control after AF4:

Accession	Annotation	Description	plasma control after AF4						
			Fr. 1	Fr. 2	Fr. 3	Fr. 4	Fr. 5	Fr. 6	Fr. 7
P02763	Acute Phase	Alpha-1-acid glycoprotein 1	1.15	0.25	0.19	0.62	0.34	0.90	0.80
P01009	Acute Phase	Alpha-1-antitrypsin	1.40	0.48	0.35	0.24	0.37	0.75	0.73
P19652	Acute Phase	Alpha-1-acid glycoprotein 2	0.39	0.09	0.09	0.14	0.19	0.36	0.29
P02751	Acute Phase	Fibronectin	0.57	0.24	0.19	0.44	0.54	0.42	0.42
P01011	Acute Phase	Alpha-1-antichymotrypsin	0.33	0.23	0.08	0.06	0.23	0.14	0.24
P00450	Acute Phase	Ceruloplasmin	0.08	0.28	0.12	0.55	3.28	1.00	0.23
P00739	Acute Phase	Haptoglobin-related protein	0.10	0.21	1.96	2.00	0.92	0.89	0.30
P00738	Acute Phase	Haptoglobin	0.11	0.89	10.99	12.39	4.71	2.72	1.30
P01023	Acute Phase	Alpha-2-macroglobulin	0.06	0.12	0.94	29.23	12.99	3.38	1.13
P02743	Acute Phase	Serum amyloid P-component	0.02	0.10	0.07	0.16	0.08	0.06	0.06
P02675	Coagulation	Fibrinogen beta chain	5.99	2.24	1.17	2.19	8.08	5.15	5.33
P00734	Coagulation	Prothrombin	0.74	0.40	0.15	0.10	0.20	0.25	0.58
P01042	Coagulation	Kininogen-1	0.34	0.20	0.25	0.25	0.19	0.16	0.34
P02671	Coagulation	Fibrinogen alpha chain	0.12	0.17	0.13	1.68	9.94	2.73	0.44
P00747	Coagulation	Plasminogen	0.15	0.17	0.14	0.07	0.06	0.08	0.13
P08697	Coagulation	Alpha-2-antiplasmin	0.08	0.06	0.01	0.00	0.00	0.02	0.06
P01008	Coagulation	Antithrombin-III	0.06	0.06	0.04	0.05	0.03	0.07	0.07
P03952	Coagulation	Plasma kallikrein	0.11	0.09	0.05	0.08	0.19	0.09	0.13
P02679	Coagulation	Fibrinogen gamma chain	0.04	0.08	0.09	2.98	18.39	5.13	0.48
P05160	Coagulation	Coagulation factor XIII B chain	0.00	0.00	0.01	0.03	0.05	0.02	0.00
P07225	Coagulation	Vitamin K-dependent protein S	0.00	0.00	0.01	0.01	0.00	0.05	0.00
P01024	Complement system	Complement C3	3.68	1.65	0.88	0.78	0.76	2.18	3.25
P04003	Complement system	C4b-binding protein alpha chain	0.21	0.40	0.49	0.74	0.53	1.10	0.37
P08603; Q02985; Q03591	Complement system	Complement factor H	0.35	0.59	0.93	0.37	0.24	0.38	0.53
P00751	Complement system	Complement factor B	0.22	0.18	0.32	0.18	0.11	0.14	0.21
P0C0L4	Complement system	Complement C4-A	0.03	0.41	0.43	0.13	0.08	0.22	0.12
P0C0L5	Complement system	Complement C4-B	0.01	0.19	0.20	0.06	0.04	0.10	0.06
P01031	Complement system	Complement C5	0.01	0.04	0.05	0.01	0.01	0.01	0.02
O75636	Complement system	Ficolin-3	0.02	0.02	0.02	0.19	0.16	0.11	0.02
P05155	Complement system	Plasma protease C1 inhibitor	0.01	0.32	0.30	0.07	0.03	0.05	0.11
P00736	Complement system	Complement C1r subcomponent	0.02	0.02	0.04	0.03	0.07	0.02	0.03
P20851	Complement system	C4b-binding protein beta chain	0.00	0.01	0.00	0.02	0.01	0.10	0.01
P02747	Complement system	Complement C1q subcomponent subunit C	0.00	0.00	0.00	0.00	0.01	0.03	0.01
P13671	Complement system	Complement component C6	0.00	0.04	0.01	0.00	0.01	0.00	0.01
P02746	Complement system	Complement C1q subcomponent subunit B	0.00	0.00	0.00	0.00	0.00	0.00	0.00
P01857	Immunoglobulins	Ig gamma-1 chain C region	0.46	13.54	14.65	3.73	1.79	2.10	6.78
P01871	Immunoglobulins	Ig mu chain C region	0.08	0.06	0.07	0.16	1.18	10.86	0.87
P01834	Immunoglobulins	Ig kappa chain C region	0.27	14.12	19.15	5.43	3.22	8.54	6.58
B9A064; P0CG04	Immunoglobulins	Immunoglobulin lambda-like polypeptide 5	0.15	7.84	7.16	1.85	0.99	2.63	3.45
A0A0B4 J1V1; A0A0B4	Immunoglobulins	Immunoglobulin heavy variable 3-21	0.16	0.19	0.29	0.17	0.15	0.35	0.19

J1X8; P01762; P01763; P01766; P01780									
P01859	Immunoglobulins	Ig gamma-2 chain C region	0.13	1.98	1.48	0.42	0.24	0.34	0.61
P01860	Immunoglobulins	Ig gamma-3 chain C region	0.07	0.80	2.09	0.48	0.15	0.12	0.38
P01714	Immunoglobulins	Immunoglobulin lambda variable 3-19	0.08	0.31	0.25	0.13	0.10	0.06	0.15
P0CG06; P0CF74; P0CG05	Immunoglobulins	Ig lambda-3 chain C regions	0.07	3.72	3.32	0.77	0.40	1.10	1.59
A0A075 B6S2; A0A0A0 MRZ7	Immunoglobulins	Immunoglobulin kappa variable 2D-29	0.01	0.00	0.00	0.00	0.00	0.00	0.01
A0A0C4 DH25	Immunoglobulins	Immunoglobulin kappa variable 3-20	0.05	0.07	0.08	0.04	0.03	0.04	0.06
P01619	Immunoglobulins	Immunoglobulin kappa variable 3-20	0.03	0.04	0.03	0.01	0.02	0.02	0.03
P01880	Immunoglobulins	Ig delta chain C region	0.13	0.08	0.09	0.09	0.08	0.18	0.09
A0A0B 4J1X5	Immunoglobulins	Immunoglobulin heavy variable 3-74	0.05	0.06	0.05	0.02	0.02	0.04	0.06
P01764; P01768	Immunoglobulins	Immunoglobulin heavy variable 3-23	0.06	0.20	0.26	0.12	0.24	0.28	0.15
A0A0C4 DH42	Immunoglobulins	Immunoglobulin heavy variable 3-66	0.03	0.27	0.43	0.23	0.16	0.39	0.18
P01876	Immunoglobulins	Ig alpha-1 chain C region	0.03	1.33	3.93	3.57	1.83	1.09	0.78
A0A0B4 J1Y9	Immunoglobulins	Immunoglobulin heavy variable 3-72	0.05	0.05	0.06	0.03	0.04	0.05	0.05
P01861	Immunoglobulins	Ig gamma-4 chain C region	0.03	0.71	0.42	1.08	0.47	0.15	0.24
P06312	Immunoglobulins	Immunoglobulin kappa variable 4-1	0.05	0.18	0.12	0.07	0.06	0.18	0.12
P80748	Immunoglobulins	Immunoglobulin lambda variable 3-21	0.03	0.16	0.36	0.09	0.06	0.10	0.11
A0A0A0 MRZ8	Immunoglobulins	Immunoglobulin kappa variable 3D-11	0.00	0.02	0.03	0.01	0.03	0.03	0.01
P01700	Immunoglobulins	Immunoglobulin lambda variable 1-47	0.02	0.09	0.17	0.12	0.23	0.15	0.06
A0A075 B6P5; P01615	Immunoglobulins	Immunoglobulin kappa variable 2-28	0.01	0.02	0.02	0.01	0.00	0.01	0.01
P01624; A0A0C4 DH55	Immunoglobulins	Immunoglobulin kappa variable 3-15	0.01	0.11	0.18	0.05	0.04	0.10	0.07
P01782	Immunoglobulins	Immunoglobulin heavy variable 3-9	0.01	0.01	0.01	0.01	0.01	0.01	0.01
A0A0C4 DH41; A0A075 B6R2; P01824; P01825; P06331	Immunoglobulins	Immunoglobulin heavy variable 4-61	0.02	0.16	0.24	0.12	0.11	0.16	0.10
P04433	Immunoglobulins	Immunoglobulin kappa variable 3-11	0.01	0.26	0.34	0.13	0.21	0.25	0.14
P01602	Immunoglobulins	Immunoglobulin kappa variable 1-5	0.02	0.11	0.11	0.04	0.05	0.07	0.06
P01591	Immunoglobulins	Immunoglobulin J chain	0.01	0.02	0.13	1.62	1.07	0.51	0.10
A0A075 B6S5	Immunoglobulins	Immunoglobulin kappa variable 1-27	0.00	0.02	0.04	0.01	0.01	0.03	0.01
P01767; P01772	Immunoglobulins	Immunoglobulin heavy variable 3-53	0.00	0.02	0.03	0.02	0.03	0.03	0.01
A0M8Q6	Immunoglobulins	Ig lambda-7 chain C region	0.00	0.12	0.15	0.02	0.01	0.01	0.04
P01611; A0A0C4 DH73	Immunoglobulins	Immunoglobulin kappa variable 1D-12	0.00	0.00	0.00	0.01	0.10	0.01	0.00
P01699	Immunoglobulins	Immunoglobulin lambda variable 1-44	0.00	0.02	0.02	0.01	0.01	0.03	0.01
P04220	Immunoglobulins	Ig mu heavy chain disease protein	0.00	0.00	0.00	0.00	0.01	0.04	0.00
P01877	Immunoglobulins	Ig alpha-2 chain C region	0.00	0.04	0.09	0.07	0.04	0.02	0.02
A0A0C4 DH24	Immunoglobulins	Immunoglobulin kappa variable 6-21	0.00	0.01	0.01	0.00	0.00	0.02	0.01
A0A087 WSY6	Immunoglobulins	Immunoglobulin kappa variable 3D-15	0.00	0.00	0.01	0.00	0.00	0.00	0.00
P04432; P01597	Immunoglobulins	Immunoglobulin kappa variable 1D-39	0.00	0.00	0.00	0.00	0.00	0.04	0.00

A0A087 WW87; P01614	Immunoglobulins	Immunoglobulin kappa variable 2-40	0.00	0.00	0.00	0.00	0.00	0.00	0.00
P04114	Lipoproteins	Apolipoprotein B-100	1.57	0.91	0.27	0.27	0.32	0.98	1.25
P02647	Lipoproteins	Apolipoprotein A-I	0.22	1.57	0.61	0.36	0.21	0.27	0.40
P02749	Lipoproteins	Beta-2-glycoprotein 1	0.06	0.41	0.23	0.10	0.10	0.11	0.10
P02652	Lipoproteins	Apolipoprotein A-II	0.08	0.66	0.22	0.05	0.07	0.04	0.16
P10909	Lipoproteins	Clusterin	0.01	0.10	0.26	0.19	0.07	0.06	0.09
P06727	Lipoproteins	Apolipoprotein A-IV	0.03	0.05	0.04	0.01	0.02	0.02	0.03
P27169	Lipoproteins	Serum paraoxonase/arylesterase 1	0.01	0.02	0.02	0.00	0.01	0.00	0.01
P02768	Other Plasma components	Serum albumin	46.96	19.27	6.64	6.71	7.18	21.26	33.37
Q14116	Other Plasma components	Interleukin-18	12.89	5.87	1.60	1.23	0.83	3.08	7.28
P02787	Other Plasma components	Serotransferrin	4.15	2.46	1.00	0.77	0.84	1.99	3.43
Q6P587	Other Plasma components	Acylpyruvase FAHD1, mitochondrial	1.60	0.82	0.30	0.50	0.60	1.19	1.23
P02790	Other Plasma components	Hemopexin	1.65	1.26	0.35	0.46	0.45	1.10	1.31
P02774	Other Plasma components	Vitamin D-binding protein	1.08	0.44	0.15	0.17	0.17	0.38	0.64
P02765	Other Plasma components	Alpha-2-HS-glycoprotein	1.11	0.57	0.20	0.19	0.18	0.45	0.67
P06276	Other Plasma components	Cholinesterase	0.83	0.34	0.18	0.21	0.23	0.55	0.54
H3BPM6	Other Plasma components	MKRN2 opposite strand protein	1.09	0.24	0.24	0.26	0.15	0.29	0.47
Q08380	Other Plasma components	Galectin-3-binding protein	0.37	0.23	0.05	0.06	0.21	0.13	0.28
Q9UJ72	Other Plasma components	Annexin A10	0.57	0.17	0.09	0.19	0.14	0.28	0.31
P0C7T7	Other Plasma components	Putative uncharacterized protein FRMD6-AS1	0.51	0.18	0.10	0.14	0.13	0.29	0.28
P35218	Other Plasma components	Carbonic anhydrase 5A, mitochondrial	0.37	0.28	0.08	0.15	0.11	0.23	0.38
P01019	Other Plasma components	Angiotensinogen	0.26	0.23	0.10	0.04	0.04	0.09	0.18
P02750	Other Plasma components	Leucine-rich alpha-2-glycoprotein	0.53	0.21	0.12	0.17	0.14	0.40	0.33
Q9NY27	Other Plasma components	Serine/threonine-protein phosphatase 4 regulatory subunit 2	0.32	0.12	0.04	0.05	0.02	0.17	0.20
P25311	Other Plasma components	Zinc-alpha-2-glycoprotein	0.46	0.19	0.06	0.24	3.08	0.82	0.23
Q4JDL3	Other Plasma components	Tyrosine-protein phosphatase non-receptor type 20	0.20	0.09	0.02	0.02	0.01	0.09	0.15
P04217	Other Plasma components	Alpha-1B-glycoprotein	0.28	0.10	0.05	0.05	0.07	0.15	0.19
P02042; P68871; P69891; P69892	Other Plasma components	Hemoglobin subunit delta	0.32	0.11	0.11	0.21	0.12	0.20	0.19
Q86WP2	Other Plasma components	Vasculin	0.37	0.24	0.12	0.08	0.13	0.15	0.26
P19823	Other Plasma components	Inter-alpha-trypsin inhibitor heavy chain H2	0.28	0.17	0.15	0.09	0.09	0.16	0.20
P82970	Other Plasma components	High mobility group nucleosome-binding domain-containing protein 5	0.27	0.14	0.08	0.11	0.25	0.22	0.20
P19827	Other Plasma components	Inter-alpha-trypsin inhibitor heavy chain H1	0.48	0.15	0.05	0.27	1.46	0.45	0.33
Q96HR3	Other Plasma components	Mediator of RNA polymerase II transcription subunit 30	0.25	0.10	0.05	0.05	0.04	0.15	0.19
Q14624	Other Plasma components	Inter-alpha-trypsin inhibitor heavy chain H4	0.28	0.15	0.09	0.46	0.17	0.14	0.12
B4DZS4	Other Plasma components	T-complex protein 11 X-linked protein 1	0.12	0.10	0.06	0.03	0.03	0.09	0.14
P07098	Other Plasma components	Gastric triacylglycerol lipase	0.18	0.06	0.03	0.03	0.03	0.07	0.09
P02766	Other Plasma components	Transthyretin	0.15	0.16	0.18	0.16	0.13	0.18	0.15
Q8NGB8	Other Plasma components	Olfactory receptor 4F15	0.17	0.09	0.05	0.77	0.30	0.14	0.15
Q9NRM6	Other Plasma components	Interleukin-17 receptor B	0.05	0.06	0.01	0.01	0.01	0.01	0.05
Q9UIY3	Other Plasma components	RWD domain-containing protein 2A	0.09	0.07	0.08	0.19	0.15	0.27	0.08
Q10469	Other Plasma components	Alpha-1,6-mannosyl-glycoprotein 2-beta-N-acetylglucosaminyltransferase	0.06	0.84	0.60	0.20	0.09	0.12	0.30

P01583	Other Plasma components	Interleukin-1 alpha	0.06	0.02	0.02	0.01	0.04	0.02	0.10
Q16832	Other Plasma components	Discoidin domain-containing receptor 2	0.10	0.07	0.04	0.03	0.02	0.04	0.07
Q96IZ5	Other Plasma components	RNA-binding protein 41	0.01	0.01	0.00	0.01	0.01	0.02	0.02
Q9BXI3	Other Plasma components	Cytosolic 5'-nucleotidase 1A	0.09	1.71	2.07	0.91	0.49	1.01	1.03
P18615	Other Plasma components	Negative elongation factor E	0.06	0.21	3.37	3.60	1.27	0.64	0.42
P08185	Other Plasma components	Corticosteroid-binding globulin	0.05	0.05	0.03	0.01	0.01	0.02	0.04
P20742	Other Plasma components	Pregnancy zone protein	0.06	0.07	0.13	0.61	1.07	0.35	0.11
P02760	Other Plasma components	Protein AMBP	0.03	0.23	0.29	0.07	0.06	0.07	0.12
P43652	Other Plasma components	Afamin	0.03	0.03	0.02	0.02	0.02	0.09	0.04
P02753	Other Plasma components	Retinol-binding protein 4	0.02	0.02	0.01	0.02	0.03	0.01	0.02
Q86WK7	Other Plasma components	Amphoterin-induced protein 3	0.03	0.01	0.01	0.01	0.00	0.00	0.02
P36955	Other Plasma components	Pigment epithelium-derived factor	0.02	0.01	0.00	0.00	0.00	0.00	0.00
P55957	Other Plasma components	BH3-interacting domain death agonist	0.01	0.01	0.04	0.03	0.02	0.02	0.01
A8MT65	Other Plasma components	Zinc finger protein 891	0.01	0.01	0.01	0.00	0.00	0.01	0.02
Q6ZTU2; Q96L91	Other Plasma components	EP400 N-terminal-like protein	0.03	0.02	0.00	0.00	0.00	0.01	0.02
P69905	Other Plasma components	Hemoglobin subunit alpha	0.01	0.01	0.03	0.03	0.03	0.01	0.01
O94760	Other Plasma components	N(G),N(G)-dimethylarginine dimethylaminohydrolase 1	0.01	0.00	0.00	0.01	0.00	0.01	0.01
Q8N140	Other Plasma components	EP300-interacting inhibitor of differentiation 3	0.01	0.03	0.04	0.19	0.07	0.02	0.02
O75638	Other Plasma components	Cancer/testis antigen 2	0.00	0.01	0.00	0.00	0.00	0.00	0.00
Q99619	Other Plasma components	SPRY domain-containing SOCS box protein 2	0.04	0.07	0.69	0.94	0.38	0.14	0.12
Q9NWF4	Other Plasma components	Solute carrier family 52, riboflavin transporter, member 1	0.04	0.02	0.04	0.12	0.11	0.20	0.03
P16260	Other Plasma components	Graves disease carrier protein	0.01	0.00	0.00	0.00	0.00	0.00	0.01
Q96MC2	Other Plasma components	Dynein regulatory complex protein 1 OS=Homo sapiens GN=DRC1 PE=2 SV=2	0.02	0.02	0.02	0.07	0.07	0.12	0.03
Q8NHV9	Other Plasma components	Rhox homeobox family member 1	0.01	0.01	0.02	0.07	0.10	0.02	0.01
P22792	Other Plasma components	Carboxypeptidase N subunit 2	0.01	0.06	0.06	0.03	0.02	0.02	0.02
P27482	Other Plasma components	Calmodulin-like protein 3	0.00	0.02	0.07	0.21	0.14	0.04	0.02
Q10589	Other Plasma components	Bone marrow stromal antigen 2	0.01	0.06	0.07	0.09	0.45	0.12	0.05
Q8N8B7	Other Plasma components	Transcription elongation factor A N-terminal and central domain-containing protein	0.00	0.00	0.00	0.01	0.01	0.03	0.00
Q8NCY6	Other Plasma components	Myb/SANT-like DNA-binding domain-containing protein 4	0.01	0.00	0.00	0.00	0.02	0.02	0.00
Q9C0E8	Other Plasma components	Protein lunapark	0.00	0.00	0.03	0.08	0.54	0.12	0.01
Q9BX74	Other Plasma components	TM2 domain-containing protein 1	0.00	0.00	0.00	0.00	0.00	0.00	0.00
P04278	Other Plasma components	Sex hormone-binding globulin	0.00	0.01	0.00	0.00	0.00	0.00	0.00
P63261; P60709; Q6S8J3	Other Plasma components	Actin, cytoplasmic 2	0.00	0.00	0.00	0.01	0.00	0.00	0.00
Q16048	Other Plasma components	Putative pro-MCH-like protein 1	0.00	0.00	0.00	0.02	0.05	0.02	0.00
Q68G75	Other Plasma components	LEM domain-containing protein 1	0.00	0.04	0.06	0.03	0.00	0.02	0.01
Q13434	Other Plasma components	Putative E3 ubiquitin-protein ligase makorin-4	0.00	0.00	0.00	0.00	0.01	0.00	0.00
Q14376	Other Plasma components	UDP-glucose 4-epimerase	0.00	0.00	0.00	0.00	0.00	0.00	0.00
P10916	Other Plasma components	Myosin regulatory light chain 2, ventricular/cardiac muscle isoform	0.00	0.02	0.03	0.02	0.02	0.10	0.01
O00442	Other Plasma components	RNA 3'-terminal phosphate cyclase	0.00	0.18	0.37	0.02	0.01	0.00	0.19
E7EML9	Other Plasma components	Serine protease 44	0.00	0.00	0.01	0.00	0.01	0.11	0.01
A6NGD5	Other Plasma components	Putative zinc finger and SCAN domain-containing protein 5C	0.00	0.01	0.02	0.02	0.01	0.02	0.00
Q96E09	Other Plasma components	Protein FAM122A	0.00	0.00	0.00	0.01	0.00	0.00	0.00

Q9BUG6	Other Plasma components	Zinc finger and SCAN domain-containing protein 5A	0.00	0.00	0.00	0.01	0.01	0.00	0.00
P25788	Other Plasma components	Proteasome subunit alpha type-3	0.00	0.02	0.01	0.00	0.00	0.00	0.00
Q14954	Other Plasma components	Killer cell immunoglobulin-like receptor 2DS1	0.00	0.00	0.00	0.00	0.02	0.00	0.00
A6NMT0	Other Plasma components	Homeobox protein DBX1	0.00	0.00	0.00	0.00	0.00	0.07	0.00
Q9HAJ7	Other Plasma components	Histone deacetylase complex subunit SAP30L	0.00	0.00	0.00	0.02	0.00	0.00	0.00
Q96A32	Other Plasma components	Myosin regulatory light chain 2, skeletal muscle isoform	0.00	0.01	0.02	0.01	0.00	0.00	0.00
P04004	Tissue Leakage	Vitronectin	0.17	0.25	0.24	0.10	0.09	0.15	0.15
P49662	Tissue Leakage	Caspase-4	0.01	0.01	0.00	0.00	0.00	0.00	0.01
O43866	Tissue Leakage	CD5 antigen-like	0.07	0.30	0.69	0.53	0.32	0.44	0.20
P06396	Tissue Leakage	Gelsolin	0.05	0.07	0.03	0.02	0.01	0.03	0.03
Q9UPQ4	Tissue Leakage	Tripartite motif-containing protein 35	0.06	0.02	0.01	0.02	0.01	0.07	0.05
Q96A61	Tissue Leakage	Tripartite motif-containing protein 52	0.01	0.00	0.00	0.00	0.00	0.00	0.01
P53672	Tissue Leakage	Beta-crystallin A2	0.00	0.02	0.16	0.14	0.05	0.03	0.02
Q96PD5	Tissue Leakage	N-acetylmuramoyl-L-alanine amidase	0.01	0.02	0.00	0.00	0.00	0.00	0.01
P12273	Tissue Leakage	Prolactin-inducible protein	0.00	0.00	0.00	0.00	0.00	0.00	0.00